

December 2016

Sulfate Resistance of Nanosilica Contained Portland Cement Mortars

Iani Batilov Batilov

University of Nevada, Las Vegas, batilovi@unlv.nevada.edu

Follow this and additional works at: <https://digitalscholarship.unlv.edu/thesesdissertations>



Part of the [Civil Engineering Commons](#), [Engineering Science and Materials Commons](#), and the [Materials Science and Engineering Commons](#)

Repository Citation

Batilov, Iani Batilov, "Sulfate Resistance of Nanosilica Contained Portland Cement Mortars" (2016). *UNLV Theses, Dissertations, Professional Papers, and Capstones*. 2850.

<https://digitalscholarship.unlv.edu/thesesdissertations/2850>

This Thesis is protected by copyright and/or related rights. It has been brought to you by Digital Scholarship@UNLV with permission from the rights-holder(s). You are free to use this Thesis in any way that is permitted by the copyright and related rights legislation that applies to your use. For other uses you need to obtain permission from the rights-holder(s) directly, unless additional rights are indicated by a Creative Commons license in the record and/or on the work itself.

This Thesis has been accepted for inclusion in UNLV Theses, Dissertations, Professional Papers, and Capstones by an authorized administrator of Digital Scholarship@UNLV. For more information, please contact digitalscholarship@unlv.edu.

SULFATE RESISTANCE OF NANOSILICA CONTAINED
PORTLAND CEMENT MORTARS

By

Iani B. Batilov

Bachelor of Science in Civil and Environmental Engineering

University of Nevada, Las Vegas

2012

A thesis submitted in partial fulfillment
of the requirements for the

Master of Science in Engineering – Civil and Environmental Engineering

Department of Civil and Environmental Engineering and Construction

Howard R. Hughes College of Engineering

The Graduate College

University of Nevada, Las Vegas

December 2016

Copyright by Iani B. Batilov 2016

All Rights Reserved



Thesis Approval

The Graduate College
The University of Nevada, Las Vegas

November 18, 2016

This thesis prepared by

Iani B. Batilov

entitled

Sulfate Resistance of Nanosilica Contained Portland Cement Mortars

is approved in partial fulfillment of the requirements for the degree of

Master of Science in Engineering – Civil and Environmental Engineering
Department of Civil and Environmental Engineering and Construction

Nader Ghafoori, Ph.D.
Examination Committee Chair

Kathryn Hausbeck Korgan, Ph.D.
Graduate College Interim Dean

Samaan Ladknay, Ph.D.
Examination Committee Member

Mohamed S. Kaseko, Ph.D.
Examination Committee Member

Mohamed Trabia, Ph.D.
Graduate College Faculty Representative

ABSTRACT

Sulfate Resistance of Nanosilica Contained Portland Cement Mortars

By

Iani B. Batilov

Dr. Nader Ghafoori, Examination Committee Chair

Professor of Civil Engineering

Department of Civil and Environmental Engineering and Construction

University of Nevada, Las Vegas

Soils, sea water and ground water high in sulfates are commonly encountered hostile environments that can attack the structure of concrete via chemical and physical mechanisms which can lead to costly repairs or replacement. Sulfate attack is a slow acting deteriorative phenomenon that can result in cracking, spalling, expansion, increased permeability, paste-to-aggregate bond loss, paste softening, strength loss, and ultimately, progressive failure of concrete. In the presented research study, Portland cement (PC) mortars containing 1.5% to 6.0% nanosilica (nS) cement replacement by weight were tested for sulfate resistance through full submersion in sodium sulfate to simulate external sulfate attack. Mortars with comparable levels of cement replacement were also prepared with microsilica (mS). Three cement types were chosen to explore nS' effectiveness to reduce sulfate expansion, when paired with cements of varying tricalcium aluminate (C_3A) content and Blaine fineness, and compare it to that of mS. Mortars were also made with combined cement replacement of equal parts nS and mS to identify if they were mutually compatible and beneficial towards sulfate resistance. Besides sulfate attack expansion of mortar bars, the testing program included investigations into transport and microstructure properties via water absorption, sulfate ion permeability, porosimetry, SEM with EDS, laser diffraction, compressive strength, and heat of hydration. Expansion measurements indicated that mS replacement mortars outperformed both powder form nS, and nS/mS combined replacement mixtures. A negative effect of the dry nS powder

replacement attributed to agglomeration of its nanoparticles during mixing negated the expected superior filler, paste densification, and pozzolanic activity of the nanomaterial. Agglomerated nS was identified as the root cause behind poor performance of nS in comparison to mS for all cement types, and the control when paired with a low C_3A sulfate resistant cement.

Testing the effects of mixing methodology and nS dispersion (mechanical blending vs. ultrasonic dispersion vs. aqueous solution) on sulfate resistance became a separate focus of the study. Use of the aqueous form of nS resulted in a more sulfate resistant and impermeable mortar than all other tested methods of mixing and dispersing dry form nS. At 6% replacement, aqueous nS contained mortars were more resistant to expansion than those with mS. Excessive ultrasonic dispersion of dry nS in the mixing water was shown to likely cause further agglomeration that harmed permeability and sulfate resistance.

Overall, nS proved effective at improving sulfate resistance of mortars provided good dispersion could be achieved, otherwise mS remained the more effective, reliable, and economic choice. Parts of this study, a testing phase exploring the effectiveness of aqueous form nS on mortar resistance to physical sulfate attack via partial submersion, is still ongoing.

ACKNOWLEDGEMENTS

Finding the courage and inspiration to take on such a daunting research project, and then finding the stamina and path forward to see it through to this culminating product of the work, is in no small part due to the invaluable mentorship I've had from my academic advisor, Dr. Nader Ghafoori. I'll be forever grateful for all the technical and professional guidance, all the motivation, encouragement, insight, opportunities, and push for excellence that I have experienced working with him. I have similar praise for the very talented and very knowledgeable Meysam Najimi, from whom I've learned much about concrete going all the way back to my undergraduate days where he was my TA for the civil materials lab. Thank you for all the discussion, help with the testing, and too many peer reviews to count.

I am very thankful to the committee members Dr. Samaan Ladkany, Dr. Mohamed S. Kaseko, and Dr. Mohamed Trabia for their feedback, guidance, and suggestions. I would like to recognize and thank Mr. Peter Faught, often behind the scenes, but he's the man that keeps everything in that laboratory running. On many occasions he saved the day when I accidentally broke something. Thank you for being so kind, for procuring things and finding creative solutions, and for the amazing work on retrofitting the cyclic environmental chamber you did for me.

I want to thank my family for their love and unwavering support. I appreciate your patience and your forgiveness for my lack of presence or early departure at many family functions. I also have nothing but praise and love for my girlfriend Brittany Radke, who has put up with me through all the lab work, the writing, the long nights, and just created the most accommodating environment for research at home anyone could ask for. Thank you for being my rock...or should I say concrete?

DEDICATION

First, I dedicate this work to my amazing parents, Mr. Batil Batilov and Mrs. Galina Batilova. Thank you for sacrificing so much and taking such big risks in your lives to create a brighter future for me and my sister Donna. Thank you for fighting so hard and persevering through grueling times so that we may now call this country our second home and have such amazing opportunities to pursue our dreams, passions, and happiness.

Second, I want to dedicate this work to my late grandmother Mrs. Donka Dimitrova Ilieva. She was the kindest, most caring, poised, and selfless person I know. She never made it about herself, and never wanted someone to go out of their way for her. Some of my most cherished childhood memories are spent in her care. She was the embodiment of unspoken altruism and I would like her to be remembered.

TABLE OF CONTENTS

ABSTRACT	iii
ACKNOWLEDGEMENTS.....	v
DEDICATION.....	vi
TABLE OF CONTENTS.....	vii
LIST OF TABLES.....	xv
LIST OF FIGURES	xvii
INTRODUCTION.....	1
1 SULFATE ATTACK	6
1.1 Sources of Sulfates	6
1.1.1 Internal Sources of Sulfates.....	6
1.1.2 External Sources of Sulfates.....	8
1.2 Chemical Sulfate Attack.....	9
1.2.1 Ettringite and Gypsum.....	10
1.2.2 Magnesium Sulfate.....	17
1.2.3 Thaumasite Formation.....	17
1.2.4 Delayed Ettringite Formation (DEF)	20
1.3 Physical Sulfate Attack (PSA)	21
1.4 Effects of Cement Composition on Sulfate Attack.....	25
1.4.1 Tricalcium Aluminate (C ₃ A) Content.....	25
1.4.2 Tricalcium Silicate (C ₃ S) to Dicalcium Silicate (C ₂ S) Ratio	26

1.4.3	Mineral Admixtures.....	27
1.5	Effects of Permeability on Sulfate Attack.....	29
1.5.1	Water-to-Cement Ratio (w/c).....	30
1.5.2	Cement Fineness.....	31
2	NANOSILICA.....	33
2.1	Pozzolans.....	33
2.2	Silica Fume (Microsilica).....	35
2.2.1	Historical Background.....	36
2.2.2	Microsilica Effects on Fresh & Rheological Properties.....	36
2.2.3	Microsilica Effects on Hardened Properties.....	38
2.2.4	Microsilica on Durability and Sulfate Resistance.....	39
2.3	Sources and Production of Nanosilica.....	43
2.4	Nanosilica Effects on Fresh & Rheological Properties.....	44
2.4.1	Water Demand and Workability.....	44
2.4.2	Bleeding and Segregation.....	45
2.4.3	Setting Time.....	45
2.4.4	Heat of Hydration.....	46
2.5	Nanosilica Effects on Hardened Properties.....	47
2.6	Nanosilica on Durability and Sulfate Resistance.....	48
2.6.1	Permeability Effects of Nanosilica.....	48
2.6.2	Sulfate Resistance.....	50

3	MATERIALS AND EXPERIMENTAL PROGRAM.....	54
3.1	Materials	54
3.1.1	Ordinary Portland Cements	54
3.1.2	Aggregate	55
3.1.3	Water	57
3.1.4	Chemical Admixture	58
3.1.5	Nanosilica.....	58
3.1.6	Silica Fume (Microsilica)	61
3.1.7	Sodium Sulfate (Na_2SO_4) Solution.....	62
3.1.8	Particle Size Distribution of Cements and Pozzolans	63
3.2	Mortar Mixture Proportions	65
3.3	Mixing Procedure	68
3.4	Experimental Program & Setup.....	72
3.4.1	Phase I – Chemical Sulfate Attack via Full Submersion Exposure.....	72
3.4.2	Phase II – Mixing Methodology and Dispersion of Nanosilica	75
3.4.3	Phase III – Nanosilica on Physical Sulfate Attack via Partial Submersion Exposure....	77
3.5	Measurements	79
3.5.1	Flow (ASTM C 1437)	79
3.5.2	Heat of Hydration	81
3.5.3	Compressive Strength (ASTM C 109).....	82
3.5.4	Mass Loss and Observable Deterioration.....	84

3.5.5	Sulfate Expansion of Mortar Bars (ASTM C 1202).....	86
3.5.6	Water Absorption (ASTM C 642).....	89
3.5.7	Rapid Sulfate Permeability Test (RSPT)	91
3.5.8	Mercury Intrusion Porosimetry (MIP)	92
3.5.9	Scanning Electron Microscopy (SEM) and Energy-Dispersive X-Ray Spectroscopy (EDS).....	93
RESULTS AND DISCUSSION		97
Overview of Manuscripts.....		97
4	SULFATE RESISTANCE OF NANOSILICA AND MICROSILICA CONTAINED MORTARS.....	99
4.1	Abstract.....	99
4.2	Introduction.....	99
4.3	Research Significance	102
4.4	Experimental Procedure	103
4.4.1	Materials.....	103
4.4.2	Mixture Proportions.....	104
4.4.3	Mixture and Sample Preparation.....	105
4.4.4	Sulfate Solution.....	106
4.5	Experimental Results and Discussion.....	106
4.5.1	Influence of Nanosilica	108
4.5.2	Influence of Microsilica	116
4.5.3	Comparison between Nanosilica and Microsilica	117

4.5.4	Strength Loss.....	119
4.5.5	Mass Loss.....	121
4.6	Conclusions.....	122
5	BLAINE AND TRICALCIUM ALUMINATE EFFECTS ON THE SULFATE RESISTANCE OF NANOSILICA AND MICROSILICA CONTAINED MORTARS.....	124
5.1	Abstract.....	124
5.2	Introduction.....	124
5.3	Research Significance.....	129
5.4	Experimental Procedure.....	129
5.4.1	Materials.....	129
5.4.2	Mixture Proportions.....	131
5.4.3	Mixture and Sample Preparation.....	132
5.4.4	Sulfate Solution.....	132
5.4.5	RSPT, Mercury Intrusion Porosimetry, Heat of Hydration.....	133
5.5	Experimental Results and Discussion.....	133
5.5.1	Sulfate Attack Expansion.....	133
5.5.2	Rapid Sulfate Permeability Test (RSPT).....	139
5.5.3	Mercury Intrusion Porosimetry (MIP).....	141
5.5.4	Heat of Hydration.....	145
5.5.5	Discussion.....	148
5.5.6	Compressive Strength.....	149

5.6	Conclusions.....	151
6	EFFECT OF COMBINED NANOSILICA AND MICROSILICA ON RESISTANCE TO SULFATE ATTACK.....	154
6.1	Abstract.....	154
6.2	Introduction.....	155
6.3	Experimental Program.....	157
6.3.1	Materials.....	157
6.3.2	Mixture Proportions.....	159
6.3.3	Mixing Procedure	159
6.3.4	Sulfate Solution.....	160
6.3.5	Absorption and RSPT.....	160
6.4	Results and Discussion.....	161
6.4.1	Sulfate Attack Expansion.....	161
6.4.2	Supplemental Testing.....	165
6.4.3	Water Absorption and RSPT	168
6.4.4	Mercury Intrusion Porosimetry (MIP)	170
6.4.5	Compressive Strength.....	172
6.5	Conclusion.....	174
7	INFLUENCE OF DISPERSION METHODS ON SULFATE RESISTANCE OF NANOSILICA CONTAINED MORTARS.....	176
7.1	Abstract.....	176

7.2	Introduction.....	176
7.3	Experimental Procedure	182
7.3.1	Materials.....	182
7.3.2	Mixture Proportions.....	183
7.3.3	Mixing and Testing Program.....	184
7.3.4	Sulfate Solution.....	186
7.4	Experimental Results and Discussion.....	186
7.4.1	Sulfate Expansion – Aqueous Solution VS Ultrasonic Dispersion VS Mechanical Dispersion	187
7.4.2	Sulfate Expansion – Ultrasonic Dispersion and Aqueous Solution	188
7.4.3	Sulfate Expansion – Mechanical Dispersion & HRWRA Dosing Method.....	191
7.4.4	Effects on Absorption, Sulfate Ion Permeability, and Porosimetry	194
7.4.5	Compressive Strength.....	201
7.5	Conclusions.....	204
8	INFLUENCE OF NANOSILICA ON PHYSICAL SULFATE ATTACK RESISTANCE OF MORTARS..	206
8.1	Abstract.....	206
8.2	Update on Research Activities	206
9	CONCLUSION AND RECOMMENDATIONS.....	211
9.1	Summary of Research Activities	211
9.2	Summary of Conclusions.....	212
9.3	Future Research Needs.....	213

APPENDIX A: CONVERSION FACTORS	215
APPENDIX B: RELEVANT COMPOUND FORMULAS & CEMENT CHEMISTRY	216
BIBLIOGRAPHY	218
CURRICULUM VITAE.....	230

LIST OF TABLES

Table 3-1: Properties of Portland Cements Tested	54
Table 3-2: Sieve Analysis and Material Finer than No. 200 Sieve	55
Table 3-3: Specific Gravity and Absorption of Fine Aggregate per ASTM C 128.....	56
Table 3-4: Deleterious Substance and Alkali-Silica Reactivity Testing of Fine Aggregate.....	57
Table 3-5: Properties of HRWRA	58
Table 3-6: Properties of Dry Silicon Dioxide Nanoparticle Powder.....	60
Table 3-7: Properties of Aqueous Silica Nanoparticle Dispersion	60
Table 3-8: Properties of Silica Fume (Microsilica)	61
Table 3-9: Properties of Anhydrous Sodium Sulfate Powder	63
Table 3-10: Mortar Mixture Proportions for Phase I of Testing Program	66
Table 3-11: Mixture Proportions for Phase II of Testing Program	67
Table 3-12: Mixture Proportions for Phase III of Testing Program.....	67
Table 3-13: Specifications of SEM Used for Imaging and EDS Analysis of Mortars	95
Table 3-14: Specifications of FESEM Used for Imaging of dry nS, mS, and Aqueous nS	96
Table 4-1: Chemical Composition and Physical Properties of Cement, nS, and mS.....	104
Table 4-2: Mortar Mixture Proportions for Moderate and Low C ₃ A Cements	105
Table 4-3: Expansion Measurements at Key Time Periods.....	107
Table 5-1: Chemical Composition and Physical Properties of Cement, nS, and mS.....	130
Table 5-2: Mortar Mixture Proportions for Low and High C ₃ A Cements	131
Table 5-3: Expansion Measurements at Key Time Periods.....	134
Table 6-1: Chemical Composition and Physical Properties of Cement and nS	158
Table 6-2: Mortar Mixture Proportions	159
Table 6-3: Expansion Measurements at Key Time Periods.....	161
Table 7-1: Literature Review of Different nS Forms and Methods of Dispersion or Mixing.....	179

Table 7-2: Chemical Composition and Physical Properties of Cement and nS	183
Table 7-3: Mortar Mixture Proportions	184

LIST OF FIGURES

Figure 1-1: SEM and EDX Analyses of Gypsum and Ettringite, the Products of ‘Traditional’ Chemical Sulfate Attack (Nehdi et al. 2014).....	10
Figure 1-2: Micrographs of Paste Containing Gypsum and Calcium Sulfoaluminates hydrated with lime in (A) and without lime in (B) (Mehta 1973).....	15
Figure 1-3: Expansion in Cement Pastes as a Function Of The Amount Of Ettringite Formed (Odler & Gasser 1988).....	16
Figure 1-4: Example SEM and EDX of Thaumasite (Bassuoni & Nehdi 2009)	18
Figure 1-5: Example of Severe TSA Damage in Lab Samples (Rahman & Bassuoni 2014).....	19
Figure 1-6: Effect of Combined ASR and DEF on Precast Beam (Skalny et al. 2002)	21
Figure 1-7: BSE Image of Aggregate Particle with Surrounding Ettringite-filled Gap (Thomas et al. 2008)	21
Figure 1-8: Phase diagram of Sodium Sulfate (Flatt 2002).....	24
Figure 1-9: Scaling of Concrete Foundation Slab due to Physical Sulfate Attack (Haynes et al. 1996)	25
Figure 1-10: Link between C_3A of Cements and Rate of Deterioration (Verbeck 1967)	26
Figure 1-11: Correlation between Permeability and w/c for matured cement paste (Powers 1958)	30
Figure 1-12: Effects of w/c on MIP of Cement Pastes Cured for 7 Days (Cook & Hover 1999)	31
Figure 2-1: Effects of Microsilica (MS) on Strength to (w/c) Ratio Curve (Hewlett & Massazza 2003)	39
Figure 2-2: SEM of the ITZ Between Cement Paste and Aggregate at 28 days for A) Mixture without mS, B) Mixture with mS (ACI Committee 234 2006; Bentur & Cohen 1987)	41
Figure 2-3: Expansion of Mortar Bars in Sulfate Solution Tested per ASTM C 1012 (ACI Committee 234 2006)	42

Figure 2-4: Flow Table Spread of Mortars Containing 0% to 3.5% nS (L. Senff et al. 2009)	45
Figure 2-5: Effects of nS on Rate of Heat Development for High Slag Mixtures (Zhang et al. 2012) ..	46
Figure 2-6: Capillary Suction of 5% and 10% Contained Mortars (Tobón et al. 2015)	49
Figure 2-7: Cumulative MIP Pore Volume Curves for 0.9% nS Concrete and an OPC Control (Du et al. 2014a)	50
Figure 2-8: Relative Expansion to Control of Mineral Admixture contained Mortars after 12 Months of Internal Sulfate Attack due to Contaminated Sand (Atahan & Dikme 2011)	51
Figure 2-9: Expansion of Mineral Admixture contained Mortars after 12 Months of External Sulfate Attack due to 5% Na ₂ SO ₄ (Atahan & Dikme 2011)	52
Figure 2-10: 3 Years of Expansion of Mortars Immersed in 5% MgSO ₄ Solution (Tobón et al. 2015)	53
Figure 3-1: SEM Image of the Dry Nanosilica Powder Used in this Study	59
Figure 3-2: SEM Image of Aqueously Dispersed Nanosilica Dried Out of Solution	59
Figure 3-3: SEM Image of Microsilica	62
Figure 3-4: Laser Diffraction Particle Size Analysis of Cements and Pozzolans	64
Figure 3-5: Epicyclic Mixer used for Preparation of Mortars	68
Figure 3-6: Setup of Ultrasonic Cleaner for Ultrasonic Dispersion of Nanosilica	69
Figure 3-7: Measurement of Mortar Flow per ASTM C 1437 Procedure	71
Figure 3-8: Phase I Sodium Sulfate Solution Tanks	74
Figure 3-9: Phase I Sodium Sulfate Tank Opened to Show Contents	74
Figure 3-10: Humidity Controller and Humidifier in Environmental Chamber for Phase III	78
Figure 3-11: Constant Environment Partial Submersion Exposure Setup for Phase III	79
Figure 3-12: ASTM C 230 Mortar Flow Table	80
Figure 3-13: Heat of Hydration Test Setup	81
Figure 3-14: Loading Machine for Testing Mortar Cube Compressive Strength	83

Figure 3-15: Axial Compression Loading Machine Used for Mortar Cylinder Testing.....	84
Figure 3-16: Cement M Control Mortar (M0) Cubes Tested for Mass Loss.....	85
Figure 3-17: Set of Mortar Cylinders Part of the Physical Sulfate Attack Testing in Phase III	85
Figure 3-18: Length Comparator with Mortar Bar Loaded in for Measurement.....	88
Figure 3-19: Mortar Bars of a Cement M mixture after 1.5 years of Immersion in Sodium Sulfate Solution.....	88
Figure 3-20: Schematic of RSPT Test Setup Adopted from (CCAA 2011).....	91
Figure 3-21: RSPT Setup of Three RSPT Testing Cells	92
Figure 3-22: FESEM Used for Imaging of dry nS, mS, and Aqueous nS	96
Figure 4-1: Control Mixture Expansion.....	108
Figure 4-2: 7.2% C ₃ A Cement A Mixture Series Expansion with nS and mS Replacement.....	109
Figure 4-3: Absorption of Cement A Mortars with 0%, 3%, and 6% Dry nS Replacement	110
Figure 4-4: Laser Diffraction Particle Size Analysis of nS, mS, cements A and B	112
Figure 4-5: 7.2% C ₃ A Cement A Expansion of Mortars with dry nS, aqueously dispersed nS, and mS Replacement.....	113
Figure 4-6: 4.1% C ₃ A Cement B Mixture Series Expansion with mS and nS Replacement.....	114
Figure 4-7: 4.1% C ₃ A vs 7.2% C ₃ A Cement Mixture Series Expansion with nS Replacement.....	115
Figure 4-8: 7.2% C ₃ A Cement A Mortar Cube Compressive Strengths at, a) 26 Weeks, b) 52 Weeks	119
Figure 4-9: 4.2% C ₃ A Cement B Mortar Cube Compressive Strengths at, a) 26 Weeks, b) 52 Weeks	120
Figure 4-10: 4.1% C ₃ A vs 7.2% C ₃ A Cement mortar cubes after 1 year exposure to Na ₂ SO ₄ solution: a) A0 mortar cubes with observable surface softening and cracking around edges pointed out with arrows, b) B0 mortar cubes with no edge cracking, c) A3mS cubes with some edge cracking, d) B3mS	

without observable cracking, e) A3nS with observable edge cracking, f) B3nS with observable edge cracking	121
Figure 5-1: Sulfate Attack Expansion for Control Mortars	135
Figure 5-2: Cement L (4.1% C ₃ A / SSA = 285 m ² /kg) Mortar Series Expansion	136
Figure 5-3: Cement H (12.3% C ₃ A / SSA = 546 m ² /kg) Mortar Series Expansion	137
Figure 5-4: Cement L vs Cement H nS Contained Mortars	138
Figure 5-5: RSPT Results for Select Mortars (error bars represent ±SD)	139
Figure 5-6: MIP Results for Cement L and Cement H Mortars	142
Figure 5-7: Classification of Total Intrusion Pore Volume for Select Mortars	143
Figure 5-8: Heat of Hydration Results	146
Figure 5-9: Laser Diffraction Particle Analysis of nS, mS, Cement L, and Cement H	149
Figure 5-10: Compressive Strength, a) Cement L at 28 Days, b) Cement H at 28 Days, c) Cement L at 6 Months, d) Cement H at 6 Months, e) Cement L at 1 Year, f) Cement H at 1 Year	150
Figure 6-1: Expansion Measurements for Cement M Mortar Mixtures	162
Figure 6-2: Expansion Measurements for Cement L Mortar Mixtures	163
Figure 6-3: Test Strip pH Measurements of Mixing Water vs Tap Water	166
Figure 6-4: Laser Diffraction Particle Size Analysis of nS, mS, and Cements L and M	167
Figure 6-5: Water Absorption of Select Mortars (error bars represent ±SD)	168
Figure 6-6: RSPT vs Expansion at 1.5 years of Sulfate Attack for Select Mortar Mixtures (error bars represent ±SD)	169
Figure 6-7: MIP Pore Size Distribution for Cement M Mortars	171
Figure 6-8: Cement L Mortar Cube Compressive Strengths at, a) 26 Weeks, b) 52 Weeks	173
Figure 6-9: Cement M Mortar Cube Compressive Strengths at, a) 26 Weeks, b) 52 Weeks	173
Figure 7-1: Laser Diffraction Particle Size Analysis of dry nS and OPC	181

Figure 7-2: Expansion of the Mechanical Dispersion, Ultrasonic Dispersion, and Aqueous Solution 3% nS Mortars	187
Figure 7-3: Expansion of the Mechanical Dispersion, Ultrasonic Dispersion, and Aqueous Solution 6% nS Mortars	188
Figure 7-4: Expansion of the 3% and 6% nS Ultrasonic Dispersion VS Aqueous Solution Mortars	189
Figure 7-5: Expansion of the Mechanical Dispersion 3% nS Mortars.....	190
Figure 7-6: Expansion of the Mechanical Dispersion 6% nS Mortars.....	192
Figure 7-7: Water Absorption Results (error bars represent \pm SD).....	194
Figure 7-8: Example of Ultrasonically Induced Re-Agglomeration of ZrO_2 Particles due to Excessive Ultrasonic Treatment (Vasylykiv & Sakka 2001)	196
Figure 7-9: RSPT Test of Select nS Contained Mortars (error bars represent \pm SD).....	198
Figure 7-10: MIP Pore Size Distribution for CNTL, M6nS-10-I, and AQ6nS Mortars	201
Figure 7-11: Compressive Strength of Mortars at 3 Days and 26 Weeks (error bars represent \pm SD)	202
Figure 8-1: Constant Low Humidity Exposure Setup for Physical Sulfate Attack	208
Figure 8-2: Specimens Exposed to Cyclic Exposure Conditions after 12 Months.....	208
Figure 8-3: Specimens Exposed to Constant Condition Exposure after 12 Months	209

INTRODUCTION

Concrete is one of the most versatile and commonly used construction materials in the world. The United States (US) alone uses over 300 million cubic meters (400 million cubic yards) a year (Kosmatka et al. 2002). Concrete applications take place in a broad spectrum of environments, many of which expose the material to conditions that can cause deterioration and can lead to costly repairs and replacement. The annual repair, protection, and strengthening costs for concrete structures in the US are estimated to be between \$18 and \$21 billion (ICRI 2006). Structures found lacking in durability, that have experienced untimely deterioration under hostile environments have also been the subject of expensive litigation (Skalny et al. 2002). Development of durable concrete lessens concrete's environmental impact by both reducing the amount of virgin cement used and prolonging the service life of the structure, which saves on energy and resources associated with its maintenance, repair, and untimely replacement. These are some of the factors behind the concrete industry's drive towards the development of materials, mixtures, and technologies that can result in durable concrete, mitigate maintenance costs, and extend the service life of concrete structures.

Nanotechnology developments have made significant impacts to multiple industries. Research into nano-engineered construction materials has garnered a lot of attention over the last 50 years since P. Feynman discussed the significance of manipulating matter at the nanoscale in his 1959 lecture *"There's Plenty of Room at the Bottom"* (Sanchez & Sobolev 2010; Sahin & Oltulu 2008). There has been a surge of interest in nanomaterials and their potential applications in producing high performance, sustainable, and durable concrete. Nanosilica has become particularly popular. This attention is due to the material's fine particle size and aggressive pozzolanic nature. The high pozzolanic reactivity stems from its inherently high surface area that surpasses that of its predecessor microsilica (mS), also known as silica fume (Singh et al. 2013; Pengkun Hou et al. 2013). Nanosilica (nS) is commercially available in various nano-scale sizes dependent on the method of

synthesis and may be offered in dry powder form or in a dispersant stabilized suspension (Campillo et al. 2004). Although the fresh rheological and hardened properties of cement pastes, mortars, and concrete with nS replacement have been studied over the recent years there is still limited literature on the sulfate durability effects of nS. The work presented in this thesis explores the role nS can have in reducing sulfate related expansion and how the nanomaterial performs when put up against the more common and at this time relatively more economical silica fume.

The results and true body of discussion in this thesis are presented as a collection of manuscripts developed in completed form for publication in reputable journals of science and technology in civil engineering materials. Some have already been published and some are in various stages of peer review. With this in mind, following this introduction, the thesis is organized in a series of chapters with the following intent:

Chapter 1 | This is a background chapter that presents an overview of sulfate attack and covers its many forms, reactions, and mechanisms of deterioration. Sources of sulfates are described, both those introduced internally and those concrete may encounter externally. The multiple forms of chemical sulfate attack are covered with a more elaborate discussion of the conventional form of sulfate attack. The conventional form of chemical sulfate attack centers around the chemical reactions between the sulfate ions and the hydrated cement compounds to form ettringite and gypsum. Following that magnesium sulfate, thaumasite, and delayed ettringite formation are also covered under chemical sulfate attack. The physical sulfate attack mechanisms of deterioration are discussed in a separate section of the chapter. After this overview, different factors that affect sulfate attack susceptibility are discussed. Those relevant aspects of the cement chemical composition and factors that affect the physical transport properties of the hardened cementitious composites.

Chapter 2 | This is a background chapter on nanosilica. It starts with a section on pozzolans and a section on its predecessor silica fume. These are followed by a section on the development and synthesis of the nanomaterial. The same chapter then covers the many effects of nanosilica on the fresh and hardened properties of cementitious composites such as concrete with particular attention given to its effects on sulfate resistance.

Chapter 3 | This chapter serves to detail the various materials used and the scope of the testing program. The various cement types, nanosilica, silica fume, and other mortar ingredient materials are described. The source of water used for mixing and the preparation of the sodium sulfate is listed as well. All testing phases and the mixture proportions used within are presented. A detailed mortar mixing procedure and testing program setup is described that includes a separate section for every type of experimental measurement made.

Chapter 4 | This is the first manuscript chapter. Its objective was presenting a side-by-side comparison study intended to identify the effects of nanosilica (nS) on chemical sulfate attack resistance of Portland cement (PC) mortars and its effectiveness in comparison to similar replacement levels of the more widely implemented microsilica (mS). This manuscript presents results of mortar mixtures from Phase I of the testing program. Only mixtures using cement Type I/II and cement Type V are compared, because they have different tricalcium aluminate (C_3A) content but otherwise similar fineness. The focus group of mixtures contained either nS or mS only.

Chapter 5 | This is the second manuscript chapter. Its objective was to highlight the effect of dry powder nS paired with cements of contrastingly different fineness and C_3A content on the sulfate resistance of mortars. Results from several Phase I mortar mixtures with incrementally higher

cement replacement with nS or mS and either the 4.1 or 12.3% C₃A cement of different Blaine fineness (Type V and Type III) are presented and discussed in that manuscript chapter.

Chapter 6 | This is the third manuscript chapter. Its objective was to highlight the effect of combined nanosilica (nS) and microsilica (mS) on sulfate resistance of Portland cement (PC) mortars evaluated against all cement control mortars and mixtures with equivalent contents of only one form of silica. This manuscript chapter presents results of silica contained mortars from Phase I of the testing program that had 6% cement replacement of either nS, mS, or 3% of each.

Chapter 7 | This is the fourth manuscript chapter. The results presented in this chapter stem from Phase II of the testing program. Its objective was to evaluate the influence of various dispersion methods on the sulfate attack resistance of nanosilica (nS) contained mortars. Multiple mechanical or ultrasonic dispersion methods, HRWRA dosing procedures, and both dry and aqueous solution forms of nS were used to prepare a series of mortars with 0%, 3%, and 6% replacement of Portland cement with nS. Mortars were subjected to 6 months of exposure in a 5% sodium sulfate solution.

Chapter 8 | This chapter is a progress update on Phase III of the testing program where the mortar mixtures containing 3% or 6% of either nS or mS using two types of cements were subjected to a two exposure environments intended to simulate physical form of sulfate attack. The objective of this study was to evaluate the effectiveness of colloidal nanosilica as a nanomaterial and pozzolanic admixture to prevent effects of physical sulfate attack on mortars. This work is still ongoing in order to collect results after more severe deterioration of the mortar samples is observed and quantified via mass loss and a visual rating system. Therefore, at this time, this chapter only includes some of the preliminary observations and a brief discussion of the current state of the tested specimens.

Chapter 9 | This is a closing chapter that summarizes all research activities within this body of work and offers a summary of conclusions that touches on the outcome of the work presented within each of the preceding manuscript chapters. There are some recommendations for further research and thoughts on the future of nanosilica in developing durable sulfate resistant concrete.

1 SULFATE ATTACK

One of the significant advantages of concrete is that in most cases, it performs well in a broad range of environmental and atmospheric conditions. When designed and constructed with consideration of the chemical and physical demands that it will be subjected to, concrete is inherently durable and will often exceed its intended design service life. Concrete structures offer decades of service life with relatively little maintenance. Besides its low cost, one of the great advantages of concrete is that it can innately hold up well to soils, waters, and air that expose it to a variety of aggressive chemicals that include acids, sulfates, chlorides, CO₂, and de-icing salts (Dyer 2014). This body of work focuses on the concrete deteriorative mechanisms known as sulfate attack. Sulfate attack is not one process but a category of complex and overlapping chemical and physical phenomena that stem from interaction between a sulfate source and the hydrated phases and physical structure of the cementitious composite (Skalny et al. 2002). Following is a synopsis of the multiple chemical and physical forms of sulfate attack. However, the author must disclose that the body of research work presented herein explores the effects of nanosilica on a narrow selection of them. In brief, sodium sulfate is the only external source of sulfate tested, under a limited variety of laboratory controlled conditions (temperature, humidity, pH, cyclic exposure), and over a limited exposure period. Now follows an overview of the broad and complex world of sulfate attack.

1.1 Sources of Sulfates

1.1.1 *Internal Sources of Sulfates*

A common internal source of sulfate is calcium sulfate [CaSO₄], which is also an important component intentionally added in ordinary Portland cements (OPC). It is added to OPC clinker during grinding either in the form of anhydrite [CaSO₄], hemihydrate [CaSO₄*0.5H₂O], or dihydrate also commonly referred to as gypsum [CaSO₄*2H₂O] to control the setting rate of the cement (Skalny et al. 2002).

Usually around 5% of gypsum or anhydrite is added during grinding of the clinker because it helps regulate the early stages of setting and provide a sufficient workability window (Mehta & Monteiro 2006). It has a retarding effect on the hydration of the aluminates by suppressing their solubility and an accelerating effect on the hydration of the silicates C_3S and C_2S (Mehta & Monteiro 2006). The dosage added is usually optimized based on its effects on accelerating early strength and maintaining workability of the specific cement produced. Due to the careful control of chemistry, burning, and grinding processes in place at cement plants, excessive dosages of gypsum are a rare occurrence.

A more likely internal source of excessive sulfates might come from an aggregate used that may unknowingly contain sulfates (such as gypsum) or sulfides (such as iron sulfide). Iron sulfide, also known as pyrite, may oxidize in the presence of oxygen and moisture to form an acidic sulfate solution that can cause sulfate and acid attack (Skalny et al. 2002). Sulfates may also be introduced internally by use of certain mineral or chemical admixtures, which is why their mineral and chemical make-up should be screened prior to application. Although rare, mixing water could also be a source of sulfates introduced internally since tap water in some localities may have sulfate contents in excess of 150 parts per million (ppm) (Skalny et al. 2002). This is a relatively low concentration for external sulfate exposure. It is used as the low end boundary of the concentration range (150 to 1500 ppm) defined by ACI as moderate class S1 sulfate exposure. This range comes from the sulfate exposure table in the *Guide to Durable Concrete* by ACI Committee 201 (ACI Committee 201 2008). Nevertheless, sulfates from use of contaminated mixing water are not impeded by the impermeability of the concrete, so they have access to the entirety of the concrete structure and can at minimum accelerate or compound the effects of possible sulfate attack from an external source.

1.1.2 External Sources of Sulfates

External sulfate attack would not occur without the presence of water to dissolve the sulfate ions from their natural state and bring them in contact with the concrete structure. For marine structures, seawater is an obvious source. Seawater is a high concentration sulfate solution that, depending on its salinity, contains anywhere from 2500 to 3000 mg/L (Dyer 2014). The sulfates are paired mostly with sodium and magnesium, although potassium and calcium is present in smaller quantities too.

Inland, there are naturally occurring sulfates in soils and clays that are of various solubility and can be transported and brought in contact with concrete through groundwater, rainwater, and irrigation water. Four of the more soluble sulfate-rich minerals encountered are Epsomite [$\text{MgSO}_4 \cdot 7\text{H}_2\text{O}$], Mirabilite [$\text{NaSO}_4 \cdot 10\text{H}_2\text{O}$], Glauberite [$\text{Na}_2\text{Ca}(\text{SO}_4)_2$], and Gypsum [$\text{CaSO}_4 \cdot 2\text{H}_2\text{O}$] (Dyer 2014). Most minerals encountered are natural sulfates of calcium, magnesium, sodium, and potassium (Skalny et al. 2002; Hewlett & Massazza 2003; Mehta 1993). Alkali soils encountered in large areas of North America may have sulfate contents of several percent. Issues experienced in the past with concrete in sewers, pipes, culverts, and foundations drew a lot of the initial attention to sulfate attack (Hewlett & Massazza 2003). The distribution of sulfates in clays is very irregular and it is not uncommon to encounter pockets of crystalline gypsum or bands of certain sulfate compound deposits. Sulfate concentration also exhibits significant variability with depth. In regions where rainfall exceeds evaporation, sulfates are typically absent from the upper 1 m (3 ft) of soil due to rainwater leaching of the upper deposits. In more hot and arid regions such as the US Southwest and Canada prairies, there might be a concentration of sulfates near the surface due to deposition of sulfates from the evaporation of top soil moisture (Hewlett & Massazza 2003). Construction activities can disrupt deposits and expose sulfide minerals such as pyrite [FeS_2] to air, which can oxidize into sulfate minerals. Its rate of oxidation can be accelerated in high pH conditions such as those present in close proximity to hydrated Portland cement structures (Dyer 2014). Concentrations of sulfates in

groundwater also vary broadly and are a function of a number of factors including: the solubility of minerals present in the hosting soil, industrial effluent or fertilizer contamination, and the mobility of the groundwater. In North American alkali soils and other arid regions around the world, sulfate concentrations of 10 g/L or more are not uncommon (Hewlett & Massazza 2003).

There are also industrial wastes such as those from mining, coal combustion, other fossil fuel processing, and metallurgical processes that could leach out sulfates if exposed to groundwater or precipitation (Skalny et al. 2002). Industrial effluents and fertilizers that come in direct contact with concrete or are picked up by groundwater may contain ammonium sulfate $(\text{NH}_4)_2\text{SO}_4$ (Neville 1998; Mehta 1993). Exposure to sulfuric acid $[\text{H}_2\text{SO}_4]$ can also lead to a very aggressive combination of both sulfate and acid attack. There are industrial processes that either use or produce H_2SO_4 as a by-product. A big source of sulfuric acid is sulfur dioxide (SO_2) from the burning of fossil fuels that then oxidizes in the atmosphere and comes into contact with concrete via precipitation (Dyer 2014). Near urban areas, high acidity of rainwater and fogs has been reported with recorded pH readings of 2.5-3.5 which is in large part due to SO_2 (Mehta 1993). Another source of sulfate are sulfur-reducing and oxidizing bacteria present in various wastewaters and soils where there is decay of organic matter. The bacteria convert sulfur compounds into H_2S gas that oxidizes in the atmosphere to form sulfur. This sulfur is then taken in by the oxidizing bacteria and converted into H_2SO_4 (Dyer 2014; Mehta & Monteiro 2006).

1.2 Chemical Sulfate Attack

There are multiple reaction processes between sulfates and the hydrated cement paste that would classify as a chemical form of sulfate attack. Multiple overlapping mechanisms of chemical sulfate attack may be simultaneously occurring in a given case. The presence of either is subject to multiple factors that include: the type and concentration of sulfates, chemistry of hydrated cement, and the

exposure conditions of the structure. It is important to point out that although rooted in chemical reactions between sulfates and the hydrated cement phases, the deteriorative effects of chemical sulfate attack can be physical in nature. The observable effects of sulfate attack are sometimes said to stem from physiochemical reactions. The physical form of sulfate attack discussed later is differentiated from the chemical processes since it is based on stresses exerted by sulfate salt crystallization directly on the microstructure of the hydrated cement paste and aggregates. In that salt weathering process, the stresses are not stemming from reaction products deposited from any of the chemical forms of attack presented in the current section.

1.2.1 Ettringite and Gypsum

The formation of gypsum [$\text{CaSO}_4 \cdot 2\text{H}_2\text{O}$ or $\text{C}\bar{\text{S}}\text{H}_2$] and ettringite [$3\text{CaO} \cdot \text{Al}_2\text{O}_3 \cdot 3\text{CaSO}_4 \cdot 32\text{H}_2\text{O}$ or $\text{C}_6\bar{\text{A}}\bar{\text{S}}_3\text{H}_{32}$] formed from reactions between the sulfate ions and the hydrated cement phases are often referred to as the ‘traditional’ or ‘classic’ forms of sulfate attack.

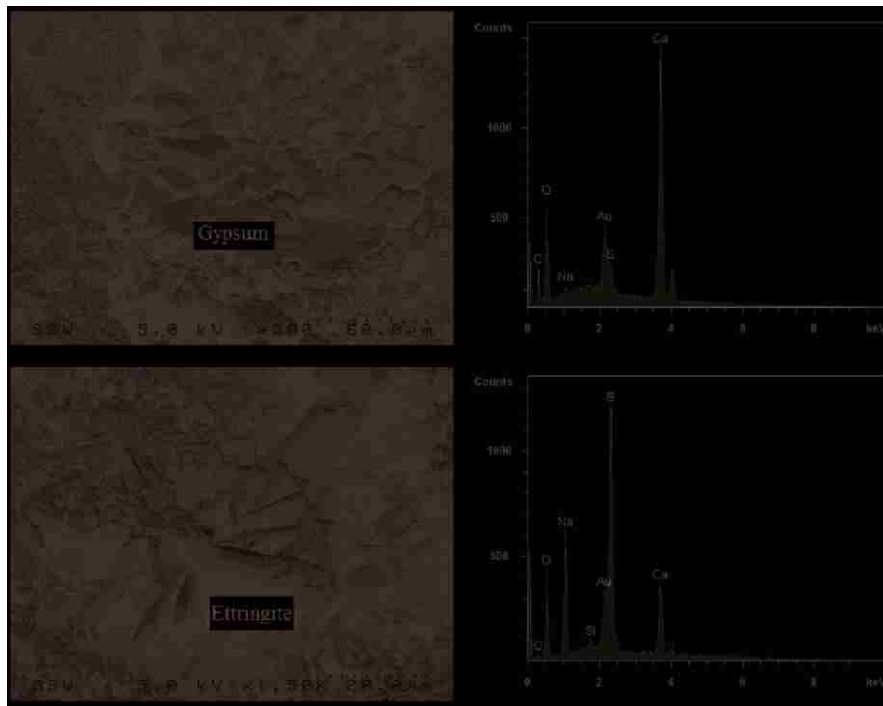
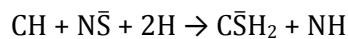


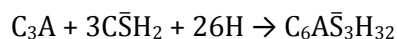
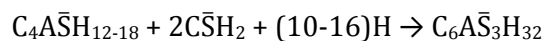
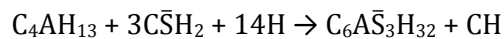
Figure 1-1: SEM and EDX Analyses of Gypsum and Ettringite, the Products of ‘Traditional’ Chemical Sulfate Attack (Nehdi et al. 2014)

A spectral electron microscopy (SEM) image and Energy Dispersive X-Ray (EDX) Spectroscopy analysis of each are presented in **Figure 1-1**. The sulfate ions target calcium hydroxide [Ca(OH)₂ or CH], any un-hydrated C₃A, and the alumina-bearing hydration phases of C₃A (Kosmatka & Wilson 2016; Cohen & Bentur 1988; Neville 1998). The targeted hydration products of C₃A are tetracalcium aluminate hydrates [4CaO*Al₂O₃*13H₂O or C₄AH₁₃] and calcium sulfoaluminate hydrate [3CaO*Al₂O₃*CaSO₄*12-18H₂O or C₄A \bar{S} H₁₂₋₁₈] also known as monosulfate. The latter mineral is one of the more common members of the AFm group of hydrated calcium sulfo-aluminates; the products of C₃A and C₄AF hydration (Winter 2012a). Ettringite is part of the AFt group of hydrated calcium sulfo-aluminates. The difference between both is that AFm phases contain one (mono-) SO₄ group and the AFt phases contain three SO₄ groups; the F stands for iron [Fe] which can partially replace the aluminum in these hydrated phases (Winter 2012a; Skalny et al. 2002). The reactions described next use sodium sulfate [Na₂SO₄ , N \bar{S}] as the source of [SO₄²⁻] ions and provide a good overview of the processes that generate sulfate attack gypsum and ettringite. During the first stage of reactions, the sulfate ions will separate from their cation, in this case Na⁺, and usually first target CH to produce gypsum.



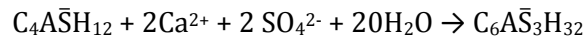
NH – NaOH, other cement chemistry notations of compounds can be found in Appendix B

Then usually gypsum supplies all of the calcium and sulfate ions needed to react with each C₃A phase to produce ettringite as the equations below show (Cohen & Bentur 1988).



Cement chemistry notations of compounds can be found in Appendix B

For monosulfate only, another possible route to produce ettringite from sulfate attack is that calcium (Ca^{2+}) ions are pulled directly from CH and in the presence of sulfate ions they jointly react with the AFm phase as indicated below (Dyer 2014).



The latter scenario occurs more frequently where potassium or sodium sulfate are the present sulfate source since they are relatively more soluble than gypsum (Richardson 2002). Once CH is depleted, calcium silicate hydrates [C-S-H] can also begin to slowly release calcium ions which will start a gradual decalcification of the C-S-H represented by a decline in the Ca/Si gel ratio (Dyer 2014). C-S-H is the main binding phase of concrete responsible for strength. When the accessible AFm phases are depleted, if there is a steady supply of sulfate ions, they will continue to react with calcium to form more gypsum. Gypsum deposition will continue until sulfate ions can permeate further into the concrete structure and access fresh AFm reserves either through the pore structure or through newly formed access from sulfate attack induced cracks. This conventional form of sulfate attack will continue producing ettringite and/or gypsum as long as there is a constant and steady supply of sulfate ions and removal of the sodium hydroxide [NaOH]. If NaOH or a similar alkali by-product of the reaction between the sulfate salts and hydrated cement paste accumulates, the reactions will reach an equilibrium dependent on the sulfate concentration (Neville 1998). In the case of a 5% sodium sulfate solution, approximately 1/3 of the $[\text{SO}_4^{2-}]$ ions will deposit as calcium sulfate when equilibrium is reached (Hewlett & Massazza 2003). In scenarios where there is flowing water high in sulfates that supplies fresh sulfates and removes the alkaline hydroxide ion (OH^-) binding by-products, the reactions can continue to completion which is why these exposure conditions are more deleterious to structures.

Having reviewed the chemical interactions between sulfate ions and the cement based hydrates, now the mechanisms through which ettringite and gypsum can deteriorate concrete will be discussed.

Concrete under this 'conventional' form of chemical sulfate attack is disrupted by expansive stresses induced by the formed gypsum and ettringite. These stresses are combined with a loss of strength and cohesion of the hydrated cement paste and its bond to aggregate due to depletion of CH and gradual decalcification of the C-S-H gel. The observable damage of the expansive stresses can be cracking, spalling, and delamination that characteristically starts at edges and corners of a structure and progresses throughout. The affected area can also become brittle, friable, and even soft due to the loss of strength and cohesion of the paste (Skalny et al. 2002; Neville 1998). There is debate as to the prevailing mechanisms of expansion and some researchers speculate that a combination of them could contribute to the overall volume changes associated with the sulfate attack products ettringite and gypsum.

The first of the prevailing theories of expansion is founded on the concept of topochemical reactions and directional crystal growth based on which the sulfate attack products take up a larger volume than their components (Mehta 1993; Neville 1998). Sulfate attack damage of concrete occurs when products exert deleterious pressures against the confining interspatial spaces of the hydrated cement paste phases and aggregate. A topochemical reaction is also described as a solid-state reaction, where the products of the reaction are formed on the solid surface of one its components. The products grow perpendicular to the surface of the solid phase through a solid-liquid interface. In this theory, sulfate and calcium ions from the dissolution of sulfate salts and CH react with the surface of the aluminate phase, which progressively dissolves and releases aluminate then used to form ettringite. Progressively, the aluminate phase is replaced with ettringite and since the oriented acicular crystalline structure and configuration of the ettringite formed is of larger volume than the aluminate phase that hosted it, there is an overall expansion effect (Neville 1998; Odler 1991). This approach is opposite to the concept of through-solution reaction, where the components go through a stage where they completely dissolve in solution and then precipitate to their product forms. A through-

solution reaction would not result in expansion of the system since movement of the newly formed products would be possible. On top of that, the ettringite formed from a purely chemical standpoint would result in a net chemical volume shrinkage (Mehta 1993). There is evidence that both topo-chemical and through-solution formation of ettringite take place, the latter of which does not cause expansion (Odler 1991). The predominance of the topo-chemical mechanism of ettringite formation has shown to directly correlate with the lime (CaO) saturation level of the liquid medium (Odler 1991). This is suspected to be the case because the topo-chemical reaction favors conditions where the dissolution rate of the alumina from the solid aluminate phase surface is lower compared to the supply of calcium and sulfate ions to it.

There is uncertainty as to the extent that gypsum formation might directly contribute to expansion. There is a hypothesis that gypsum will continue to form in the pore system of hydrated Portland cement and lead to expansion provided the pore solution continues to meet a certain supersaturation of calcium and sulfate ions (Odler 1991). Such expansion is also based on the topo-chemical and oriented crystal growth theory where gypsum crystals are precipitated from a sulfate saturated solution perpendicular to the crystalline CH surface (Skalny et al. 2002). Then again, the formation of gypsum in the presence of sulfates may just be a by-product of the dissolution of the CH and decalcification of C-S-H that leads to loss of strength and cohesion. Gypsum then simply serves as a convenient source of sulfate and calcium ions used in the ettringite forming reactions with the aluminate phases. This may be the prevalent role gypsum plays in the overall expansion associated with sulfate attack. For the pressures exerted by either mechanism of ettringite formation to cause volumetric expansion and cracking, the stiffness of the constraining system needs to be weaker. This is eventually the case with continuous precipitation of gypsum and decalcification of the C-S-H phase (Mehta 1993).

The second prevailing theory of sulfate attack expansion suggests that the ettringite phase experiences a swelling effect due to water adsorption. Osmotic forces are suspected to cause swelling of the microcrystalline ettringite formed from sulfate attack reactions that through this mechanism induces stresses against the hardened paste structure and causes expansion and cracking (Mehta 1993). Mehta and other researchers suggest that in a system saturated with sulfate, hydroxyl, and calcium ions, a poorly crystalline and colloidal type ettringite will form with particles around 1 μm long (Odler 1991). Ettringite crystals that are well-formed and observed in solutions absent of lime, have been measured to be around 4-6 μm or more and not reported to cause measurable expansion while those of the colloidal form do (Mehta 1973). Micrographs of ettringite formed with and without lime from that study are shown in **Figure 1-2**.

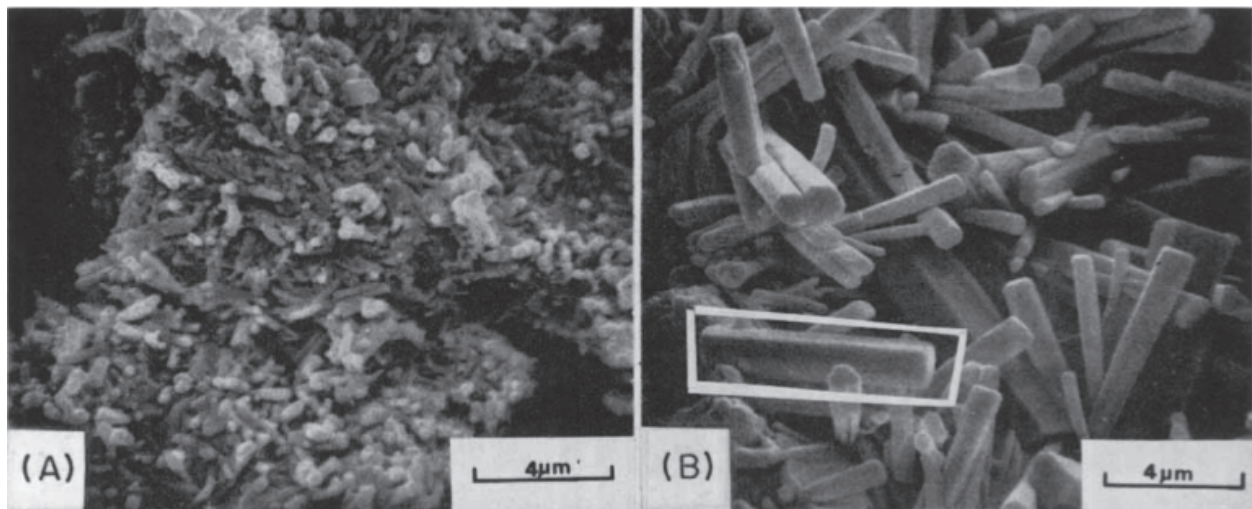


Figure 1-2: Micrographs of Paste Containing Gypsum and Calcium Sulfoaluminates hydrated with lime in (A) and without lime in (B) (Mehta 1973)

Sulfate expansion is attributed to the swelling of this poorly crystalline form of ettringite that adsorbs water due to its high surface area. Favorable conditions of the swelling theory also include a moist and permeable environment that can supply and accommodate movement of water. Interconnected capillary pores and cracks in the cement composite could provide such an environment and the

supply of ions needed to foster formation and swelling of this form of ettringite (Mehta 1993). In a test of cement pastes with 15% gypsum, as presented in **Figure 1-3**, the expansiveness of ettringite is significantly increased in samples that were cured in water versus ones cured in a sealed environment (Odler & Gasser 1988).

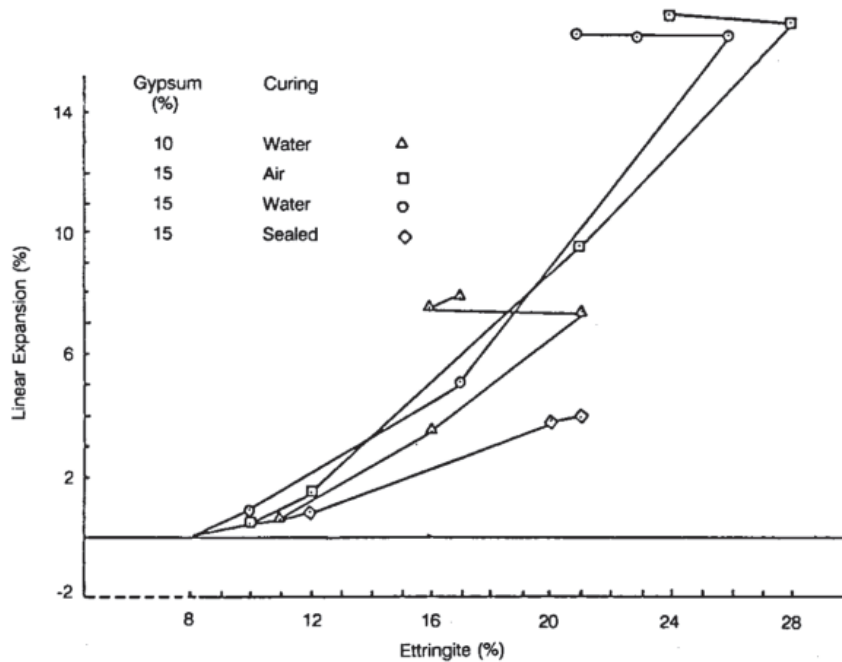
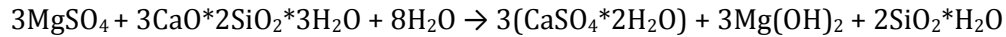


Figure 1-3: Expansion in Cement Pastes as a Function Of The Amount Of Ettringite Formed (Odler & Gasser 1988)

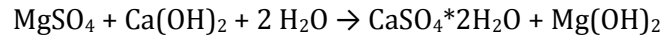
Nevertheless as the figure shows, some expansion was still observed with the sealed samples. The body of research suggests that it is possible both topo-chemical and oriented crystal growth and swelling mechanisms may act in parallel to contribute to the total expansion caused by ettringite (Mehta 1993; Neville 1998). This is supported by more evidence presented by Rosetti et al (Rosetti et al. 1982) that the swelling effect of ettringite alone is unable to explain the total expansion observed and an anisotropic growth of ettringite causing crystallization pressure must also be involved.

1.2.2 *Magnesium Sulfate*

In the presence of magnesium sulfate ($\text{MgSO}_4 \cdot 7\text{H}_2\text{O}$) there is an additional reaction between the Mg^{2+} cation and the hydrated cement paste that is not present in reactions with potassium, calcium, and sodium sulfates. For the latter group, the sulfate ions are the only agent that directly targets the hydrated cement phases as discussed in the previous section. What makes magnesium sulfate more aggressive is that it directly targets the C-S-H phase in parallel to the sulfate ion reactions that target CH and the aluminate phases discussed earlier (Neville 1998). The hydrated calcium silicates react with magnesium sulfate through the reaction below to form more gypsum, magnesium hydroxide ($\text{Mg}(\text{OH})_2$), and silica oxide gel (Mehta & Monteiro 2006; Hewlett & Massazza 2003).



The reaction between magnesium sulfate and CH that produces gypsum is summarized as:



Another reason why the degradation of the C-S-H phase is much faster than that observed with other sulfates is the very low solubility of $\text{Mg}(\text{OH})_2$ and its lower solution pH of 10.5 (Skalny et al. 2002; Neville 1998). As the surrounding solution saturates with respect to $\text{Mg}(\text{OH})_2$, the pH becomes too low to maintain the stability of the C-S-H phase, and the silicate hydrate phases start to liberate lime in the form of CH to establish equilibrium (Hewlett & Massazza 2003). This released CH is quickly also converted to $\text{Mg}(\text{OH})_2$, thus perpetuating the rapid decalcification and eventual degradation of the C-S-H phase (Skalny et al. 2002).

1.2.3 *Thaumasite Formation*

This form of chemical sulfate attack, also referred to directly as thaumasite sulfate attack (TSA), is more prevalent in colder climates since the formation of this mineral form is more conducive in temperatures below 15 °C (Dyer 2014). Thaumasite [$3\text{CaO} \cdot \text{SiO}_2 \cdot \text{CO}_2 \cdot \text{SO}_3 \cdot 15\text{H}_2\text{O}$] is described to be a needle-shaped crystal sulfate bearing mineral that is similar to ettringite, but the aluminate content

is replaced with a silica and some of the SiO_4^{2-} ions are swapped for calcium carbonate $[\text{CO}_3^{2-}]$ (Richardson 2002). A sample SEM and EDX analysis of this compound is shown in **Figure 1-4**.

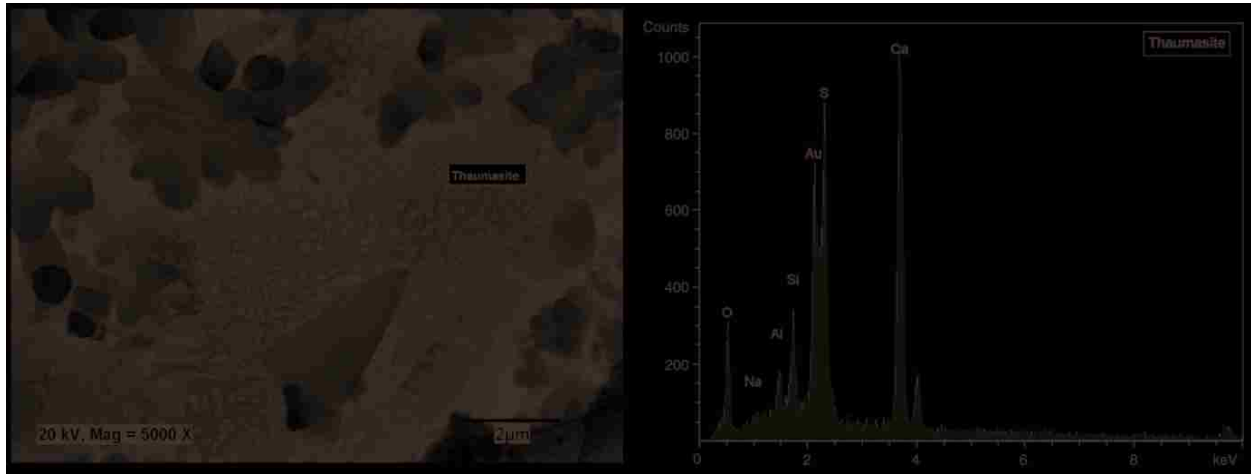
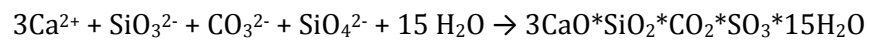
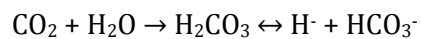


Figure 1-4: Example SEM and EDX of Thaumascite (Bassuoni & Nehdi 2009)

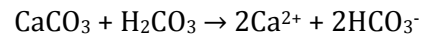
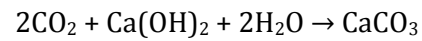
In the presence of sulfate and carbonate $[\text{CO}_3^{2-}]$ or bicarbonate ions $[\text{HCO}_3^-]$, calcium silicates from the C-S-H phase, and favorable temperature and pH conditions (less than 15 °C & >10.5 pH), thaumasite may form as represented by the following reaction:



The source of carbonate and bicarbonate ions are usually limestone aggregates, limestone filler in cement, and groundwater high in carbon dioxide. Carbon dioxide in groundwater can lead to carbonation of the CH phase, production of calcite $[\text{CaCO}_3]$, and dissolution of CaCO_3 into bicarbonate ions that can contribute to thaumasite formation (Collett et al. 2004). One path to the production of bicarbonate ions is through dissolving CO_2 in water that forms carbonic acid. The acid can directly dissociate into hydrogen and bicarbonate ions available for thaumasite formation:



Alternatively, the CO₂ can carbonate the CH phase of hydrated cement paste to form calcite. Then carbonic acid can help dissolve that calcite to get calcium and bicarbonate ions following the process below (Dyer 2014):



As previously mentioned earlier, the formation of thaumasite favors colder temperature with 5° C reported as most conducive to TSA (Skalny et al. 2002). The effects of TSA on concrete results in progressive decomposition of the C-S-H phase and its observable effects are significant softening and strength loss. Complete disintegration of the concrete resembles a soft and whitish mush (Dyer 2014). Examples of TSA are shown in **Figure 1-5**. Many field cases of TSA damage to slabs, tunnels, piles, and other foundation structures with nature of damage and probable causes are summarized by Rahman & Bassuoni (Rahman & Bassuoni 2014).



Figure 1-5: Example of Severe TSA Damage in Lab Samples (Rahman & Bassuoni 2014)

1.2.4 Delayed Ettringite Formation (DEF)

This form of sulfate attack is only present in cases where there is an internal source of sulfates such as gypsum. The addition of gypsum serves to control the early setting behavior of the C_3A and C_4AF phases and prevents an undesired premature stiffening of the paste referred to as a “flash set”. Gypsum reacts with the aluminate and ferrite phases to form a hydration retarding semipermeable layer of ettringite around them during those early stages of hydration and slows down their otherwise very fast rate of reaction (Brown & Taylor 1999). Once the gypsum supplied sulfate has been exhausted, the ettringite formed during this early hydration period converts to monosulfate (Dyer 2014). The cause of delayed ettringite formation (DEF) is due to the low decomposition temperature of ettringite, which is unstable at temperatures above 60-70 °C (Richardson 2002). When concrete experiences higher temperatures (>70 °C) during curing, which can be the case in steam-cured pre-cast units and large mass concrete pours where excessive heat from hydration can develop, ettringite does not form during curing (Richardson 2002). Instead, the sulfate is absorbed by the C-S-H phases and some forms into poorly crystalline monosulfate or syngenite $[K_2Ca(SO_4)_2 \cdot H_2O]$, and some stays in the pore fluid solution (Taylor 1997). Following this curing period in elevated temperatures, if the concrete is subsequently exposed to a moist condition, such as water or high humidity air, ettringite will reform and precipitate into large crystals. This ‘delayed’ ettringite then fills up pore spaces and aggregate-paste interfacial zones forming bands of the mineral that cause expansive stresses and subsequent map cracking similar to that of Alkali-Silica reaction (ASR). In fact, many cases of DEF also exhibit signs of ASR attack since the occurrence of the latter in many field cases has been reported to precede DEF. The presence of alkali susceptible aggregate has proven to magnify the effects of DEF possible by ASR initiating the micro cracks which are then filled and further expanded by the precipitated ettringite (Taylor 1997). Examples of DEF and a back-scattered electron (BSE) microscopy image showing the telltale accumulation of ettringite around aggregate are presented in **Figure 1-6** and **Figure 1-7**.



Figure 1-6: Effect of Combined ASR and DEF on Precast Beam (Skalny et al. 2002)

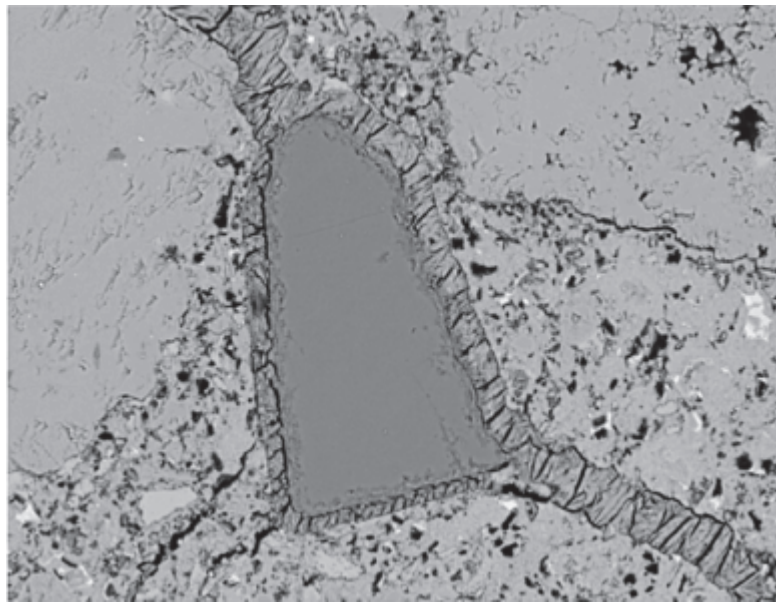


Figure 1-7: BSE Image of Aggregate Particle with Surrounding Ettringite-filled Gap (Thomas et al. 2008)

1.3 Physical Sulfate Attack (PSA)

Physical sulfate attack (PSA), also referred to as salt weathering and salt hydration distress, is a physical erosion mechanism that can affect concrete much in the same way it can affect natural rock formations of porous rock such as limestone (Kosmatka & Wilson 2016; Haynes & Bassuoni 2011). It

gained more focused attention after the mid-90s prior to which it was commonly misidentified as chemical sulfate attack (Haynes et al. 1996). The stress inducing mechanism is the crystallization of the salt itself and not an expansive product of chemical reactions between the sulfate salt and any of the hydrated cement phases. That is what differentiates physical sulfate attack from the multiple chemical forms of sulfate attack discussed earlier. The salt's fluctuation between its hydrous and anhydrous form is associated with a volumetric change between the two states that can fatigue and wear down concrete or other porous rock. This phenomena is analogous to the deteriorative freeze-thaw effects of water. The presence of salt weathering does not rule out the presence of any chemical form of sulfate attack that is likely concurrently happening (Skalny et al. 2002). In many exposure conditions, both forms of sulfate attack are contributing to the overall rate of a concrete structure's deterioration due to the all-encompassing sulfate attack. In high-sulfate environments where concrete is exposed to wetting and drying cycles, the damage from this form of sulfate attack might be more significant than the chemical form (Skalny et al. 2002). Physical sulfate attack is a point of interest since sodium sulfate is among the most aggressive salts known to weather concrete (Haynes et al. 1996). The *ACI Guide to Durable Concrete* recognizes that groundwater containing sodium sulfate, sodium carbonate, sodium chloride, and sea water are common causes of this form of salt weathering (ACI Committee 201 2008).

PSA commonly occurs at an area designated as the evaporative front. This is the point where the dissolved sulfate ions in solution have permeated through the afflicted concrete by capillary suction, absorption, ionic diffusion, or any other mechanism of transport and reached the point where the solution is evaporating. The solution will supersaturate with respect to the particular ionic species and the salt will crystallize (Skalny et al. 2002; Haynes & Bassuoni 2011). If the evaporative front is at the surface of the concrete, which happens if the supply of salt solution through the material is higher than the rate of evaporation, the sulfate salts crystallize outside the material and form

efflorescence that is mostly harmless and not believed to cause mechanical damage (Binda & Baronio 1987). If the transport rate of salt solution through the material is less than that of evaporation at the exposed face, the evaporative front would move into the material and form subflorescence which can cause mechanical damage (Binda & Baronio 1987; Haynes & Bassuoni 2011).

The distress mechanism of PSA based on sodium sulfate stems from this salt's cyclic phase transformation between its anhydrous form thenardite [Na_2SO_4] and its hydrous form mirabilite [$\text{Na}_2\text{SO}_4 \cdot 10\text{H}_2\text{O}$]. The hydration transformation of this salt results in a volume expansion of about 314% (Tsui et al. 2003). This transition has been shown to occur through a rapid dissolution and precipitation of mirabilite (Rodriguez-Navarro & Doehne 1999). The expansive hoop stresses that this phase transition generates can range anywhere from 10 to 20 MPa (1450-2900 psi), well in excess of the tensile strength of most stones and concrete (Flatt 2002). The damage mechanism relies on cycles of impregnation and drying that accumulate a threshold level of thenardite at the subsurface evaporative front. When water fills this now thenardite rich area, dissolution of the thenardite creates a solution supersaturated in respect to mirabilite. At that point, mirabilite precipitates and causes the destructive expansive stresses at this precipitation front (Tsui et al. 2003). What initiates the phase changes of thenardite to mirabilite are fluctuations of the ambient temperature and relative humidity of the environment. Refer to the phase diagram of sodium sulfate in **Figure 1-8**. At lower levels of humidity and higher temperatures, thenardite is the stable phase of sodium sulfate. At lower temperatures and higher humidity, mirabilite is the stable phase. If sufficient thenardite is present to saturate a solution at a higher temperature such as 40°C and then the temperature drops to 20°C, the solution will become supersaturated with respect to mirabilite and will precipitate the hydrous crystal resulting in the associated hoop stresses.

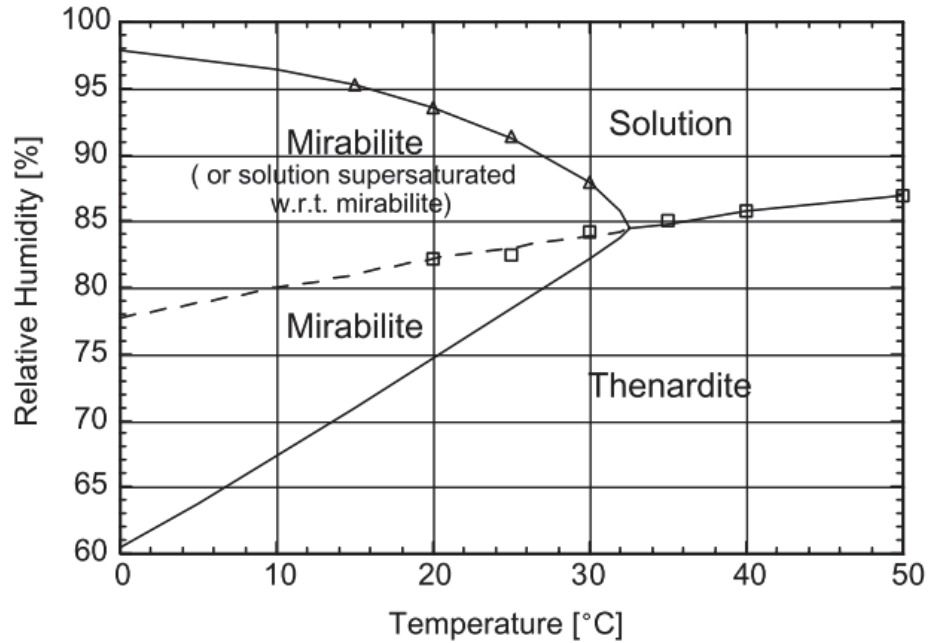


Figure 1-8: Phase diagram of Sodium Sulfate (Flatt 2002)

Damage due to physical sulfate attack is scaling primarily along the exterior above the soil or water line. The exposed concrete foundation slab in **Figure 1-9** exhibits distinctive scaling due to PSA. Factors that influence the degree of PSA are the supply rate and concentration of the sulfate solution, location of the evaporative front, the concrete pore size distribution, and its tensile strength (Haynes & Bassuoni 2011). There is also some theoretical correlation between higher crystallization pressures in smaller nanometric pores under full saturation conditions, although stresses of similar magnitude can also develop in larger pores in partially saturated conditions (Scherer 2004).



Figure 1-9: Scaling of Concrete Foundation Slab due to Physical Sulfate Attack (Haynes et al. 1996)

1.4 Effects of Cement Composition on Sulfate Attack

Some of the cement composition properties listed here are shown to have an effect on the performance of concrete against sulfate attack.

1.4.1 Tricalcium Aluminate (C_3A) Content

From extensive field and laboratory studies started in the early 1930s, some of which were conducted in California by the Portland Cement Association (Verbeck 1967; McMillan et al. 1949) and others in Florida by the US Army Corps of Engineers (Mather 1967), a direct correlation was identified between C_3A and the sulfate resistance of concrete. In the Portland Cement Association study, various types of cement, tested with difference cement contents and water-cement ratios indicated that higher C_3A content experienced a faster rate of deterioration, refer to **Figure 1-10** (McMillan et al. 1949). As discussed in 1.2.1 Ettringite and Gypsum, the hydrated phases of C_3A such as monosulfate are integral to the formation of ettringite in the presence of sulfates.

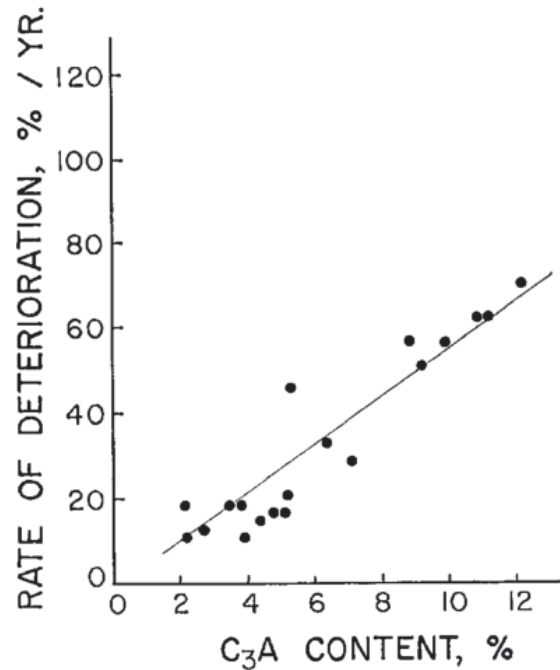


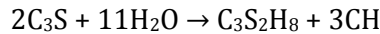
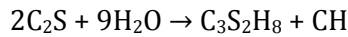
Figure 1-10: Link between C₃A of Cements and Rate of Deterioration (Verbeck 1967)

Studies like these in the 1920s and 1930s led to the development of sulfate resistant cements such as ASTM C 150 Type V (ASTM-C150 2007) that are alumina-poor [C₃A] and ferrite [C₄AF] rich (Skalny et al. 2002). The ASTM Type V cement limits the cement C₃A content to within 5% and limits the sum of C₄AF and twice the C₃A to 25% (ASTM-C150 2007). Modern day understanding is that the relationship is not as straight forward. The alumina in cement that has remained bound in ettringite form after hydration does not typically participate in sulfate attack unless the alkalinity drops below the mineral's stable pH of 10-11 (Dyer 2014; Skalny et al. 2002).

1.4.2 Tricalcium Silicate (C₃S) to Dicalcium Silicate (C₂S) Ratio

There is a correlation that a higher cement C₃S/C₂S ratio can make a cement more susceptible to sulfate attack because increasing the C₃S content results in more CH formed during hydration (Shanahan & Zayed 2007; Dyer 2014). Calcium hydroxide is the first phase targeted by sulfates for the formation of gypsum and serves as a ready source of calcium ions for ettringite. Based on the

products of hydration for both silicate phases, C_3S produces more than twice the CH that C_2S does (Neville 1998). The stoichiometric equations presented below assuming $C_3S_2H_8$ is the product C-S-H phase illustrate that point (Kosmatka & Wilson 2016).



A solution highly saturated with lime [CaO] can enhance the formation of microcrystalline type ettringite which is more capable of crystalline swelling due to the water imbibition theory (Mehta 1973; Mehta 1983). The lime saturated solution may also limit the solubility of the aluminate phase which better facilitates the topo-chemical mechanisms of ettringite formation from the surface of the aluminate phase (Mehta 1973; Mehta 1983). In a study of mortars of similar C_3A content tested for expansion under 5% sodium sulfate, the 1 year expansion for mortars made with a cement C_3S/C_2S ratio of 4.5 was 0.981%. That of the cement with a C_3S/C_2S ratio of 2.2 was 0.209% (Shanahan & Zayed 2007).

1.4.3 Mineral Admixtures

Mineral admixtures can be paired successfully with Portland cements (PC) to increase the sulfate resistance of concretes and mortars (Dyer 2014). Use of fly ash, ground granulated blast-furnace slag (GGBFS), silica fume, and other artificial or natural cementitious or pozzolanic admixtures is an American Concrete Institute (ACI) recognized strategy for designing concrete mixtures with resistance against sulfate attack (ACI Committee 201 2008). Mitigating sulfate attack is a combination of retarding the ingress and movement of water while selecting ingredients that would disrupt the reactions associated with sulfate attack (ACI Committee 201 2008). Reducing the C_3A content alone might in some cases be insufficient since the hydrated phases CH and C-S-H are still susceptible to calcium leaching that can lead to loss of strength and cohesion without the occurrence of expansion (Neville 1998). Coal burning power plants and metallurgical furnaces producing iron, silicon metals,

and ferrosilicon alloys have become major sources of these mineral admixtures that would have otherwise been sent to landfills as a waste by-product (Mehta & Monteiro 2006). A few of these mineral admixtures are briefly discussed.

Fly ash is a mostly silicate glass that forms from the condensation of molten coal ash collected from the exhaust gases at coal-fired power stations (Neville 1998). It is composed of spherical particles mostly less than 1 to 100 μm , with an average diameter reported as 20 μm (Mehta & Monteiro 2006). There is a high-calcium form of fly ash classified by ASTM C 618 as Class C, that has a lime $[\text{CaO}]$ content from 10% to more than 30% (Kosmatka & Wilson 2016). Class C fly ash is considered partially cementitious due to the reactive calcium content present in its composition generally in the forms of tricalcium aluminate $[\text{C}_3\text{A}]$, anhydrite $[\text{C}\bar{\text{S}}]$, and tetracalcium trialuminosulfate $[\text{C}_4\text{A}_3\bar{\text{S}}]$ (Mehta & Monteiro 2006). There is also a low-calcium fly ash, designated as Class F by ASTM C 618, that is mostly siliceous. Class C fly ash when in conformance to ASTM C 618 has at least 50% of combined content of silicon $[\text{SiO}_2]$, aluminum $[\text{Al}_2\text{O}_3]$, and ferric oxide $[\text{Fe}_2\text{O}_3]$. For Class F fly ash, that requirement is at least 70% (Kosmatka & Wilson 2016). The beneficial aspect of this mineral admixture is the pozzolanic effect it has on the hydrated cement paste. The silica reacts with the CH phase of the hydrated cement to form secondary C-S-H that binds up the calcium ions and makes them harder for sulfates to extract except where MgSO_4 or acidic conditions are encountered (Wee et al. 2000). Only class F fly ash is recommended for sulfate resistance as the high-calcium Class C variety will serve as another source of calcium ions for reaction in the presence of sulfate ions. As reported in comparison studies, use of high-calcium fly ash can lead to more expansion than that observed with cement only samples (Ferraris et al. 2006). Low-calcium fly ash addition will also reduce the permeability of the paste due to its fine sized particles acting as a filler and the formation of secondary C-S-H that will have a void filling effect (Dyer 2014). The total CH available in the matrix will also be reduced by replacing the cement used in the mixtures, as fly ash is typically used to

replace 25-35% of the cement by mass (ACI Committee 201 2008). There is also evidence that pozzolanic reactions facilitate more alumina to be absorbed in the C-S-H phase, therefore reducing its availability for ettringite formation (Dyer 2014).

GGBFS is another by-product of smelting iron ore for metal (Dyer 2014). Limestone is added in the furnace to remove silicon, magnesium, and aluminum impurities in the ore. Then the formed slag is rapidly cooled to form glass granules that when ground to a powder of 400 to 500 m²/kg Blaine fineness exhibit good cementitious and pozzolanic properties (Mehta & Monteiro 2006). The behavior of GGBFS is similar to high-calcium fly ash, although the former has been in concrete application much longer. Higher levels of cement replacement and using GGBFS with low Al₂O₃ content has shown to be more effective at mitigating sulfate attack since the total aluminates and CH available for reaction are reduced through dilution (Dyer 2014). GGBFS is also usually of finer particle size than the cement it is paired with. Therefore, it serves as a filler and refines the grain size of the hydrate phases which helps reduce the sulfate ingress permeability of concrete (Dyer 2014).

Silica fume is also a very effective mineral admixture. It is also a pozzolanic type mineral admixture but more reactive than fly ash or GGBFS due to its finer size. It consumes the CH phase to produce secondary C-S-H which strengthens and densifies the paste. The effects of using silica fume on durability and the sulfate resistance of concrete are discussed in the next chapter.

1.5 Effects of Permeability on Sulfate Attack

So far, only the effects of the cement chemistry on sulfate attack have been discussed. The following are properties that affect the permeability of the hardened cement paste. Preventing the ingress of sulfate ions into the hydrated cementitious matrix is of significant importance. Even sulfate resistant cement that is chemically resistant to reactions with the sulfate ions can be subject to deterioration

after a sufficiently long period of exposure, or at the hands of magnesium sulfate, and the salt weathering effect some of the sulfate minerals are capable of (Skalny et al. 2002). The durability of concrete is significantly influenced by the permeability of its pore structure.

1.5.1 Water-to-Cement Ratio (w/c)

The water-to-cement (w/c) ratio (or water-to-binder ratio) of a mix design is one of the most influential factors on the total porosity and pore size distribution (Skalny et al. 2002). Through his research, T. C. Powers (Powers 1958) demonstrated a strong correlation between increasing the w/c and an increase in the total porosity as shown in **Figure 1-11**. As the curve shows, there are exponential increases in the permeability at w/c above 0.45-0.50. The reduction in total porosity and pore size refinement effects due to reducing the w/c is evident in **Figure 1-12** from a mercury porosimetry study on hardened cement pastes (Cook & Hover 1999).

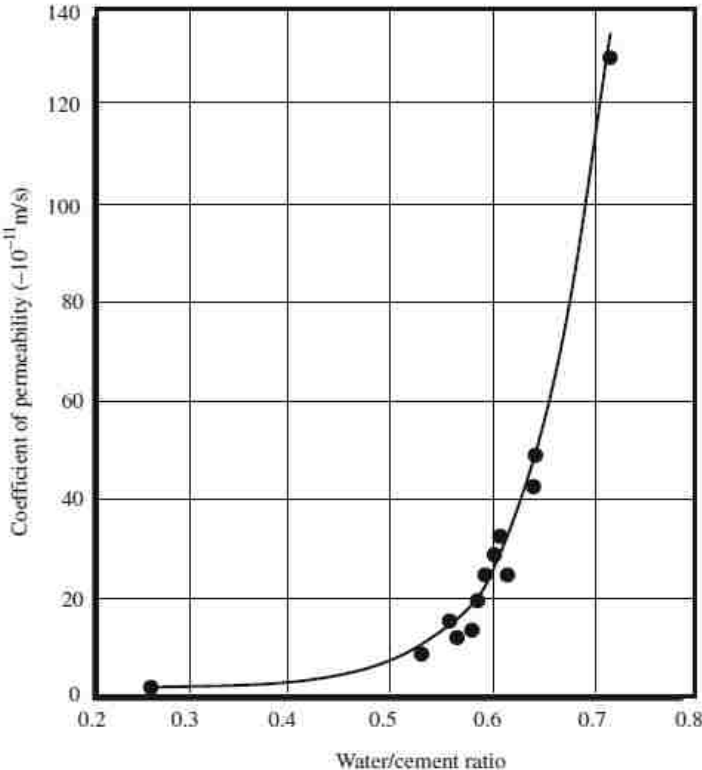


Figure 1-11: Correlation between Permeability and w/c for matured cement paste (Powers 1958)

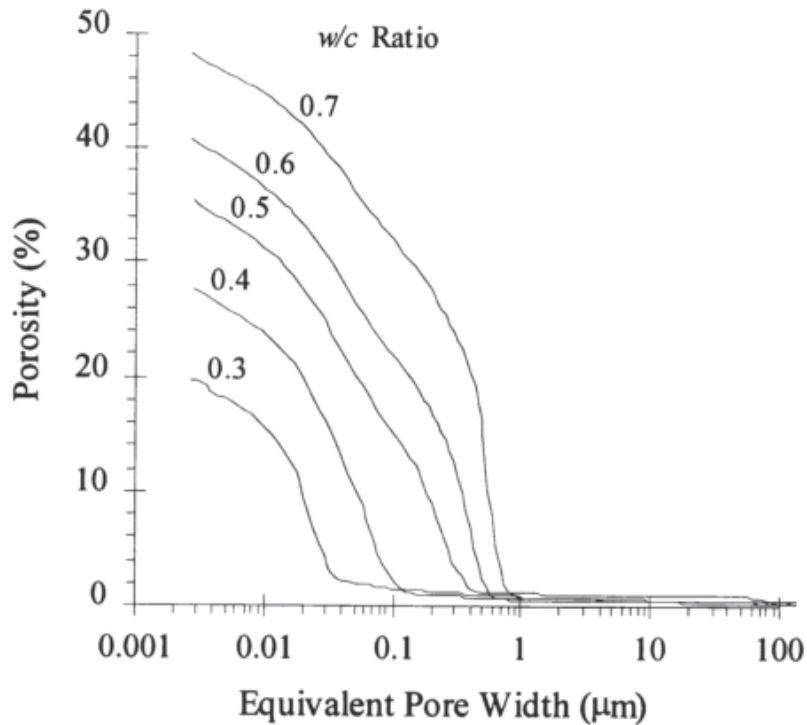


Figure 1-12: Effects of w/c on MIP of Cement Pastes Cured for 7 Days (Cook & Hover 1999)

The total volume of pores and their interconnectivity affects the permeability of the pore system to sulfate ions or any other deleterious agents in a penetrating solution (Skalny et al. 2002). A low w/c reduces the diffusivity of sulfate ions through the matrix and at a minimum will slow the rate of sulfate attack. A reduced w/c also correlates with an increase in compressive strength making the cement matrix more resistant to expansive stresses (Dyer 2014). The ACI Guide to Durable concrete reduces the maximum recommended w/c depending on the severity of sulfate exposure from 0.50 for class 1 exposure (>150 and < 1500 ppm SO₄ in water) to 0.40 for class 3 exposure (10,000 ppm SO₄ in water or greater) (ACI Committee 201 2008).

1.5.2 Cement Fineness

The effects of cement fineness are primarily on high early strength (Kosmatka & Wilson 2016). Over the years, cement manufacturers have been generally increasing fineness of all cement types to

increase early strength (Skalny et al. 2002). Increasing the fineness of the cement increases the reactive area of the cement particles during hydration and results in a grain refinement effect (Mehta & Monteiro 2006). This makes these cements more capable of binding free ions such as chloride and sulfate in large part due to the reactive nature of aluminates (Richardson 2002). Increasing the fineness of the cement exposes a larger portion of the C₃A phase that can react with sulfates and result in increased expansion (Odler 1991). Cement fineness has also been also correlated to increased expansion due to delayed ettringite formation in samples cured at 90 °C (Kelham 1996).

2 NANOSILICA

The concrete industry has widely adopted the use of chemical and mineral admixtures in concrete design. Balancing performance and cost, controlling application specific properties, increasing durability, increasing sustainability, lowering maintenance costs, and extending the service life of structures are among the many growing demands of modern day concrete designs (Skalny et al. 2002). This has resulted in chemical and mineral admixtures having an ever growing role in developing quality concrete that can perform well. Concrete, being a composite material, there is general agreement that its microstructure properties affect its bulk properties and performance. This is why developing advanced new materials and admixtures that can positively and economically alter the microstructure of concrete to achieve performance goals has been the latest frontier in concrete design. Over the last few decades, nanotechnology, or the manipulation matter at the nanoscale level, has led to revolutions in physics, chemistry, biology, and other industries where new materials and techniques have been discovered (Sanchez & Sobolev 2010). An influx of novel and commercially available nanomaterials has led to a renewed research effort in testing their application in concrete and understanding how their manipulation of concrete at the nanoscale level can alter the bulk properties as a whole (Singh et al. 2013). There is compelling evidence that ultra-fine particles, such as nanosilica, can improve both the plastic and hardened properties of concrete. Nanosilica (nS) can be described as a synthesized high-purity, highly reactive siliceous pozzolan nanoparticle admixture (Campillo et al. 2004; Quercia & Brouwers 2010). Exploring its effects on sulfate resistance with mortars has been the central objective in this study.

2.1 Pozzolans

Nanosilica, due to its ultra-fine particle size and high silica (SiO_2) purity, can be classified as a highly reactive siliceous pozzolan. Pozzolanic materials encompass a broad group of natural or artificial materials that exhibit pozzolanic activity. Pozzolans are either silicious or aluminosilicious

materials that alone exhibit little to no cementitious behavior, but when in the presence of moisture and calcium hydroxide (CH) in a finely divided form, they will react with CH to form additional stable calcium silicate hydrate (C-S-H) phases that possess cementitious properties (Neville 1998). This makes pozzolans a desirable material because they can take the CH phase, that otherwise has no cementitious value to the matrix besides maintaining a high pH that keeps the C-S-H phase stable, and react with it to form additional “glue” binder that strengthens the paste and reduces its permeability (Kosmatka & Wilson 2016). The reactive alumina, if present, will react to form various calcium-aluminate phases similar to the alumina phases (C_3A and C_4AF) native to the cement. Those reactions are concurrently happening but are outside the focus of this discussion.

In Section 1.2 on chemical sulfate attack, it was made clear that CH is the primary hydrated phase targeted by sulfates, so converting as much of it into secondary C-S-H via a pozzolan is an effective strategy for increasing the sulfate resistance of the cementitious matrix. Overall, there are three main advantages of using a pozzolanic material in concrete stemming from the nature and products of the pozzolanic reaction (Mehta & Monteiro 2006). Pozzolanic reactions are slower than hydraulic ones, so mixtures with a high pozzolan content liberate heat of hydration slower (Mehta & Monteiro 2006). This could be beneficial if developing excessive internal temperatures due to hydration in mass concrete pours or high temperatures developed during hot weather pouring are concerns. If temperatures develop that prevent ettringite from precipitating during the initial stages of hydration, it could result in the delayed ettringite formation (DEF) form of sulfate attack. The second benefit is the consumption of CH during the pozzolanic reactions, the benefits of which are not only with sulfate resistance, but overall reductions of susceptibility to aggressive ions and acidic conditions. The third benefit is the increases in strength and reduced permeability due to deposition of secondary C-S-H. In terms of sulfate attack, increasing the compressive strength of the cement paste makes it more resistant to expansive stresses from the product sulfate attack compounds. The secondary C-S-H

precipitated from the pozzolanic reactions and reduces permeability by filling up the voids, which refine the pore size distribution and make the pore system more impermeable to sulfate ingress (Mehta & Monteiro 2006).

2.2 Silica Fume (Microsilica)

Nanosilica is commonly compared to silica fume in many of the studies discussed in the literature review later in this chapter due to their inherent similarities. At first glance, both on a chemical level are purely siliceous pozzolans. Both are silicon dioxide (SiO_2) presented in a spherical reactive non-crystalline form. The main differentiating factor between both is their fineness and the associated specific surface area (SSA). Nanosilica is generally composed of spherical particles less than 100 nm and a nitrogen absorption measured surface area that often exceeds $80 \text{ m}^2/\text{g}$ (Campillo et al. 2004). Silica fume is composed of particles generally smaller than $1.0 \mu\text{m}$ in diameter with an average particle size (APS) of $0.1 \mu\text{m}$ or less (Kosmatka & Wilson 2016; Holland 2005; ACI Committee 234 2006). Since silica fume particles mostly span the microscale range, this pozzolan is also referred to as microsilica (mS) which is the predominant nomenclature used in this study. Most silica fume has a measured surface area of about $20 \text{ m}^2/\text{g}$ via the nitrogen absorption method (Kosmatka & Wilson 2016) which ranks it among the highly active pozzolan admixtures (Mehta & Monteiro 2006).

Microsilica is an industrial by-product of electric-arc furnaces used to produce silicon metals and ferrosilicon alloys from high-purity quartz and coal (Neville 1998; Kosmatka & Wilson 2016). Hot gaseous SiO leaving the furnaces, oxidizes into SiO_2 and as it cools it condenses into the distinctive ultra-fine amorphous silica particles that are then collected in bag filters. In that amorphous glass form and fineness, the SiO_2 particles are very active in an environment conducive to pozzolanic reactions.

Silica fume deemed suitable for use in cementitious mixtures as a pozzolan material needs to meet ASTM C 1240 (AASHTO M 307) standards where recognized. Commercially it is available as an undensified powder, a water based slurry, or in a densified/compacted powder form (Kosmatka & Wilson 2016). Certain cement manufacturers also offer blended cements where silica fume could constitute 7-12% of the binder content (ACI Committee 234 2006). Silica fume collected from electric-arc furnaces that manufacture silicon metal usually features a SiO₂ content above 90% by mass and 99% percent purity is not unheard of (Kosmatka & Wilson 2016). For silica fume collected from electric-arc furnaces that manufacture ferrosilicon alloys, the silica content directly correlates with the amount of silicon in the alloy produced and if the alloy produced contains only 50% silicon, the by-product silica fume will likely not meet the 85% minimum requirement by ASTM C 1240 (Kosmatka & Wilson 2016).

2.2.1 Historical Background

Silica fume has been around a lot longer than nanosilica. It was first collected for testing in 1947 in Kristiansand, Norway. Most of the research on silica fume and its properties was done in Nordic countries and its first structural application was also in Norway in 1971 (Kosmatka & Wilson 2016). Improvements in strength and observed durability against sulfate exposure comparable to sulfate-resisting cement mixtures were among the first identified benefits of silica fume from the testing done in the 1950s (Hewlett & Massazza 2003). The US Army Corps of Engineers first opted to use silica fume for repairing the Kinzua Dam in Pennsylvania due to its high abrasion resistance (Kosmatka & Wilson 2016).

2.2.2 Microsilica Effects on Fresh & Rheological Properties

2.2.2.1 Water Demand and Workability

Adding silica fume to a mixture, due to its large SSA, significantly increases the internal surface area of the mixture which increases its cohesiveness (Hewlett & Massazza 2003). This “stickiness” of the

mixture typically requires an increase of the slump to maintain favorable workability via use of chemical admixture. The high surface area of the pozzolan causes an increase in water demand. When the fresh mixture is agitated, vibrated, pumped, or worked in any way, the spherical mS particles will lubricate the cement paste and aggregate, imbuing the mixture with greater mobility than cement only concrete of comparable slump (Hewlett & Massazza 2003).

2.2.2.2 Bleeding and Segregation

Bleeding is significantly reduced with the addition of mS. Concrete mixtures with 5-10% silica fume and a water-to-cement ratio less than 0.50 may not bleed at all (Kosmatka & Wilson 2016). The placing, finishing, and curing practices for mixtures containing silica fume need stricter control to protect the concrete from drying since the lack of bleed water means there is an increased risk of plastic shrinkage cracking. The reduction in bleed water may allow finishing of flatwork to commence sooner (Hewlett & Massazza 2003; Kosmatka & Wilson 2016).

2.2.2.3 Setting Time

Since pozzolanic reactions take longer than those of ordinary Portland cement and depend on the CH released from setting of the paste to commence, the setting time of mixtures containing microsilica can theoretically increase (Hewlett & Massazza 2003). That, however, has not been observed for the generally smaller 5-10% dosages of mS used in practice (Kosmatka & Wilson 2016). In testing on concrete mixtures containing 20% mS, an increase in setting time of 6-20% was recorded (Siddique & Khan 2011).

2.2.2.4 Heat of Hydration

The heat of hydration that mS contributes could be equal to or greater than that of Portland cement depending on its dosage and surface area (Kosmatka & Wilson 2016). A mixture containing mS

designed for the same compressive strength at 28 days as one designed only with cement, would develop less heat of hydration than the latter. Microsilica can accelerate the hydration of ordinary Portland cement phases C_3S , C_2S , and C_4AF due to its high surface area and pozzolanic reactivity (Siddique & Khan 2011; Kurdowski & Nocuń-Wczelik 1983). In the presence of CH, mS starts dissolving to create a condition where there is a supersaturation of silica in respect to a silica-rich phase that starts forming at the surface of the mS particles. At that point, the partially dissolved mS particles all serve as new topochemical precipitation sites for more C-S-H which accelerates hydration at all stages (Siddique & Khan 2011).

2.2.3 Microsilica Effects on Hardened Properties

Microsilica will increase the strength of cementitious mixtures, the degree of which depends on the type of mix, cement type, dose of mS, use of water reducing admixture, and the specific aggregate and curing methods used (Hewlett & Massazza 2003). Due to its fineness, large surface area, and highly reactive amorphous nature, mS can contribute to the compressive strength early on as well (Kosmatka & Wilson 2016). Given that good placement and curing practices are followed, the strength gains of adding mS can be seen within the period of 3 to 28 days in cured samples (Kosmatka & Wilson 2016). Concrete mixtures containing mS support the conventional relation between water-to-cement ratio (w/c) and strength but the curve shifts right towards higher compressive strengths for a given w/c as shown in **Figure 2-1**. Cementitious mixtures containing mS also see improvements in tensile and flexure strength relatively proportional to those seen for compressive strength (Hewlett & Massazza 2003).

High strength mS contained concrete has shown to improve abrasion and impact resistance of concrete and has been adopted for many such applications including the repair work at dams and channels (Hewlett & Massazza 2003). In Norway, high strength (95 MPa) mS concrete has become

the preferred paving material for high wear surfaces and has reduced the wear on roads where installed by a factor of 5-10 in comparison to high-quality black-top (Hewlett & Massazza 2003).

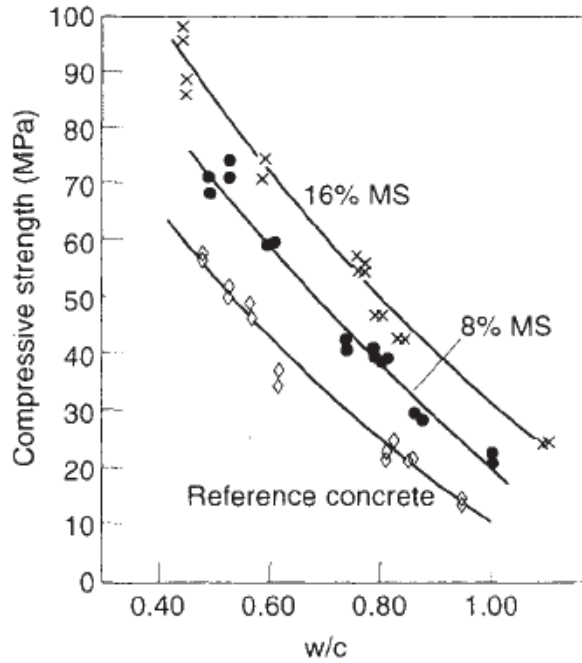


Figure 2-1: Effects of Microsilica (MS) on Strength to (w/c) Ratio Curve (Hewlett & Massazza 2003)

2.2.4 Microsilica on Durability and Sulfate Resistance

The way mS affects the hardened and durability characteristics of cementitious composites is based on its physical effects on the microstructure of the paste and its chemical effects as a pozzolan.

2.2.4.1 Physical Effects of Microsilica

By reducing bleeding of mix water due to its ultra-fine particles and high surface area, mS prevents segregation and pockets of bleedwater from forming under coarse aggregate and rebar which can become weak spots and reduce bonding (ACI Committee 234 2006). As discussed in its effects on heat of hydration, due to its fine particle size, mS provides nucleation sites where the hydrated cement phases and secondary C-S-H can precipitate. This densifies the hardened cement paste and

accelerates hydration (ACI Committee 234 2006). This effect is not unique to mS, but has shown to occur in other testing where inert ultra-fine fillers such as CaCO_3 produced a similar effect. Microsilica improves the particle packing of hardened concrete by occupying the spaces in between cement grains, not unlike how cement grains occupy the spaces between the fine aggregate, and the fine aggregate occupies the spaces between the coarse aggregate (ACI Committee 234 2006). This particle packing effect requires that the surface forces of particles, which increase as particle fineness enters the macro and nano-range, are reduced by a sufficient dose of water reducing admixture (ACI Committee 234 2006). This phenomenon has been proven in testing of mixtures with 5% or less mS cement replacement by observing a measurable reduction in water demand due to mS occupying the space between the cement particles which would have otherwise been filled with water (Bache 1981). The primary physical effect of mS on the microstructure of hardened paste is its densification and porosity reduction at the cement paste-aggregate transition zone also referred to as the interfacial transition zone (ITZ) since it also applies for other wall and barrier conditions (ACI Committee 234 2006). The ITZ is a zone approximately 50 μm that forms between the cement paste and boundary conditions, such as the aggregate. This zone is generally weaker in strength, shown to be more porous, and exhibits poorer particle packing than that of the bulk cement paste (ACI Committee 234 2006). More of the CH phase precipitates in this region and it tends to precipitate in larger crystals that are characteristically oriented parallel to the aggregate surface as shown in **Figure 2-2**. The effects of mS are apparent in the mS contained mixture also shown in the same figure. Without mS, the large CH phase crystals that precipitate in the ITZ do not contribute much to strength and create a weak zone since they are easily cleaved (Monteiro et al. 1985). Multiple researchers have proven that mS can densify the ITZ to a state of similar strength, permeability, and porosity to that of the bulk paste and essentially eliminate its role as the weaker link (ACI Committee 234 2006). Durability of the cementitious composite is also significantly improved through the densification of

the ITZ since the more porous structure of the ITZ significantly contributes to the total ionic diffusivity and fluid permeability of the cement-aggregate matrix.

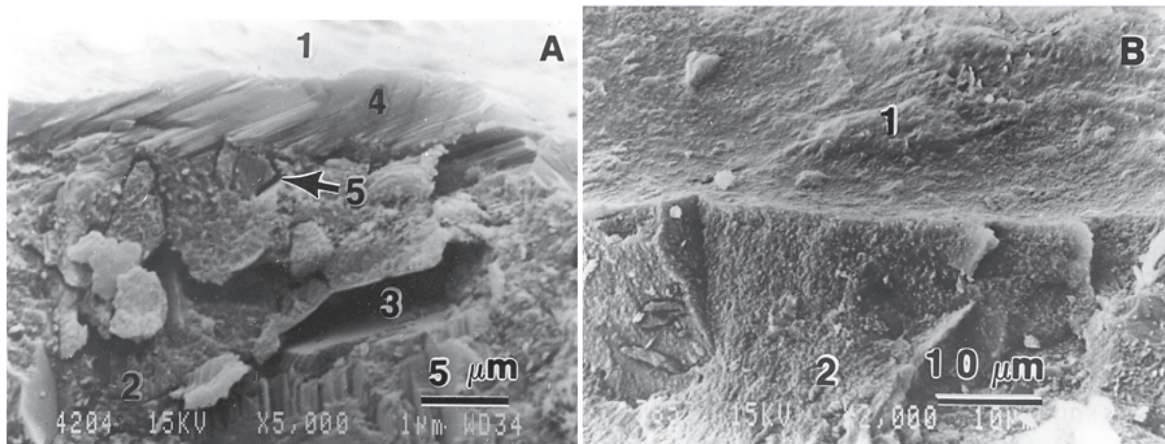


Figure 2-2: SEM of the ITZ Between Cement Paste and Aggregate at 28 days for A) Mixture without mS, B) Mixture with mS (ACI Committee 234 2006; Bentur & Cohen 1987)

Note: 1 = aggregate surface; 2 = cement paste; 3 = voids; 4 = CH; 5 = microcracks

2.2.4.2 Chemical Effects of Microsilica

The chemical effects of mS stem from its pozzolanic reactivity as discussed in the section on Pozzolans. The pozzolanic reaction mechanism of mS and its hydration in cement pastes is commonly described via the gel model theory (ACI Committee 234 2006). Upon contact with water, mS is believed to dissolve and change into a silica-rich gel that absorbs most of the neighboring water. The gel then starts agglomerating between the grains of hydrating cement and coats the hydrating cement particles as well. The CH that starts precipitating out of the alite and belite hydration is reacted with at the exposed surfaces of the silica-rich gel to form secondary C-S-H that fills the voids and interparticle spaces left behind by the cement produced C-S-H. This chemical process of consuming the CH phase and converting it to secondary C-S-H contributes to the physical mechanisms described

in the previous section towards creating a very dense paste and ITZ structure (ACI Committee 234 2006).

2.2.4.3 Microsilica on Sulfate Resistance

The sulfate resistance of concrete, mortars, and pastes can be significantly increased with the addition of mS. Both the physical and chemical effects of mS discussed in the previous sections contribute to its resistance to sulfate attack. The primary mechanism via which mS reduces and prevents sulfate attack is attributed to its ability to decrease the total permeability of the cementitious composite. This effect is complemented by the reduction of the CH phase which is primarily responsible for the decalcification of paste and is the main target of sulfates due to its high solubility (ACI Committee 234 2006; Skalny et al. 2002).

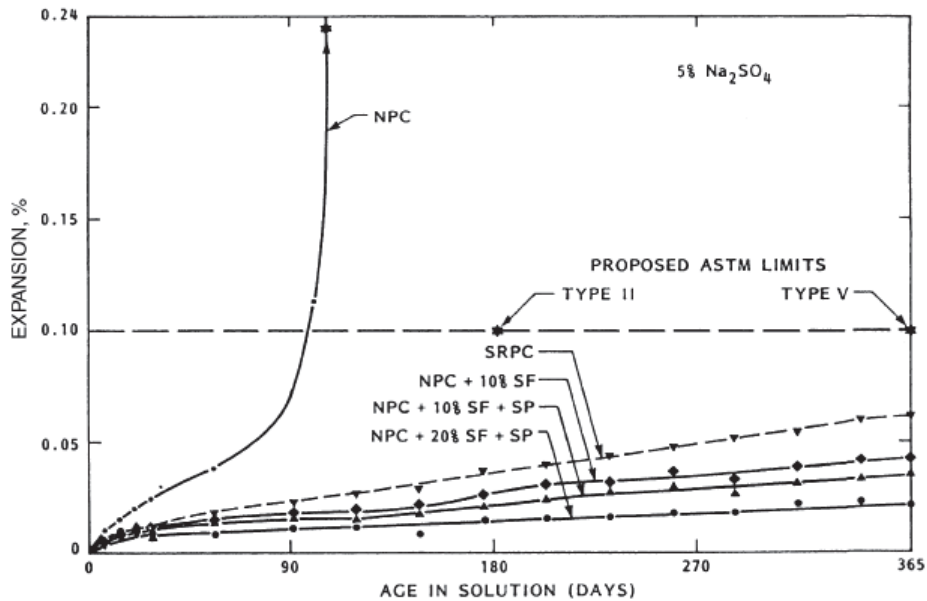


Figure 2-3: Expansion of Mortar Bars in Sulfate Solution Tested per ASTM C 1012 (ACI Committee 234 2006)

The permeability improvements are considered more important since reduction of CH is not as effective at mitigating magnesium and acid based sulfate attack that can directly target the C-S-H phase. In laboratory testing measuring mortar bar expansion under exposure to 5% Na₂SO₄ solution,

mS contained mortar bars made with a high C₃A cement (11.8%) exhibited less expansion than those made with a sulfate-resistant cement used on its own, see *Figure 2-3* (ACI Committee 234 2006).

2.3 Sources and Production of Nanosilica

Nanosilica (nS) is not a byproduct of another industrial process as was the case for silica fume. It is manufactured and there are multiple methods for its synthesis that produce nS of different nanoscale particle sizes and forms. Outside of its relatively recent application in concrete, nS has been used in other industries such as ceramics, lens, glass, rubbers and paints (Campillo et al. 2004). It has been used as an anti-sliding agent, to achieve refractory behavior, thermal resistance, anti-reflective surface treatments, and more (Campillo et al. 2004).

Some of the methods used to synthesize nS are reviewed here. One method is based on the sol-gel process that can be done at room temperatures (Quercia & Brouwers 2010). The process entails adding starting materials, often sodium silicate [Na₂SiO₄] paired with organometallics such as tetramethoxysilane (TMOS) [CH₃OSi(OCH₃)₃] or tetraethoxysilane (TEOS) [Si(OC₂H₅)₄], into a solvent and precipitating silica gel by changing the pH of the solution (Quercia & Brouwers 2010). The silica gel can then be filtered, dried, and burned to procure nS in powder form, or dispersed back into a solution typical of 20-40% wt. solid SiO₂ with a stabilizing agent such as Na, K, NH₃, or others (Quercia & Brouwers 2010). Nanosilica can also be produced by vaporization of quartz material at a temperature between 1500 and 2000 °C with an electric-arc furnace, which is the method most similar to how silica fume is collected (Quercia & Brouwers 2010). The nS particles are condensates of the SiO vapor that is oxidized in a cyclone. There is also a biological method developed where nS is produced using digested humus from California red worms generating nS ranging in size between 55 nm to 245 nm with an 88% process efficiency (Quercia & Brouwers 2010). The worms are fed rice husk or biological waste material that naturally contains at least 22% silica. There is a precipitation

method for generating nS that involves precipitating nS from a solution that uses precursors such as sodium silicates [Na_2SiO_4], burned rice husk ash, semi-burned rice straw ash, magnesium silicate, and others. There is a newer method involving the treatment of the mineral olivine [$(\text{Mg}^{+2}$ or $\text{Fe}^{+2})_2\text{SiO}_4$] with sulfuric acid [H_2SO_4] through which particularly fine nS (6 to 30 nm) is precipitated (Quercia & Brouwers 2010).

2.4 Nanosilica Effects on Fresh & Rheological Properties

2.4.1 Water Demand and Workability

Multiple studies have indicated that the addition of nS, even in smaller doses than mS, has increased the water demand to retain a favorable workability. This is directly attributed to the high surface area of the nanomaterial, which is often in excess of $80 \text{ m}^2/\text{g}$ (Singh et al. 2013; Tobón et al. 2010). There is an observed reduction of spread, increase in the cohesion, and higher measured rheological yield stresses measured for mortars containing increasing dosages of nS (Luciano Senff et al. 2009). In a rheological study where nS of 9nm APS and SSA of $300 \text{ m}^2/\text{g}$ present in 30% wt. slurry was compared against mS with a SSA of $18.41 \text{ m}^2/\text{g}$, plasticity was measured via a mortar flow table and rheometer (L. Senff et al. 2009). Increases in torque measured with the rheometer and reduction in spread as measured on the flow table were correlated to reductions in mixture plasticity and increases in viscosity. Addition of nS reduced plasticity more so and at a faster rate than mS at the same dosages. **Figure 2-4** from the mortar spread testing done in that study indicated that as the dose of nS increased from 0 to 3.5%, the table spread decreased. This loss of workability and increase in paste cohesiveness, even at small doses, stems from the higher surface area particles of nS in comparison to mS.

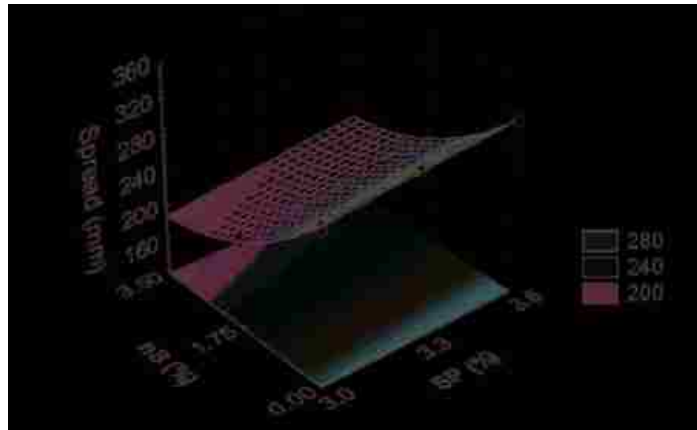


Figure 2-4: Flow Table Spread of Mortars Containing 0% to 3.5% nS (L. Senff et al. 2009)

2.4.2 Bleeding and Segregation

Since nS has shown to increase the cohesiveness and viscosity of mixtures with increases in the dose, it has also been very effective at preventing segregation of aggregates. It is actually used in high-performance and self-compacting concretes mainly as an anti-bleeding agent (Kontoleonos et al. 2012). By increasing the cohesiveness and internal friction of the mix, its tendency to segregate is also reduced. Researchers have reported concrete mixtures prepared with a proprietary nS admixture slurry called Gaia, exhibit very satisfactory workability without segregation or bleeding (Sobolev & Gutiérrez 2005).

2.4.3 Setting Time

Small doses of nS have shown to reduce setting times (Luciano Senff et al. 2009; Zhang et al. 2012). In one study on mortars, just 2.5% nS by weight of cement reduced the setting time by 60% by shortening the dormant period (Luciano Senff et al. 2009). The reduction in the setting time has been correlated to the extreme fineness of the nS particles and their associated high surface area that significantly exceeds that of mS as well (Zhang et al. 2012). In a study of using nS on concretes with approximately 50% slag, the 2% nS contained mortars exhibited significant reduction in initial and

final setting time in comparison to a slag and cement control and a mixture with comparable 2% of mS which did not reduce the setting time much from the control (Zhang et al. 2012).

2.4.4 Heat of Hydration

Besides accelerating hydration, the addition of nS has shown to increase the rate of heat evolution and peak temperatures generated during the first 24 hours (Singh et al. 2013; Said et al. 2012). Because pozzolanic reactions are typically slower and depend on the hydration of the cement phases first to access reserves of CH, the acceleration of the hydration kinetics has been mostly attributed to the ultrafine nature of the nanoparticles and their associated high surface area (Said et al. 2012). Nanosilica can also accelerate the hydration of other mineral admixtures such as slag and fly ash. The cumulative heat generated with nS and other mineral admixtures will be higher with increasing dosages of nS (Zhang et al. 2012). Refer to **Figure 2-5** for the effects of nS on mixtures containing almost 50% of slag (Zhang et al. 2012).

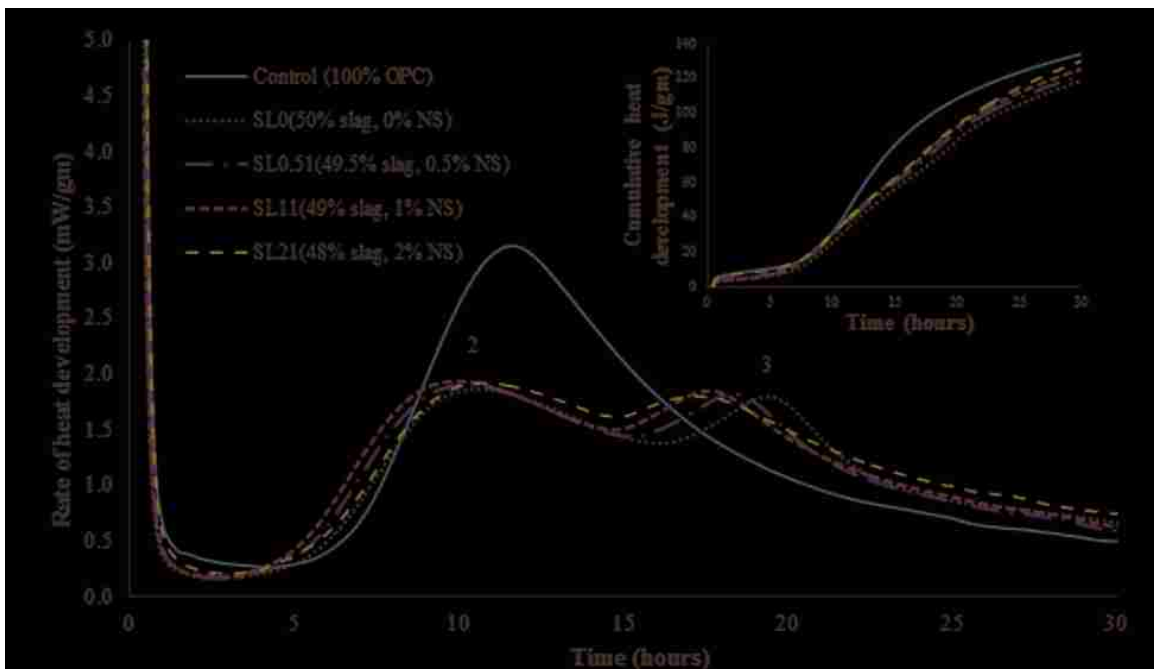


Figure 2-5: Effects of nS on Rate of Heat Development for High Slag Mixtures (Zhang et al. 2012)

Note that as the nS content increases from 0% to 2%, both peak 2 (cementitious hydration reactions of silica and alumina phases) and peak 3 (pozzolanic reactions) shift to an earlier age and the cumulative curves indicate the higher the nS content, the more cumulative heat is generated from the cementitious and pozzolanic hydration reactions combined. In cement only mixtures, the addition of nS not only reduces the dormant period but can accelerate the rate of reactions leading to a higher heat evolution peak, all due to the high reactive surface area of its nanoparticles (Luciano Senff et al. 2009; Said et al. 2012).

2.5 Nanosilica Effects on Hardened Properties

The particle packing effect of nS, similar to that observed with mS, helps fill the voids between the cement particles. This packing densification contributes to strength since it reduces the capillary porosity of the hydrated paste (Singh et al. 2013). The pozzolanic benefits of nS are also accelerated due to the nanoscale size of the SiO₂ particles and their high surface area which facilitate more silica and CH contact. Well dispersed nS also contributes much more C-S-H nucleation sites in between cement grains that can densify the paste beyond what is possible with mS. The denser secondary C-S-H formed at the expense of CH leads to increases in strength at all ages (Kawashima et al. 2013). For optimal strength contributing nucleation and paste densification effects to take place, good dispersion of the nS particles is important otherwise weak zones and voids could form compromising strength and permeability (Li et al. 2004). The microstructural and pozzolanic effects of nS are reported to increase the compressive and flexural strength in concretes, mortars, and pastes in numerous studies (Singh et al. 2013; Sanchez & Sobolev 2010). There is broad variability in the reported magnitude of strength improvements from nS application, anywhere from 20% to more than 60% which is likely due to the broad variability in nS particle sizes that are tested, their method of mixing and dispersion, and the cements and other mineral admixtures that nS is paired with. Based on its characteristic physical and chemical behavior in cementitious composites, it is likely that given

equally good dispersion, nS of finer average particle size and larger SSA can result in larger gains in strength between two otherwise identical mix designs.

2.6 Nanosilica on Durability and Sulfate Resistance

Nanosilica has proven to embody a lot of the same chemical and physical effects as mS although in many direct comparison cases, beyond what is achieved with mS at the same dosage. In most studies, smaller replacements often less than 6% by cement weight, have proven to be as effective as or more so than higher dosages of mS or other pozzolanic additives. Nanosilica has also shown to accelerate the pozzolanic reactions and improve the performance of mixtures featuring large contents of other mineral admixtures that it is paired with in testing. Those include fly ash and slag, both of which on their own usually come with the tradeoff of slower development of strength (Sanchez & Sobolev 2010; Singh et al. 2013). In terms of durability, nS contained mixtures have exhibited reductions in permeability and reduced chemical susceptibility to sulfates in large part due to the paste and ITZ densifying effect paired with a more rapid pozzolanic consumption of CH. Some select studies that have explored durability and sulfate resistance effects of nS are reviewed in this section.

2.6.1 Permeability Effects of Nanosilica

Khazadi et al, tested a 5.25% replacement of cement by weight using a 15% aqueous dispersion of 5 nm sized nS on concrete and tested it for water absorption and chloride ion diffusion to a depth of 20-30 mm (Khazadi et al. 2010). They observed a reduction in the percent water absorbed at all ages up to 7 days and calculated a smaller capillary coefficient of the nS contained mixture in comparison to the OPC control. Tobón et al. tested the porosity and capillary suction via absorption of 5% MgSO₄ solution, of 5 and 10% nS contained mortars versus a control (Tobón et al. 2015). They also tested sulfate resistance by measuring expansion of mortar bars in 5% MgSO₄ solution for 3 years which is referred to in the next section. They used nS with an APS of 99 nm and a SSA of 51.4

m²/g in a 40% solids aqueous solution. Nanosilica at 5% and 10% replacement in mortars, decreased the rate and total volume of water absorbed via capillary suction as shown in **Figure 2-6**. Increasing the dose of nS further reduced absorption via capillary suction.

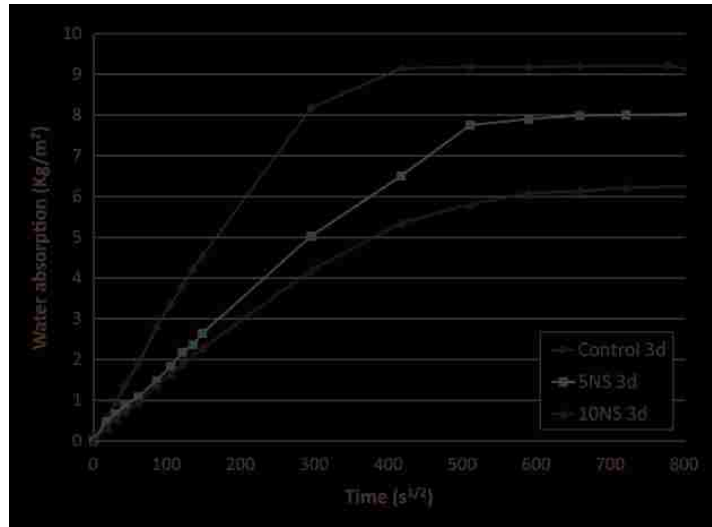


Figure 2-6: Capillary Suction of 5% and 10% Contained Mortars (Tobón et al. 2015)

From the mercury intrusion porosimetry (MIP) testing, Tobón et al. found that pore refinement resulting in the decrease of capillary pores 10 nm in diameter and larger was achieved with 10% nS, which indicates nS made the mixtures more impermeable. By measuring the percent mercury retained in their sample from the MIP extrusion curves, they were able to correlate higher dosages of nS with a greater tortuosity of the pore system likely due to less interconnectivity and refined pore diameters. K. L. Lin et al., tested 0%, 1%, and 2% doses of nS paired with 20% sludge ash mortars of varying ash particle sizes (Lin et al. 2008). The nS used was 10 nm dry powder with a SSA of 670 m²/g. Base on MIP testing of porosity, the researchers showed that at 7 days curing and 2% nS content, the average pore radius size of the mortar can be reduced from 65.8-93.8 nm to 50.5-68.2 nm, depending on the sludge ash particle size which would correlate with reduced permeability and strength gain. Du et al. also showed that capillary pores were refined with the addition of nS, and the resistance to water and chloride ion ingress were both improved at dosages of nS as low as 0.3% (Du et al. 2014a). The researchers used powder form nS, with an APS of 13 nm and SSA of 200 m²/g and

tested it on concrete. The MIP results indicated that with 0.9% nS, large capillary porosity was refined and overall capillary porosity mainly responsible for fluid transfer was reduced, as shown in **Figure 2-7**.

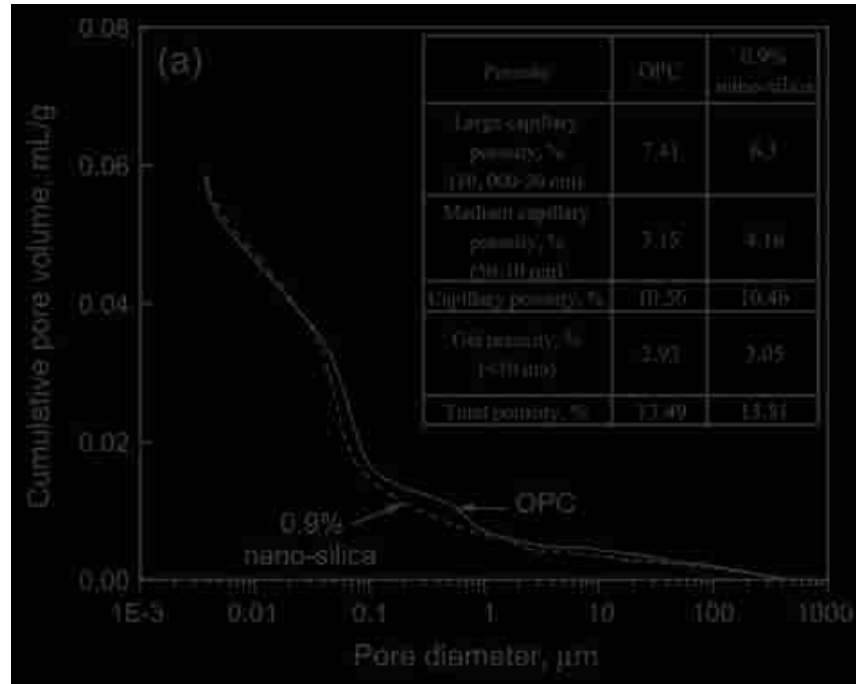


Figure 2-7: Cumulative MIP Pore Volume Curves for 0.9% nS Concrete and an OPC Control (Du et al. 2014a)

In the same study, rapid chloride migration and chloride diffusivity testing indicated that 0.3% of nS proved effective at increasing resistance of chloride ion ingress, but agglomeration of the nS was used to explain why significant improvements between the 0.3% and 0.9% nS concrete mixtures was not observed.

2.6.2 Sulfate Resistance

Atahan and Dikme tested the resistance of 2%, 4%, and 6% nS contained mortars to internal and external sulfate attack measured as expansion of mortar bars (Atahan & Dikme 2011). The internal sources of sulfate attack sample were cast with contaminated sands with up to 2% water soluble sulfates. Those were stored in limewater solution. The external sulfate attack samples without

contaminated sand were placed in 5% sodium sulfate solution. They used a Type I, 7.6% C₃A cement and a 50 nm/>80 m²/g nS in a 50% wt. aqueous dispersion. The sulfate resistance of nS was measured separately against other mineral admixtures used at higher dosages including: 6-12% mS, 15-45% fly ash (FA), and 20-60% slag (GGBFS). Per ACI durability guidelines (ACI Committee 201 2008), a Portland cement and mineral admixture mortar tested for expansion per ASTM C 1012 qualifies as sulfate resistant if it shows an expansion less than or equal to 0.10% at 12 months. After 12 months, the mixtures with the most contaminated sand and as little as 4% nS content, exhibited less than the threshold expansion qualifying them as sulfate resistant. At least 9% mS was required to achieve the same effect. FA and GGBFS mixtures also performed well but at the much higher replacements. In **Figure 2-8** from that study, showing the relative expansion of the mineral admixture containing mortars against that of the control for internal sulfate attack by a 2% SO₃ contaminated sand, the strong performance of nS at much smaller doses can be observed. In **Figure 2-9**, showing the 3, 6, and 12 month expansion of control and the mineral admixture containing mortars for external sulfate by Na₂SO₄, nS content of no higher than 2% is more than capable of maintaining expansion levels way below the 0.1% limit at 12 months.

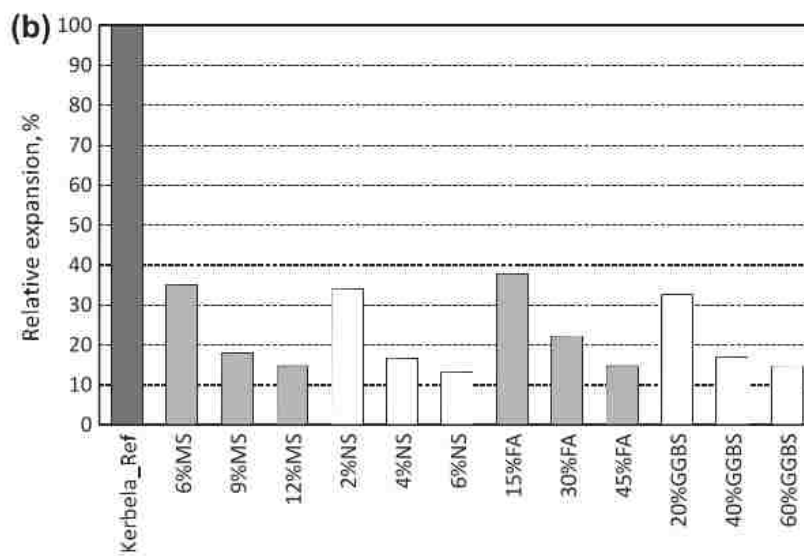


Figure 2-8: Relative Expansion to Control of Mineral Admixture contained Mortars after 12 Months of Internal Sulfate Attack due to Contaminated Sand (Atahan & Dikme 2011)

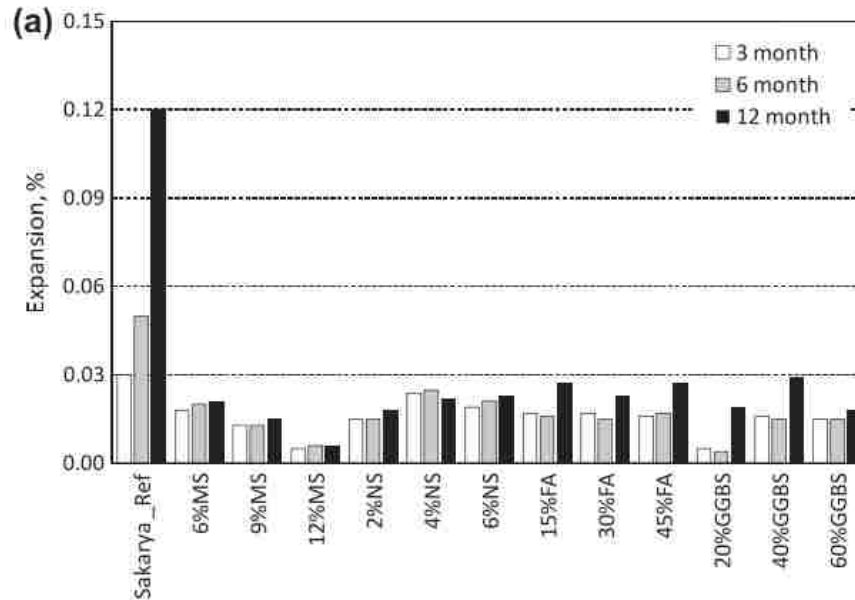


Figure 2-9: Expansion of Mineral Admixture contained Mortars after 12 Months of External Sulfate Attack due to 5% Na_2SO_4 (Atahan & Dikme 2011)

Tobón et al. also tested the sulfate resistance of 1, 3, 5, and 10% nS contained mortars exposed to 5% MgSO_4 solution for 3 years (Tobón et al. 2015). They used nS with an APS of 99 nm and a SSA of 51.4 m^2/g in a 40% solids aqueous solution. The expansion results reproduced in **Figure 2-10**, indicated that there was a decreasing trend in measured expansion with increases in the dose of nS. At least 5% nS was necessary to exhibit less expansion than the 0.10% threshold set by ACI at approximately 52 weeks (12 months) for good sulfate resistance. Since MgSO_4 can target the C-S-H phase, including that produced via pozzolanic reactions between the nS and CH, most of the beneficial effect of nS in regard to sulfate resistance could be attributed to its physical effects on reducing permeability via paste and ITZ densification and pore size refinement. Nevertheless, the pozzolanic reactions still contribute to those physical effects by densifying the paste and blocking capillary pore interconnectivity as secondary C-S-H is deposited.

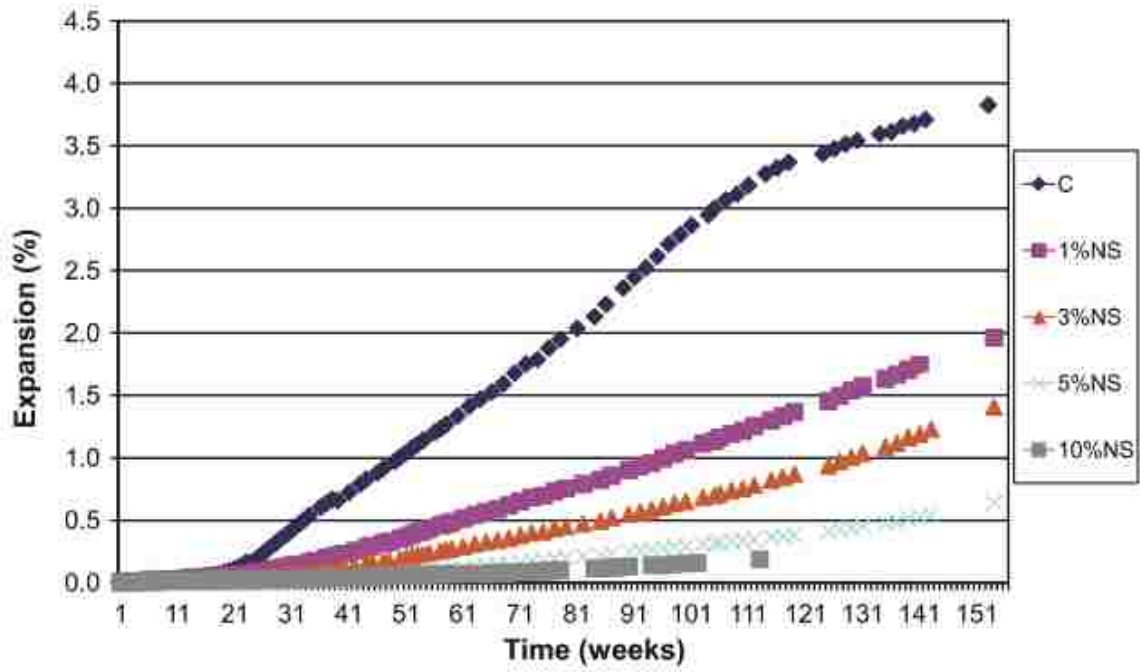


Figure 2-10: 3 Years of Expansion of Mortars Immersed in 5% $MgSO_4$ Solution (Tobón et al. 2015)

3 MATERIALS AND EXPERIMENTAL PROGRAM

3.1 Materials

The raw mixture and testing materials used in this body of research are described in more detail.

3.1.1 Ordinary Portland Cements

The objectives of this research include identifying the effects of nanosilica on sulfate resistance when paired with cements of different types. Particular attention was made to selecting cements of contrasting tricalcium aluminate (C_3A) content and fineness. Three locally sourced cements were procured and their chemical and physical properties are summarized in **Table 3-1**. All three cements are in conformance with their specified ASTM C 150 cement type designation (ASTM-C150 2007).

Table 3-1: Properties of Portland Cements Tested

	Cement L (Low C_3A)	Cement M (Moderate C_3A)	Cement H (High C_3A)
ASTM C 150 Designation	Type V	Type I/II	Type III
<i>Chemical Composition</i>			
Silicon Dioxide (SiO_2), %	21.7	21.1	20.8
Aluminum Oxide (Al_2O_3), %	4.1	4	5.4
Ferric Oxide (Fe_2O_3), %	4.0	2	1.2
Calcium Oxide (CaO), %	63.2	62.7	63.5
Magnesium Oxide (MgO), %	2.8	2.1	2.7
Sulfur Trioxide (SO_3), %	1.8	2.8	3.3
Loss on Ignition, %	0.7	1.8	1.2
Insoluble Residue, %	0.1	0.71	0.1
Total Alkali ($Na_2O + K_2O$), %	0.46	0.59	0.44
Free Lime (CaO), %	0.8	0	0.8
<i>Physical Properties</i>			
Time of Set Initial Vicat, min	150	145	70
Specific Surface Area, m^2/kg	285 ^a	341 ^a	546 ^a
325 Mesh (45 μm), % passing	72.9	--	99.7
Avg. Particle Size (APS), μm	35-45 ^b	20-30 ^b	15-20 ^b
<i>Per Bogue Calculation^c</i>			
Tricalcium Silicate (C_3S), %	54.0	57.0	53.0
Dicalcium Silicate (C_2S), %	21.5	17.5	19.6
Tricalcium Aluminate (C_3A), %	4.1	7.2	12.3
Tetracalcium Aluminoferrite (C_4AF), %	12.2	6.1	3.7
$(C_3S) / (C_2S)$ Ratio	2.51	3.26	2.70

^aby Blaine ASTM C 204 air-permeability test

^bEstimated from MasterSizer Laser Diffraction Particle Distribution Analysis

^cBogue Modified Equation for Interground Gypsum & Limestone (Winter 2012a)

Copies of the mill certificates for the cements used in this thesis are provided in the appendix. All cements were stored in sealed plastic lined 55 gallon steel drums. Prior to mixing, sufficient quantities of cement were transferred into 5 gallon buckets and kept indoors to reach ambient room temperatures of 21 ± 2 °C (70 ± 3 °F) at minimum 48 hours prior to mixing.

3.1.2 Aggregate

In terms of durability, aggregate can play an influential role. The surface quality, density, porosity, permeability, and chemical reactivity of the aggregate can all affect the overall permeability of concrete and mortar along with their resistance to chemical sulfate attack (Skalny et al. 2002). Only fine aggregate was used in the scope of this study because all samples tested were mortars. The fine aggregate was provided from a Southern Nevada quarry. Its gradation, as summarized in **Table 3-2**, was within the ranges specified in ASTM C 33 Standard Specification for Concrete Aggregates (ASTM International 2003b). Physical properties of the fine aggregate are summarized in **Table 3-3**.

Table 3-2: Sieve Analysis and Material Finer than No. 200 Sieve

Sieve Size	Target Range	Percent Passing
9.50-mm (3/8-in.)	100	100
4.75-mm (No. 4)	95 to 100	100
2.36-mm (No. 8)	80 to 100	95
1.18-mm (No. 16)	50 to 85	65.0
600- μ m (No. 30)	25 to 60	43
300- μ m (No. 50)	5 to 30	24
150- μ m (No. 100)	0 to 10	9
75- μ m (No. 200)	0 to 3	2.7
Fineness Modulus	2.3 to 3.1	2.64

Per ASTM C 117 and ASTM C 136

Table 3-3: Specific Gravity and Absorption of Fine Aggregate per ASTM C 128

Physical Property	Testing Results
Relative Density (Specific Gravity) Oven-Dry	2.755
Relative Density (Specific Gravity) Saturated-Surface Dry	2.777
Apparent Relative Density (Apparent Specific Gravity)	2.818
Absorption, %	0.81
Damp Loose Unit Weight per ASTM C 29	85 pcf @ 1.5% moisture

There are deleterious substances in aggregate that can affect the chemical durability of concrete. Aggregate that might be reactive in the lime-saturated environment of hydrated cement paste can pose particular issues if it exhibits volume instability or releases aggressive ionic species, such as sulfates, in the paste (Mehta & Monteiro 2006). If the aggregate is reactive with the alkali in the cement, it can lead to alkali-silica reactions (ASR) which as discussed earlier can predicate and exacerbate delayed ettringite formation (DEF) (Skalny et al. 2002; Thomas et al. 2008). ASR alone can create extensive cracking that provides pathways for ingress of sulfates, chloride, acids, and other aggressive ions from the outside environment that can target the hydrated silicates or reinforcement (Mehta & Monteiro 2006). The fine aggregate used in this study met the limitations for deleterious substances and alkali reactivity as indicated from the testing summarized in **Table 3-4**.

The fine aggregate was air dried in open horse troughs. At least 48 hours prior to mixing, sufficient aggregate was collected in 5 gallon buckets and stored in the laboratory to allow it to acclimate to the ambient room temperature of 21 ± 2 °C (70 ± 3 °F).

Table 3-4: Deleterious Substance and Alkali-Silica Reactivity Testing of Fine Aggregate

Deleterious Substances	Testing Standard	Testing Results	Max Allowable
Organic Impurities	ASTM C 40	Less than Color Plate No. 1	Not Detrimental
Clay Lumps and Friable Particles	ASTM C 142	0%	3.0%
Lightweight Particles	ASTM C 123	0 Specific Gravity 2.0	0.3%
Soundness of Aggregates	ASTM C 88	Sodium Sulfate 1.7% Loss	0.10%
Sand Equivalent Value (SE)	ASTM D 2419	93	NA
Alkali-Silica Reactivity Testing			
Potential Alkali-Reactivity of Aggregate (Mortar Bar Method)	ASTM C 1260	0.055%	0.10%
Accelerated Detection of Potentially Deleterious Expansion of Mortar Bars Due to Alkali-Silica Reaction	AASHTO T 303	0.033%	0.10%

3.1.3 Water

Most of the water used in Clark County, NV comes from Lake Mead, which is a manmade reservoir supplied by the Colorado River. A smaller proportion comes from groundwater. Over its journey through Colorado Basin and the Grand Canyon, the water picks up natural minerals, primarily calcium and magnesium, which imbue a significant hardness to the local tap water (Henderson 2015). The hardness of local tap water is reported to exceed 300 ppm (Donaldson et al. 2012). Dissolved sulfates in the tap and groundwater are also not uncommon and have been reported as high as 500 mg/L in Nevada (Donaldson et al. 2012). It was not desired to inadvertently introduce internal sulfate and magnesium in the mortars being tested for external sodium sulfate attack. If tap water from a local source was used, this could have introduced a risk for magnesium sulfate attack which was not within the scope of this research. Secondly, the effects of nanosilica on permeability might have been unclear in the results if there were sulfate ions already dispersed throughout the hydrated cement and aggregate matrix. To avoid these unpredictable variables, all the water used for mixing as well

as preparation of the sodium sulfate solution was commercially bottled distilled water from a single source.

3.1.4 Chemical Admixture

A polycarboxylate based high-range water-reducing admixture (HRWRA) was used to achieve the desired flow per ASTM C 109 (ASTM International 2002). The HRWRA satisfied the requirements of AASHTO M194 (Type A and F), ASTM C 494 (Type A and F) and ASTM C 1017. Properties of the HRWRA are presented in **Table 3-5**.

Table 3-5: Properties of HRWRA

Admixture Property	HRWRA Used
Chemical Type	Polycarboxylate Acid
Volatiles	59.70%
Specific Gravity	1.09
pH	3 to 8
Water Reduction Range	up to 40%

3.1.5 Nanosilica

The amorphous nanosilica (nS) used in this body of research was supplied in a porous dry powder form with manufacturer reported average particle sizes (APS) ranging from 15-20 nm (0.59-0.787×10⁻⁶ in) and a reported SSA of 640 m²/g (3.13×10⁶ ft²/lb). An aqueous dispersion of 25% by weight, 5-35 nm amorphous nS, was also procured and used in phase II and III of the research program. Scanning electron microscope (SEM) images of the dry and aqueous nS used in this study are shown in **Figure 3-1** and **Figure 3-2**, respectively. The aqueously dispersed nS had to be dried out of its colloidal solution prior to observing in the vacuum chamber of the SEM. More information on the SEM work performed in this study is available in a later section.

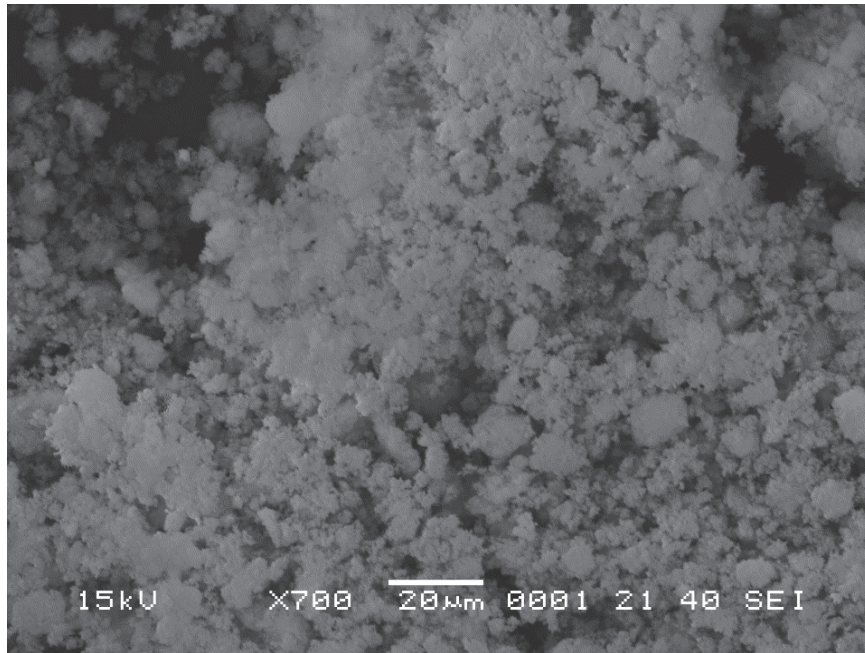


Figure 3-1: SEM Image of the Dry Nanosilica Powder Used in this Study

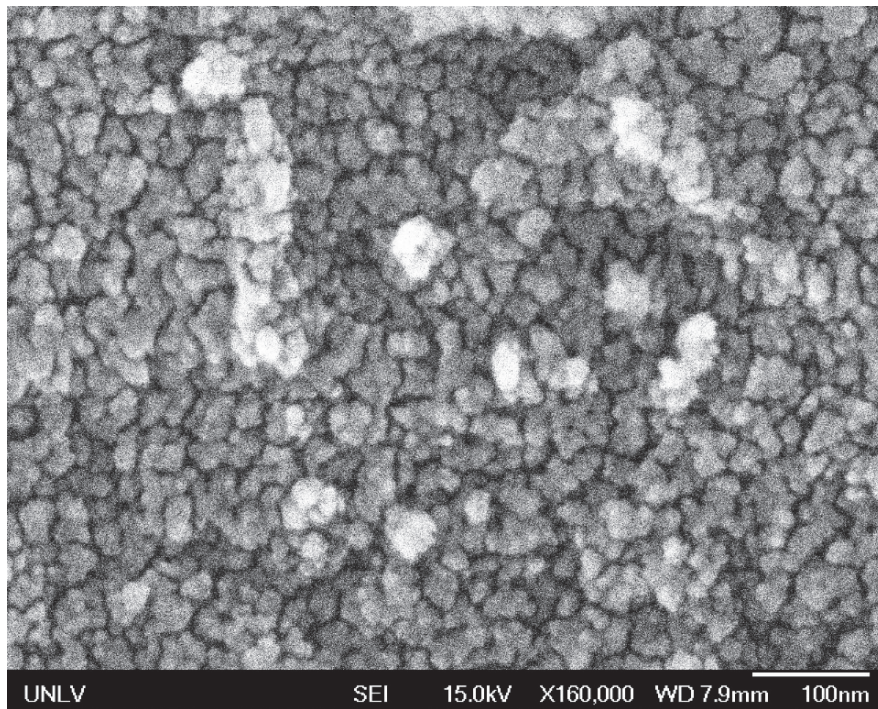


Figure 3-2: SEM Image of Aqueously Dispersed Nanosilica Dried Out of Solution

The chemical and physical properties of the dry nanosilica powder used in this study are presented in **Table 3-6**. For the aqueous dispersion refer to **Table 3-7**.

Table 3-6: Properties of Dry Silicon Dioxide Nanoparticle Powder

Material Property	
Color	White Powder
Morphology	Porous and Nearly Spherical
Average Particle Size (APS)	15-20 nm
Specific Surface Area (SSA)	640 m ² /g
Porosity	0.6 mL/g
Bulk Density	0.08 to 0.10 g/cm ³
True Density	2.648 g/cm ³
Silicon Dioxide (SiO ₂) Purity	>99.5%
Typical Impurities	
Al	≤ 0.002% (20 ppm)
Fe	≤ 0.001% (10 ppm)
Ca	≤ 0.002% (20 ppm)
Mg	≤ 0.001% (10 ppm)
Cl	≤ 0.001% (10 ppm)

Table 3-7: Properties of Aqueous Silica Nanoparticle Dispersion

Material Property	
Appearance	Translucent Liquid
Solution pH	8 to 11
Solution SiO ₂ Content	>25.5%
Solvent	75% water
Viscosity	50-100
Particle Morphology	Spherical and Amorphous
Average Particle Size (APS)	5-35 nm
Silicon Dioxide (SiO ₂) Purity	>99.99%
Typical Impurities	
Co	≤ 0.0075% (≤75 ppm)
Fe	≤ 0.00001% (≤0.1 ppm)

3.1.6 Silica Fume (Microsilica)

The microsilica used in this study as a comparison pozzolan to nanosilica is in accordance with ASTM C 1240 specifications for silica fume used in cementitious mixtures. As discussed in Section 2.2, microsilica is a very fine pozzolanic material comprised primarily of amorphous silica that is a by-product of the production of elemental silicon or ferrosilicon alloys. Undensified type silica fume was used in this study with the chemical and physical properties summarized in **Table 3-8**. A SEM image of the mS used in this study is shown in **Figure 3-3**.

Table 3-8: Properties of Silica Fume (Microsilica)

Chemical Properties	Testing Results	ASTM C 1240 Criteria
Silicon Dioxide (SiO ₂)	94.72%	85.0% MIN
Sulfur Trioxide (SO ₃)	0.23%	N/A
Chloride (Cl ⁻)	0.11%	N/A
Total Alkali	0.49%	N/A
Moisture Content	0.27%	3.0% MAX
Loss of Ignition	2.82%	6.0% MAX
pH	8.47	N/A
Physical Properties		
State of Material	Amorphous - sub-micron powder	
Color	Gray to medium gray powder	
Oversize % Retained on 45 µm (No. 325) sieve	2.88%	10% MAX
Density (Specific Gravity)	2.23	N/A
Bulk Density	322.96 kg/m ³	N/A
Specific Surface Area (SSA)*	22.65 m ² /g	15 m ² /g MIN
Average Particle Size (APS)**	0.1-1.0 µm	NA
Accelerated Pozzolanic Activity Index - with Portland Cement at 7 days	133.04%	105% MIN

* Estimated from MasterSizer Particle Distribution Analysis

** by BET Analysis

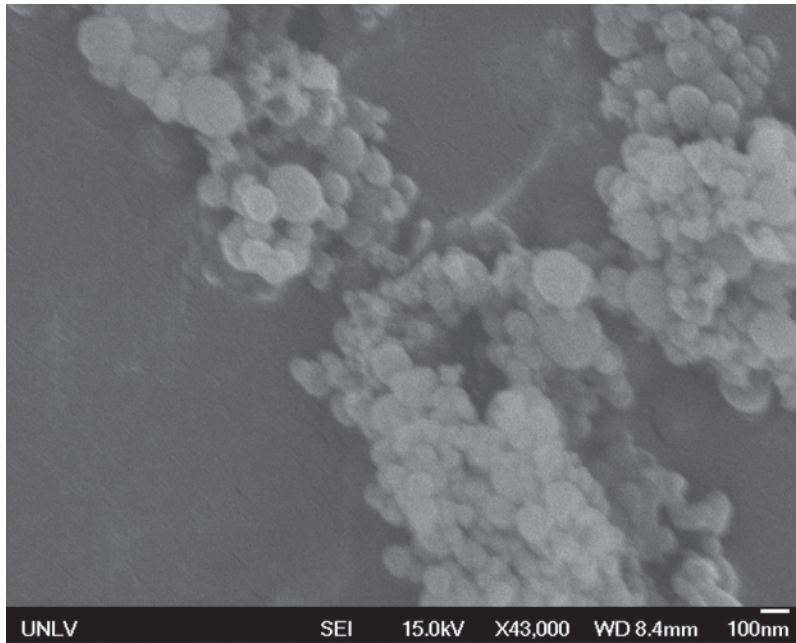


Figure 3-3: SEM Image of Microsilica

3.1.7 Sodium Sulfate (Na_2SO_4) Solution

For the preparation of the sodium sulfate solution used throughout the experimental program, food grade high purity sodium sulfate in anhydrous powder form was procured from a single source for mixing with distilled water to prepare solutions of the desired concentration. The dry sulfate supply was kept bagged in a plastic, watertight sealed bucket and stored indoors at room temperature of 21 ± 2 °C (70 ± 3 °F). For a summary of the chemical and physical properties of the anhydrous form sodium sulfate procured, refer to **Table 3-9**.

The 5% Na_2SO_4 solution used in Phase I and Phase II and the 10% Na_2SO_4 solution used in Phase III, were prepared per ASTM C 1012 (ASTM International 2004). For the full submersion tests in Phase I and Phase II, a solution-to-mortar volume ratio of 4 was maintained at all times and the solution was kept in circulation using 0.90 gallons-per-minute (GPM) submersible pumps. To replenish the sulfate ion concentration of the solution used for the ASTM C 1012 mortar bar expansion tests (Mehta

1975), the pH of each solution tank was manually rebalanced to 7.0±1 daily with 0.5N H₂SO₄ for the first 6 months and then weekly for the remainder of the extended 1.5 year fully submerged test. For Phase II, all samples were housed within one sulfate solution tank and the pH was continuously maintained at 6.5±1 with a pH controller and peristaltic pump system that dosed 0.5N H₂SO₄ as needed during the 6 month full submersion test.

Table 3-9: Properties of Anhydrous Sodium Sulfate Powder

Chemical Properties	Testing Results	Food Chemical Specified Criteria*
Sodium Sulfate (Na ₂ SO ₄)	99.80%	99% MIN
Water Insoluble	0.01%	0.03% MAX
Moisture	0.01%	NA
Impurities & Trace Metals		
NaCl	0.15%	0.5% MAX
Na ₂ CO ₃	0.50%	0.5% MAX
As	0.3 ppm	3.0 ppm MAX
Fe	1.0 ppm	10 ppm MAX
Physical Properties		
State of Material	White granular crystalline powder	
Average Particle Size (APS)**	0.1-1.0 µm	NA
Density	88.0 lbs/ft ³	

* Limits of impurities and trace metals based on Food Chemicals Codex, 5th Ed.

** Based on Screen Analysis in Certificate of Analysis included in the Appendix

3.1.8 Particle Size Distribution of Cements and Pozzolans

Samples of all three cements and the two dry forms of pozzolan (nanosilica and microsilica) were submitted for particle size distribution analysis via a MasterSizer laser diffraction analyzer. Prior to measurements, each material was ultrasonically dispersed in solution for 1 minute. The results are presented in **Figure 3-4**. The average particle sizes reported for each cement in **Table 3-1** were based on this analysis. The results for each cement were in close agreement of just a few percent from the reported fineness of each by the cement manufacturer in terms of percent passing the No. 325 Mesh

(45 μm). For the Type V cement, the manufacturer reported 72.9% percent passing 325 mesh while the diffraction analysis indicated 74.6% based on adding up all percent of sample measurements for 45 micron and less. For Type III cement, the manufacturer reported 99.7%, and 97.9% was measured through diffraction. In both cases the difference is less than 2%. The distribution of cement particles seems to correlate with the reported Blaine fineness too. The higher the reported SSA, the farther to the left each cement curve was towards a smaller particle size gradation. As expected, the particle size distribution curve of the Type III cement with the highest SSA of 546 m^2/kg is farthest to the left.

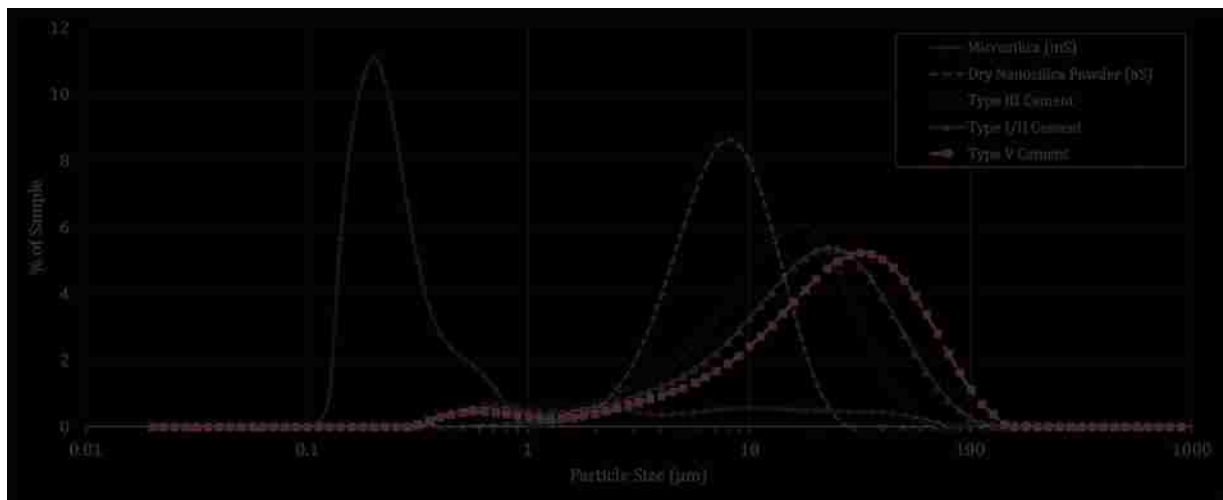


Figure 3-4: Laser Diffraction Particle Size Analysis of Cements and Pozzolans

The mS particles exhibited a broader distribution of particle sizes than nS. More than 84% of them ranged in size between 0.1 to 1.0 μm , which was in agreement with the mS manufacturer data and most typical industry reported mS size of $\leq 1.0 \mu\text{m}$ (ACI Committee 234 2006; Holland 2005). The nS particle size distribution indicated that most particles ranged between 3 and 12 μm . This gradation is significantly larger than the manufacturer-specified nS particle size range of 0.015 to 0.020 μm , which indicates that after blending the dry nS powder with water, the particles agglomerated in clusters held together by weak forces (capillary, Van der Waals, and electrostatic) (Taurozzi et al.

2011; Jiang et al. 2009). This is an observed tendency of ultrafine nanoparticles in general (Taurozzi et al. 2011; Jiang et al. 2009). The effects of this agglomeration on the effectiveness of dry powder nS to increase the sulfate resistance and decrease the permeability of mortars, is reported and discussed in the compilation of manuscripts presented in the next chapter.

3.2 Mortar Mixture Proportions

The mixture proportions for all mortar series tested are summarized in tables corresponding to each of the three phases of the experimental program, the objectives of which are outlined in Section 3.4. For Phase I, refer to **Table 3-10**. For Phase II, refer to **Table 3-11**. For Phase III, refer to **Table 3-12**. The nomenclatures for each mixture were chosen to easily differentiate the cement type and level of cementitious replacement with either nS and/or mS. Particular mixture nomenclature used within each of the manuscripts in the next chapters applies only to that manuscript. Therefore, a specific mixture proportion table is included within each manuscript. All mortar mixtures in this research program were prepared with a constant water-to-cement ratio (w/c) of 0.485 as recommended for the ASTM C 1012 test (ASTM International 2004). The fine aggregate-to-binder ratio for all mortar mixtures in the program was set to a constant 2.75-to-1 by mass as specified in ASTM C 109 (ASTM International 2002).

Table 3-10: Mortar Mixture Proportions for Phase I of Testing Program

Sample Designation	Binder Content			Measured Flow, %*	HRWRA Used, g	3-Day Compressive Strength,	
	Cement	nS	mS			psi	MPa
Low C₃A - Cement L							
L0	100%	--	--	145%	0.0	3,851	26.6
L3mS	97%	--	3.0%	127%	0.0	3,463	23.9
L4.5mS	95.5%	--	4.5%	115%	0.0	3,350	23.1
L6mS	94%	--	6.0%	97%	0.0	3,419	23.6
L1.5nS	98.5%	1.5%	--	122%	0.0	3,478	24.0
L3nS	97%	3.0%	--	98%	0.0	3,560	24.5
L4.5nS	95.5%	4.5%	--	100%	4.0	3,376	23.3
L6nS	94.0%	6.0%	--	102%	7.0	3,226	22.2
L1.5mS+1.5nS	97%	1.5%	1.5%	118%	0.0	3,872	26.7
L2.25mS+2.25nS	96%	2.25%	2.25%	100%	2.5	3,408	23.5
L3mS+3nS	94%	3.0%	3.0%	98%	4.0	3,504	24.2
Moderate C₃A - Cement M							
M0	100%	--	--	148%	0.0	4,296	29.6
M3mS	97%	--	3.0%	108%	0.0	4,420	30.5
M4.5mS	95.5%	--	4.5%	103%	0.0	4,623	31.9
M6mS	94%	--	6.0%	95%	4.0	4,463	30.8
M1.5nS	98.5%	1.5%	--	117%	0.0	5,013	34.6
M3nS	97%	3.0%	--	97%	4.2	4,641	32.0
M4.5nS	95.5%	4.5%	--	98%	9.4	4,560	31.4
M6nS	94.0%	6.0%	--	100%	20.0	4,337	29.9
M1.5mS+1.5nS	97%	1.5%	1.5%	107%	0.0	4,879	33.6
M2.25mS+2.25nS	96%	2.25%	2.25%	118%	4.0	4,602	31.7
M3mS+3nS	94%	3.0%	3.0%	102%	9.0	4,363	30.1
High C₃A - Cement H							
H0	100%	--	--	123%	5.8	5,164	35.6
H3mS	97%	--	3.0%	110%	5.6	5,146	35.5
H4.5mS	95.5%	--	4.5%	100%	9.0	4,975	34.3
H6mS	94%	--	6.0%	105%	9.5	5,088	35.1
H1.5nS	98.5%	1.5%	--	100%	14.0	4,673	32.2
H3nS	97%	3.0%	--	97%	18.0	4,527	31.2
H4.5nS	95.5%	4.5%	--	97%	28.7	5,462	37.7
H6nS	94.0%	6.0%	--	110%	43.5	4,984	34.4
H1.5mS+1.5nS	97%	1.5%	1.5%	98%	8.8	5,878	40.5
H2.25mS+2.25nS	96%	2.25%	2.25%	98%	13.0	5,506	38.0
H3mS+3nS	94%	3.0%	3.0%	96%	16.0	5,720	39.4

*Flow measured according to ASTM C 1437 with flow table conforming to ASTM C 230

Table 3-11: Mixture Proportions for Phase II of Testing Program

Sample Designation	nS Dispersing Method	HRWRA, mL		Binder Content			3-Day Compr. Strength,		
		Blender	Mixer	Cement	Dry nS	Aq. nS	Measured Flow, %*	MPa	psi
CTRL	n/a	--	5.0	100%	--	--	130%	31.2	4,527
M3nS-10-I	10 min. mechanical	--	10.0	97%	3.0%	--	101%	40.9	5,926
M3nS-10-II	10 min. mechanical	5.0	5.0	97%	3.0%	--	95%	48.6	7,051
M3nS-10-III	10 min. mechanical	10.0	--	97%	3.0%	--	85%	47.1	6,836
M3nS-10-IV	10 min. mechanical	10.0	5.0	97%	3.0%	--	106%	43.5	6,314
M3nS-20-I	20 min. mechanical	--	10.0	97%	3.0%	--	84%	47.8	6,930
M6nS-10-I	10 min. mechanical	--	20.0	94%	6.0%	--	98%	48.8	7,080
M6nS-10-II	10 min. mechanical	10.0	10.0	94%	6.0%	--	88%	49.4	7,158
M6nS-10-III	10 min. mechanical	20.0	--	94%	6.0%	--	75%	51.4	7,448
M6nS-10-IV	10 min. mechanical	20.0	5.0	94%	6.0%	--	103%	48.7	7,064
M6nS-20-I	20 min. mechanical	--	20.0	94.0%	6.0%	--	79%	50.0	7,251
U3nS-10	10 min. ultrasonic	--	10.0	97%	3.0%	--	109%	44.3	6,427
U3nS-20	20 min. ultrasonic	--	10.0	97%	3.0%	--	102%	46.4	6,737
U6nS-10	10 min. ultrasonic	--	20.0	94.0%	6.0%	--	90%	49.6	7,191
U6nS-20	20 min. ultrasonic	--	20.0	94%	6.0%	--	74%	47.9	6,951
AQ3nS	aqueous solution	--	13.0	97.0%	--	3.0%	80%	43.4	6,290
AQ6nS	aqueous solution	--	30.0	94%	--	6.0%	49%	44.6	6,473

*Flow measured according to ASTM C 1437 with flow table conforming to ASTM C 230

Table 3-12: Mixture Proportions for Phase III of Testing Program

Sample Designation	Binder Content			Measured Flow, %*	HRWRA Used, mL
	Cement	nS	mS		
Low C₃A - Cement L					
L0	100%	--	--	131%	0.0
L-3mS	97%	--	3.0%	127%	0.0
L-6mS	94%	--	6.0%	113%	5.0
L-AQ3nS	97%	3.0%	--	116%	5.0
L-AQ6nS	94.0%	6.0%	--	92%	25.0
Moderate C₃A - Cement M					
M0	100%	--	--	126%	0.0
M-3mS	97%	--	3.0%	121%	0.0
M-6mS	94%	--	6.0%	102%	5.0
M-AQ3nS	97%	3.0%	--	103%	20.0
M-AQ6nS	94.0%	6.0%	--	75%	70.0

*Flow measured according to ASTM C 1437 with flow table conforming to ASTM C 230

3.3 Mixing Procedure

The general mortar mixing procedure used was adopted from ASTM C 305 “Standard Practice for Mechanical Mixing of Hydraulic Cement Pastes and Mortars of Plastic Consistency” with some modifications for the addition of nS and/or mS. The mortar mixing sequence was as follows:

1. The electrically driven epicyclic type mechanical mixer used in this study was a Hobart Model AS200T with a flat beater paddle, see **Figure 3-5**. It was set up for mixing with a clean bowl and paddle that were slightly moistened with a damp rag.



Figure 3-5: Epicyclic Mixer used for Preparation of Mortars

2a. Dry nS Powder:

Phase I: The measured dose of dry nS powder was combined with most of the mixing water in a commercial blender. The mixture was blended for 1 minute to produce a homogenous milky white silica slurry and then transferred to the mixer bowl using the remainder of the mixing water to wash out any remaining slurry from the blender.

Phase II: (Mechanical Mixing Method) The measured dose of dry nS powder was combined with most of the mixing water in a commercial blender. The mixture was blended for either 10 or 20 minutes. The premeasured dose of HRWRA was added 30 seconds after the start of

blending if indicated so in the dispersion and mixing methodology tested for that mortar. The silica slurry was then transferred to the mixer bowl using the remainder of the mixing water to wash out any remaining slurry from the blender. (Ultrasonic Dispersion Method) A 1000 mL glass beaker containing the mortar mixing water was suspended in a Branson Model 1200 (50/60 Hz) ultrasonic cleaner filled with distilled water for the ultrasonic dispersion via the indirect method. The premeasured dose of nS powder was slowly added to the beaker over a period of 1 minute before continuing for either 10 or 20 additional minutes of ultrasonic dispersion. See **Figure 3-6** for the ultrasonic dispersion setup.



Figure 3-6: Setup of Ultrasonic Cleaner for Ultrasonic Dispersion of Nanosilica

Phase III: Dry nS powder was not tested in this phase.

2b. Aqueous nS Solution:

Phase I: Aqueous nS dispersion was not tested in this phase.

Phase II: The premeasured dose of aqueous nS solution was combined and stirred with all the mixing water directly in the mixer bowl. To maintain the w/c, the mixing water quantity was adjusted to account for the water content of the aqueous dispersion.

Phase III: See Phase II procedure.

2c. Microsilica:

Phase I: The measured dose of microsilica was added directly to the premeasured dose of cement and manually stirred until a homogenous dry binder powder was achieved.

Phase II: Microsilica was not tested in this phase.

Phase III: See Phase I procedure.

3. Once either the mixing water or nS slurry (water + Dry nS or water + aqueous nS) were in the mixer bowl, the binder (cement only or cement + mS) was added and mixing was started at the slow speed setting (140 ± 5 rpm) for 30 seconds.
4. After the first 30 seconds, the premeasured dose of fine aggregate was slowly fed into the mixing bowl over the next 30 seconds of mixing at the slow speed setting.
5. At the 1 minute mark, the mixer was stopped, and then turned on for another 30 seconds now on the medium speed setting (285 ± 10 rpm). If mixture appeared very dry, some of the HRWRA was added within the first 10 seconds of this mixing period.
6. At the 1 minute 30 second mark, the mixer was stopped for 1 ½ minutes. During that time, the bowl was removed from the mixer, and any mortar stuck to the side of the bowl was scraped down using a stainless steel scooper. Then, the entire batch was hand stirred and kneaded for the remainder of the period to better intermix the paste and aggregate.
7. At the end of the 1 ½ minute mechanical mixing break, the mortar batch was moved back to the mixer and then mixed for another 1 minute at the medium speed setting. The remainder of the HRWRA dose was added at the start of this period if required for workability.
8. Following the 1 minute of medium speed mixing, the flow of the mortar mixture was measured following ASTM C 1437 procedure on a flow table conforming to ASTM C 230 specifications (ASTM International 2001; ASTM International 2003a). See **Figure 3-7** for how flow was measured. If the desired flow was not achieved, the mortar batch was returned to the mixer bowl and mechanically mixed at medium speed for another 1 minute at the

beginning of which more HRWRA was added. This step was repeated until the desired flow was achieved.

9. Mortar bar, cube, disk, and cylinder molds were packed and compacted using a model Synttron PowerPulse electromagnetic table.
10. Samples were then wrapped in plastic and left at room temperature 21 ± 2 °C (70 ± 3 °F) for 24 hours. After the 24 hours, they were removed from their molds using compressed air if necessary and transferred to a moist cure room for 3 days (72 hours). This was determined to be the minimum period needed to attain the recommended compressive strength of 20.0 ± 1.0 MPa (3000 ± 150 psi) per ASTM C 1012 prior to immersion in the sodium sulfate solution.
11. Any samples not intended for exposure to sulfate attack but requiring continued curing for supplemental testing at a later age were kept in the moist cure room for Phase I and Phase III or in the case of Phase II, cured in saturated limewater tanks. Limewater tanks contained 3 g/L of lab grade hydrated lime [$\text{Ca}(\text{OH})_2$] to achieve saturation as recommended in ASTM C 511.

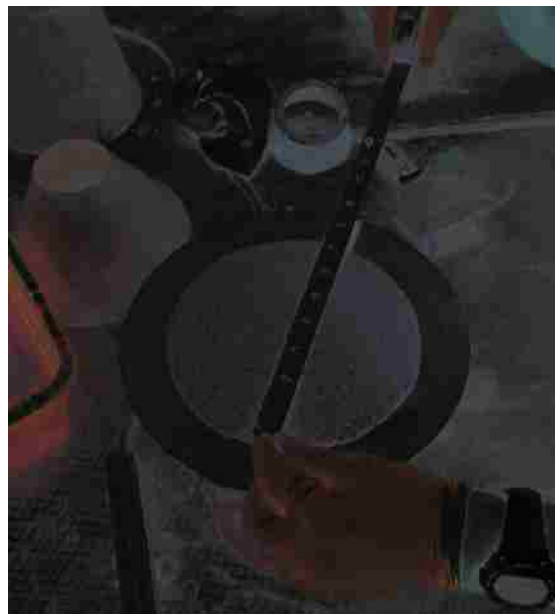


Figure 3-7: Measurement of Mortar Flow per ASTM C 1437 Procedure

3.4 Experimental Program & Setup

A summary of the testing program organized in three distinctive phases is presented herein.

3.4.1 Phase I – Chemical Sulfate Attack via Full Submersion Exposure

The tests performed under this initial phase set out to achieve a few objectives and narrow down the focus of Phase II. At the core of this phase, was the ASTM C 1012 test for measuring chemical sulfate attack induced expansion of mortar bars. The objectives of this testing phase can be summarized as follows:

- 1) Identify the effectiveness of nS at improving the sulfate resistance of mortars prepared with cements of low (<5%), moderate (6-8%), and high (>10%) C₃A content, which as discussed earlier, correlates with the chemical susceptibility of the hydrated cement to sulfate attack. The significance of fineness in comparison to the C₃A content for mortars containing nS, mS, or both was also a point of interest given the properties of the three cement types chosen for the test.
- 2) Include mortars with similar replacements of mS to establish a direct point of comparison between nS and its more industry recognized predecessor.
- 3) Understand how increasing the dosage of nS affects the sulfate resistance of mortars and how it compares to both the control and the comparable mS contained mixtures.
- 4) Evaluate if there are potential benefits from combining nS and mS in equal doses from the standpoint of possible reduced sulfate induced expansion due to the following: combined filler effects, acceleration of pozzolanic activity, and superior permeability improvements in comparison to either pozzolan applied separately in the same high-sulfate exposure environment.

In addition to measuring the sulfate attack induced expansion of mortar bars at the frequencies recommended in ASTM C 1012 over a period of a year and a half, the following additional tests were performed:

- Compressive strength testing at 28 days, 3 months, 6 months, and 1 year of 5 cm (2-in) mortar cubes for each mixture. The compressive strength of cubes exposed to sodium sulfate attack were compared against the compressive strength of cubes stored in a moist cure room at the same age.
- Mass loss and observable expansion damage or cracking on 5 cm (2-in) mortar cubes for all mixtures.
- Water absorption and Rapid Sulfate Permeability Testing (RSPT) of select mortar mixtures performed on 4" diameter x 2" thick mortar disks.
- Heat of Hydration for select mortars performed on 4" diameter x 4" cylinders.
- Mercury Intrusion Porosimetry (MIP) of select mixtures.
- Scanning Electron Microscopy (SEM) imaging and Energy-Dispersive X-Ray Spectroscopy of mortar fragments for evidence of gypsum and ettringite.

More information on the procedure of these tests is provided in Section 3.5. Mortar samples prepared following the mixing procedure outlined in Section 3.3 and intended for full submersion exposure to sulfate attack were placed in the lidded plastic tanks shown in **Figure 3-8** that contained the 5% sodium sulfate solution. Each sulfate tank contained all the needed mortar bar, cube, and disk samples for two mixture designs as well as a sufficient volume of sodium sulfate solution. As shown in **Figure 3-9**, each tank featured an individual submersible electric water pump used to circulate the solution, and a raised plastic rack to store the mortar bars above the cubes and facilitate solution exposure on all sides.



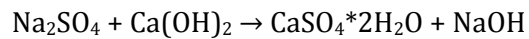
Figure 3-8: Phase I Sodium Sulfate Solution Tanks



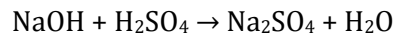
Figure 3-9: Phase I Sodium Sulfate Tank Opened to Show Contents

The pH of each tank was monitored daily for the first 6 months and then weekly for the remaining year with a waterproof digital pH tester. The pH of the solution was manually rebalanced to 7.0 ± 1 daily with $0.5N \text{ H}_2\text{SO}_4$ for the first 6 months and then weekly for the remainder of the extended 1.5 year fully submerged test to replenish the sulfate ion concentration. The formation of gypsum due to

the reaction between sodium sulfate and the CH phase consumes the sulfate ions and simultaneously releases NaOH which changes the solution pH from acidic to basic (Mehta 1975). The following reaction shows this:



The gypsum that precipitates continues to play a role in the ettringite bearing sulfate attack reactions discussed before. The NaOH concentration in the solution builds up while the SO_4 ion concentration drops which causes a reduction in the sulfate attack reactions unless the solution is replaced. An easier approach to replenish the sulfate ions is to titrate the NaOH with sulfuric acid [H_2SO_4] via the following reaction:



This will restore the pH of the solution to a neutral level that is still relatively acidic compared to the high alkalinity of the hydrated cement paste. Doing so will maintain a consistent and aggressive rate of sulfate attack that is more representative to field conditions where the alkalinity of concrete is unable to change the pH or sulfate concentration of its surrounding sulfate-rich environment.

3.4.2 Phase II – Mixing Methodology and Dispersion of Nanosilica

The testing program of Phase II was built upon the results of Phase I. As discussed in more detail within the results, agglomeration of the dry nS powder proved to be a significant factor in its effectiveness as a pozzolan and as a nanoparticle material. Its state of agglomeration seems to strongly influence its ability to increase the sulfate resistance of mortars. The objectives of this phase became testing different methods of mixing and different forms of nS. The scope of Phase II tested the effects on sulfate resistance of the following:

- Different methods of preparing mechanically blended nS and mixing water slurry that considered varying blending times and the time at which the HRWRA dosage added to optimize both the nS dispersion and fresh mortar workability.

- Dispersion of nS via ultrasonic mixing that considers varying the sonication time.
- Effectiveness of aqueous nS dispersion in comparison to the mechanically or ultrasonically blended dry powder nS mixtures tested.

The mortar series tested in Phase II all utilized cement M due to its moderate C₃A content and average Blaine fineness. Cement M was chosen because based on the expansion results from Phase I, a trend would become clear within a shorter test period of 6 months.

All mortar samples of the Phase II mixtures listed in **Table 3-11** that were exposed to sodium sulfate attack were placed within a single plastic tank with a lid that was larger than the Phase I variety. Four submersible water pumps were used to keep the 5% sodium sulfate solution in circulation. To replenish the sulfate ion supply during this phase, the pH was continuously maintained at 6.5±1 with a pH controller and peristaltic pump system that dosed 0.5N H₂SO₄ as needed during the 6 month full submersion test. This facilitated a more consistent and aggressive sulfate attack environment than what was possible via manual titration during Phase I.

Along with measuring the sulfate attack induced expansion of mortar bars at the frequencies recommended in ASTM C 1012 over a period of 6 months, the following additional tests were performed:

- Compressive strength testing at 6 months, of 5 cm (2-in) diameter x 10 cm (4-in) mortar cylinders for each mixture. The compressive strength of cylinders exposed to sodium sulfate attack were compared against compressive strength of cubes stored in saturated limewater curing tanks.
- Water absorption and RSPT of select mortar mixtures performed on 4" diameter x 2" thick mortar disks.
- Heat of hydration for select mortars performed on 4" diameter x 4" cylinders.

- Mercury Intrusion Porosimetry (MIP) of select mixtures.
- Scanning Electron Microscopy (SEM) imaging and Energy-Dispersive X-Ray Spectroscopy of mortar fragments for evidence of gypsum and ettringite.

More information on the procedure of these tests is provided in Section 3.5.

3.4.3 Phase III – Nanosilica on Physical Sulfate Attack via Partial Submersion Exposure

The objective of the testing program in Phase III was to take the optimal mixing methodology and form of nS delivery from Phase II and test it for physical sulfate attack. The nS containing mortar mixtures for Cement L and Cement M were tested for resistance to sodium sulfate induced physical sulfate attack against the control and mixtures of comparable cement replacements with mS. To facilitate physical sulfate attack, 3”diameter x 6” mortar cylinder samples of each of the mixtures listed in **Table 3-12** were partially submerged in 10% sodium sulfate solution. With partial submersion, the sulfate solution is drawn into the sample via capillary sorption, absorption, and diffusion. As the solution moves through the sample and evaporates from its air exposed surfaces, it deposits crystalline form thenardite and mirabilite crystals.

For this test, eight (8) mortar cylinders were cast for each mixture. Half of those were placed in an environmentally controlled chamber where the temperature and humidity were fluctuated over a repeating 48 hour cycle to force hydrous to anhydrous crystalline form transitions of the sodium sulfate. Using digital timers set to alternate in the ON position every 24 hours, a humidifier and space heater unit were rigged up to their respective humidity and temperature controllers, and set to cycle the environmental chamber between a high humidity/lower temperature and low humidity/higher temperature state. The high humidity/lower temperature state of >85% relative humidity (RH) and ambient room temperatures of (24 ± 2 °C (70 ± 3 °F)) was conducive to mirabilite precipitation as shown in the sodium sulfate phase diagram on **Figure 1-8**. The low humidity/higher temperature

state of < 35% RH and higher temperature of 35 – 40 °C (95 – 104 °F) was conducive to the crystallization of thenardite and more ingress of sulfate solution in the sample. These repeatedly simulated phase changes between thenardite and mirabilite aggravate the rate of sample deterioration and fatigue due to physical sulfate attack. The humidity controller, shown in **Figure 3-10**, with a set-point of 85% RH turns ON an ultrasonic humidifier whenever the humidity drops below that set-point during the high humidity low temperature phase of the cycle.



Figure 3-10: Humidity Controller and Humidifier in Environmental Chamber for Phase III

The remaining four cylinder samples were also partially submerged in 10% sodium sulfate solution but placed in an environment of constant temperature (24 ± 2 °C (70 ± 3 °F)) and constantly low relative humidity (25-30% RH). In this condition, the sulfate solution drawn into the mortar samples would naturally evaporate at the exposed faces of the specimen above the rubber barrier. If the evaporative front is below the surface of the sample to cause subflorescence, there should be observable physical sulfate attack. To increase the rate of evaporation and attempt to force subflorescence, a box fan was oriented to continuously move air over the exposed surfaces of the cylindrical samples. The constant environment setup is shown in **Figure 3-11**.



Figure 3-11: Constant Environment Partial Submersion Exposure Setup for Phase III

3.5 Measurements

Various tests were conducted as part of the main objective of this work and certain supplemental testing was conducted to aid the discussion and interpretation of results. In the sub-sections that follow, the various forms of testing conducted within the scope of this thesis work are further explained.

3.5.1 Flow (ASTM C 1437)

The test method for mortar bar expansion ASTM C 1012 recommends that for blends of Portland cement (PC) and either pozzolan or slag, a w/c should be chosen that yields a flow within 5% that of a pure PC mortar mixture with w/c of 0.485. Changing the w/c for the silica contained mortars would significantly affect their porosity and pore structure as discussed in Section 1.5.1. The changes to the permeability of the silica contained mortar would no longer be purely based on the pozzolan, so

HRWRA was used to maintain a constant w/c. To achieve comparable workability to the control, that per ASTM C 109 for mortars is $110\pm 5\%$, the HRWRA dosage was adjusted for each mixture to achieve such workability. As evident in the mixture proportion tables presented in Section 3.2, the necessary HRWRA dosages to target that desired flow increased with higher pozzolan content and higher Blaine fineness of the cement (i.e. cement H required more HRWRA than cement L for comparable mixture designs).

Mortar flow in this study was tested per the procedure laid out in ASTM C 1437, the standard test method for flow of hydraulic cement mortar. The flow table used in this test, similar to the one shown in **Figure 3-12**, met ASTM C 230 specifications.



Figure 3-12: ASTM C 230 Mortar Flow Table

Mixtures that did not meet the desired flow after completion of the mixing procedure were returned to the mixer and additional HRWRA was added. With some mixtures, particularly those with 6% nS and those with cement H, even very high doses of HRWRA did not bring the flow up to the desired level which. This was a function of the maximum workability improvements achievable with the particular HRWRA used in this study. Four readings were taken of the mortar spread after lifting the

mold and the flow is calculated as the average increase of the mold base diameter 10 cm (4") expressed as a percentage. The calculation of average flow, where D1-D4 are the individual diameter measurements of the mortar spread after dropping the table 25 times in 15 seconds, can be represented by the following equation:

$$Avg. Flow = \frac{\left(\frac{(D1 + D2 + D3 + D4)}{4} - 10 \text{ cm}\right)}{10 \text{ cm}} * 100\%$$

Eq. 1: Average Flow of Mortar

3.5.2 Heat of Hydration

Heat of hydration was measured for the control, 6% mS, 6% dry nS, and 6% aqueous dispersion nS mortars of both the cement L and cement H series. The mortar specimens cast for this test were 10 cm (4-in) diameter by 10 cm (4-in) cylinders. Immediately after mixing, compacting, and wrapping in plastic following the procedure detailed for all mortars, the cylinder molds were placed in individual well insulated adiabatic casings. Examples are shown in **Figure 3-13**. The mortar cubes seen in the figure are only used as weights. A type K thermocouple wire was embedded at the center of each sample and connected to a data logger that collected temperature readings every 30 seconds for the first 48 hours of hydration.



Figure 3-13: Heat of Hydration Test Setup

3.5.3 Compressive Strength (ASTM C 109)

In Phase I of the testing program, compressive strength was measured with 5 cm (2-in) mortar cubes following the ASTM C 109 standard. Four cubes were tested at each age. Compressive strength was measured at 3 days of moisture room curing to verify that the ASTM C 1012 recommended minimum compressive strength of 20.0 ± 1.0 MPa (3000 ± 150 psi) was achieved prior to immersion in the sodium sulfate solution. Mortar cubes, both moisture room cured and sulfate solution exposed, of all Phase I mixtures were tested at 28 days, 12 weeks, 26 weeks (6 months), and 52 weeks (1 year).

The reported compressive strength is calculated based on the average maximum force recorded by the testing machine divided by the area (A) of the loaded surface. The calculation, where P1 to P4 represent individual maximum force readings recorded by the uniaxial loading machine, can be summarized by the following equation:

$$\text{Avg. Compressive Strength (psi)} = \frac{\left(\frac{P1 + P2 + P3 + P4}{4} \right)}{A}$$

Eq. 2: Average Compressive Strength

For compressive strength expressed in pounds-per-square inch (psi), the loading is in pounds and the area of applied force in inches squared. The machine used for the compression tests of the mortar cubes was a computer controlled Tinius Olsen Testing Machine (refer to **Figure 3-14**) and the maximum applied force was measured via a loading cell connected to a Model P3 strain indicator and recorder.



Figure 3-14: Loading Machine for Testing Mortar Cube Compressive Strength

In Phase II, the compressive strength of mortars was measured with 5 cm (2-in) diameter x 10 cm (4-in) cylinders. Three cylinders were tested at each age. Compressive strength was measured at 3 days of moisture room curing to verify that the ASTM C 1012 recommended minimum compressive strength of 20.0 ± 1.0 MPa (3000 ± 150 psi) was achieved prior to immersion in the sodium sulfate solution. Cylinder specimens, both limewater tank cured and sulfate solution exposed, of all Phase II mixtures were tested at 26 weeks (6 months) which aligned with the conclusion of the sulfate expansion measurement test. The machine used for the Phase II compressive strength testing was a Gilson Model MC-500CL (500,000 lbs capacity) axial concrete compression machine shown loading a sample in **Figure 3-15**. The specimens were fitted with spherical bearing blocks and centered on the loading plates to ensure equal distribution of stress. Then the load was gradually applied until specimen failure.



Figure 3-15: Axial Compression Loading Machine Used for Mortar Cylinder Testing

3.5.4 Mass Loss and Observable Deterioration

In Phase I, after the 3 days of moisture room curing, two mortar cubes of each mixture were transferred into individual 5% sodium sulfate solution filled containers. After 24 hours, their combined saturated weight was recorded as the initial mass. At the conclusion of the Phase I test, after 1.5 years of sulfate exposure, the samples were removed, patted dry, and re-weighed for their combined mass. Any observable cracking was also noted. Any mass loss at an age of (t), could be calculated as:

$$\text{Mass Loss at } (t) = \frac{M_i - M_t}{M_i} \times 100$$

Eq. 3: Mass Loss

Where M_i is the initial total mass of the cubes and M_t is the total mass of the cubes at the age of (t). The two assigned mass loss cubes for the mixture M0 (the cement M control) after 1.5 years of sulfate exposure are shown in **Figure 3-16**. Generally, there was not significant mass loss but some observable edge softening and cracking were seen as shown in the figure.

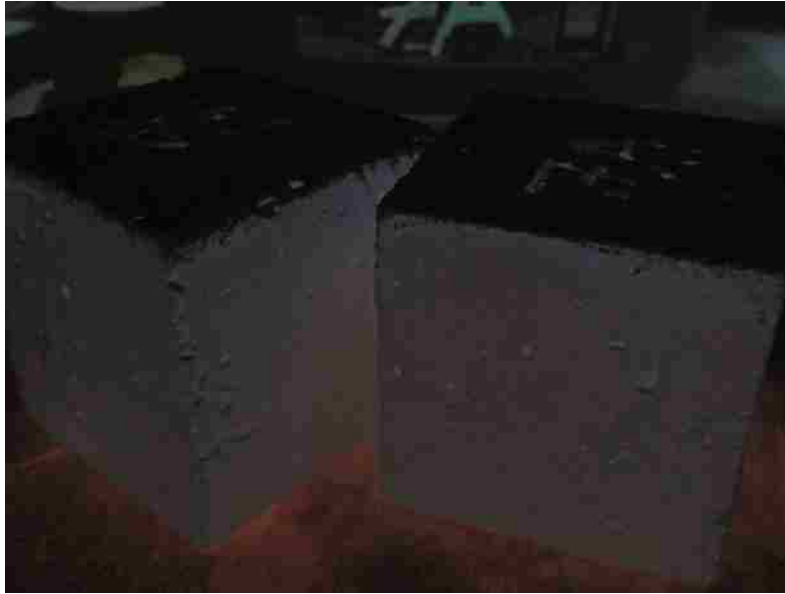


Figure 3-16: Cement M Control Mortar (M0) Cubes Tested for Mass Loss

For Phase III, each of the eight cylinders for the mixtures tested, were individually numbered 1-8 and weighed-in promptly after demolding. The first four samples of each mixture were assigned to the cyclic environmental chamber exposure, and the latter four to the constant temperature and humidity exposure conditions. The mortar specimens used for the partial submersion physical sulfate attack test (examples shown in **Figure 3-17**) are still undergoing exposure but the mass loss at the conclusion of the test will be calculated using Eq. 3.



Figure 3-17: Set of Mortar Cylinders Part of the Physical Sulfate Attack Testing in Phase III

3.5.5 Sulfate Expansion of Mortar Bars (ASTM C 1202)

In Phase I, the sulfate attack induced expansion was measured per the ASTM C 1012 “Standard Test Method For Length Change of Hydraulic-Cement Mortars Exposed to a Sulfate Solution”, by casting four mortar bars in stainless steel molds that conform to ASTM C 490 specifications. For Phase II, three mortar bars were cast. Stainless steel gage studs were embedded at each end of the 25 x 25 x 285 mm (1-in x 1-in x 11 ¼ in) mortar bars. Each mortar bar was labeled with its unique mixture nomenclature, a “T” at one end and a “B” at the other end near the steel gauges to indicate the proper top and bottom orientation of the mortar bar, and a small arrow that served as a reminder to rotate the specimen in the same direction every reading. The length comparator used in this study featured a Humboldt digital micrometer gauge capable of measuring length change differences from a reference bar with an accuracy of 0.0001-in. The center of the standard 170 ± 3.0 mm ($11 \frac{5}{8} \pm 1/8$ -in) stainless steel reference bar was covered in a rubber tube to minimize temperature changes during measuring. The length comparator is shown in **Figure 3-18** and it satisfied all other ASTM C 490 specifications. Comparator measurements for the mortar bars of each mixture were taken from the point they were added into the sulfate solution, then after 3 days, then weekly up until 3 months, then every 2 weeks up until 6 months, and then monthly until the conclusion of the test in the case of Phase I.

The procedure for taking comparator readings, one mixture at a time, can be summarized as follows:

1. All mortar bars for a given mixture were retrieved and transported in a shallow plastic container filled with sufficient sulfate solution from their respective sulfate tank to keep them in a submerged and saturated state. This avoided any immediate drying shrinkage of the samples if they were left exposed outside of solution too long during measurements.
2. Before each mortar bar reading, the reference bar was loaded in and the digital gauge was reset to zero. The reference bar was also labelled and always loaded into the comparator with

the same end into the bottom and top stud holes. The reference bar was slowly rotated in the same direction every time and the bottom stud hole was cleaned with a fabric towel before and after each reading to remove any water and debris that pooled up there.

3. After the reference bar was measured, the first specimen of the mixture was loaded into the comparator, in the proper orientation, and slowly rotated clockwise. The lowest reading measured by the comparator while rotating of the sample a few times was recorded.
4. The mortar bar was taken out of the comparator and promptly returned to the solution in the transport container.
5. The bottom comparator stud hole was cleaned again.
6. To verify that the digital gauge was taking an accurate measurement of the sample, following each mortar bar measurement, the reference bar was loaded into the comparator again to ensure the reading still read 0.0000-in and the gauge did not misread the previous measurement. If it did not, the gauge was reset again and the same mortar bar re-measured.
7. The process of measuring the reference bar, then mortar bar, then reference bar again was repeated for all four mortar bars of each Phase I mixture, or all 3 mortar bars for each Phase II mixture.
8. After measuring all retrieved mortar bars for a given mixture, they were returned to their respective sulfate tank, and the sulfate solution borrowed in the transport container was poured back in the tank. The process repeated for the next mixture.

The length change reported in the results is the average percent length change that was calculated using the following equation:

$$\text{Length } \Delta (t) = \frac{L_x - L_i}{G} \times 100$$

Eq. 4: Calculation for Length Change of Mortar Bars per ASTM C 490

Where ' L_x ' is the comparator reading of the mortar bar specimen at age x after the gauge was reset to zero with the reference bar, ' L_i ' is the initial comparator reading of the mortar bar specimen after the gauge was reset to zero with the reference bar, and G is the nominal gauge length, set as 10-in (25.4 cm) for this type of apparatus.



Figure 3-18: Length Comparator with Mortar Bar Loaded in for Measurement



Figure 3-19: Mortar Bars of a Cement M mixture after 1.5 years of Immersion in Sodium Sulfate Solution

3.5.6 Water Absorption (ASTM C 642)

The water absorption test performed per ASTM C 642 helped identify density, percent absorption, and percent void volume of hardened cementitious composites. Absorption is a transport process that involves the ingress of fluid, in this case water, by capillary action which relates to the pore structure of the mortar but not necessarily its permeability (Richardson 2002). This test was useful to develop conversions between mass and volume of the mortars and to find other characteristic properties such as the oven-dried mass, saturated mass after immersion, saturated mass after boiling, and the immersed apparent mass. By finding these values, the absorption after immersion, absorption after immersion and boiling, bulk density after immersion and boiling, apparent density, and the volume of permeable pore space (voids) could be found through this test method. The test was carried out following the ASTM C 642 standard procedure on three, 28-day cured 10 cm (4-in) diameter x 5 cm (2-in) thick, mortar disks for each mixture as outlined here:

- *To find Oven-Dried Mass:* Each mortar disk specimen was oven-dried at a temperature of 100 to 110 °C for a minimum of 24 hours. After this drying period, the disks were allowed to cool at the dry ambient air temperatures in the lab that fell within the 20 to 25 °C range set in the standard. Then the mass was recorded. The sample was oven-dried for another 24 hour period and once cooled, the mass was recorded again. This was repeated until the difference between the last mass recorded and the one preceding it did not exceed 0.5%. When that was the case, the samples were considered dry and the last mass recorded was the oven-dried mass.
- *To find Saturated Mass After Immersion:* Following the conclusion of the process for finding the oven-dried mass, the fully cooled mortar disk samples were immersed in approximately 21 °C water for a minimum of 48 hours. After the first 24 hours, the samples were towel dried and their mass recorded, after the second 24 hour period, they were towel dried again and their mass measured again. If the increase in mass between both measurements was less than

0.5%, the last mass measurement was the assigned saturated mass after immersion. If there was an increase in mass more than 0.5%, the samples were returned to immersion in the water for another 24 hours and then re-measured again. This was continued as required until the increase in mass from immersion was less than 0.5%. The last mass measurement once the criteria was satisfied, was assigned as the saturated mass after immersion.

- *To find Saturated Mass After Boiling:* Once the saturated mass after immersion was found, the mortar disk specimens were placed in a steel pot filled with tap water until samples were fully submerged. The water was then brought to a boil for 5 hours and then allowed to cool for no less than 14 hours to a final measured temperature in the range of 20 to 25 °C. Each specimen was then surface dried with a towel and its mass recorded. This measurement was assigned as the saturated mass after boiling.
- *To find the Immersed Apparent Mass:* The last mass measurement was made by suspending the specimen by wire and determining its immersed apparent mass.

Having found the four characteristic mass properties in the previous steps, the following calculations were used to determine the absorption, bulk densities, apparent density, and the void volume of permeable pore space based on this test:

$$\text{Absorption after immersion, \%} = [(B - A)/A] \times 100$$

$$\text{Absorption after immersion and boiling, \%} = [(C - A)/A] \times 100$$

$$\text{Bulk density, dry} = [A/(C - D)]\rho = g_1$$

$$\text{Bulk density after immersion} = [B/(C - D)]\rho$$

$$\text{Bulk density after immersion and boiling} = [C/(C - D)]\rho$$

$$\text{Apparent Density} = [A/(A - D)]\rho = g_2$$

$$\text{Volume of permeable pore space (voids), \%} = (g_2 - g_1)/g_2 \times 100$$

Where

A = mass of oven-dried sample in air, g

B = mass of surface-dry sample in air after immersion, g

C = mass of surface-dry sample in air after immersion and boiling, g

D = apparent mass of sample in water after immersion and boiling, g

g_1 = bulk density, dry, Mg/m³

g_2 = apparent density, Mg/m³

ρ = density of water = 1 Mg/m³ = 1 g/cm³.

3.5.7 Rapid Sulfate Permeability Test (RSPT)

The RSPT test, as proposed in the Sulfate-Resisting Concrete report by the Cement Concrete & Aggregates Australia (CCAA 2011), is similarly setup to the traditional rapid chloride permeability test (RCPT) per ASTM C 1202. In this study, a 10% Na₂SO₄ solution was used across the 0.3N NaOH instead of 3% NaCl. Three, 28-day cured 10 cm (4-in) diameter x 5 cm (2-in) thick, mortar disks were used for each average permeability reading that is presented in the results.

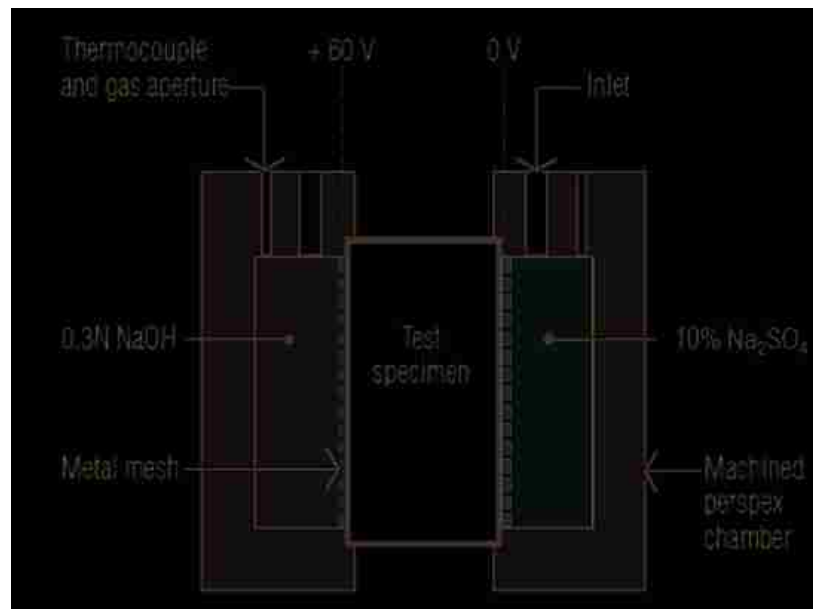


Figure 3-20: Schematic of RSPT Test Setup Adopted from (CCAA 2011)



Figure 3-21: RSPT Setup of Three RSPT Testing Cells

3.5.8 Mercury Intrusion Porosimetry (MIP)

The porosity of a material like concrete, is the proportion of the total volume of concrete occupied by pores, while the pore size distribution of a porous material is more indicative of its permeability (Dyer 2014). The pore structure that its porosity is comprised of is considered one of the characteristics of concrete that has the most influence on its behavior. Everything from compressive strength, absorption, permeability, and durability of concrete is affected by its pore structure (Cook & Hover 1993). Out of the multiple techniques available for measuring the pore size distribution and studying a porous material's microstructure, one of the most common and favored in the concrete industry is mercury intrusion porosimetry (MIP) (Neville 1998; Cook & Hover 1993). The output of this test can be presented in multiple ways. They results are presented either with a cumulative curve of pore size versus intrusion volume (cm^3) or porosity (%), or a pore size versus $dV/d\log D$ curve with distinctive peaks centered over where there are concentrated distributions of pores in that pore

size range. The theory behind this method is based on the concept that for squeezing a non-wetting fluid (such as mercury) into a pore of diameter 'd', a pressure 'P' that is inversely proportional to this diameter must be applied (Vočka et al. 2000). For cylindrical pores, this relationship is represented by the Washburn (Laplace) equation:

$$P = \frac{-4\gamma\cos\theta}{d}$$

Eq. 5: Washburn (Laplace) Equation used in MIP

Where "Y" is the surface tension of the non-wetting liquid, and "θ" is its contact angle with the pore walls (Cook & Hover 1993; Cook & Hover 1999). The "-4" in the equation presented is a constant shape factor based on the assumption that pores are of circular cross-section (Cook & Hover 1993). Most researchers use the circular pore cross-section assumption, although other factors for elliptical and slit type pores exist (Cook & Hover 1993). For mercury, its surface tension in a vacuum at 20 °C is approximately 480 dynes/cm (0.480 N/m) (Cook & Hover 1999) and its contact angle used in the MIP testing of this program was 140 degrees.

MIP of select mortars was sent out for testing by trained technicians at a certified laboratory. Small <0.5" mortar fragments, collected from multiple samples representative of the chosen mixtures for the test, were oven-dried at 50 °C for 48 hours and then desiccated in a vacuum for another 12 hours before shipping to the testing lab. The fragment samples were all collected from the interior of mortar disk or cylinder specimens split by tensile stresses. Doing so avoids any mold wall effects and any micro-cracks associated with compressive loading.

3.5.9 Scanning Electron Microscopy (SEM) and Energy-Dispersive X-Ray Spectroscopy (EDS)

Use of the scanning electron microscope (SEM) to observe and study the microstructure of concrete and other cementitious composites has become a prominent tool for petrographers and researchers

alike. The images recorded by SEM are based on rastering an electron beam over the specimen and detecting the electrons and other radiations emitted from it (Poole & Sims 2016). Under the electron beam, the specimen reflects, emits, and backscatters electrons and radiation which provide different information about the specimen that is detected and displayed on the monitor. Secondary electrons (SE) show the topography of the specimen, while backscattered electrons (BSE) indicate information about the composition of the specimen material compounds based on their atomic mass (Poole & Sims 2016). For concrete, mortar, and any other materials that are not electrically conductive, the specimens are sputter coated with a thin (about 20 nm) surface layer of either carbon or gold, which helps dissipate electrons and prevents “charging” of the observed area which oversaturates the electron receptors (Poole & Sims 2016). SEM’s are often equipped with electron probe microanalyzers (EPMA) or multichannel analyzer detectors that are capable of analyzing x-ray radiations emitted from the specimen at the point of electron bombardment. The x-rays emitted are characteristic to the elements present in the specimen at the point of interest (Poole & Sims 2016). There are wavelength-dispersive spectrometers (WDS) capable of providing finer quantitative analysis of the elemental makeup for a compound, and there are energy dispersive spectrometers (EDS) that are able to rapidly capture a qualitative full x-ray energy spectrum of the specimen over a set counting time (Poole & Sims 2016). The latter is more popular with concrete and mortar research since it provides faster data analysis and generates x-ray energy spectrums that are distinguishable between the variety of ingredients and phases of hydrated cement paste.

Images were taken of the raw dry nS powder, dried out aqueous nS, and mS that were presented in an earlier section. Additionally, small mortar fragments collected from select mortar mixtures were prepared for SEM by first over drying them for 24 hours at 70-80 °C. Once cooled over another 24 hours, the specimens were then gold coated with a thin, approximately 20 nm, layer of gold for conductance using an automated sequence sputter coating machine. The SEM used to study the

mortar samples was a model JSM-5610 microscope equipped with secondary and backscattered electron detectors and an Oxford ISIS EDS system, capable of qualitative, pseudo-quantitative analyses, and x-ray mapping. More information on the JSM-5610 is provided in **Table 3-13**.

Table 3-13: Specifications of SEM Used for Imaging and EDS Analysis of Mortars

JEOL Model JSM-5610 SEM Specifications	
Resolution (High Vacuum Mode):	1 μm
Accelerating voltage:	x0.5 to 30kV (53 steps)
Images:	SEI, BEI (COMPO, TOPO,Shadow), EBSD, CL
Magnification	x35 to 100,000 (in 136 steps)
Specimen size	< 150mm
Specimen stage	Eucentric goniometer Range of Motion: X=80mm, Y=40mm, Z=5 to 48mm, T=-10° to 90°, R=360°
Electron Gun	W filament
Emitter	Tungsten hairpin filament
Gun Bias	Automatically settable for all accelerating voltages
Image Shift	+12 micrometer or -12 micrometer
Displayed image	640 x 480 pixels
Analytical Functions	Oxford ISIS EDS system
Detectable element range:	₅ B to ₉₂ U

For the images of all forms of silica, a model JSM-6700F Field Emission Scanning Electron Microscope (FESEM) with higher magnification capabilities was used. The JSM-6700F was optimized for imaging nano-scale specimens. The magnification range is x500 to x430,000 (5 μm to 10 nm). This FESEM was also equipped with SE and BSE detectors. The FESEM is shown in **Figure 3-22** and additional characteristics of the unit are summarized in **Table 3-14**.



Figure 3-22: FESEM Used for Imaging of dry nS, mS, and Aqueous nS

Table 3-14: Specifications of FESEM Used for Imaging of dry nS, mS, and Aqueous nS

JEOL Model JSM6700 FESEM Specifications	
Resolution (High Vacuum Mode)	5 nm
Accelerating voltage:	x0.5 to 30kV
Images:	SEI, BEI (COMPO, TOPO, Shadow)
Magnification	x500 to 430,000
Specimen size	< 50 mm
Specimen Observation Stage	Eucentric goniometer Range of Motion: X=80mm, Y=40mm, Z=2 to 18mm, T=-10° to 90°, R=360°
Electron Gun	Field Emission Gun w/ Cold Cathode
Emitter	Tungsten Single Crystal
Gun Bias	Automatically settable for all accelerating voltages
Displayed image	1024 x 1024 pixels
Image Shift	+1 nanometer or -1 nanometer

RESULTS AND DISCUSSION

Overview of Manuscripts

The results and discussion are presented as an integrated manuscript format where each section is written as a standalone manuscript with introductions, presentation of the results, discussion relevant to their interpretation, conclusions, and any other applicable subsections. A list of manuscripts is presented here as an overview of the focus and topics discussed within. Each manuscript is intended for publication in recognized journals in civil engineering materials and technology. Some are already published and others are in various states of peer review or preparation for submittal.

LIST OF MANUSCRIPTS

Sulfate Resistance of Nanosilica and Microsilica Contained Mortars

Brief Abstract: A side-by-side comparison study intended to identify the effects of nanosilica (nS) on chemical sulfate attack resistance of Portland cement (PC) mortars and its effectiveness in comparison to similar replacement levels of the more widely implemented microsilica (mS).

Blaine and Tricalcium Aluminate Effects on the Sulfate Resistance of Nanosilica and Microsilica Contained Mortars

Brief Abstract: This study was set out to determine the effect of dry powder nS paired with cements of contrastingly different fineness and C_3A content on the sulfate resistance of mortars. Several mortar mixtures of incrementally higher cement replacement with nS or mS were prepared with a 4.1 and 12.3% tricalcium aluminate (C_3A) PC of different fineness.

Effect of Combined Nanosilica and Microsilica on Resistance to Sulfate Attack

Brief Abstract: In this study, the effect of combined nanosilica (nS) and microsilica (mS) on sulfate resistance of Portland cement (PC) mortars was evaluated against all cement control mortars and mixtures with equivalent contents of only one form of silica.

Influence of Dispersion Methods on Sulfate Resistance of Nanosilica Contained Mortars

Brief Abstract: This study evaluates the influence of various dispersion methods on the sulfate attack resistance of nanosilica (nS) contained mortars. Multiple mechanical or ultrasonic dispersion methods, HRWRA dosing procedures, and both dry and aqueous solution forms of nS were used to prepare a series of mortars with 0%, 3%, and 6% replacement of Portland cement with nS.

Influence of Nanosilica on Physical Sulfate Attack Resistance of Mortars (STATUS UPDATE ONLY)

Brief Abstract: The objective of this study was to evaluate the effectiveness of colloidal nanosilica as a nanomaterial and pozzolanic admixture to prevent effects of physical sulfate attack on mortars. Physical sulfate attack is simulated via partial submersion in 10% sodium sulfate solution and either a constant or cyclic ambient condition. This work is still ongoing in order to collect results after more severe deterioration of the mortar samples is observed and quantified via mass loss and a visual rating system.

4 SULFATE RESISTANCE OF NANOSILICA AND MICROSILICA CONTAINED MORTARS

4.1 Abstract

Presented is a side-by-side comparison study intended to identify the effects of nanosilica (nS) on chemical sulfate attack resistance of Portland cement (PC) mortars and its effectiveness in comparison to similar replacement levels of the more widely implemented microsilica (mS). Several mortar mixtures were prepared with a 4.1 and 7.2% tricalcium aluminate (C3A) PC by progressive cement replacement with nS or mS. The mortars tested were measured for expansion, compressive strength, and mass loss. Results indicated that nS replacement benefited the studied mortars. However, in the dry powder form and method of mixing used in this study, poor dispersion and agglomeration of the nS was suspected to hinder mortar permeability in comparison to mS and low C3A cement mortars. Replacement with nS in aqueous dispersion, however, proved to be significantly more effective than equivalent replacement of dry powder nS and mS.

4.2 Introduction

Concrete is one of the most versatile and commonly used construction material in the world and the US alone uses over 300 million cubic meters (400 million cubic yards) a year (Kosmatka et al. 2002). Concrete applications take place in a broad spectrum of environments many of which expose it to conditions that can deteriorate the material, requiring costly repairs or replacement. Sulfate attack is a slow acting deteriorative phenomenon that can lead to progressive failure of concrete exposed to continuous contact with a high sulfate source. External sources include seawater, soils/clays or groundwater high in sulfates, and sewage. Internally sulfate attack can come from cement with excessive gypsum, sulfate rich aggregate, and mineral admixtures (Skalny et al. 2002).

Sulfate attack manifests itself in chemical or physical form, albeit often a combination thereof. The quantifiable and observable effects of sulfate attack include cracking, spalling, expansion, increased permeability, paste to aggregate bond loss, paste softening, and strength loss. Outside of the physical form of sulfate attack due to salt crystallization and its hydrous to anhydrous phase fluctuation, most of the aforementioned effects on concrete are primarily due to the formation of ettringite and gypsum. Excessive ettringite and gypsum in concrete are undesirable since both are expansive and non-strength contributing compounds. Ettringite causes expansive stresses in the pores of the concrete paste, and gypsum causes both expansive stresses and loss of stiffness, adhesion and strength of the cement paste (Skalny et al. 2002; Cohen & Bentur 1988). While sulfate attack alone may not be sufficient to cause failure; cracking, spalling, an increase of porosity and permeability can facilitate and aggravate a host of other deteriorative phenomena such as carbonation, freeze-and-thaw damage and reinforcement corrosion. The challenges and cost with repairing and replacing deteriorated concrete, in addition to the potential for expensive litigation and other unnecessary expenses is the driving factor behind developing sulfate resistant and in general highly durable concrete (Skalny et al. 2002).

The chemical reactions between sulfates and the hydrated cement compounds are well detailed in existing literature (Skalny et al. 2002; Hewlett & Massazza 2003). There is a well-established direct correlation between the tricalcium aluminate [C_3A] content of the cement used in a concrete mixture and the observed degradation of the cement paste due to sulfate attack (Mehta & Monteiro 2006; Mather 1967; ACI Committee 201 2008). Mineral admixtures such as fly ash, silica fume (microsilica), and slag have proven effective at mitigating sulfate attack and are recommended options for durable concrete design by ACI Committee 201 in their Guide to Durable Concrete (ACI Committee 201 2008). Microsilica is a by-product of the silicon and ferrosilicon smelting industries. Physically, microsilica is a filler with particles significantly finer than PC which can refine the concrete pore structure and

improve the quality of the transition zone between aggregate particles and the cement paste. Doing so microsilica effectively decreases the permeability of the concrete which both reduces the passage of harmful ions such as sulfate and the leaching of calcium from the decomposition of Ca(OH)_2 and C-S-H due to sulfate attack. Chemically, microsilica is a pozzolan which chemically reacts with the available Ca(OH)_2 to form a secondary C-S-H. This pozzolanic reaction, paired with a reduction of the available C3A due to the replacement of the cement with microsilica, leads to a reduction in the production of gypsum and ettringite which depend on those precursor constituents (Hewlett & Massazza 2003; Wee et al. 2000). There is strong evidence that control of permeability may be more important than control of cement chemistry in regards to concrete resistance to sulfate attack. This can be successfully achieved through the use of lower water/cement ratios and quality pozzolans such as microsilica in appropriate levels of replacement (Mehta 1993; Khatri et al. 1997).

Concrete research has in the recent years shifted its attention to the nanoscale and in turn nanosilica has become a new mineral admixture being tested following the success of its predecessor. Like microsilica, nanosilica is primarily composed of SiO_2 , but with finer 10 to 150 nm colloidal or amorphous particles available as dry powder or in a stabilized suspension. Based on the current body of research (Singh et al. 2013; Choolaei et al. 2012; Quercia & Brouwers 2010; Tobón et al. 2015; Khanzadi et al. 2010; Said et al. 2012; Sanchez & Sobolev 2010; Sobolev & Gutiérrez 2005), nanosilica also affects concrete durability on a chemical and physical level albeit slightly different from microsilica due to its much finer size. The physical impact is that nS also has a filler effect and takes up the very small nano-scale voids between cement grains in the young and still hydrating cement paste (Singh et al. 2013). This improved particle size distribution and packing in the concrete will result in better strength, durability, and impermeability (Singh et al. 2013; Choolaei et al. 2012). Microstructural analysis has shown that nanosilica also has a paste compaction effect where the silica particles reacts with and serve as a nucleation sites for the C-S-H crystal phase during the initial

hydration. Due to this effect, nanosilica reduces the average C-S-H crystal size which makes the cement paste and interfacial transition zone (ITZ) between the cement paste and aggregate stronger and denser (Singh et al. 2013). This densification of the cement paste results in a more impermeable and stronger mortar or concrete mix. Chemically, due to its larger surface area ($80 \text{ m}^2/\text{g}$ or more), the pozzolanic reaction of nanosilica with $\text{Ca}(\text{OH})_2$ is more aggressive than microsilica and manifests at an earlier age. This accelerated pozzolanic activity could retard the rate of calcium leaching during sulfate attack since $\text{Ca}(\text{OH})_2$ is consumed faster by nS. Nanosilica is also reported to result in higher levels of combined C-S-H gel in later stages of curing (Singh et al. 2013; Quercia & Brouwers 2010). Based on these existing observations it can be hypothesized that nanosilica may improve the sulfate resistance of concrete more effectively than microsilica. In a recent study by Tobón and associates (Tobón et al. 2015) on Portland cement mortars blended with 0, 1, 3, 5, and 10% nanosilica cement replacement, nanosilica reduced sulfate attack related expansions during a 154 week continuous immersion in 5% magnesium sulfate solution. Mortars with 5 and 10% nanosilica replacement decreased expansion by 90% and 95% compared to the control mortar respectively after two years of immersion. Other research showed a superior performance of concretes, mortars and cement pastes with nanosilica replacement in terms of increases of strength, paste densification, impermeability, and chloride penetration resistivity (Singh et al. 2013; Khanzadi et al. 2010; Said et al. 2012; Sobolev & Gutiérrez 2005). These results so far indicate that nanosilica could be very effective in producing highly sulfate resistant concrete, possibly more so than its predecessor microsilica. This study aims to assess this hypothesis.

4.3 Research Significance

The effect of nanosilica on chemical sulfate resistance of PC composites has not yet been extensively evaluated and compared to its predecessor microsilica. Accordingly, this study will provide valuable data regarding the effects of nano and microsilica on the chemical sulfate resistance of PC mortars.

In terms of industrial applications, once more economically viable, the findings of this study can provide an insight into an alternative mineral admixture for improving sulfate durability of PC concrete.

4.4 Experimental Procedure

The studied mortars were subjected to a 79 week (1.5 year) full submersion exposure in 5% sodium sulfate (Na_2SO_4) solution and their expansion, strength, and mass loss were measured.

4.4.1 Materials

Two cement types were tested with very similar specific surface areas (SSA) and different tricalcium aluminate (C_3A) content. The intent was to minimize the cement fineness effect and bring out durability performance against chemical sulfate attack based on C_3A content and nanosilica (nS) or microsilica (mS, also known as silica fume) replacement. The moderate C_3A cement A had a 7.2% and the low C_3A cement B had a 4.1% C_3A content. The chemical and physical properties of the cements used are presented in **Table 4-1**. The nS used was supplied in a porous white dry powder form with particle sizes ranging from 15-20 nm and a specific surface area of 640 m^2/g . It was mechanically blended with the premeasured mixing water for 1 minute prior to use in each mortar mixture. The mS used in the experiment, was a gray amorphous sub-micron powder and was manually dispersed in the cement for each mortar mixture. The chemical and physical properties of the nano- and microsilica are also presented in **Table 4-1**. A polycarboxylate based high-range water-reducing admixture (HRWR) was utilized for achieving the desired flow per ASTM C 109 (ASTM International 2002). In a follow up testing phase, an aqueous dispersion of 25% by weight 5-35 nm amorphous nS was also used in a comparison study between different forms and methods of mixing nS. The fine aggregate used for the mortars in this study was from a Nevada based quarry and had an oven-dry specific gravity of 2.76, absorption of 0.81% and a fineness modulus of 2.64. Its gradation was well inside the upper and lower limits of ASTM C 33 (ASTM International 2003b). Mortar mixing water

and water used for the preparation of the sodium sulfate solution was commercially bottled distilled water obtained from a single source.

Table 4-1: Chemical Composition and Physical Properties of Cement, nS, and mS

	Cement A (Moderate C ₃ A)	Cement B (Low C ₃ A)	micro-Silica (mS)	nano-Silica (nS)
<i>Chemical Composition</i>				
Silicon Dioxide (SiO ₂), %	21.1	21.7	94.72	99.5
Aluminum Oxide (Al ₂ O ₃), %	4	4.1	--	0.002
Ferric Oxide (Fe ₂ O ₃), %	2	4.0	--	0.001
Calcium Oxide (CaO), %	62.7	63.2	--	0.002
Magnesium Oxide (MgO), %	2.1	2.8	--	0.001
Sulfur Trioxide (SO ₃), %	2.8	1.8	0.23	--
Loss on Ignition, %	1.8	0.7	2.82	--
Insoluble Residue, %	0.71	0.1	--	--
Total Alkali (Na ₂ O + K ₂ O), %	0.59	0.46	0.49	--
Free Lime (CaO), %	0	0.8		
<i>Physical Properties</i>				
Time of Set Initial Vicat, min	145	150	--	--
Specific Surface Area, m ² /g	0.341 ^a	0.285 ^a	22.65 ^b	640 ^b
325 Mesh (45 μm), % passing	--	72.9	97.12	
Avg. Particle Size (APS), μm	20-30 ^c	35-45 ^c	0.1-1.0 ^c	0.015-0.020
<i>Per Bogue Calculation^d</i>				
Tricalcium Silicate (C ₃ S), %	57.0	54.0	--	--
Dicalcium Silicate (C ₂ S), %	17.5	21.5	--	--
Tricalcium Aluminate (C ₃ A), %	7.2	4.1	--	--
Tetracalcium Aluminoferrite (C ₄ AF), %	6.1	12.2	--	--
(C ₃ S) / (C ₂ S) Ratio	3.26	2.51	--	--

^a by Blaine air-permeability test

^b by BET Analysis

^c Estimated from MasterSizer Particle Distribution Analysis

^d Bogue Modified Equation for Interground Gypsum & Limestone (Winter 2012a)

4.4.2 Mixture Proportions

Table 4-2 presents the mixture proportions of the mortar mixtures tested in this study. As can be seen, eight mortar groups were prepared for each cement type (moderate and low C₃A); one control mixture with no nS or mS replacement, followed by seven mortar mixtures with progressively higher levels of cement replacement using mS or nS at increments of 1.5% by mass. The water-to-binder ratio was kept constant at 0.485 for all mixtures according to ASTM C 1012 (ASTM International

2004). The fine aggregate-to-binder ratio was 2.75-to-1 by mass as specified in ASTM C 109 (ASTM International 2002).

Table 4-2: Mortar Mixture Proportions for Moderate and Low C₃A Cements

Sample Designation	Binder, %			Measured Flow, %*	3-Day Strength, MPa	Compressive Strength, psi
	Cement	nS	mS			
Moderate C₃A Cement A						
A0	100%	--	--	148%	29.6	4,296
A3mS	97%	--	3.0%	108%	30.5	4,420
A4.5mS	95.5%	--	4.5%	103%	31.9	4,623
A6mS	94%	--	6.0%	95%	30.8	4,463
A1.5nS	98.5%	1.5%	--	117%	34.6	5,013
A3nS	97%	3.0%	--	97%	32.0	4,641
A4.5nS	95.5%	4.5%	--	98%	31.4	4,560
A6nS	94%	6.0%	--	100%	29.9	4,337
Low C₃A Cement B						
B0	100%	--	--	145%	26.6	3,851
B3mS	97%	--	3.0%	127%	23.9	3,463
B4.5mS	95.5%	--	4.5%	115%	23.1	3,350
B6mS	94%	--	6.0%	97%	23.6	3,419
B1.5nS	98.5%	1.5%	--	122%	24.0	3,478
B3nS	97%	3.0%	--	98%	24.5	3,560
B4.5nS	95.5%	4.5%	--	100%	23.3	3,376
B6nS	94%	6.0%	--	102%	22.2	3,226

*Flow measured according to ASTM C 1437 with flow table conforming to ASTM C 230 (ASTM International 2003a)

4.4.3 Mixture and Sample Preparation

Mortar mixtures were batched using an electrically driven epicyclic mechanical mixer following the mortar preparation procedure of ASTM C 305 (ASTM International 1999). For the nS contained mortars, the mixing procedure began with adding the nS powder to the mixing water and mechanically mixing together for 1 minute in a commercial blender before transferring to the mixer. For the mS contained mortars, the mS was homogeneously stirred together with the dry cement prior to placing in the mixer and adding the mixing water. For each studied mixture, 4 mortar expansion bars were prepared per ASTM C 1012 (ASTM International 2004) and 36, 5 cm (2 in), mortar cubes were prepared per ASTM C 109 (ASTM International 2002) for strength testing. Additionally two, 10

cm (4 in), diameter disks were made for supplemental testing. For the nS and mS replacement mixtures, the HRWR was utilized to reach the ASTM C 109 recommended flow of $110\pm 5\%$.

All mortar sample molds were hand packed and compacted using an electromagnetic vibrating table. The sample molds for each mortar mixture were plastic wrapped and kept at room temperature of 21 ± 3 °C (69.8 ± 5.4 °F) for a day then followed by 3 days of curing in a moist room to achieve the required compressive strength of 20 ± 1.0 MPa (2900 ± 145 psi) per ASTM C 1012 prior to sulfate exposure. After the 3 days of moist room curing, three mortar cubes were tested for compression strength to confirm the minimum strength. Following the 3 day curing period, the mortar bars and half of the mortar cubes were transferred to 5% sodium sulfate solution tanks. The remaining cubes were moved to a curing room and tested in compression at the same age of samples immersed in sulfate solution.

4.4.4 Sulfate Solution

The 5% Na₂SO₄ solution was prepared per ASTM C 1012 with a minimum solution to mortar volume ratio of 4. The solution in each container was kept in circulation using submersible pumps. The solution pH was manually rebalanced to 7.0 ± 1 daily with 0.5N H₂SO₄ for the first 6 months and then weekly for the remainder of the extended 1.5 year fully submerged test.

4.5 Experimental Results and Discussion

Table 4-3 documents key expansion readings of all mortar mixtures tested during the 1.5 year sulfate submersion period for convenient reference during the discussion of results. **Figure 4-1** presents the expansion of the control mixtures made purely with cement, without any nS or mS replacement. As evident in the expansion behavior of the control mixtures A0 and B0 in **Figure 4-1**, the low C₃A mixture (B0) performed better than the mixture with the moderate concentration of C₃A (A0). With a progressively longer period of exposure to the sulfate solution, the difference in the expansion

observed between the two mixtures broadened. This implies that at earlier ages, the two mortar mixtures initially exhibit similar behavior and the effect of the different C₃A concentration in the binder is not as apparent. This difference becomes more and more significant under prolonged exposure and clearly distinct past the first 3 months of the test period. There is a linear trend in the expansion of the A0 mortar bars, and an exponential decay reduction in the expansion rate of the B0 mortar bars. Due to the similar cement fineness between the two mixtures, it is reasonable to assume that during initial sulfate exposure, the permeability of the cement paste had a more significant effect on controlling the rate of expansion and the sodium sulfate had not yet permeated through enough of the paste to reach the more abundant C₃A reserves of the A0 mortar. As the sulfate solution permeated deeper into the mortar bars and the monosulfate, calcium and sulfate ions became more abundant, the more favorable C₃A conditions stood out in the expansion behavior and the differences between the two mixtures became more apparent. The expansion of B0 was 20% and 52% less than that of A0 at 8 weeks and 1.5 years of sodium sulfate exposure, respectively.

Table 4-3: Expansion Measurements at Key Time Periods

	A0 CNTL	A3mS 3% mS	A4.5mS 4.5% mS	A6mS 6% mS	A1.5nS 1.5% nS	A3nS 3% nS	A4.5nS 4.5% nS	A6nS 6% nS
4 WEEKS	0.011%	0.009%	0.010%	0.010%	0.011%	0.013%	0.012%	0.012%
8 WEEKS	0.016%	0.012%	0.015%	0.015%	0.019%	0.020%	0.017%	0.019%
12 WEEKS	0.021%	0.017%	0.017%	0.017%	0.023%	0.025%	0.022%	0.021%
26 WEEKS	0.039%	0.028%	0.028%	0.028%	0.038%	0.041%	0.037%	0.034%
1 YEAR	0.074%	0.045%	0.045%	0.043%	0.063%	0.064%	0.058%	0.054%
1.5 YEAR	0.124%	0.056%	0.054%	0.050%	0.092%	0.089%	0.073%	0.063%
	B0 CNTL	B3mS 3% mS	B4.5mS 4.5% mS	B6mS 6% mS	B1.5nS 1.5% nS	B3nS 3% nS	B4.5nS 4.5% nS	B6nS 6% nS
4 WEEKS	0.009%	0.006%	0.006%	0.003%	0.004%	0.006%	0.009%	0.009%
8 WEEKS	0.013%	0.010%	0.010%	0.011%	0.009%	0.013%	0.012%	0.012%
12 WEEKS	0.014%	0.011%	0.013%	0.012%	0.011%	0.013%	0.015%	0.015%
26 WEEKS	0.029%	0.024%	0.026%	0.025%	0.030%	0.032%	0.032%	0.032%
1 YEAR	0.047%	0.041%	0.041%	0.037%	0.050%	0.048%	0.050%	0.050%
1.5 YEAR	0.059%	0.052%	0.050%	0.047%	0.068%	0.067%	0.068%	0.061%

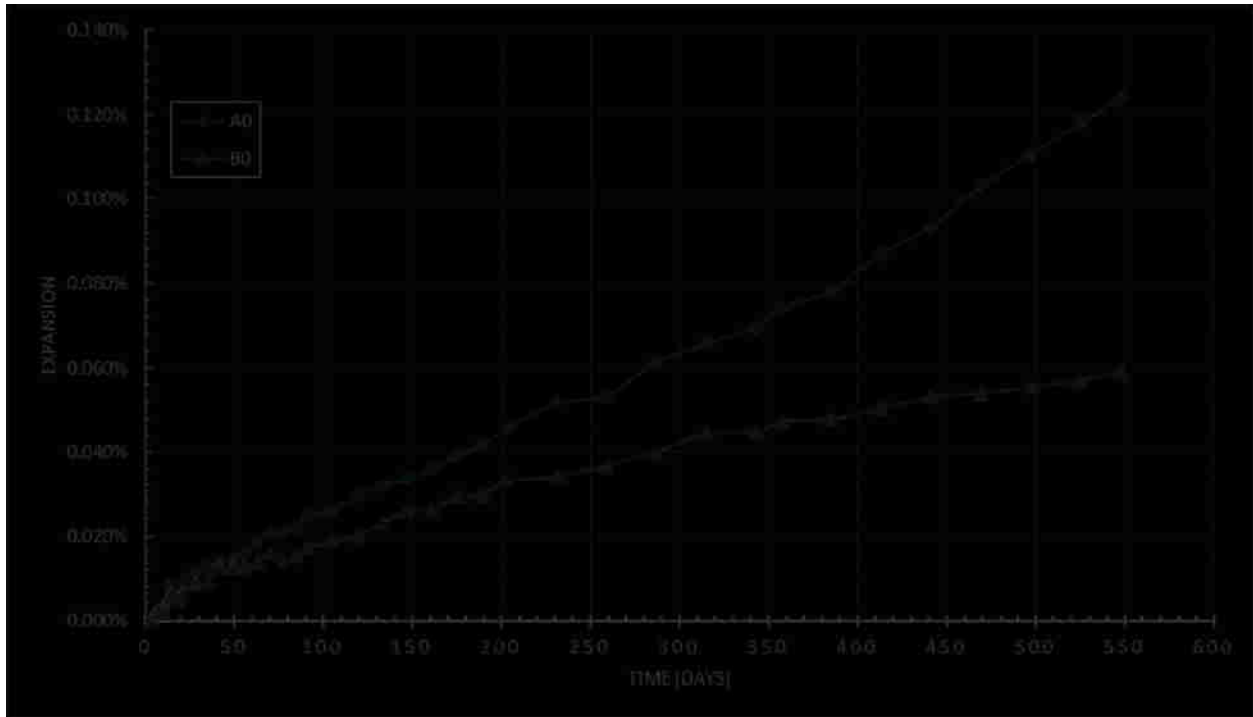


Figure 4-1: Control Mixture Expansion

4.5.1 Influence of Nanosilica

Unless otherwise stated, all statements of nS refers to dry nS powder. **Figure 4-2** shows the expansion of the moderate C₃A Cement mortar series with nS and mS replacement. As can be observed, progressive increases in the level of nS replacement resulted in improvements of the expansion behavior of the studied mortars. These improvements increased by extending the exposure time. The 1 year expansion of the mortars having 1.5, 3, 4.5, and 6% nS replacement were 15, 14, 23, and 28% less than that of the control A0 mortar, respectively. At the 1.5 year point, the same nS replacement mortars had 26, 28, 41, and 49% less expansion than the control mortar, respectively. These percent differences also point out that there were progressive improvements from increasing the percent nS replacement. The expansion for the A1.5nS was 0.063% and 0.092% at 1 and 1.5 years respectively. The expansion for A6nS at those respective ages was 0.054% and 0.063%. As can be seen from the percentages above, at either age, the improvements for 6% nS

replacement was almost twice that of the 1.5% nS replacement, when compared to the control mortar.

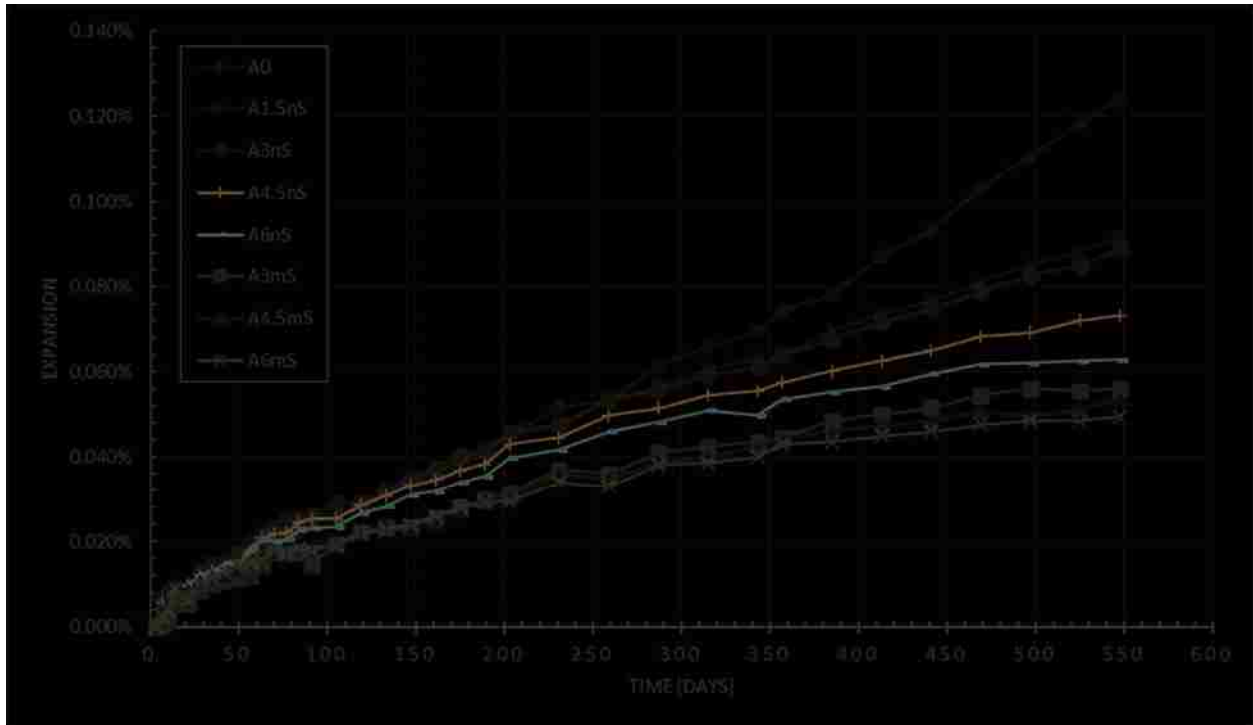


Figure 4-2: 7.2% C_3A Cement A Mixture Series Expansion with nS and mS Replacement

Measurements showed that all mortar mixtures with and without replacements had similar expansion values during the first 4 weeks. There was only a 9% difference between A0 and A6nS at this age. Furthermore, up to the 12 weeks period, the higher nS replacement mixtures exhibited more expansion than their lower replacement counterparts and even the A0 control mortar. This trend reversed following the first 12 weeks and the higher replacements of nS began to outperform the smaller replacements and the control. The early period expansion data indicated that the permeability improvements expected with nS replacement were not clearly evident. This contradicted the superior filler and paste densification effects of nS reported in other studies. In an effort to explain the results, water absorption testing on the control, 3% nS, and 6% nS replacement mortars was performed on three additional disks of each mixture according to ASTM C 642 (ASTM International 1997) to measure the changes in permeability due to nS replacement. The results are

presented in **Figure 4-3**. The absorption test revealed that the nS replacement in this study actually increased the permeability of the mixture when compared to the control mixture. The observed behavior within the first 12 weeks may be related to this increase in the permeability by use of nS. These results contradict trends observed in other studies with nS replacement (Singh et al. 2013; Said et al. 2012).

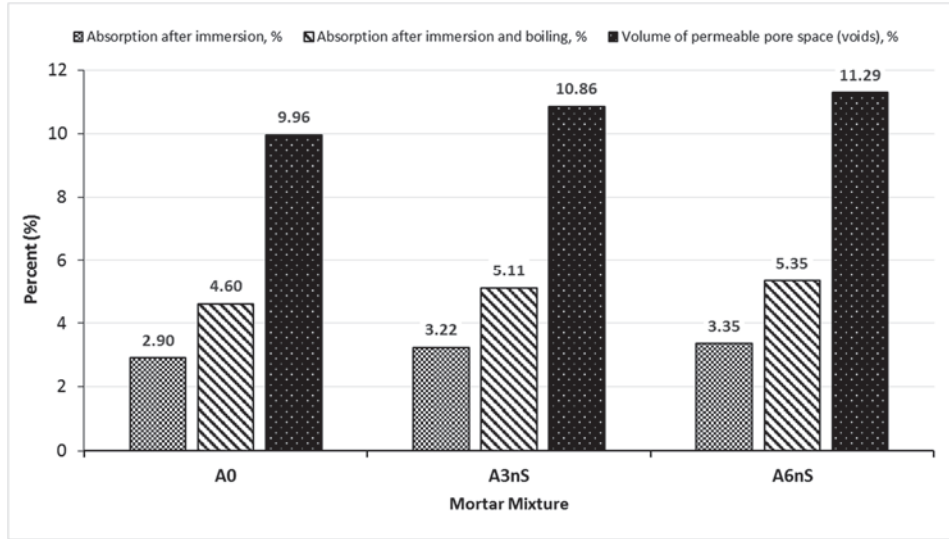


Figure 4-3: Absorption of Cement A Mortars with 0%, 3%, and 6% Dry nS Replacement

Further review of the existing literature, indicated that the most prevalent method of nS replacement in concrete was through their addition in the mixture suspended in an aqueous dispersion where the nS particles are already dispersed as a percentage of the solution mass. Due to the significantly small nature of the nS particles, it is observed that when originally in dry form, nS tends to agglomerate with the addition of water and becomes challenging to mechanically disperse without the aid of specialized dispersants (Singh et al. 2013; Campillo et al. 2004). To investigate if agglomeration of the nS during mixing was present, samples of the dry nS used in the study were submitted for laser diffraction particle analysis along with samples of mS, cement A, and cement B. Prior to measurement, the nS samples were ultrasonically mixed with water for 1 minute, the same period they were dispersed in the mixture water with a commercial blender for the mortar mixtures. The

results as presented in **Figure 4-4** indicated that the average particle size measured for nS was 3 to 12 μm which was multitudes larger than the manufacturer specified nS particle size of .015-0.020 μm . Results indicated that even with ultrasonic mixing the dry nS particles introduced in a plain water suspension tended to agglomerate to a narrowly graded size of clusters significantly larger than the individual nS particles. The agglomerated clusters were also significantly larger than the mS particles, which similarly prepared and tested under laser diffraction, exhibited a broader distribution where 84% of the sample was 0.1-1.0 μm sized particles. The mS particle size closely conformed to the mS manufacturer data and the most typical industry reported mS sizes ($\leq 1.0 \mu\text{m}$) (Holland 2005). Agglomeration of the nS could explain the larger permeability based on water absorption measured between the control and 3% to 6% nS mortars and the larger expansion observed with the nS replacement mortars during the first 12 weeks. It is plausible that the agglomerated nS not only could not fill the nm-size voids in the mortar paste, but the C-S-H paste densification effect of the nanoscale silica particles reported in literature could not easily occur since nS was bound up in clusters before it could interact with the un-hydrated cement.

The nS replacement mortars nevertheless still outperformed the A0 mixture past the 12 week period in terms of lower expansion up to 1.5 years as seen in **Figure 4-2**. The nS replacement still provided some filler effect, and the pozzolanic nature of the nS even in agglomerate form most likely contributed to additional C-S-H production. The negative physical effects of the poorly dispersed nS outweighed the positive pozzolanic effects in the short term sulfate exposure but were overcome given enough continuous exposure to the sulfate solution. The mechanical dispersion method used during mortar mixture preparation could be to blame and became a point of further study.

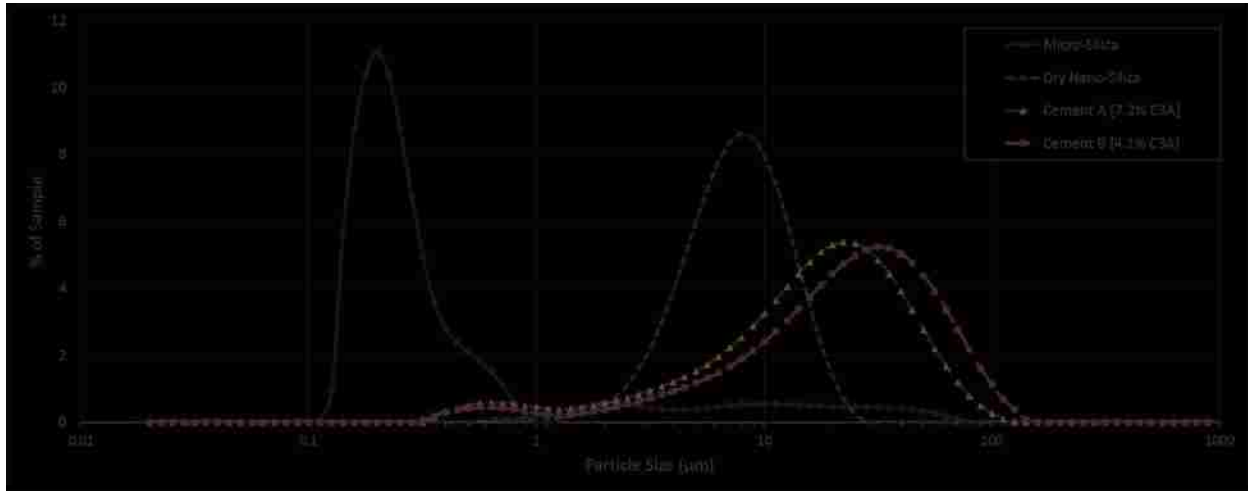


Figure 4-4: Laser Diffraction Particle Size Analysis of nS, mS, cements A and B

In the follow up study, the procured aqueous nS dispersion listed earlier was tested in mortars with the moderate C₃A cement A at 3% (mixture AQ3nS) and 6% (mixture AQ6nS) replacement under a 6 month continuous immersion in 5% Na₂SO₄ solution. During this test phase, a pH controller was used to automatically dose the 0.5N H₂SO₄ and maintain the solution at a constant pH of 6.5±1.0. This measure was implemented to simulate a more aggressive and stabilized sulfate attack environment. The expectation was that now through the use of nS in a properly dispersed aqueous solution, the nS-contained mortars would perform better than both the dry powder nS and mS replacement mortars from the original testing program. The results were supportive of this hypothesis. The control mortar (A0) expansion from the first testing phase was plotted against the control mortar of the second phase (A0.PH2) and the expansion between the two during the initial 6 months were very similar as seen in **Figure 4-5**. As evident in the same figure, the AQ3nS and AQ6nS mortars exhibited less expansion than their comparable A3nS and A6nS counterparts. At 6 months, AQ3nS had expanded 0.027% while A3nS expanded 0.041%, the aqueous nS mortar showed a 34% improvement. For AQ6nS and A6nS, the respective 6 month expansions were 0.023% and 0.034%, which equated to a 32% improvement. Also, AQ3nS did not underperform the control mortar either as was observed

between A3nS and A0. In fact, AQ3nS performed as well as both mS replacement mortars A3mS and A6mS. As clearly evident, AQ6nS performed the best with the smallest percent expansion among this focus group of mortars. At 6 months, AQ3nS showed a 4% improvement over both mS replacement mortars and AQ6nS showed an 18% improvement over A6mS. Note that unlike the higher expansion readings measured for the A3nS and A6nS against the control A0 for the first 12 weeks as discussed earlier, that was not the case for the AQ3nS and AQ6nS mortars. The aqueous nS mortars also performed better than the control at early age sulfate attack which could be reasonably attributed to improvements in the impermeability of the paste. The nS admixture under aqueous form may finally have had the opportunity to exhibit its pore refinement and densification effects as well as an even more aggressive pozzolanic reactivity in comparison to its agglomerated counterpart.

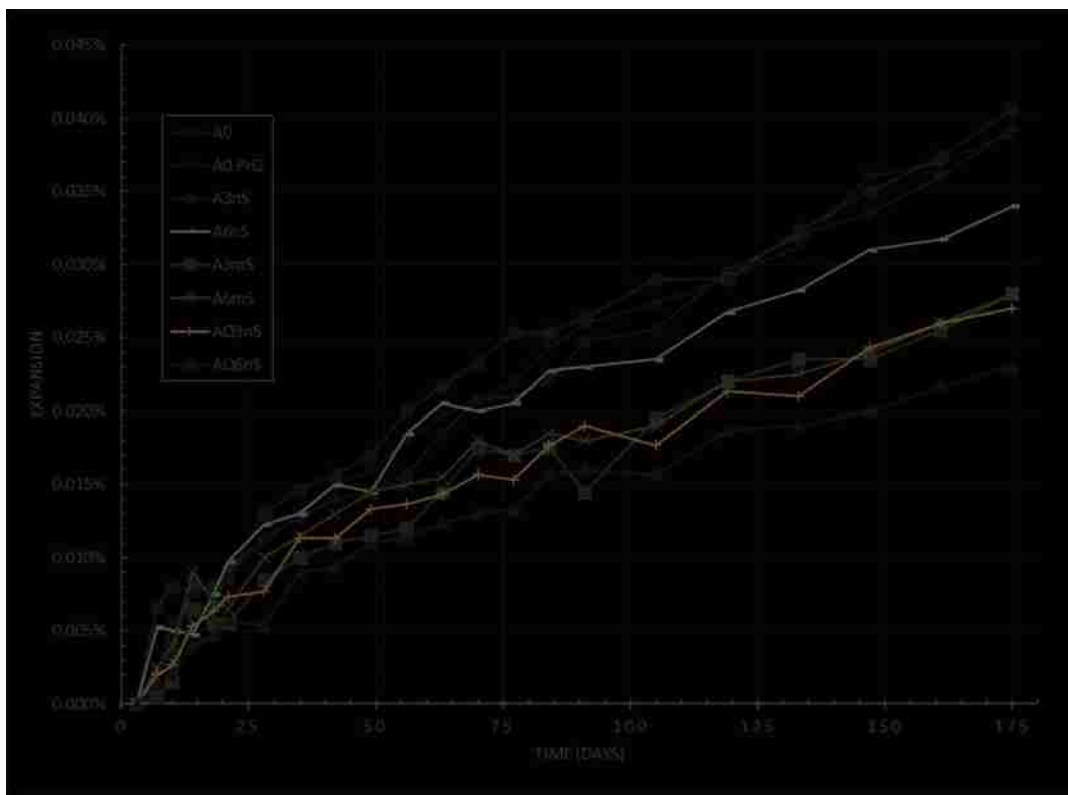


Figure 4-5: 7.2% C₃A Cement A Expansion of Mortars with dry nS, aqueously dispersed nS, and mS Replacement

In the case of the low C₃A cement, the nS-contained mortars generally showed more expansion than the control mortar B0 as seen in **Figure 4-6**. This indicates less chemical sulfate attack resistance in comparison to the control. At 1 year, even the highest nS-contained mortar tested (B6nS), did not show improvement over the smaller levels of nS replacement or the control. There was only 1% measurable difference between the expansion measurements of B1.5nS and B6nS. At 1 year, all the nS replacement expansions averaged around 0.050% which was still 6% more expansion than the control. B6nS does break off from the group and showed improvement over the lesser nS-contained mortars at the conclusion of the 1.5 year test, but that improvement was only 10% from B1.5nS to B6nS. The expansion of the B6nS mortar at 1.5 years was 0.061% which was still 3% more than the 0.059% measured for the control B0 mortar at the end of the test. The observed trend further suggested that for the low C₃A cement, the positive pozzolanic effect of nS on consuming C₃A couldn't outweigh the possible negative effects observed due to agglomeration and resulting higher mortar permeability. In fact, since cement B mortars were inherently more resistant to sulfate attack due to the low C₃A content of the cement, they were, therefore, more sensitive to any negative effects of the nS replacement.

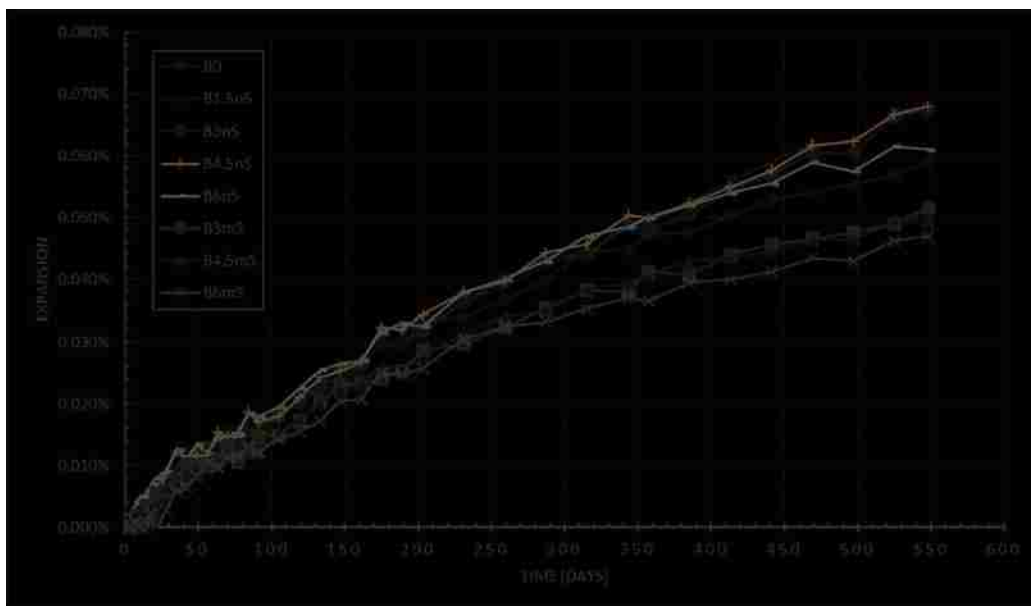


Figure 4-6: 4.1% C₃A Cement B Mixture Series Expansion with mS and nS Replacement

Figure 4-7 presents the expansion of control and nS-contained mortars for both low and moderate C_3A content cements. The inherent sulfate attack resistance of the cement B mortar mixture is evident in this figure; B0 had less expansion than all of the cement A mortars including the nS-contained mortars.

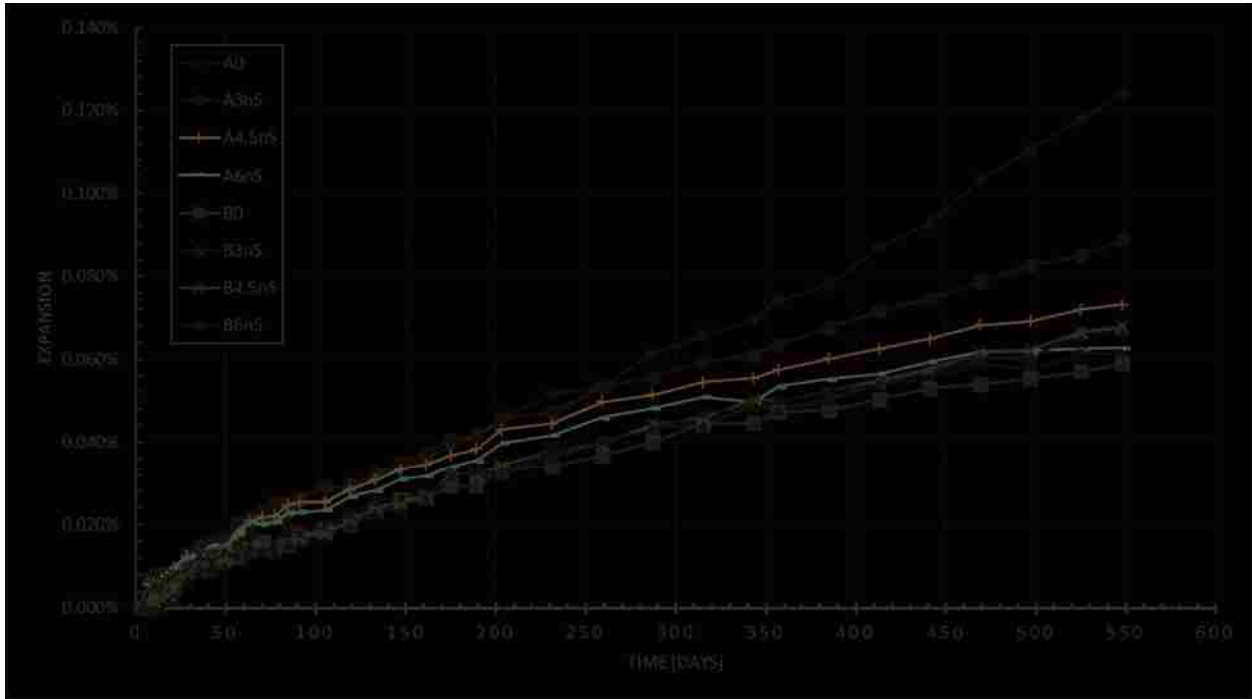


Figure 4-7: 4.1% C_3A vs 7.2% C_3A Cement Mixture Series Expansion with nS Replacement

At 1.5 years, control mixture B0 showed a 33% improvement over A3nS and a 6% improvement over A6nS. Almost all the cement B mortars surpassed the performance of the cement A mortars with the various nS replacements indicating that the benefits gained from the use of dry powder nS in cement A could not negate the negative effect of having almost twice the C_3A as cement B. The contrary was true when comparing the 26 week (6 month) expansion of the low C_3A cement B mortars with that of the aqueous nS replacement mortars. Mortars AQ3nS and AQ6nS had 0.027% and 0.023% expansion, respectively. At the same age, mortars B0, B3nS, and B6nS showed 0.029%, 0.032%, and 0.032% expansion, respectively. AQ3nS and AQ6nS respectively showed an 8% and 22%

improvement over the B0 control mortar. Compared to their respective nS replacement level for the low C₃A cement mortars, the aqueous nS mortars showed a 16% and 27% improvement for 3% and 6% replacement, respectively.

4.5.2 Influence of Microsilica

The use of mS led to significant improvements in sulfate resistance as represented in a reduction of mortar bar expansion in **Figure 4-2**. Cement A mortars with 3, 4.5, and 6% mS replacement had 40, 40, and 42% less expansion respectively than the A0 control mortar at 1 year. The same replacements at 1.5 years had 55, 56, and 60% less expansion respectively than the control. The expansion of the cement A mortars with mS replacement showed that the mS-contained mortars all exhibited very similar levels of expansion indicating that higher levels of mS replacement are not necessarily proportionally beneficial. There is only a 3% observed improvement between A3mS and A6mS at 1 year of submersion in the sodium sulfate solution, meaning that as little as 3% mS replacement provided almost as significant an improvement in chemical sulfate attack durability as if the replacement amount were doubled. The percent difference from A3mS to A6mS was 12% at the end of the test. In comparison the percent difference between the 3% and 6% nS mortars A3nS and A6nS was 34%.

Unlike the nS-contained mortars with the low C₃A cement B, the mS-contained mortars outperformed the control B0 in terms of less expansion; refer to **Figure 4-6**. Progressively higher levels of mS replacement improved the sulfate attack resistance in comparison to the control and lesser mS replacement, but similarly to the cement A mortars, the improvement from the 3% to 6% mS replacement was not significant. The improvements, however, were lower for the low C₃A cement than the moderate C₃A cement. This observation could be related to the less significant mS related chemical improvements in respect to the already sulfate resistant low C₃A cement. After 1 year, the

expansion of mortars was reduced by 13%, 2%, and 10% when the mS replacement was increased from 0 to 3, 3 to 4.5, and 4.5 to 6%, respectively. After 1.5 years, the expansion reductions for the same incremental increases of mS replacement were 12%, 4%, and 5%, respectively. The percent difference between B3mS and B6mS was only 9% indicating again that doubling the mS replacement does not translate to a proportional increase in sulfate attack resistance. Lower levels of C₃A in this cement are evident in that the control mixture B0's lower levels of expansion resulted in a smaller gap between the mS replacement mortars and the control. The improvement between B6mS and B0 at 1.5 years was 20%, more than four times less than that between A6mS and A0.

Unlike nS (dry powder form) replacement, the use of mS in the 7.2% C₃A cement A led to lower expansion than even the low C₃A cement control B0, as can be seen in **Table 4-3**. This observation can be attributed to both the chemical pozzolanic and filler benefits of mS replacement. Based on this observation, it can be deduced that the chemical and filler benefits of mS outweigh the positive effects of reducing the C₃A of the cement.

4.5.3 Comparison between Nanosilica and Microsilica

For the 7.2% C₃A cement A, as **Figure 4-2** indicated, the mS-contained mortars outperformed the control and all nS (dry powder form) contained mortars by having the smallest levels of expansion during the 1.5 year Na₂SO₄ submersion period. This can also be seen in **Table 4-3**. The A3mS mortar performed 30% better than A3nS at 1 year, and 37% better at 1.5 years. The improvement of A6mS over A6nS was 20% and 21% at 1 and 1.5 years respectively. The mS replacement mortars even at the lowest 3% - A3mS, performed better than twice the nS replacement in A6nS, the A3mS expansion at 1.5 years was 11% less than that of A6nS. It is also of interest to note that while at early age of immersion, nS-contained mortars experienced more expansion than the control A0, the mS-contained mortars consistently showed less expansion than the control. These observations at early

age can be related to the improvement in permeability by the use of well-dispersed mS as opposed to agglomerated nS. On the other hand, in well-dispersed form, the aqueous nS resulted in superior sulfate attack resistance in comparison to comparable mS-contained mortars.

For the 4.1% C₃A cement B, while nS-contained mortars did not perform better than the control B0, all the mS-contained mortars did. At 1.5 years of exposure to sodium sulfate solution the expansion measurements of mortars having 3, 4.5, and 6% mS were 23, 27, and 23% lower in comparison to their nS replacement counterparts, respectively. For cement B, the difference between the expansion trends for the progressive nS and mS contained mortars did not broaden with a longer submersion period as much as observed with the cement A mortars indicating that the difference in C₃A between the cements could be the primary factor attributed to this change in behavior. The same negative effect of agglomeration of the nS particularly stood out in cement B where the nS replacement mortars could not compete with the control and the mS mortars. The B6nS mortar with the highest nS content did show improvement, but did not surpass the control. Based on the minimal difference between the B1.5nS to B4.5nS mortars and only marginal improvement of B6nS after the 1 year mark, it is suspected that the negative physical effects on mortar permeability of poorly dispersed nS was challenged by the beneficial pozzolanic and filler effects resulting from higher nS replacements.

If larger levels of nS replacement can completely overcome the negative physical effects due to poorly dispersed nS and show improvements over no replacement in low C₃A cement mortars is unclear in this study. The same levels of replacement with aqueously dispersed nS proved to be significantly more effective with the moderate C₃A cement in later testing. It can be anticipated well-dispersed nS would perform similarly well with low C₃A cement mixtures. The overarching trend observed was that higher levels of mS replacement paired with a lower level of C₃A content in mortar cement consistently led to an improvement in resistance to chemical sulfate attack. As discussed, the spread

in expansion for all mS replacements for both cements is relatively close indicating that even small levels of mS replacement are almost as beneficial as larger levels of replacement. Higher levels of nS replacement seem to benefit mortars, but in the dry powder form and method of mixing used in this test, did not prove to be an improvement over the control for low C₃A cement mortars. Further studies and testing are ongoing to evaluate other forms of nS and methods of mixing in mortars to investigate the effects on sulfate-induced attack durability.

4.5.4 Strength Loss

The compressive strength measurements at the 28 days, 12, 26, and 52 week (1 year) period entailed testing 4 cubes of the sulfate exposed and 4 cubes of the moist room cured mortars for each cement type. Results are summarized in **Figure 4-8** and **Figure 4-9** for the 26 and 52 week tests. The strength ratio added as the secondary y-axis represents the compressive strength of the sulfate solution exposed samples over that of the cure room counterparts. When over the 1.0 line, it indicates that the average compressive strength of the sulfate exposed samples was higher than that of those tested from the cure rom for that particular mortar mixture.

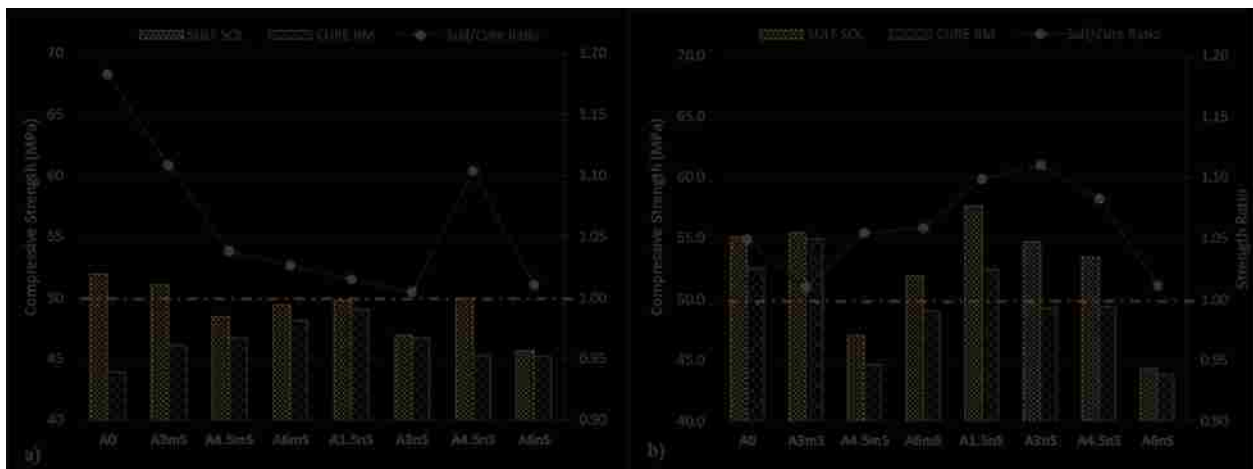


Figure 4-8: 7.2% C₃A Cement A Mortar Cube Compressive Strengths at, a) 26 Weeks, b) 52 Weeks

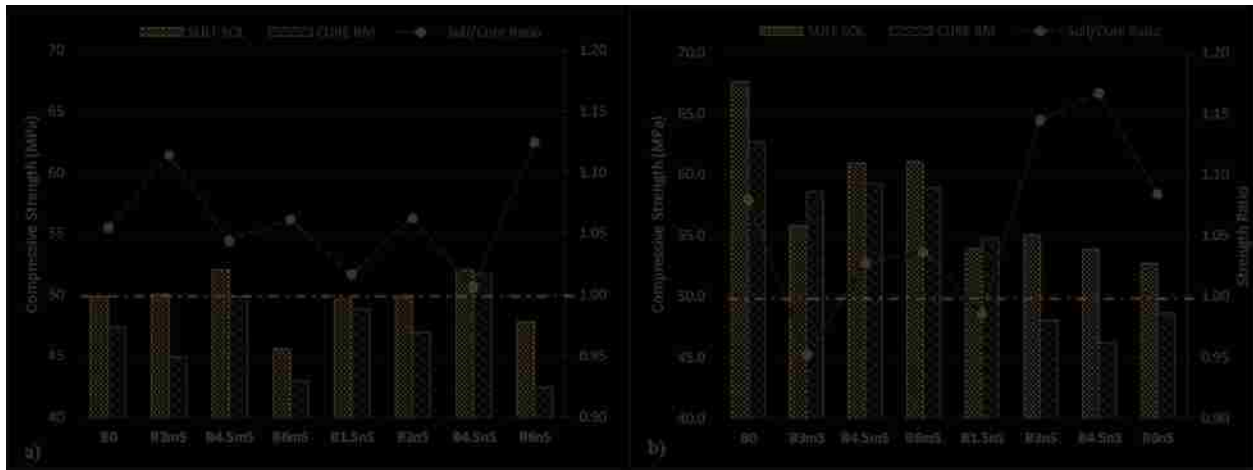


Figure 4-9: 4.2% C₃A Cement B Mortar Cube Compressive Strengths at, a) 26 Weeks, b) 52 Weeks

There was no conclusive evidence that strength loss attributed to sulfate attack occurred during this testing since almost all sulfate solution-to-moist room cured mortar strength ratios were greater than 1. Samples exposed to the sodium sulfate solution in fact showed a consistently higher increase in strength in comparison to the water-cured counterparts. This could be attributed to the generally observed trend for initial increases in strength due to filling and compaction effect of the sulfate attack related expansive compound ettringite (Rundong et al. 2010). This effect may not be permanent and given a longer period of continuous sulfate exposure, strength loss can develop.

It is possible that due to the lower water/binder ratio of 0.485 utilized in this study, compared to other studies where a higher water/binder ratio was used to increase the permeability of mortars, resulted in generally more impermeable mortars where the chemical sulfate attack could not successfully deteriorate the paste sufficiently enough to show strength loss in the 1 year test period. Unfortunately mortar cubes were not available for testing at 1.5 years since that extended period was not originally scoped at the beginning of the test. Additionally, the predominantly basic pH of the sodium sulfate solution as measured for the studied mortars at levels between 10 and 11.5 and only re-balanced at most once in a 24 hour period, possibly meant that the conditions for more extensive

degradation of the C-S-H paste due to gypsum formation could not occur. Ettringite is the more stable expansive compound generated under sulfate attack and generally higher pH (>11.5) conditions (Mehta 1993; Mehta 1975). Studies show that strength loss and softening of the C-S-H paste mostly occurs at lower than 8.0 pH levels (Mehta 1993; Mehta 1975). Under these conditions, the dissolution and depletion of calcium ions from the more easily available calcium hydroxide takes place due to the formation of gypsum and leads to more aggressive de-calcification and progressive deterioration of the C-S-H paste.

4.5.5 Mass Loss

Two, 2-in (5 cm), cube specimens from each mortar mixture, were weighed after the 3 day moist room cure period in a saturated state. They were exposed to an isolated container of 5% sodium sulfate solution for the duration of the test to observe and attempt to measure any mass loss due to chemical sulfate attack.



Figure 4-10: 4.1% C_3A vs 7.2% C_3A Cement mortar cubes after 1 year exposure to Na_2SO_4 solution: a) A0 mortar cubes with observable surface softening and cracking around edges pointed out with arrows, b) B0 mortar cubes with no edge cracking, c) A3mS cubes with some edge cracking, d) B3mS without observable cracking, e) A3nS with observable edge cracking, f) B3nS with observable edge cracking

At the conclusion of the 1.5 year test, there was no measurable mass loss for any of the mortar samples. There was some observable surface softening of the 7.2% C₃A mortars, and some localized cracking near the edges of the control and nS-contained cubes for both cement types (see **Figure 4-10**). In general the 4.1% C₃A mortars and those with mS replacement exhibited less edge cracking. As is evident in the strength testing results, there was insufficient mass loss and softening to result in quantifiable strength loss in the sodium sulfate samples compared to those mortars cured in the moist room.

4.6 Conclusions

The experimental results for this comparison study of chemical sulfate attack on Portland cement mortars with different levels of nano- and microsilica replacements indicated that:

1. Use of mS led to improvements in the expansion of mortars made with both low and moderate C₃A cements. The spread in expansion for all mS replacements for both cements is relatively close indicating that even small levels of mS replacement are almost as beneficial as larger levels of replacement.
2. For mortars made with moderate C₃A content cements, progressively higher cement replacements up to 6% nS reduced the mortar level of expansion in comparison to the control which indicates nS replacement resulted in an overall positive resistance to chemical sulfate attack.
3. For cements with low levels of C₃A, nS replacement did not prove beneficial. This reversal in the trend between the two cements could be attributed to the indication of silica nanoparticle agglomeration that hindered the manifestation of the expected superior pozzolanic and C-S-H paste densification effects expected of nS. The low C₃A cement mortars were inherently more resistant to sulfate attack and were therefore, more sensitive to any negative effects of the nS replacement. Unlike the observations made for the moderate C₃A cement mortars, the

pozzolanic benefit of the poorly dispersed nS could not overcome its negative physical effect on the low C₃A cement mortar permeability even at 1.5 years.

4. The results of this study indicated nS in its dry form was an inferior mineral admixture alternative to mS for chemical sulfate attack durability due to the inherent dispersion challenges of the significantly finer particles. Mortars with mS outperformed those with dry powder nS for both C₃A cements tested.
5. Higher levels of nS replacement seem to benefit mortars, but in the dry powder form and method of mixing used in this test, did not prove to be an improvement over the control for low C₃A cement mortars. The same levels of replacement with aqueously dispersed nS proved to be significantly more effective than dry nS and mS with the moderate C₃A cement in later testing. These results supported the explanation of the observed negative effects of poorly dispersed nS on mortar permeability and resistance to chemical sulfate attack. Currently, nS is a relatively expensive synthetically manufactured nanomaterial, and unlike mS, it is not a byproduct of another industrial process. Therefore, it would seem more economical to procure and properly mix a smaller quantity of well dispersed nS than use excessive cement replacement levels of agglomerated nS.
6. While permeability and cement chemistry both affect the rate of chemical sulfate attack, control of permeability may be more important than control of cement chemistry to produce sulfate resistant concrete. The use of mS improved the sulfate attack resistance more than the improvements resulting from the reduction of C₃A from 7.2% to 4.1%.

5 BLAINE AND TRICALCIUM ALUMINATE EFFECTS ON THE SULFATE RESISTANCE OF NANOSILICA AND MICROSILICA CONTAINED MORTARS

5.1 Abstract

This study was set out to determine the effect of dry powder nS paired with cements of contrastingly different fineness and C_3A content on the sulfate resistance of mortars. Several mortar mixtures of incrementally higher cement replacement with nS or mS were prepared with a 4.1 and 12.3% tricalcium aluminate (C_3A) PC of different fineness. Results indicated microsilica increased sulfate resistance more effectively than nanosilica due to its superior dispersion in comparison to the agglomerated state of the nS. Poor dispersion of the dry powder nanosilica used in this study is suspected to increase mortar permeability and hinder the reported filler, paste, and ITZ densification effects of nS. Mortars made with a lower Blaine and low C_3A cement paired with the agglomerated nanosilica exhibited more sulfate attack expansion in comparison to the control. Microsilica resulted in both pore and grain refinement of the mortar pastes. Increasing cement fineness proved beneficial in combination of either pozzolan regardless of the cement's C_3A content.

5.2 Introduction

Structures are often designed for a particular service life which, depending on the nature and function of the structure, could be 10 to 120 years or more (Dyer 2014). Nevertheless structures will often remain in service well past their design service life and significant effort and resources will be expended to extend their functionality and utilization before resorting to replace them. This design service life is routinely exceeded to maximize the benefit of the structure and the materials and effort invested in constructing it. More and more resources are spent to retrofit and repair concrete structures that have deteriorated due to a combination of neglect and physical and chemical

mechanisms of degradation. Estimated annual costs of repairing concrete structures in Europe has been estimated to exceed \$20 billion (Raupach 2006). The annual repair, protection, and strengthening costs for concrete structures in the US are similarly estimated to be between \$18 and \$21 billion (ICRI 2006). This tendency to extend service life and repair structures rather than replace them has directed a significant effort towards developing construction materials and technologies focused around durability. Concrete is a strong, versatile, and generally chemically inert material with the potential and proven record to last for centuries. These traits and its wide application has made it the topic of continuous research and innovation in an effort to increase its resistance to a broad spectrum of aggressive environments.

Concrete is frequently subjected to one or more chemical mechanisms of degradation. The three main mechanisms are sulfate, alkali-silica reaction (ASR), and acid attack. External sulfate attack is particularly common in the environments in which concrete structures are built. Ingress of sulfate ions released from the dissolution of sulfate minerals such as sodium, potassium, magnesium, and calcium sulfate, react with the hydrated cement compounds and lead to expansion, cracking, and loss of strength and integrity (Skalny et al. 2002). In the presence of a sulfate rich source such as seawater, high sulfate soils, groundwater, or sewage containing sulfate reducing and oxidizing bacteria; sulfate attack can occur. The chemical reactions associated with sulfate attack target the hydrated cement paste compounds C-S-H and calcium hydroxide $\text{Ca}(\text{OH})_2$ that are responsible for strength. The sulfate anions (SO_4^{2-}) primarily leach calcium ions (Ca^{+2}) first from the more soluble $\text{Ca}(\text{OH})_2$ and as it becomes depleted the C-S-H phase. Prevalently, the reaction products associated with sulfate attack are ettringite ($\text{C}_6\text{A}\bar{\text{S}}\text{H}_{32}$) and gypsum ($\text{C}\bar{\text{S}}\text{H}_2$). Both are normally occurring compounds present during initial hydration of concrete, but under sulfate attack are produced once the cement paste has hardened. At this point their volume increasing nature is deleterious since it induces expansive stresses. Sulfate attack is the combined effect of expansion from formation of ettringite and gypsum,

and the progressive loss of strength and cohesiveness due to decalcification and degradation of the $\text{Ca}(\text{OH})_2$ and C-S-H phase. The prevalent reactions associated with sulfate attack have been documented and discussed in further detail in existing literature (Skalny et al. 2002; Hewlett & Massazza 2003; Neville 1998; Odler 1991). Since the sulfate attack reaction producing ettringite also requires alumina either from an AFm phase such as monosulfate ($\text{C}_4\text{A}\bar{\text{S}}\text{H}_{12}$) or unreacted C_3A , there is a recognized direct correlation between cement C_3A content and the susceptibility to sulfate attack (Dyer 2014; Verbeck 1967).

The use of pozzolan such as silica fume as mineral admixture to mitigate sulfate attack is a recommended option for producing durable concrete by ACI in their *Guide to Durable Concrete* (ACI Committee 201 2008). Silica fume is a supplementary cementitious pozzolan that is employed in high performance concrete when a high degree of durability in terms of impermeability, resistivity, and a low diffusivity is desired. Applications include concrete bridges, parking, farming, marine and other structures that would be exposed to high sulfate or chloride conditions (Kosmatka et al. 2002). This is due to the pozzolan's effect on decreasing the permeability and chemical susceptibility of concrete against sulfate and other deleterious ions. Unlike silica fume, referred to from here-on-out as microsilica (mS), nanosilica is a relatively new mineral admixture in the concrete industry which has garnered attention due to its much more aggressive reactivity and similar benefits to concrete durability as mS. Due to its finer nanoscale sized particles, with diameters generally less than 100 nm, nS exhibits a much larger surface area (80 m^2/g and above) than mS (typically 15-30 m^2/g (Holland 2005)). This results in an accelerated pozzolanic activity that offers benefits to concrete similar in nature, but in most cases reported, superior those observed with mS. They include, faster production and overall more secondary C-S-H in comparison to mS at a given age; improved paste/ITZ densification; reduced permeability and chloride diffusivity; and increased compressive strength (Sanchez & Sobolev 2010; Singh et al. 2013; Quercia & Brouwers 2010).

The effects of cement fineness in combination with a high fineness pozzolan such as nS on sulfate durability has not yet been extensively investigated. Would a high surface area cement pair well with a high surface area pozzolan and how much significance would the C₃A content of the cement have? The common purpose behind increasing cement fineness is for high early strength (Kosmatka & Wilson 2016; Neville 1998). Cements of high fineness are popular in applications such as oil well cementing, grouting in tunneling and excavations, and other applications where achieving high early strength is desirable (Kontoleonos et al. 2012). High fineness cements also exhibit a higher rate of early heat of hydration, increase shrinkage, reduce bleeding, and increase the risk of cracking (Neville 1998). They are also more capable of binding free ions such as chlorides and sulfates (Richardson 2002). This is in part due to the reactive nature of aluminates. At an early age when the aluminates are in an unreacted state, they are very effective at binding with free ions. A higher surface area facilitated by a finer ground cement paired with a higher C₃A content means that a higher abundance of aluminates would be available for reaction with sulfate. This theory is supported by existing research. In one study the same cement was ground to two different levels of fineness, and the one with the higher surface area exhibited more expansion after 3 years of curing when both contained an identical content of inter-ground gypsum serving as the source of sulfate (Odler 1991). The higher cement fineness augments the significance of the cement's C₃A content. A higher cementitious topochemical surface area exposes more Ca(OH)₂ which would be susceptible to reaction in the presence of sulfate ions. That would then accelerate and increase the generation of sulfate attack formed gypsum (CaSO₄*2H₂O). Some of that gypsum would then target a more readily available and exposed unreacted C₃A or monosulfate and generate more of the expansive AFt phase, ettringite. In a similar sense on the other hand, a higher surface area would also make the same cement more receptive to a pozzolanic mineral admixture such as mS and nS. A high Blaine cement presents the SiO₂ particles of mS and nS with a larger topochemical reaction area from the binder. This would

accelerate the pozzolanic reactions with Ca(OH)_2 and generate secondary C-S-H faster. The pozzolanic and sulfate attack reactions would both benefit from a higher fineness of the cement phases. It is reasonable to consider that the faster the rate at which Ca(OH)_2 can form during hydration and be bound by a pozzolan as secondary C-S-H, the less there will be for reaction with sulfate ions. The hydration and pozzolanic reactions near the surface of a mortar sample would be in direct competition with those of sulfate attack for (Ca^{+2}) ions. Cements of higher Blaine have finer cement particles which reduces the space between particles and provides for better packing of the paste as it hydrates. When mS and nS are also included they serve as additional nucleation sites for where Ca(OH)_2 would form in between the hydrating cement grains. That additional Ca(OH)_2 would then proceed to react with the pozzolan around which it is formed. Additionally, the mS or nS in their own part contribute to a particle packing effect, and a densifying effect on the aggregate to cement paste interfacial transition zone referred to as the ITZ. These physical effects of mS or nS would make the binder-aggregate matrix more impermeable to sulfate ions (ACI Committee 234 2006; Neville 1998). It was this researcher's expectation that a higher Blaine cement paired with the finer particle pozzolan nS would result in a denser more impermeable cement paste and ITZ, and with overall less available Ca(OH)_2 susceptible to sulfate attack. This combination would result in an overall more sulfate resistance mortar that would exhibit less expansion under exposure to 5% sodium sulfate solution. In combination with a high fineness pozzolan, the chemistry of the cement in terms of its C_3A content, might not be as relevant. In another study, colloidal nS was tested on mortars and cement pastes made with a cement ground to two different levels of fineness, paired with either 2 or 4% nS. The higher Blaine cement paired with the larger 4% dose of nS exhibited the most in reduction in total porosity, average pore size diameter, most densification of paste microstructure, and biggest increases in compressive strength at 7 and 28 days (Kontoleonos et al. 2012). The author was interested in investigating the impacts of nanosilica (nS) on the sulfate resistance of a cement with

high Blaine (450-600 m²/kg) but also high C₃A (>8%) in comparison to that of a sulfate resistant Type V (<5% C₃A) cement of an average Blaine (280-400 m²/kg).

5.3 Research Significance

In terms of resistance to sulfate attack, the effectiveness of nS paired with cements of varying fineness and C₃A content is not yet well understood and investigated in direct comparison to the more industry established microsilica. Accordingly, this study provides valuable data and insight into the effectiveness of nS when paired with cements of different Blaine and C₃A content. In future industry applications, for cases where nS may be an economically viable pozzolan, the findings of this study can provide insight when specifying criteria for suitable PC cements or predicting the effectiveness of nS in increasing a given concrete mixtures' resistance to sulfate attack.

5.4 Experimental Procedure

The expansion data of mortars tested in this study is based on 79 weeks (1.5 year) of full submersion in 5% sodium sulfate (Na₂SO₄) solution. Compressive strength was also measured at 3 days, 28 days, 3 months, 6 months, and 1 year. Rapid sulfate ion penetration test (RSPT) and mercury intrusion porosimetry (MIP) were used to assess the porosity, diffusivity, and permeability of select mixtures. Heat of hydration was also measured for mortars with 6% mS or nS to assess the rate of hydration and pozzolan reactivity paired with each of the two cements tested.

5.4.1 Materials

The two cement types tested feature contrastingly different specific surface areas (SSA) and C₃A content. The author's intent was to investigate if cement fineness or C₃A content was a more influential factor to the durability performance against chemical sulfate attack of nanosilica (nS) or

microsilica (mS) contained mortars. Cement L had both a low C₃A content of 4.1% and a lower SSA of 0.285 m²/g (1,392 ft²/lb). Cement H had three times the C₃A content (12.3%) and almost double the SSA (0.546 m²/g (2,666 ft²/lb)). The chemical and physical properties of the cements used are presented in **Table 5-1**. The nS used was supplied in a porous white dry powder form with reported particle sizes ranging from 15-20 nm (0.59-0.787×10⁻⁶ in) and a reported SSA of 640 m²/g (3.13×10⁶ ft²/lb). The mS used in the experiment, was a gray amorphous sub-micron powder. The chemical and physical properties of the nano- and microsilica are also presented in **Table 5-1**.

Table 5-1: Chemical Composition and Physical Properties of Cement, nS, and mS

	Cement L (Low C ₃ A)	Cement H (High C ₃ A)	micro-Silica (mS)	nano-Silica (nS)
<i>Chemical Composition</i>				
Silicon Dioxide (SiO ₂), %	21.7	20.8	94.72	99.5
Aluminum Oxide (Al ₂ O ₃), %	4.1	5.4	--	0.002
Ferric Oxide (Fe ₂ O ₃), %	4.0	1.2	--	0.001
Calcium Oxide (CaO), %	63.2	63.5	--	0.002
Magnesium Oxide (MgO), %	2.8	2.7	--	0.001
Sulfur Trioxide (SO ₃), %	1.8	3.3	0.23	--
Loss on Ignition, %	0.7	1.2	2.82	--
Insoluble Residue, %	0.1	0.1	--	--
Total Alkali (Na ₂ O + K ₂ O), %	0.46	0.44	0.49	--
Free Lime (CaO), %	0.8	0.8		
<i>Physical Properties</i>				
Time of Set Initial Vicat, min	150	70	--	--
Specific Surface Area, m ² /g	0.285 ^a	0.546 ^a	22.65 ^b	640 ^b
325 Mesh (45 μm), % passing	72.9	99.7	97.12	
Avg. Particle Size (APS), μm	35-45 ^c	10-20 ^c	0.1-1.0 ^c	0.015-0.020
<i>Per Bogue Calculation^d</i>				
Tricalcium Silicate (C ₃ S), %	54.0	53.0	--	--
Dicalcium Silicate (C ₂ S), %	21.5	19.6	--	--
Tricalcium Aluminate (C ₃ A), %	4.1	12.3	--	--
Tetracalcium Aluminoferrite (C ₄ AF), %	12.2	3.7	--	--

^aby Blaine air-permeability test

^bby BET Analysis

^cEstimated from MasterSizer Particle Distribution Analysis

^dBogue Modified Equation for Interground Gypsum & Limestone (Winter 2012a)

A polycarboxylate based high-range water-reducing admixture (HRWR) was used to achieve the desired flow per ASTM C 109 (ASTM International 2002). The fine aggregate used for the mortars in this study was from a locally based quarry and had an oven-dry specific gravity of 2.76, absorption

of 0.81% and a fineness modulus of 2.64. Its gradation was well inside the upper and lower limits of ASTM C 33 (ASTM International 2003b). Mortar mixing water and water used for the preparation of the sodium sulfate solution was commercially bottled distilled water obtained from a single source.

5.4.2 Mixture Proportions

Proportions of the mortar mixtures tested in this study are presented in **Table 5-2**. Eight mortar mixtures were prepared for each cement; one control mixture with no nS or mS replacement, followed by 7 silica contained mortar mixtures. Four of them contained 1.5% to 6% of nS, the dosage increasing in 1.5% increments, and three other mixtures contained 3%, 4.5% or 6% mS. The water-to-binder ratio was kept a constant 0.485 for all mixtures according to ASTM C 1012 (ASTM International 2004). The fine aggregate-to-binder ratio was 2.75-to-1 by mass as specified in ASTM C 109 (ASTM International 2002).

Table 5-2: Mortar Mixture Proportions for Low and High C3A Cements

Sample Designation	Binder, %			Measured Flow, %*	HRWRA Used, g	3-Day Compressive Strength,	
	Cement	nS	mS			MPa	psi
Low C₃A Cement L							
L0	100	--	--	145	0.0	26.6	3,851
L3mS	97	--	3.0	127	0.0	23.9	3,463
L4.5mS	95.5	--	4.5	115	0.0	23.1	3,350
L6mS	94	--	6.0	97	0.0	23.6	3,419
L1.5nS	98.5	1.5	--	122	0.0	24.0	3,478
L3nS	97	3.0	--	98	0.0	24.5	3,560
L4.5nS	95.5	4.5	--	100	4.0	23.3	3,376
L6nS	94	6.0	--	102	7.0	22.2	3,226
High C₃A Cement H							
H0	100	--	--	123	5.8	35.6	5,164
H3mS	97	--	3.0	110	5.6	35.5	5,146
H4.5mS	95.5	--	4.5	100	9.0	34.3	4,975
H6mS	94	--	6.0	105	9.5	35.1	5,088
H1.5nS	98.5	1.5	--	100	14.0	32.2	4,673
H3nS	97	3.0	--	97	18.0	31.2	4,527
H4.5nS	95.5	4.5	--	97	28.7	37.7	5,462
H6nS	94	6.0	--	110	43.5	34.4	4,984

*Flow measured according to ASTM C 1437 with flow table conforming to ASTM C 230

5.4.3 Mixture and Sample Preparation

Mortar mixtures were batched using an electrically driven epicyclic mechanical mixer following the mortar preparation procedure of ASTM C 305 (ASTM International 1999). The nS was blended with the mixing water for 1 minute in a commercial blender. The mS powder was homogeneously intermixed with the dry cement for each mortar mixture prior to adding them to the mixer. Four mortar expansion bars were cast for measuring sulfate attack induced expansion per ASTM C 1012 criteria (ASTM International 2004). For compressive strength testing, 36, 5 cm (2-in) mortar cubes specimens were prepared per ASTM C 109 (ASTM International 2002). Supplemental 10 cm (4-in) diameter by 5 cm (2-in) disks were made for the RSPT testing. The mortar samples prepared for the heat of hydration testing were 10 cm (4-in) diameter by 10 cm (4-in) cylinders. Where necessary, the HRWR was utilized to target an ASTM C 109 recommended flow of $110\pm 5\%$. The required HRWRA dosages used for each mixture are also reported in **Table 5-2**. All mortar sample molds for each mortar mixture were then wrapped in plastic and kept at room temperature (21 ± 3 °C) for a day. This was followed by 3 days of curing in a moist room to achieve the required compressive strength of 20 ± 1.0 MPa (2900 ± 145 psi) per ASTM C 1012 prior sulfate exposure. After the 3 days of moist room curing, three mortar cubes were tested for compression strength to confirm the minimum strength. At that point, the mortar bars and half of the mortar cubes were transferred to 5% sodium sulfate solution tanks. The remaining cubes were kept in the moist curing room and tested in compression at the same age of samples immersed in sulfate solution.

5.4.4 Sulfate Solution

The 5% Na_2SO_4 solution was prepared per ASTM C 1012. Each tank was filled to maintain a calculated minimum solution to mortar volume ratio of 4. The solution in each container was kept in circulation using submersible pumps. To replenish the supply of sulfate ions in the solution (Mehta 1975), the

solution's pH was manually rebalanced to 7.0 ± 1 daily with 0.5N H_2SO_4 for the first 6 months and then weekly for the remainder of the extended 1.5 year fully submerged test.

5.4.5 RSPT, Mercury Intrusion Porosimetry, Heat of Hydration

The RSPT test, as proposed in the Sulfate-Resisting Concrete report by Cement Concrete & Aggregates Australia (CCAA 2011), is similarly setup to the traditional ASTM C 1202 rapid chloride permeability test (RCPT). In this study, a 10% Na_2SO_4 solution was used across the 0.3N NaOH instead of 3% NaCl; three 28 day-cured mortar disks were used for each reported average penetration reading. For porosity and pore size distribution analysis, small fragments of mortar collected from different samples of the select mixtures presented in the results were used for mercury intrusion porosimetry (MIP). The samples taken were all from the interior of samples to avoid any mold effects. The heat of hydration samples were prepared separately following the same mixing procedure stated earlier. Immediately after compacting and wrapping in plastic, the cylinder molds were placed in individual well insulated adiabatic casings. A type K thermocouple wire was embedded at the center of the sample and connected to a data logger that collected temperature readings every 30 seconds for the first 48 hours of hydration.

5.5 Experimental Results and Discussion

5.5.1 Sulfate Attack Expansion

Some of the key mortar bar expansion readings from the 1.5 year sulfate exposure period are summarized in **Table 5-3** as a convenient reference during the discussion of results.

Table 5-3: Expansion Measurements at Key Time Periods

	L0 CNTL	L3mS 3% mS	L4.5mS 4.5% mS	L6mS 6% mS	L1.5nS 1.5% nS	L3nS 3% nS	L4.5nS 4.5% nS	L6nS 6% nS
4 WEEKS	0.009%	0.006%	0.006%	0.003%	0.004%	0.006%	0.009%	0.009%
8 WEEKS	0.013%	0.010%	0.010%	0.011%	0.009%	0.013%	0.012%	0.012%
12 WEEKS	0.014%	0.011%	0.013%	0.012%	0.011%	0.013%	0.015%	0.015%
26 WEEKS	0.029%	0.024%	0.026%	0.025%	0.030%	0.032%	0.032%	0.032%
1 YEAR	0.047%	0.041%	0.041%	0.037%	0.050%	0.048%	0.050%	0.050%
1.5 YEAR	0.059%	0.052%	0.050%	0.047%	0.068%	0.067%	0.068%	0.061%
	H0 CNTL	H3mS 3% mS	H4.5mS 4.5% mS	H6mS 6% mS	H1.5nS 1.5% nS	H3nS 3% nS	H4.5nS 4.5% nS	H6nS 6% nS
4 WEEKS	0.012%	0.004%	0.002%	0.002%	0.007%	0.008%	0.006%	0.005%
8 WEEKS	0.021%	0.010%	0.005%	0.007%	0.014%	0.014%	0.010%	0.010%
12 WEEKS	0.024%	0.010%	0.006%	0.008%	0.018%	0.017%	0.014%	0.013%
26 WEEKS	0.050%	0.021%	0.016%	0.017%	0.035%	0.031%	0.024%	0.023%
1 YEAR	0.226%	0.036%	0.030%	0.030%	0.069%	0.054%	0.042%	0.040%
1.5 YEAR	0.827%	0.045%	0.037%	0.039%	0.178%	0.086%	0.055%	0.049%

Without the presence of either pozzolan, the expansion behavior of the control mortars clearly highlight the difference in C₃A content between the two cements. As evident in **Figure 5-1**, the low C₃A mixture (L0) performed significantly better than the mixture with the high concentration of C₃A (H0). With a progressively longer period of exposure to the sulfate solution, the difference in the expansion observed between the two mixtures broadened. This implies that at earlier ages, the two mortar mixtures initially exhibited similar behavior and the effect of the different C₃A content in the binder was not as apparent. This difference became exponentially more significant under prolonged exposure and clearly distinct past the first 3 months of the test period. There was an exponentially increasing trend in the expansion of the H0 mortar bars, and a linear trend in the expansion rate of the L0 mortar bars. The higher abundance of aluminates combined with a higher reactive area due to the fineness of cement in H0 ultimately presented itself in a much more aggressive rate of sulfate attack induced expansion. Without a pozzolan to not only physically reduce the permeability but also chemically bind calcium ions released from their main source Ca(OH)₂, the high C₃A and high SSA cement mortar H0 proved to be poorly resistant to sulfate attack. In comparison, the expansion of L0 was 60% that of H0 at 8 weeks and only 7% that of H0 after 1.5 years of sodium sulfate exposure.

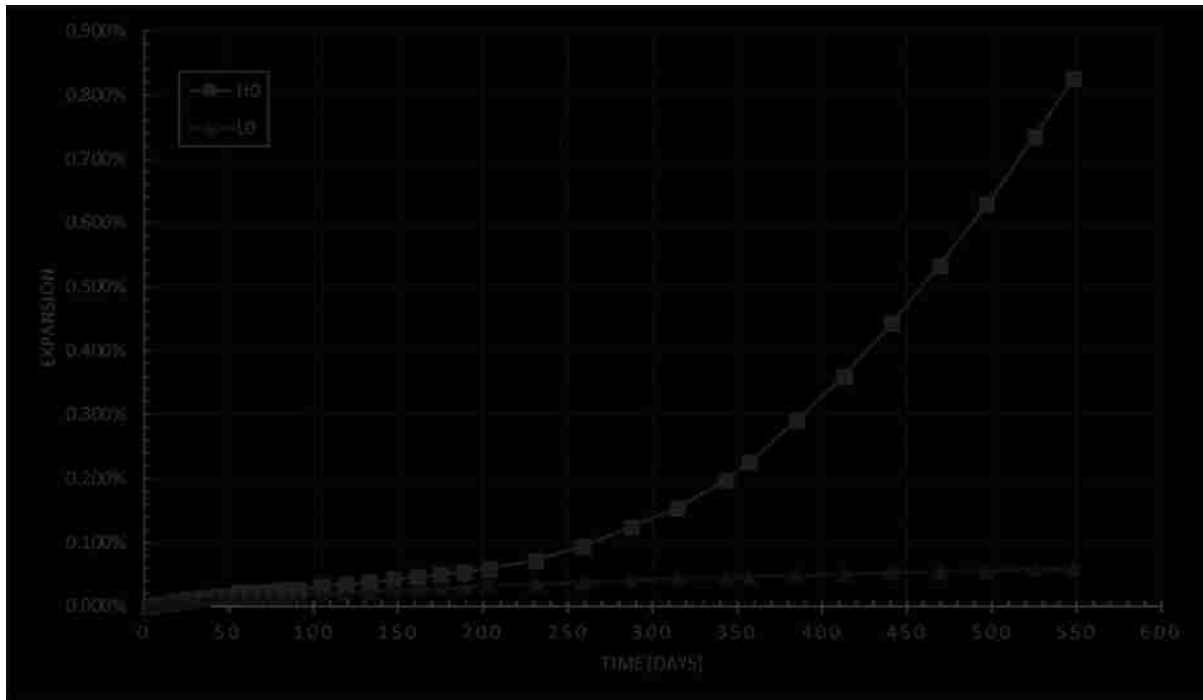


Figure 5-1: Sulfate Attack Expansion for Control Mortars

5.5.1.1 Influence of Nanosilica and Microsilica

The sulfate expansion readings of all cement L mortar mixtures are presented in **Figure 5-2**. These expansions contradicted the expectations that nS replacement would have a beneficial effect. The nS contained mortars exhibited more expansion during the 1.5 year testing period compared to the control mixture L0. There was also no clear and discernable improvement with higher levels of nS replacement from 1.5% to 4.5%. Only nS contained mortar L6nS showed marginal improvements over its lower replacement counterparts which only manifested past the 1 year exposure mark. At the conclusion of the test, L6nS exhibited 90% the expansion measured for L4.5nS. Nevertheless, the control L0 mixture had 97% the expansion of L6nS after 1.5 years of sodium sulfate exposure. For the 6 month, 1 year and 1.5 year period, L0 exhibited on average 92%, 96%, and 90% of the expansion measured for the nS contained mortars, respectively.

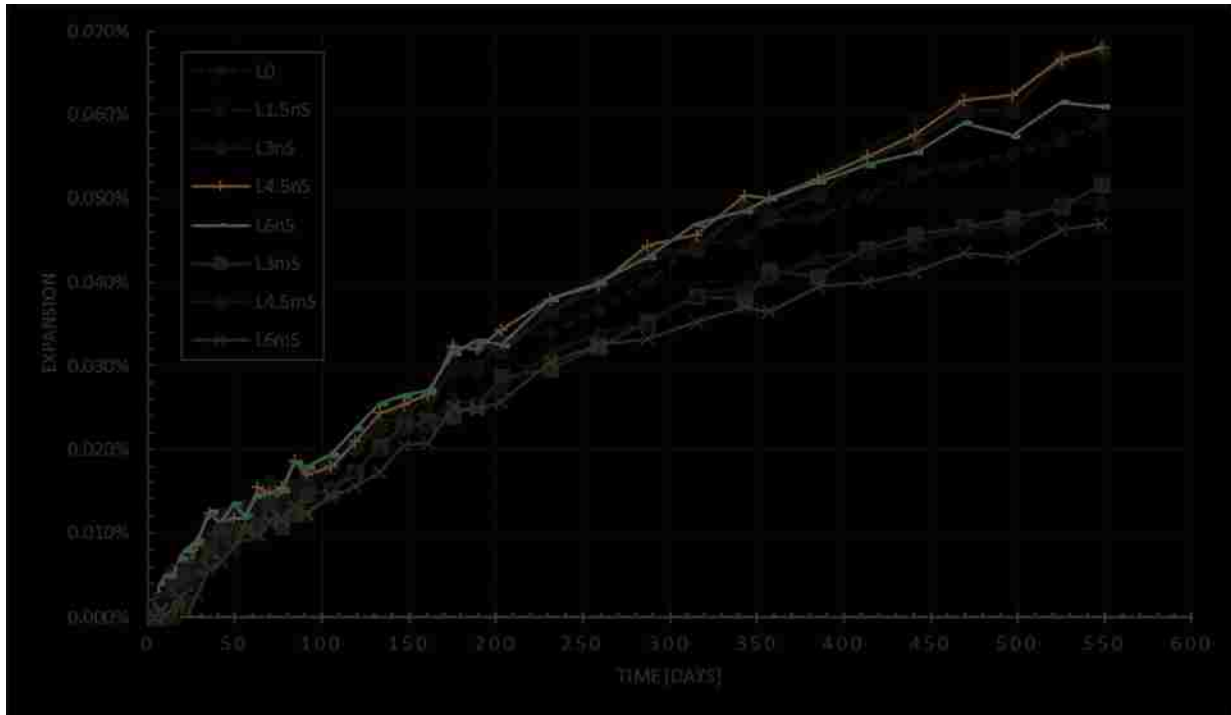


Figure 5-2: Cement L (4.1% C₃A / SSA = 285 m²/kg) Mortar Series Expansion

The mS replacement mortars for cement L all outperformed the control mixture L0. There was not a consistent and quantifiable difference between the performance of L3mS and L4.5mS. L6mS performed the best with the least expansion which after 1.5 years sulfate exposure was 80% that of the control mixture L0. The data indicated that the permeability improvements expected with nS replacement were not clearly evident in the expansive behavior of the cement L mortars. Considering that Cement L was inherently sulfate resistant due to its low C₃A content, meaning the control L0 was expected to perform favorably overall, these results contradicted the superior filler, pozzolanic, and paste densification effects of nS reported in other studies (Singh et al. 2013; Said et al. 2012; Kontoleon et al. 2012). The expectation was that nS replacement would have proven advantageous to the already sulfate resistant cement. It appeared that the nS was unable to either physically improve the permeability of the mortar or successfully deploy the full range of its reported pozzolanic benefits to limit the hydrated paste's susceptibility to the sulfate attack related reactions.

The cement L mortars containing mS on the other hand did perform favorably in terms of expansion. It was suspected the nS did not perform as intended and the cause of that was explored further with the supplemental testing presented and discussed later.

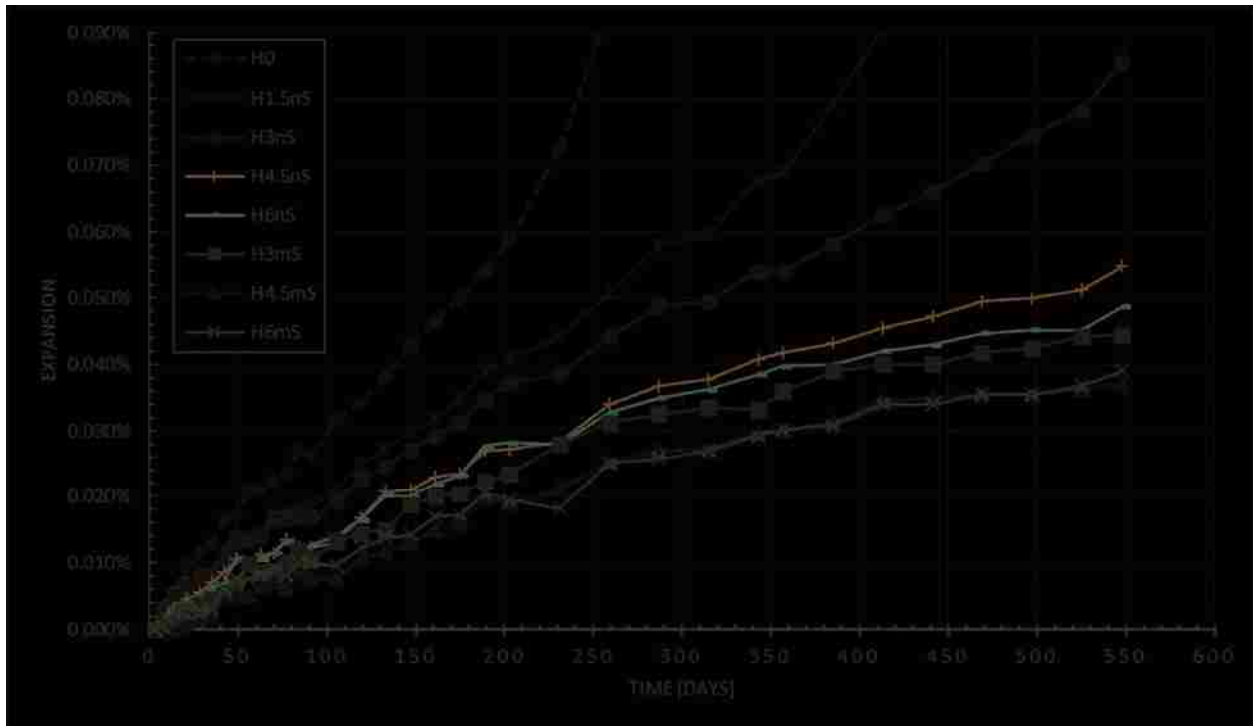


Figure 5-3: Cement H (12.3% C₃A / SSA = 546 m²/kg) Mortar Series Expansion

The results for the cement H mortar series presented in **Figure 5-3** were different. No silica contained mortar exhibited more expansion than the control mortar (H0) during the testing period. Similar to the cement L series, the mS mortars exhibited the least sulfate attack related expansion. As pointed out earlier, cement H had three times the C₃A content but also almost twice the SSA of cement L. Here the pozzolanic reactivity of both silica's seemed to have been sufficient to boost the sulfate resistance of the cement. Unlike the cement L mortars, with this series the increase of the nS content from 1.5% to 6% content proved significantly beneficial. At the conclusion of the test, H1.5nS experienced 0.178% expansion, and H6nS expanded 0.049%. H1.5nS and H6nS had 22% and 6% the expansion

measured for the control mortar H0, respectively. The impact of the pozzolan in this cement was much more significant. The mS contained mortar mixtures still outperformed the nS contained ones. Even H3mS with half the silica content of H6nS, exhibited on average 88% the expansion measured for the 6% nS mixture H6nS. When comparing H6nS with H6mS, the mS contained mortar on average had 70% the expansion of its nS counterpart; not more than 80% the expansion of H6nS at 1.5 years exposure. With both cements the performance of the nS was underwhelming.

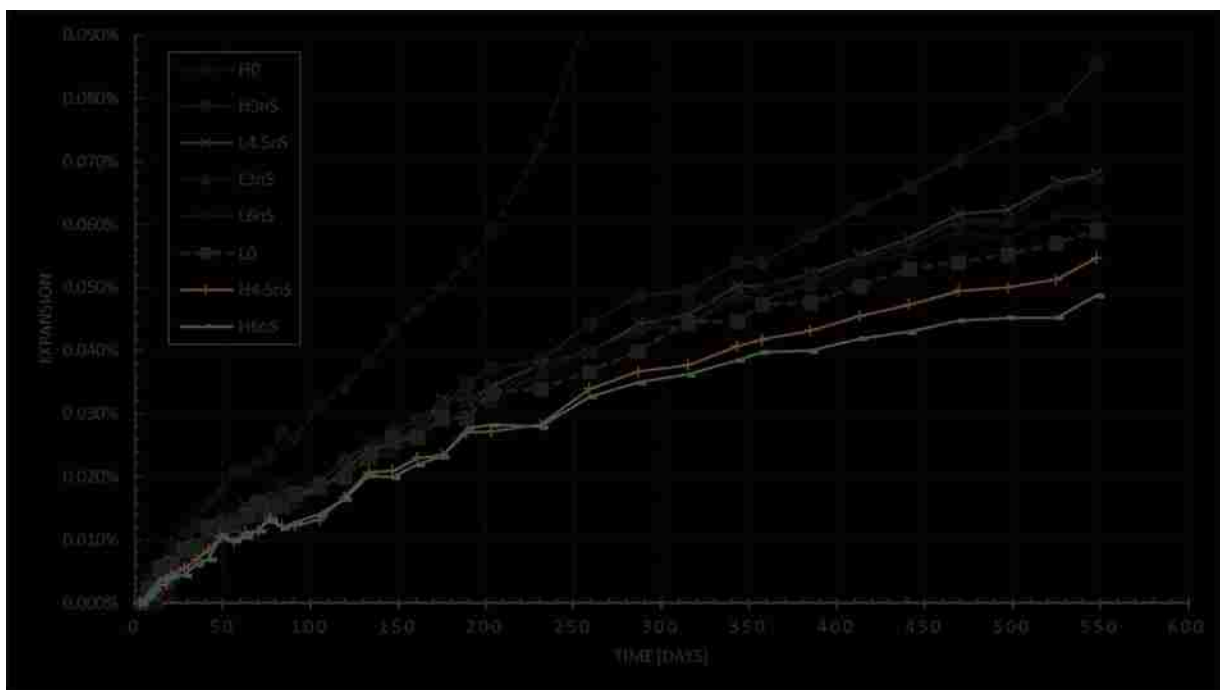


Figure 5-4: Cement L vs Cement H nS Contained Mortars

When comparing the performance of the nS contained mortars for both cements together it is worth pointing out the difference in the spread of expansion readings between those of cement L and those of Cement H as shown in **Figure 5-4**. The range of expansion readings between L0 and L6nS all fit in between the difference in expansion readings for H3nS and H4.5nS. Out of all nS contained mortars for both cements, H6nS exhibited the least expansion. This result agrees with the hypothesis that the

mixture with the higher fineness cement and the larger dose of pozzolan would exhibit the least expansion. The fact that H6mS exhibited 80% the expansion of H6nS though (after the 1.5 year exposure), was not in support of the hypothesis. The higher fineness pozzolan paired with the higher fineness cement was not the most sulfate resistant mixture in this study.

5.5.2 Rapid Sulfate Permeability Test (RSPT)

In an effort to explain the sulfate attack results, the supplemental testing program proved insightful. The results of the 6 hour RSPT test, performed on select mortars of the cement L and cement H series, are presented in *Figure 5-5*.

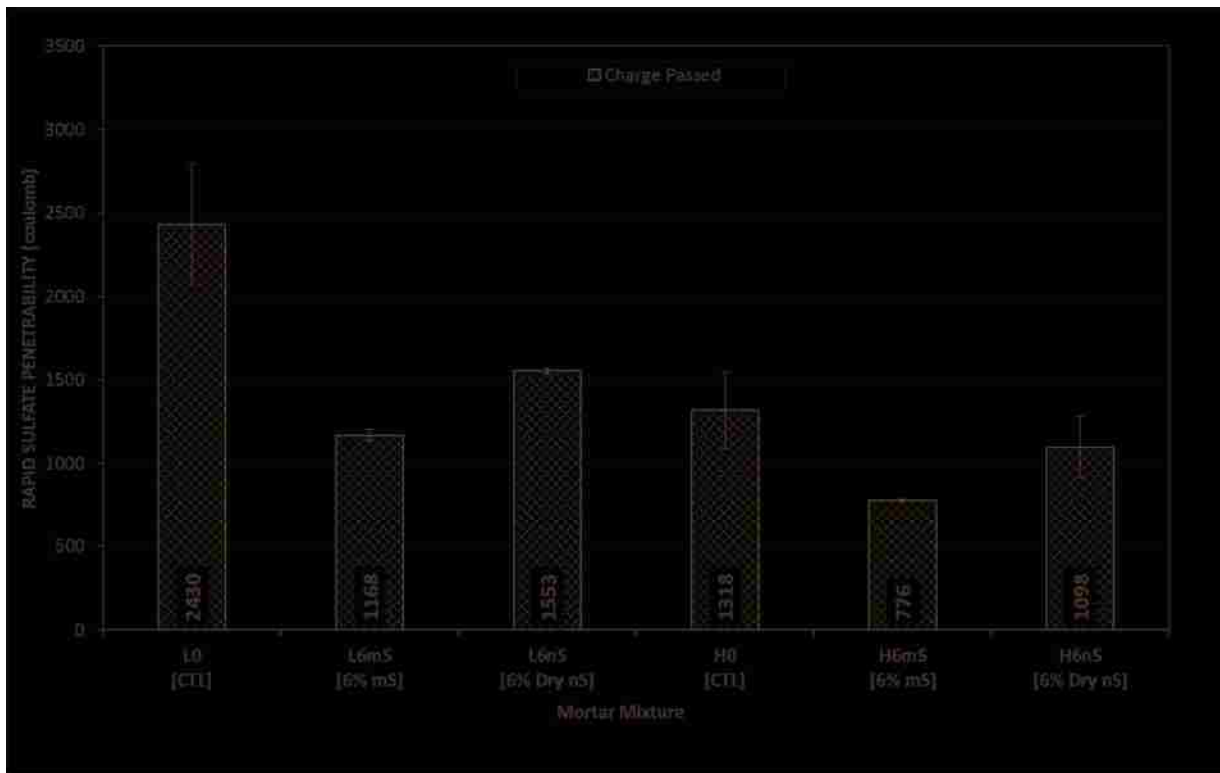


Figure 5-5: RSPT Results for Select Mortars (error bars represent \pm SD)

The test measures the penetration rate of sulfate ions which accounts for both the pore permeability and the free ion binding capacity of the mortar mixture. The coulomb charge measured in this test

accounts for all free ion movement through the mortar which along with sulfate ions includes, hydroxide and calcium (Stanish et al. 1997). The difference in sulfate penetrability between L0 and L6nS indicate that dry nS replacement did decrease the permeability of the mortar in comparison to the control L0. The 6% mS mixture had less permeability than the 6% nS one, 1168 coulomb for L6mS versus 1553 coulomb adjusted charge passed for L6nS. The trend is similar for the higher SSA/higher C₃A cement H. The 6% mS contained H6mS exhibited a lower charge passed than H6nS. The RSPT results for the pozzolan contained mixtures correlate well with the expansion measurements for these mortars. H6mS had the least expansion due to sulfate attack, L6nS had the most.

The RSPT results between the control mixtures on the other hand do not correlate with the expansion results. Recall in **Figure 5-1** that H0, exhibited the most expansion over the course of the 1.5 year test. Based on the RSPT results, H0 had a smaller rate of permeability than that measured for L0. Yet in the absence of a pozzolan, the expansion results indicated that the C₃A content played a more important role than the fineness of the cement. RSPT of the control mortar H0 tested at after 28 days of moist room curing indicated a physically more impermeable hydrated paste that did not allow easy ion mobility over the course of the 6 hour test. Nevertheless that reduced ion mobility does not reflect the chemical susceptibility of the H0 mortar to sulfate attack over a longer period of exposure. The hydrated paste might had been physically denser as expected with a higher Blaine cement, but that same paste exposed the sulfate ions with a larger surface area of monosulfates, unreacted C₃A, and Ca(OH)₂ that they could react with. As soon as sufficient pozzolan was introduced in the mixture that could cut off the supply of calcium ions by binding up the Ca(OH)₂, the trend reversed. Note in **Table 5-3** that at any given dose of mS, from 3% to 6%, the high Blaine cement H mortars outperformed the lower Blaine cement L at almost all benchmark periods of sulfate attack. That was not the case for the nS contained mortars. Only for the 4.5% and 6% nS contained mortars did the high Blaine cement mixtures consistently exhibited less expansion than their cement L counterparts. It is suspected that,

since the nS did not appear to perform as effectively as the mS, at lower doses of nS there was insufficient effective pozzolan to react with a significant enough portion of the $\text{Ca}(\text{OH})_2$ to halt the deleterious and expansive sulfate attack reactions.

5.5.3 Mercury Intrusion Porosimetry (MIP)

RSPT supported the expansion results for the nS and mS contained mortars by presenting the effects each pozzolan had on the rate of permeability between both cement types. The MIP testing provided more insight into the effectiveness of nS and mS to densify the paste and refine the pore size distribution of the mortars. The permeability of mortars and therefore their resistance to sulfate attack is dependent on the size distribution, interconnectivity, and tortuosity of their pore structure (Richardson 2002). A mortar may exhibit a higher volume of voids but it may be composed of finer less interconnected pores and larger air voids. Gel pores, integral to the dense layered C-S-H phase and generally 10 nm and smaller, are impermeable and do not contribute to transport characteristics. Pores ranging from 10 to 50 nm are considered capillary micropores and although tortuous, these can in small part contribute to permeability. The bulk of permeability and diffusivity occurs in the interconnected capillary macropores ranging from 50-10,000 nm (0.05 to 10 μm) (Tobón et al. 2015; Du et al. 2014a; Mindess et al. 2003). Pores larger than that are generally from entrapped or entrained air.

In **Figure 5-6** the MIP test results are presented for the control, 6% nS, and 6% mS contained mortars of each cement type. The diameter ranges for the relevant pore types discussed earlier are also annotated. There is a significant difference between the control mixtures for each cement type. The MIP results indicate that cement fineness strongly influenced the pore size distribution of the control mixtures and the effects each pozzolan had on their porosity and pore size distribution. L0 had a significant peak in the capillary macropore range around 0.075 microns and another one right

around the 0.005 micron boundary between gel and capillary micropores. H0 on the other hand had a smaller grouping of capillary macropores with a defined peak between 0.100 and 0.125 microns. H0 had a much larger grouping of its pores in the gel and micropore range with a peak around 0.004 microns. The total intrusion pore volume for each mortar as measured by MIP has been classified in **Figure 5-7**. H0 had a higher total intrusion volume of 0.0501 cc/g compared to that of L0, which was measured as 0.0455 cc/g. both MIP figures though indicate that the H0 mixture was of a denser and more impermeable nature. The smaller grouping of the macropore range indicated in **Figure 5-6** for H0 constituted for 0.0288 cc/g of that mixture's total intrusion volume while that of L0 was 0.0315 cc/g. Albeit chemically more susceptible to sulfate attack due to its high C₃A content, H0 was a physically more impermeable paste and both the MIP and RSPT results support that assessment.

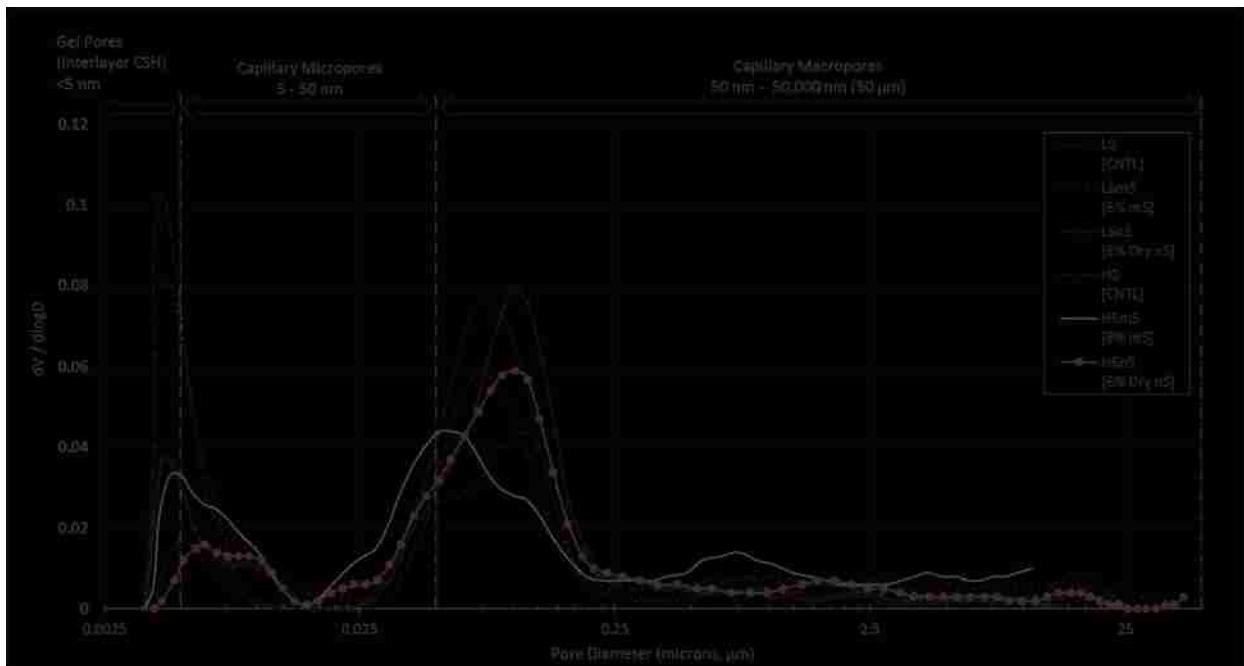


Figure 5-6: MIP Results for Cement L and Cement H Mortars

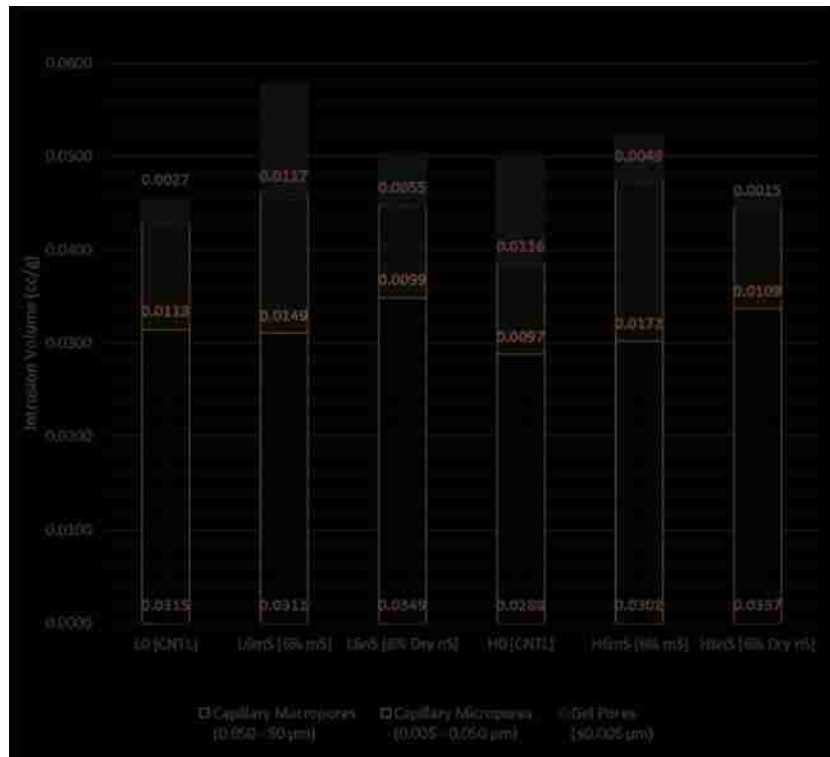


Figure 5-7: Classification of Total Intrusion Pore Volume for Select Mortars

The effects of nS and mS now follow. The addition of nS increased the total porosity for cement L from 0.0455 cc/g for the control L0 to 0.0503 cc/g for L6nS. This increase stems from both an increased total volume of capillary macropores as evident in **Figure 5-7** and their general increase in diameter as indicated by the shift of the macropore range peak to the right of the one for the control L0 in **Figure 5-6**. The nS in the L6nS mixture, instead of causing significant refinement of the pores in the macropore range, caused a shift of the curve to the right towards larger macropore diameters which could facilitate more transport of sulfate ions. There is lack of evidence that the nS added to cement L resulted in any verifiable paste densification and pore refinement. In fact the opposite was the case since these changes resulted in an increased permeability in comparison to the control mixture. There are stark differences between the mS contained mortar L6mS and L6nS. L6mS might have overall exhibited a higher porosity than the control or even L6nS with its total intrusion volume

of 0.0577 cc/g, but the pore size distribution indicates pore refinement and paste densification took place. There is a spike in the proportion of the gel pores that is represented by the strongly discernible peak in **Figure 5-6** within the 0.0005 μm boundary that constitutes for 20.3% of the total intrusion volume, and an increase in the capillary micropore range of pore diameters from 0.0113 cc/g for L0 to 0.0149 cc/g for L6mS. In **Figure 5-6**, the peak in the capillary macropore range is significantly reduced and there is a sharp increase in the peak overlapping both the gel pore and micropore range. These are all signs of pore refinement and a denser cement paste and ITZ. This was not the case with the nS contained L6nS mixture. Since the distribution of the L6nS pores in the capillary macropore range shifted towards larger diameter sizes, this could now explain why L6nS exhibited more expansion than the control under sulfate attack. With Cement L, mS was more effective at pore refinement than the nS.

For the high Blaine and high C_3A cement H, nS caused an increase in the pores in the capillary macropore range as can be seen with the peak rise in **Figure 5-6**; from 0.0288 cc/g for H0 to 0.0377 cc/g for H6nS. Instead of the shift in the capillary macropore range towards larger pore diameters as was observed with cement L, there is an increase in that group with cement H. The addition of nS significantly reduced the gel pores as well. The gel pore peak observed with H0 is the least pronounced in mixture H6nS and it has broadened and shifted mostly into the capillary micropore range. As reported in **Figure 5-7**, H0 had 0.0116 cc/g of its total pore volume in the gel pore range and with H6nS, the gel pores content dropped to 0.0015 cc/g. Although not in the same manner as cement L, the nS contained mixture H6nS, did not show signs of paste densification and pore size refinement which were contrary to expectations. In the sulfate attack testing it was observed that H6nS exhibited less expansion than the control H0, but since there is no strong evidence there was physical densification of the paste and ITZ, the author suspects that the primary beneficial aspects of

the nS tested were due to its chemical effect as a pozzolan. As a pozzolan nS would still bind up ions otherwise used by the sulfates for production of more ettringite and gypsum.

In **Figure 5-7** the total intrusion volume of the mS contained H6mS is higher than that of the control and H6nS but as mentioned earlier total porosity does not directly correlate to permeability. In **Figure 5-6** there is a clear pore refinement shift to the left in the macropore range curve between H0 and H6mS. The peak with H6mS shifted almost to the micro- to macropore boundary. The gel pore peak is reduced compared to H0, but not as significantly as H6nS, and the peak of that distribution is still within the gel pore range. Almost all of the reduction in the portion of gel pores from the control to H6mS has shifted to the capillary micropore range which still does not significantly contribute to the transport of sulfates. As shown in Error! Reference source not found., the total intrusion capillary macropore volume for H6mS was 0.0302 cc/g which is higher than the control but it is composed of a smaller diameter range capillary macropores that are relatively more impervious and tortuous than those of H0. The paste densification and pore size refinement effect of the mS paired with its chemically beneficial role as a pozzolan made it a more effective deterrent to sulfate attack which was attested by the low expansion readings during the 1.5 year sulfate solution exposure period.

5.5.4 Heat of Hydration

The results of the heat of hydration test are presented in **Figure 5-8**. Most of the heat generated is primarily dependent on the hydration of the C₃A and C₃S phases (Kosmatka & Wilson 2016). These are the phases responsible for the signature heat peak that follows the dormant initial set period and the wetting and initial C₃A hydration stage. It is indicative of the rate of hardening, final set, and early strength gain. Factors affecting that rate include the chemical composition, w/c, fineness of the cement, and the admixtures added (Kosmatka & Wilson 2016).

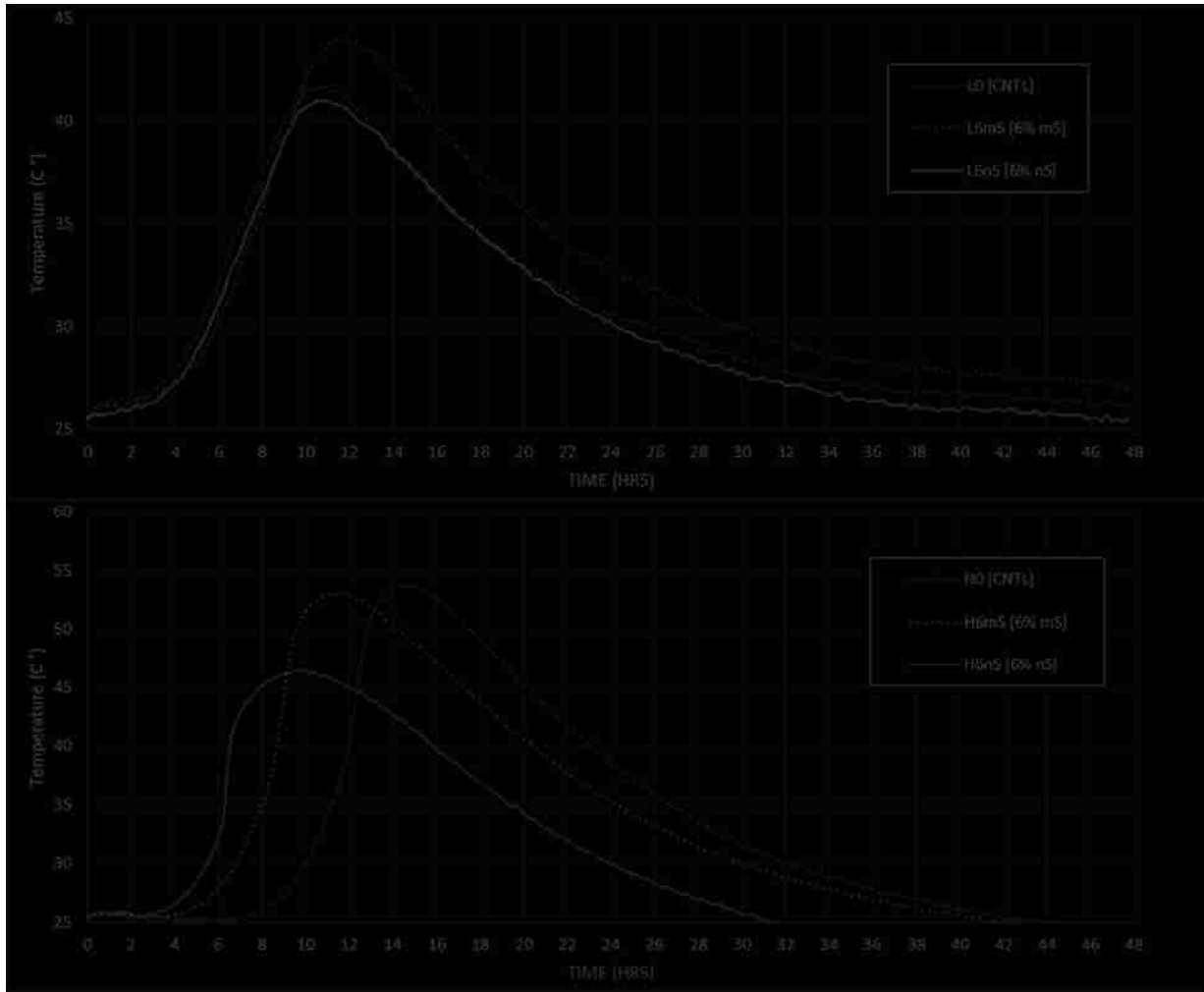


Figure 5-8: Heat of Hydration Results

With an increase in cement fineness there is an increase in the generated heat due to the grain refinement and higher reactivity of the cement (Neville 1998). When mS or nS are present in the mixture they serve as nucleation sites for the cement hydration phases and will typically accelerate the rate and increase the magnitude of the developed temperature peak during hydration of the C_3S and C_3A phase. This is indicative of both a pore and grain refinement typically observed with the addition of a pozzolan (Mehta & Monteiro 2006). For the cement L mortars, the heat of hydration for the control L0 peaked at almost 42°C. All the cement L mixtures exhibited a very similar dormant period and initial rise of the C_3S and C_3A phase peak. The differences were primarily in the maximum

temperature developed at the peak. Contrary to expectation, the addition of 6% nS decreased the temperature peak to 41°C for L6nS. The heat of hydration did not indicate grain refinement of the paste during these early stages of hydration took place. This supports the lack of evidence for pore refinement also observed with the MIP results for L6nS.

The mS contained L6mS on the other hand showed a significant increase in the peak of the C₃S and C₃A phase hydration. The curve peaked out at 44°C, a 2 degree increase over the control mortar L0. These results reaffirm the paste densification observed with MIP and confirm that mS caused both pore size and grain size refinement. For the higher fineness cement H, the 6% nS contained mixture H6nS did reduce the dormant period and shift the peak from around hour 15 for the control H0, to around hour 9. Nevertheless, in a similar nature to cement L, the peak dropped from 54°C for H0, down to 46.4°C for H6nS. The reduction in the peak was much more significant than that observed with cement L. The overall curve for H6nS was also broader than the control mortar H0.

There is a reported acceleration of alite hydration in the presence of active silica which could explain the acceleration in setting times with the high fineness cement H (Kurdowski & Nocuń-Wczelik 1983; ACI Committee 234 2006). The higher SSA of cement H exposes more alite to the silica gel and perhaps the higher SiO₂ purity of the nS as reported in **Table 5-1** results in more acceleration of the alite reactivity in comparison to that in the presence of mS. These heat of hydration results indicate either some limited grain refinement did occur with nS and the higher SSA cement or most of the acceleration was due to the increased alite reactivity in the presence of active silica. Since the MIP results did not show strong evidence of refinement and paste densification of the nS contained mortars, for H6nS the latter is likely the case. A faster rate of alite reaction does result in a faster production of the Ca(OH)₂ which is then available sooner to react with the pozzolan before exposure to sulfates. After all H6nS did exhibit less expansion than H0 under sulfate attack and increasing the

dose of nS for the cement H mortars, proved beneficial. In comparison, the addition of mS caused a lesser reduction in the dormant period before the C₃S and C₃A peak. The peak temperature dropped from 54°C for H0 to 53°C and a clear acceleration of the reactions is evident by the shift of the peak from around 15 hours down to 11 hours. The mS contained H6mS had evidence of pore refinement as indicated by MIP and the heat of hydration is likely supporting evidence for both grain refinement and alite reactivity acceleration. As shown earlier, the sulfate resistance of H6mS was better than that of H6nS. The expansion measured for H6mS under sulfate attack was overall the lowest.

5.5.5 Discussion

The testing results indicated that nS was not as effective as anticipated and upon investigative literature review, agglomeration of the nS particles was suspected as the likely cause. Like other ultrafine nanoscale particles, nS particles have an inherent tendency to agglomerate when introduced into a liquid due to their sensitivity to Van der Waals, capillary and electrostatic forces (Taurozzi et al. 2012; L Senff et al. 2010; Quercia & Brouwers 2010). When in agglomerated form, the performance of the nS is not based on the size of the individual particles but rather based on the agglomerates themselves. The effectiveness of nS as a nanoscale filler, seeding site for cement hydrates, and reactivity as a pozzolan could all be affected by the size of the agglomerates (Kong et al. 2012). Samples of the nS powder were submitted for laser particle diffraction alongside samples the mS and both cement types. The results are presented in **Figure 5-9**. Prior to measurement, each sample was ultrasonically mixed with water for 1 minute. The cement average particle size and percent passing the 325 mesh are summarized in **Table 5-1**. The nS particle size distribution indicated that most particles ranged between 3 and 12 µm. This gradation is significantly larger than the manufacturer-specified nS particle size range of 0.015 to 0.020 µm and confirms that the nS used in the mixtures tested was predominantly in an agglomerated form.

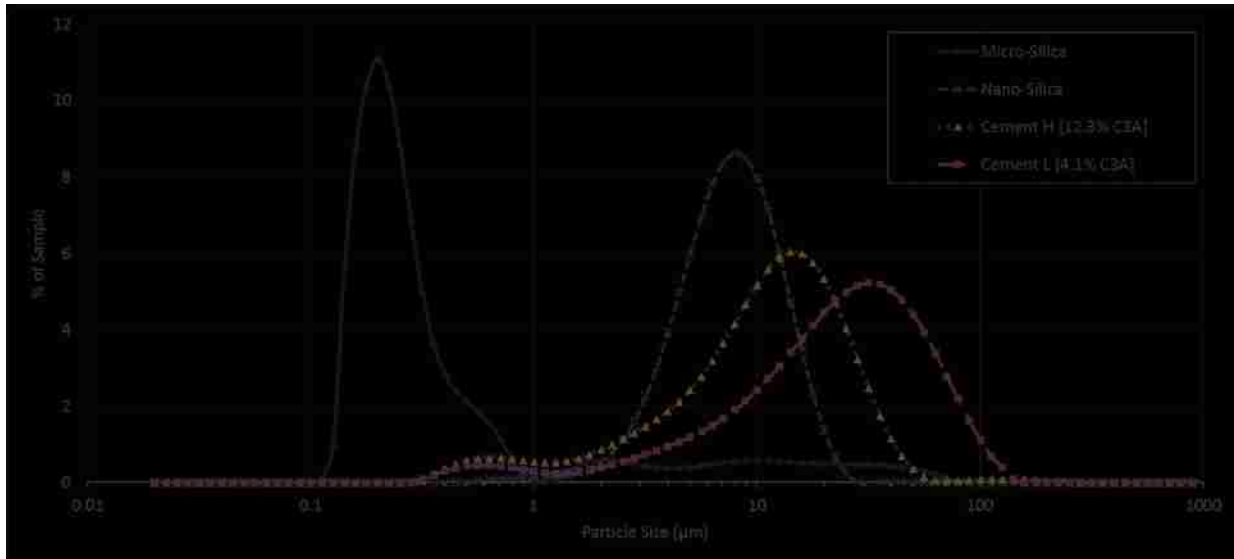


Figure 5-9: Laser Diffraction Particle Analysis of nS, mS, Cement L, and Cement H

As shown in **Figure 5-9**, the range of nS agglomerates is larger than that of the mS particles. The mS particles both exhibited a broader distribution of particle sizes and more than 84% of them ranged in size between 0.1 to 1.0 μm which was in agreement with the mS manufacturer data and most typical industry reported mS size of $\leq 1.0 \mu\text{m}$ (ACI Committee 234 2006; Holland 2005). The nS agglomerates still have a pozzolanic effect but it is impeded and mostly limited to the surface of the agglomerate cluster (Kong et al. 2012). Since nS was in agglomerated form, the physical benefits of the nanoscale particles had not occurred. In essence it was the sulfate resistance performance of agglomerated nS that was measured against a better dispersed mS.

5.5.6 Compressive Strength

Four cubes of the sulfate exposed and four cubes of the moisture room cured mixtures for each cement type were tested in compression at the 28 days, 12, 26 weeks (6 months), and 52 weeks (1 year). The results for the 28 days, 6 month and 1 year compressive testing of cement L and cement H are presented in **Figure 5-10**.

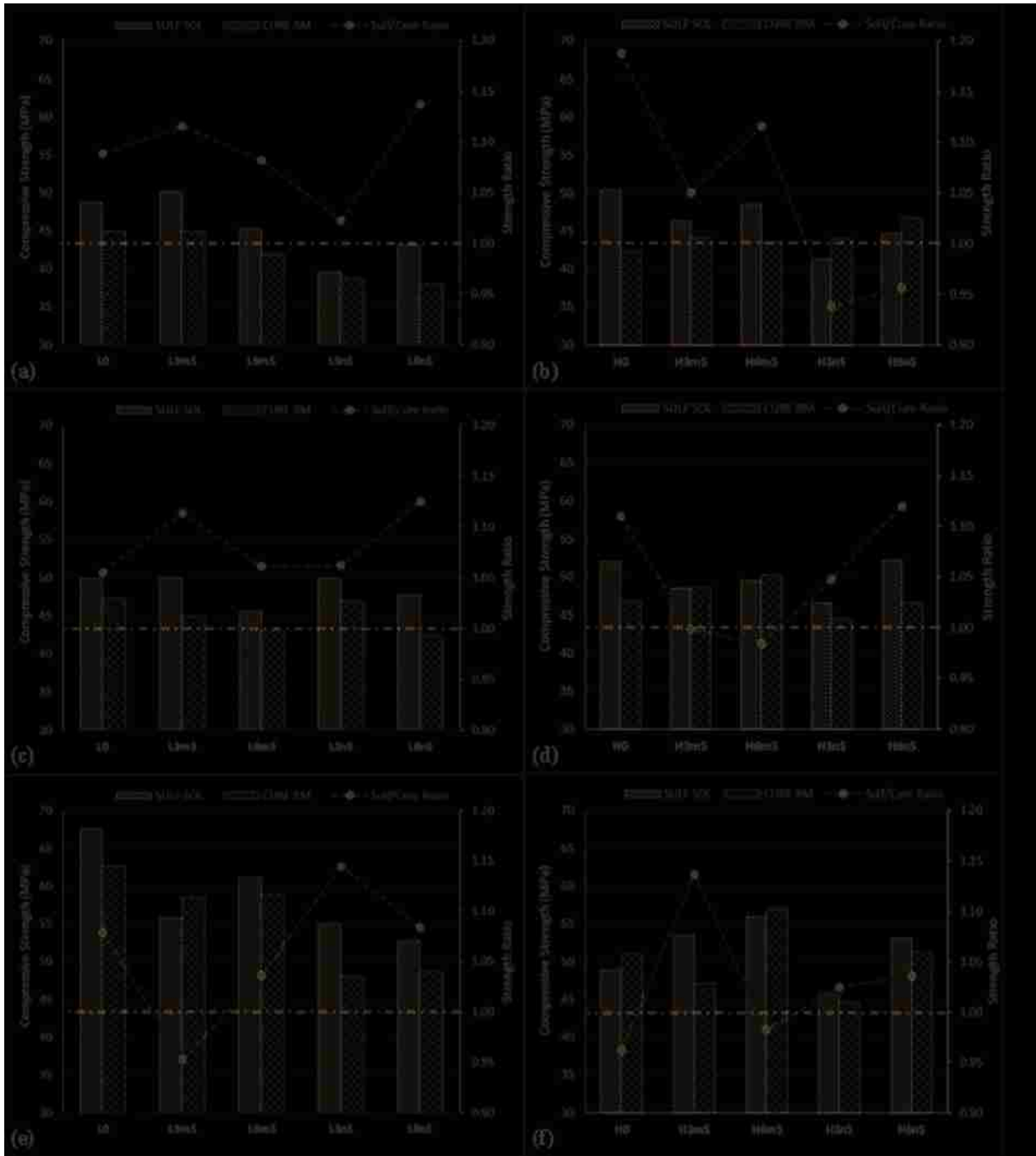


Figure 5-10: Compressive Strength, a) Cement L at 28 Days, b) Cement H at 28 Days, c) Cement L at 6 Months, d) Cement H at 6 Months, e) Cement L at 1 Year, f) Cement H at 1 Year

The strength ratio added as the secondary y-axis represents the compressive strength of the sulfate solution exposed samples over that of the cure room counterparts. When over the 1.0 line, it indicates

that the average compressive strength of the sulfate exposed samples was higher than that of those tested from the curing room for that particular mortar mixture. With some exceptions, for most mixtures even at 28 days, the compressive strength of the sulfate solution exposed samples is often higher than that of cured room counterparts. There are reports of an initial increase of compressive strength due to a filling and compaction effect from the sulfate attack generated expansive compounds like ettringite (Rundong et al. 2010). After a longer period of exposure to sulfates, when the available pore space for expansive compound growth is filled, more and more expansive stresses will develop that would lead to micro-cracks that will reverse that sulfate induced strengthening effect. The mS contained mixtures generally returned higher compressive strengths at all ages tested. For Cement L, the higher 6% dose of nS in L6nS resulted in weaker mortars in compressive strength when tested at 6 months and 1 year in comparison to the control and both mS contained mixtures. This could be attributed to a higher quantity of weak zones caused by the agglomerated nS. This was not observed with cement H, but it is likely that the higher fineness cement was more effective at utilizing the pozzolan and the net effect in terms of compressive strength for the nS contained cement H mortars was positive. Increasing the nS content for cement L resulted in a decreased compressive strength while the opposite was the case for cement H. In the case of mS, doubling the dose resulted in an increase in the compressive strength, and the better dispersion of that pozzolan is likely the cause.

5.6 Conclusions

This study sought to assess the impacts of cement fineness and C_3A content on the effectiveness of nanosilica (nS) and microsilica (mS) in regards to the sulfate resistance of Portland cement (PC) mortars. Comparisons were made against control mixtures of each cement without any pozzolan and mortars containing matching contents of un-densified powder microsilica. The outcomes of this comparison study were as follows:

1. Without the presence of either of the two pozzolans nS or mS, the susceptibility of either cement to sulfate attack induced expansion was governed primarily by the C_3A content of the cement.
2. Cement fineness was more influential in the presence of a pozzolan. In combination with at least 3% mS or 4.5% agglomerated nS, the higher SSA / high C_3A cement H mortars exhibited less expansion than the lower SSA / low C_3A cement L0. These same minimum nS and mS replacements also exhibited less expansion than their low C_3A cement counterparts. Poor dispersion of the nS in comparison to mS, as verified with laser particle diffraction, was likely the reason why a higher dose of nS was required to achieve reduced sulfate attack expansion in comparison to the control L0.
3. For the low 4.1% C_3A and lower SSA ($285 \text{ m}^2/\text{kg}$) cement L, the nS proved ineffective at increasing the sulfate resistance and the nS contained mixtures exhibited more expansion than the control mixture L0. It is believed that the agglomerated particles increased the permeability of the mortars by increasing the total intrusion volume of the capillary macropores and enlarging their average pore diameter as shown in the MIP results.
4. For the high 12.3% C_3A and high SSA ($546 \text{ m}^2/\text{kg}$) cement H, nS increased the sulfate resistance of the mortars and resulted in expansion readings less than those of the control mixture H0. The beneficial effect does not seem to stem from a paste densification and pore refinement as shown in through the MIP testing. The nS contained mortars exhibited an increase in volume of capillary macropores and a significant reduction of the gel pores in comparison to the control mixture H0. The sulfate resistance of the nS contained mortars with cement H is primarily attributed to the pozzolanic effect of the nS agglomerates that limit the availability of calcium ions for reaction with the sulfate.

5. With both cements, mS proved more effective than agglomerated nS in mitigating the sulfate induced expansion. The mS was more effective both on a chemical level as a pozzolan that was indicated by the RSPT test, and on a physical level serving as a better filler, densifying the paste, and refining the pore size distribution as shown through the MIP, heat of hydration, and compressive strength tests.

Nanosilica is a nanomaterial that has shown in other studies to imbue beneficial properties to the fresh and hardened properties of concrete. Many of these are of interest to an industry with a growing interest in increasing the durability and longevity of structures and construction materials. As evident in this study dispersion is of significant importance in the potency and effectiveness of nS as a mineral admixture. Nanosilica is commercially synthesized both in dry and solution colloidal forms. The latter might prove to be the preferable method of delivery unless good mixing practices and dispersion of the powder form nS in mixing water is verified through preliminary testing.

6 EFFECT OF COMBINED NANOSILICA AND MICROSILICA ON RESISTANCE TO SULFATE ATTACK

6.1 Abstract

In this study, the effect of combined nanosilica (nS) and microsilica (mS) on sulfate resistance of Portland cement (PC) mortars was evaluated against all cement control mortars and mixtures with equivalent contents of only one form of silica. Silica contained mortars had 6% cement replacement of either nS, mS, or 3% of each. An additional mixture with 3% mS was also tested. The series of mortars were prepared with both a moderate C₃A (7.2%) and a low C₃A (4.1%) cement to evaluate the effectiveness of each silica replacement paired with a chemically sulfate and non-sulfate resistant cement. The mortars in this study were subjected to a 1.5 year period of full submersion sulfate attack in a 5% sodium sulfate (Na₂SO₄) solution. The mortars tested were measured for expansion and compressive strength. Additional testing for absorption, rapid sulfate penetration, and mercury porosimetry of select mortar mixtures paired with laser diffraction particle analysis of the suspended silica particles supplemented the interpretation and explanation of the results. The expansion measurements indicated that mS replacement mortars outperform both nS only, and nS+mS combination replacement mixtures. A negative effect of the dry nS powder replacement attributed to agglomeration of its fine sized silica particles during mixing negated the expected superior pozzolanic activity of the nanomaterial. In the case of the low C₃A sulfate resistant cement, the dry nS replacement of 6% exhibited more expansion than the control. The nS+mS combination mortar mixtures for both cement types performed better than those with nS only but not better than the mS only mortars. Combining both silica types did not merge the strengths of both forms of pozzolan admixtures as hypothesized. In light of the results most of the beneficial contribution from the cement replacement with the combination mixtures could be attributed to the mS proportion given

that the combination mixtures' expansion performance was comparable to that of the 3% mS only mortars.

6.2 Introduction

Concrete's versatility and broad application in all aspects of civilized infrastructure and the built world means that twice as much of it is used in comparison to all other construction materials combined (Kosmatka & Wilson 2016). Cement manufacturing is an energy and resource intensive process that accounts for approximately 1.1% of the US national greenhouse gas emissions, equal to more than 75 million metric tons of CO₂ equivalents (Kosmatka & Wilson 2016). There is a continuous effort to improve the sustainability and energy efficiency of both the production of cement, and concrete itself as a material. One strategy is the use of supplementary cementitious materials (SCMs) to improve the durability performance of concrete. Durable concrete made through the use of SCMs lessens concrete's environmental impact by both reducing the amount of virgin cement used and prolonging the service life of the structure, which saves on energy and resources associated with its maintenance, repair, and untimely replacement.

Durability of concrete in most applications is synonymous with quality concrete. Quality concrete needs to be capable of resisting a host of chemical and physical phenomenon one of which is sulfate attack. While sulfate attack alone may not be sufficient enough to cause complete failure; its effect on concrete such as expansive stress induced cracking, spalling, paste decalcification, increasing of porosity and permeability, can facilitate and aggravate a host of other deteriorative phenomena such as carbonation, freeze-and-thaw damage and reinforcement corrosion. Internal and external sulfate sources, as well as causes and effects of sulfate attack are well detailed in existing literature (Skalny et al. 2002; Hewlett & Massazza 2003). Among the SCMs recommended for mitigating chemical sulfate attack by authorities in the industry such as ACI Committee 201, is microsilica (mS), a by-product of the silicon and ferrosilicon smelting industries (ACI Committee 201 2008). The sulfate

attack mitigating effects of mS are that it reduces overall permeability by densifying the cement paste and interfacial transition zone (ITZ) with the aggregate, and reduces the available hydration product calcium hydroxide $\text{Ca}(\text{OH})_2$ by reacting with it and forming secondary C-S-H. This pozzolanic reaction, paired with a reduction of the available C_3A due to replacement of the cement with microsilica, deters the precipitation of excessive gypsum and expansive ettringite which depend on a steady supply of calcium, hydroxide, and sulfate ions (Hewlett & Massazza 2003; Skalny et al. 2002).

There has been an exponentially growing interest in learning and understanding the relationship between the nanostructure of the cementitious matrix and its impact on the properties, behavior and performance of concrete (Campillo et al. 2004). With the development of the tools and technology to study concrete at this nanoscale came a wave of new research and testing of the application of a host of new synthesized nanoscale SCMs (Sobolev & Gutiérrez 2005). One of the first to gain attention and most widely used has been nanosilica (nS), essentially nano-sized ($<100\text{nm}$) silicon dioxide (SiO_2) particles. The particles of mS are larger in comparison to nS, but typically $< 1 \mu\text{m}$ (Holland 2005). The smaller particle sizes of nS correlate with a specific surface area of $80 \text{ m}^2/\text{g}$ or more while that of mS is typically $15\text{-}25 \text{ m}^2/\text{g}$ (Campillo et al. 2004). This high surface area makes nS a much more reactive pozzolan that consumes $\text{Ca}(\text{OH})_2$ faster than mS. This makes nS suitable to pair up with other SCMs such as fly ash to compensate for its slow rate of strength development (Said et al. 2012). During hydration, nS forms seeding sites from the additional C-S-H it generates and stimulates the growth of a much more compact C-S-H phase that is not limited to growing on the grain surface of the hydrating alite (C_3S), it starts growing in the pore spaces as well (Singh et al. 2013). Additionally, since nS also rapidly consumes free Ca^+ ions freed from the dissolution of $\text{Ca}(\text{OH})_2$ to produce secondary C-S-H, it prevents calcium leaching much faster than mS, especially if the concrete is exposed to sulfates during an early age. Given these observations the author set out to test the effectiveness of combining mS and nS against sulfate attack to see if nS can complement mS as a filler at the nanoscale level, and

as an aggressive pozzolan that can help mS in developing a more sulfate resistant and impermeable mortar. Beyond densifying the paste and ITZ, the nS could react with more of the Ca(OH)_2 before sulfate ions react with it to form gypsum and consecutively ettringite which should also manifest in a reduced expansion and ion diffusivity.

6.3 Experimental Program

The mortars in this study were subjected to a 79 week (1.5 year) full submersion exposure in a 5% sodium sulfate (Na_2SO_4) solution. The linear expansion of mortar bars, mortar cube compressive strength, water absorption, and rapid sulfate ion penetration (RSPT) were measured.

6.3.1 Materials

Mortars were prepared with two locally sourced cements with contrastingly different C_3A contents. Cement L was a Type V low alkali cement that contained 4.1% C_3A . Cement M was a Type I cement that contained 7.2% C_3A . The chemical and physical properties of the cements are presented in ***Error! Reference source not found.*** The nS used was supplied as a porous white dry powder form with particle sizes ranging from 15-20 nm and a specific surface area of 640 m^2/g . It was mechanically blended with the premeasured mixing water for 1 minute prior to use in each mortar mixture. The mS used in the experiment, was a gray amorphous sub-micron powder and was homogeneously intermixed with the cement for each mortar mixture. The chemical and physical properties of the nano- and microsilica are also presented in ***Table 6-1***. A polycarboxylate based high-range water-reducing admixture (HRWRA) was utilized for achieving the desired flow per ASTM C 109. The fine aggregate used for the mortars in this study was from a Nevada based quarry and had an oven-dry specific gravity of 2.76, absorption of 0.81% and a fineness modulus of 2.64. Its gradation was well inside the upper and lower limits of ASTM C 33. Mortar mixing water and water used for the

preparation of the sodium sulfate solution was commercially bottled distilled water obtained from a single source.

Table 6-1: Chemical Composition and Physical Properties of Cement and nS

	Cement A (Moderate C ₃ A)	Cement B (Low C ₃ A)	micro- Silica (mS)	Dry Powder nano-Silica (nS)
<i>Chemical Composition</i>				
Silicon Dioxide (SiO ₂), %	21.1	21.7	94.72	99.5
Aluminum Oxide (Al ₂ O ₃), %	4	4.1	--	0.002
Ferric Oxide (Fe ₂ O ₃), %	2	4.0	--	0.001
Calcium Oxide (CaO), %	62.7	63.2	--	0.002
Magnesium Oxide (MgO), %	2.1	2.8	--	0.001
Sulfur Trioxide (SO ₃), %	2.8	1.8	0.23	--
Loss on Ignition, %	1.8	0.7	2.82	--
Insoluble Residue, %	0.71	0.1	--	--
Total Alkali (Na ₂ O + K ₂ O), %	0.59	0.46	0.49	--
Free Lime (CaO), %	0	0.8		
<i>Physical Properties</i>				
Time of Set Initial Vicat, min	145	150	--	--
Specific Surface Area, m ² /g	0.341 ^a	0.285 ^a	22.65 ^b	640 ^b
325 Mesh (45 μm), % passing	--	72.9	97.12	
Avg. Particle Size (APS), μm	20-30 ^c	35-45 ^c	0.1-1.0 ^c	0.015- 0.020
<i>Per Bogue Calculation^d</i>				
Tricalcium Silicate (C ₃ S), %	57.0	54.0	--	--
Dicalcium Silicate (C ₂ S), %	17.5	21.5	--	--
Tricalcium Aluminate (C ₃ A), %	7.2	4.1	--	--
Tetracalcium Aluminoferrite (C ₄ AF), %	6.1	12.2	--	--

^aby Blaine air-permeability test

^bby BET Analysis

^cEstimated from MasterSizer Particle Distribution Analysis

^dBogue Modified Equation for Interground Gypsum & Limestone (Winter 2012b)

Table 6-2: Mortar Mixture Proportions

Sample Designation	Binder, %			Measured Flow, %*	3-Day Compressive Strength,	
	Cement	nS	mS		MPa	psi
Low C₃A Cement L						
L0	100	0	0	145	26.6	3,851
L3mS	97	0	3	127	23.9	3,463
L6mS	94	0	6	97	23.6	3,419
L6nS	94	6	0	102	22.2	3,226
L3mS+3nS	94	3	3	98	24.2	3,504
Moderate C₃A Cement M						
M0	100	0	0	148	29.6	4,296
M3mS	97	0	3	108	30.5	4,420
M6mS	94	0	6	95	30.8	4,463
M6nS	94	6	0	100	29.9	4,337
M3mS+3nS	94	3	3	102	30.1	4,363

*Flow measured according to ASTM C 1437 with flow table conforming to ASTM C 230

6.3.2 Mixture Proportions

The mixture proportions of the mortars tested are presented in **Table 6-2**. Besides the control mixture for each cement type, there were 4 mortars mixtures with a total of 3% or 6% cement replacement with either 3% mS only (L3mS and M3mS), 6% mS only (L6mS and M6mS), 6% nS only (L6nS and M6nS), or an equal 3% proportion of each form of silica (L3mS+3nS and M3mS+3nS). The (w/b) was kept at a constant 0.485 for all mixtures according to ASTM C 1012. The fine aggregate-to-binder ratio was 2.75-to-1 by mass as specified in ASTM C 109.

6.3.3 Mixing Procedure

Mortar mixtures were batched using an electrically driven epicyclic mechanical mixer following the mortar preparation procedure of ASTM C 305. The mixing procedure began with either blending the nS with the mixing water for 1 minute in a commercial blender or hand mixing the mS with the dry cement prior to placing in the mixer. For each testing mixture, 4 mortar expansion bars were prepared per ASTM C 1012 and 36, 5 cm (2-in), mortar cubes specimens were prepared per ASTM C 109 for strength testing. Additionally multiple 10 cm (4-in), diameter disks were made for supplemental testing. For the nS and mS replacement mixtures, the HRWRA was utilized as required

to reach the ASTM C 109 recommended flow of $110\pm 5\%$. All mortar sample molds were hand packed and compacted using an electromagnetic vibrating table. The sample molds for each mortar mixture were plastic wrapped and kept at room temperature (21 ± 3 °C) for 24 hours then followed by 3 days of curing in a moist room to achieve the required compressive strength of 20 ± 1.0 MPa (2900 ± 145 psi) per ASTM C 1012 prior to sulfate exposure. After the 3 days of moist room curing, three mortar cubes were tested for compression strength to confirm the required minimum strength. Following the 3 day curing period, the mortar bars and half of the mortar cubes were transferred to 5% sodium sulfate solution tanks. The remaining cubes were kept in the moist curing room and tested in compression at the same age of samples immersed in sulfate solution

6.3.4 Sulfate Solution

The 5% Na_2SO_4 solution was prepared per ASTM C 1012. Sufficient solution was prepared for each container to maintain the recommended minimum solution to mortar volume ratio of 4. The solution in each container was kept in circulation using submersible pumps. To replenish the sulfate ion concentration in the solution (Mehta 1975), the solution pH was manually rebalanced to 7.0 ± 1 daily with 0.5N H_2SO_4 for the first 6 months and then weekly for the remainder of the 1.5 year fully submerged test.

6.3.5 Absorption and RSPT

All absorption testing was performed with three mortar disks per ASTM C 642 to find the average reading presented in the results. The RSPT test, as proposed in the Sulfate-Resisting Concrete report by the Cement Concrete & Aggregates Australia (CCAA 2011), is similarly setup to the traditional rapid chloride permeability test (RCPT) per ASTM C1202. In this study, a 10% Na_2SO_4 solution was used across the 0.3N NaOH instead of 3% NaCl; similar to absorption, three mortar disks were used for each average diffusivity reading presented in the results.

6.4 Results and Discussion

6.4.1 Sulfate Attack Expansion

The expansion readings at key milestones along the 1.5 year test are reported in **Table 6-3** for convenient reference during the discussion of results. Through comparison of the control mixtures' expansion of both cement types it is evident how significantly different both cements perform under chemical sodium sulfate attack. True to expectations, the low C₃A control mixture L0 outperforms the moderate C₃A control mortar M0. At one year, L0 exhibits 44% less expansion than M0. That percent difference increases to 71% at the conclusion of the test. As the sulfate solution permeated deeper into the mortar bars and the aluminate phase monosulfate, calcium and sulfate ions became more abundant, the more favorable C₃A conditions stood out in the expansion behavior and the differences between the two mixtures quickly became apparent.

Table 6-3: Expansion Measurements at Key Time Periods

	M0	M3mS	M6mS	M6nS	M3mS+3nS
4 WEEKS	0.011%	0.009%	0.010%	0.012%	0.007%
8 WEEKS	0.016%	0.012%	0.015%	0.019%	0.011%
12 WEEKS	0.021%	0.017%	0.017%	0.021%	0.014%
26 WEEKS	0.039%	0.028%	0.028%	0.034%	0.027%
1 YEAR	0.074%	0.045%	0.043%	0.054%	0.045%
1.5 YEAR	0.124%	0.056%	0.050%	0.063%	0.058%
	L0	L3mS	L6mS	L6nS	L3mS+3nS
4 WEEKS	0.009%	0.006%	0.003%	0.009%	0.008%
8 WEEKS	0.013%	0.010%	0.011%	0.012%	0.010%
12 WEEKS	0.014%	0.011%	0.012%	0.015%	0.013%
26 WEEKS	0.029%	0.024%	0.025%	0.032%	0.025%
1 YEAR	0.047%	0.041%	0.037%	0.050%	0.038%
1.5 YEAR	0.059%	0.052%	0.047%	0.061%	0.048%

With the moderate C₃A cement series, all silica replacements by the end of the test period had a positive impact on reducing the rate and level of expansion as presented in **Figure 6-1**. Contrary to expectations, the nS mixtures' expected superior performance over their mS counterparts was not observed. Out of all silica replacement mortars for this cement, the 6% nS replacement mixture M6nS

exhibited the most expansion after the control. In fact, the control mortar performed better during the first 8 weeks as can be seen in **Table 6-3** before the M6nS expansion readings dropped below those of M0. At 4 weeks, the M0 measured expansion was 0.011% versus 0.012% measured for M6nS, a 9% difference. By 8 weeks M0 had 0.016% and M6nS 0.019%, the difference increased to 16%. The mS replacement mortars outperformed M6nS, including M3mS which had half the cement replacement of M6nS. This trend was consistent at early age and through the conclusion of the test. At 4 weeks, M3mS showed an expansion of 0.009%, which compared against the 0.012% of M6nS, was 36% better. Although M6nS narrowed the difference over time, at 1 year, M3mS outperformed M6nS by 18%, and then 11% at 1.5 years. As evident, the dry nS had a negative impact on the expansion performance of the mortar.

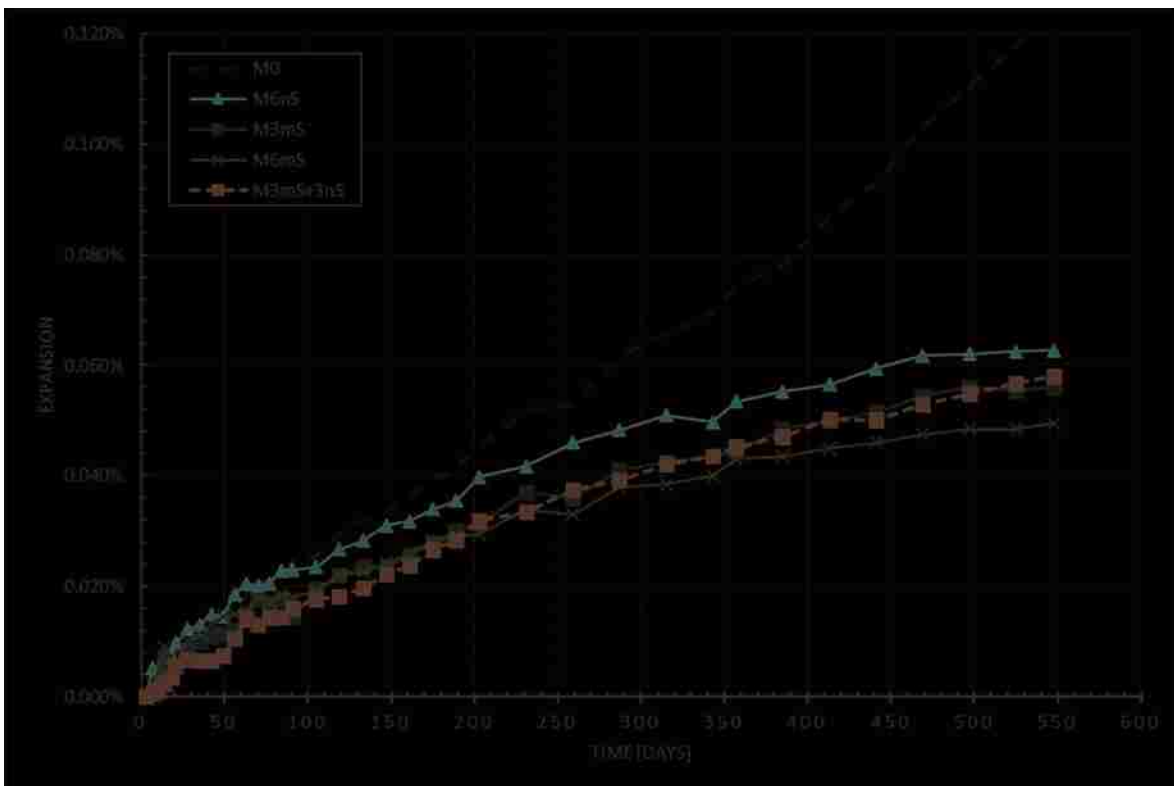


Figure 6-1: Expansion Measurements for Cement M Mortar Mixtures

The expectation that equal replacements of nS and mS in M3nS+mS would combine the strengths of both forms of silica to create a more impermeable and sulfate resistant mixture than either pure form of replacement was also not met. As evident in **Figure 6-1**, M3mS+3nS outperformed M6nS but exhibited more expansion than M6mS. It did perform better than M6mS during the first 26 weeks, starting with a strong 39%, 35%, and 18% improvement over M6mS at 4, 8, and 12 weeks respectively. By the 26th week, M3mS+3nS fell behind and concluded the test with 0.058% expansion versus the 0.050% measured for M6mS, the mS only mixture performed 16% better. As can be seen in **Figure 6-1**, with half the cement replacement, M3mS performs almost as well as the combination mortar leading to the conclusion that most of the beneficial contribution to sulfate resistance in the combination mortar stems from the mS replacement. The positive contribution of dry nS replacement might be only that of reducing the overall availability of C₃A by reducing the cement content by another 3%.

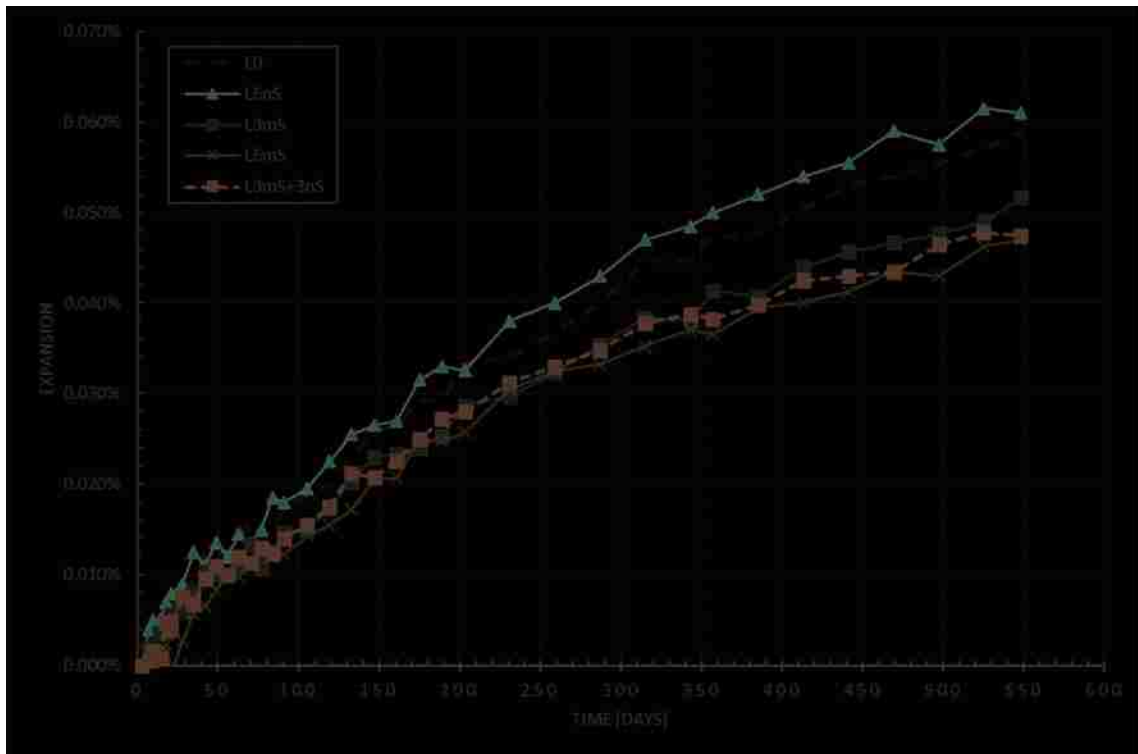


Figure 6-2: Expansion Measurements for Cement L Mortar Mixtures

For the moderate C_3A cement M, nS replacement proved deleterious, but the negative effects seemed further exasperated in the low C_3A cement L mortar mixture series presented in **Figure 6-2**. Cement L has 4.1% C_3A which meets the 5% limit imposed for Type V high sulfate resistance cements per ASTM C 150. As such, cement L is chemically resistant to sulfate attack and inherently more sensitive to any negative effects of the silica SCMs that might have been more subtle with cement M. After 12 weeks of sulfate exposure in the sodium sulfate tanks, the trend became clear, the 6% nS mortar L6nS exhibited more expansion than the control L0. Up until then similarly to cement M, L6nS has a slight edge on the control, 0.012% for L6nS versus 0.013% for L0 at 8 weeks, and averaging around 4-5% improvement over the control. After the longer period of exposure, the trend reversed and L6nS consistently exhibited more expansion than the control (averaging 7% more than L0). The rest of the silica replacement mixtures, L3mS, L6mS, and L3mS+3nS outperformed the control as was the case with the cement M series. Also similar to cement M, the 6% mS mixture L6mS outperformed all mortars in terms of the least expansion over the 1.5 year test. At 1 year, L6mS had 0.037%, and at 1.5 years, it had 0.047%, which were 26% and 23% less than L0 respectively. Nevertheless with cement L, M6mS was in close competition with L3mS+3nS and L3mS; usually less than 10% improvement over either. Similarly to cement M, the combination replacement mixture L3mS+3nS, seemed to thread the needle between L3mS and L6mS, performing on average 8% better than L3mS but exhibiting expansion up to 5% more than L6mS. Results indicate that with a sulfate resistant cement a smaller dose of 3% mS is almost as effective as doubling it and with either cement combining dry nS with mS is not preferable to pure mS. With cement M increasing the dose of mS proved more impactful to the mixture's sulfate resistance but doubling the replacement did not proportionally halve the measured expansion.

6.4.2 Supplemental Testing

Sulfate expansion results indicated that nS replacement had a generally negative effect on the sulfate resistance of the mortar mixtures tested. To better understand why, the researchers turned to existing literature and supplemental testing. Other research with nS has revealed that due to its ultrafine particle size, it has an inherent tendency to agglomerate when introduced into a liquid (L Senff et al. 2010; Quercia & Brouwers 2010). This effect is characteristic of most ultrafine particles in the nanoscale range of 1 to 100 nm, since they are sensitive to Van der Waals, capillary and electrostatic forces (Taurozzi et al. 2011). The stability of the nanoscale silica particles in the fluid system is greatly affected by the electrostatic charge on the solid particle surface which correlates to a particle fluid suspension measurement referred to as the zeta potential (Jiang et al. 2009). The zeta potential reflects the hydrodynamic diameter of the suspended particles and their potential for agglomeration. If the measured zeta potential absolute value is more than 30mV, then the suspension is considered electrostatically stable. The zeta potential is sensitive to multiple variables of the solution one of which is the pH. To electrostatically stabilize the solution the pH must be away from the isoelectric point by more than 2, the point at which the zeta potential is essentially null and attractive Van der Waal forces overcome electrostatic repulsion (Jiang et al. 2009; ISO 14887 2000). With nS, that isoelectric point is between 2 and 2.5 (Sieger et al. 2004). Under the alkali environment of the cement hydration products which is ordinarily at a pH of around 12.5 (Neville 1998), the absolute value of the zeta potential for nS as measured by Shih et al. (2006) can be estimated to be approximately 50 mV. These conditions are favorable and the silica particles have a strong electrokinetic barrier that causes the particles to repel which tends to prevent agglomeration. This might be of little help if the nS introduced with the Portland cement is already in an agglomerated state.



Figure 6-3: Test Strip pH Measurements of Mixing Water vs Tap Water

Prior the introduction in the cement, the dry nS powder is blended with the distilled mixing water. Although pure water is neutral with a pH of 7, distilled water tends to be acidic since when exposed to air it reacts with carbon dioxide from the atmosphere that forms a diluted form of carbonic acid (H_2CO_3). The carbonic acid releases hydrogen ions (H^+) which can bring the pH of the distilled water down below 5 (Bibby Scientific n.d.). Therefore during mixing, the zeta potential of the nS particles in this environment will be lower. Test strip pH measurements taken of the distilled water used in this study indicated its pH was less than 6, see **Figure 6-3**. That measured of local tap water was around 8. The zeta potential does vary depending on the nS particle size and concentration, but was not a measurement made within the scope of this study. It has been reported as -33.4 ± 1.8 mV, around -30 mV for 10 nm particles, or less than 40 mV for 50-80 nm silica particles at a concentration of 0.1 g/L (Bihari et al. 2008; Sieger et al. 2004; Bizi 2012). Based on these reports, the zeta potential of the nS-distilled water solution in this study could be assumed in the range of -30 to -40 mV. As indicated earlier, nanosilica becomes electrostatically unstable in dispersion when the absolute value of the zeta potential approaches or drops below 30 mV. Furthermore the mechanical blending agitates the particles and their frequency of collision and interaction which could facilitate more agglomeration.

Although the zeta potential was not tested for the nS used in this study, to confirm agglomeration of the nS when mixed in with the distilled water, samples of the dry nS used in the study were submitted for laser diffraction particle analysis along with samples of the mS, cement L, and cement M. Prior to taking each measurement, the nS was ultrasonically mixed with the distilled water for 1 minute, the same period the nS was dispersed with the mixing water in a blender for the mortar mixtures. As evident in **Figure 6-4**, the average particle size measured for the nS was 6 to 10 μm , which was significantly larger than the manufacturer specified nS particle size of 0.015-0.020 μm . Results of this test confirmed that even with the ultrasonic means of agitating the distilled water suspension, the dry nS tested in this study tended to agglomerate in clusters that were larger than those measured for mS. The laser diffraction results for mS being similarly tested and prepared, showed smaller particle sizes and exhibited a broader range of size distribution where 84% of the sample was in the 0.1-1.0 μm particle size range. The mS particle measurements conformed with the mS manufacturer data and most typical industry reported mS sizes of equal to or less than 1.0 μm (Holland 2005).

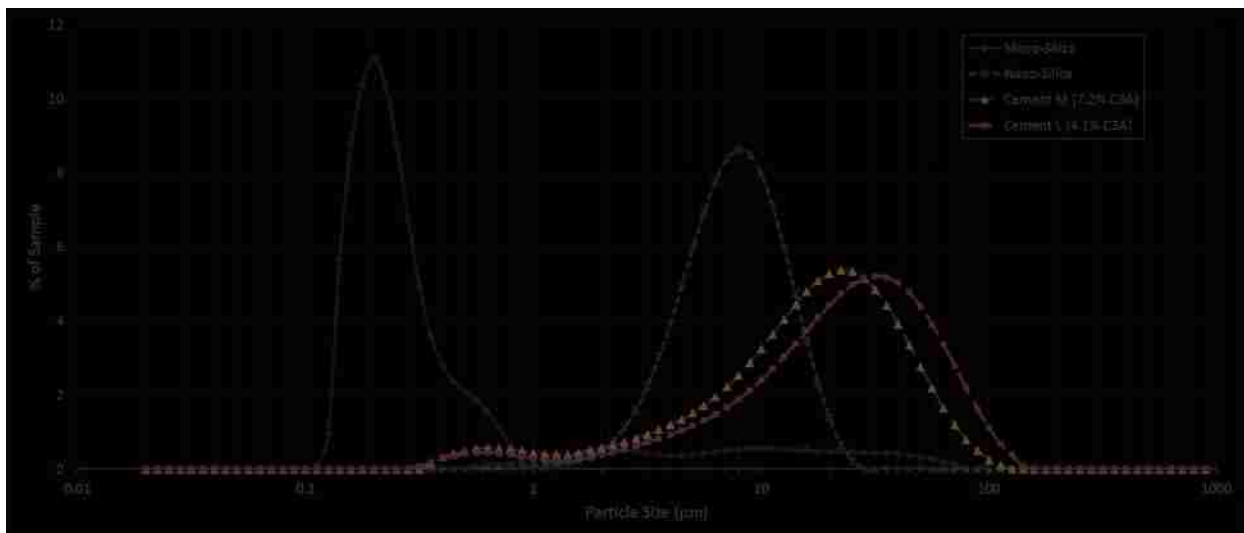


Figure 6-4: Laser Diffraction Particle Size Analysis of nS, mS, and Cements L and M

6.4.3 Water Absorption and RSPT

There is evidence of nS agglomeration but even in that state, with cement M, nS replacement resulted in an improvement in sulfate durability. To better understand the physical and chemical effect the agglomerated nS had on the mortars, water absorption and RSPT were performed on the control, 3% mS, 6% mS, and 6% nS mortars. The absorption results as presented in **Figure 6-5** showed that for both cements, the 6% nS mortars actually had the smallest measured volume of permeable pore space, 8.30% for L6nS and 8.65% for M6nS. For cement L that is 13% less than the L6mS mortar, and for cement M, M6nS had 19% less than M6mS. This indicates that the agglomerated dry nS was effective at reducing the porosity of the mortars whether as a filler or through some refinement of the cement paste porosity. Nevertheless the nS contained mortars still exhibited more expansion than the mS only and nS+mS combination mixtures.

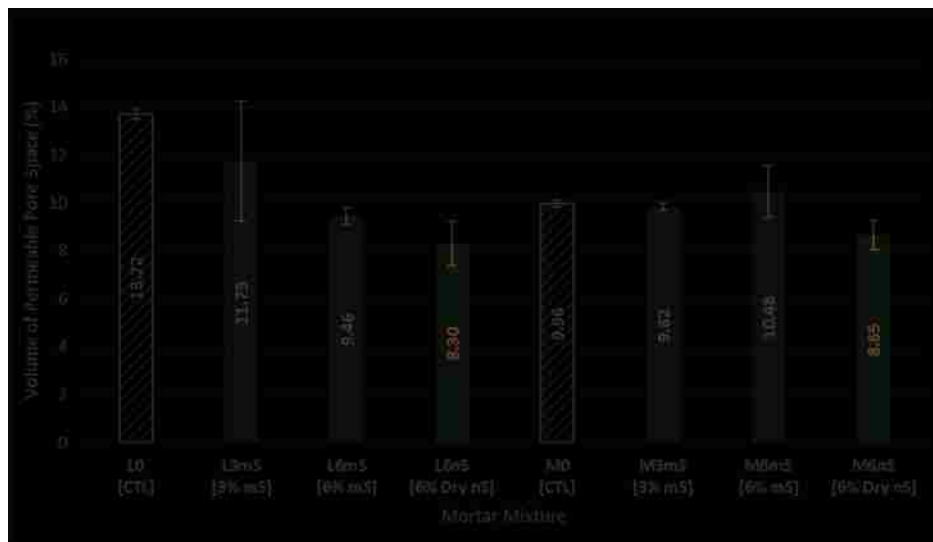


Figure 6-5: Water Absorption of Select Mortars (error bars represent \pm SD)

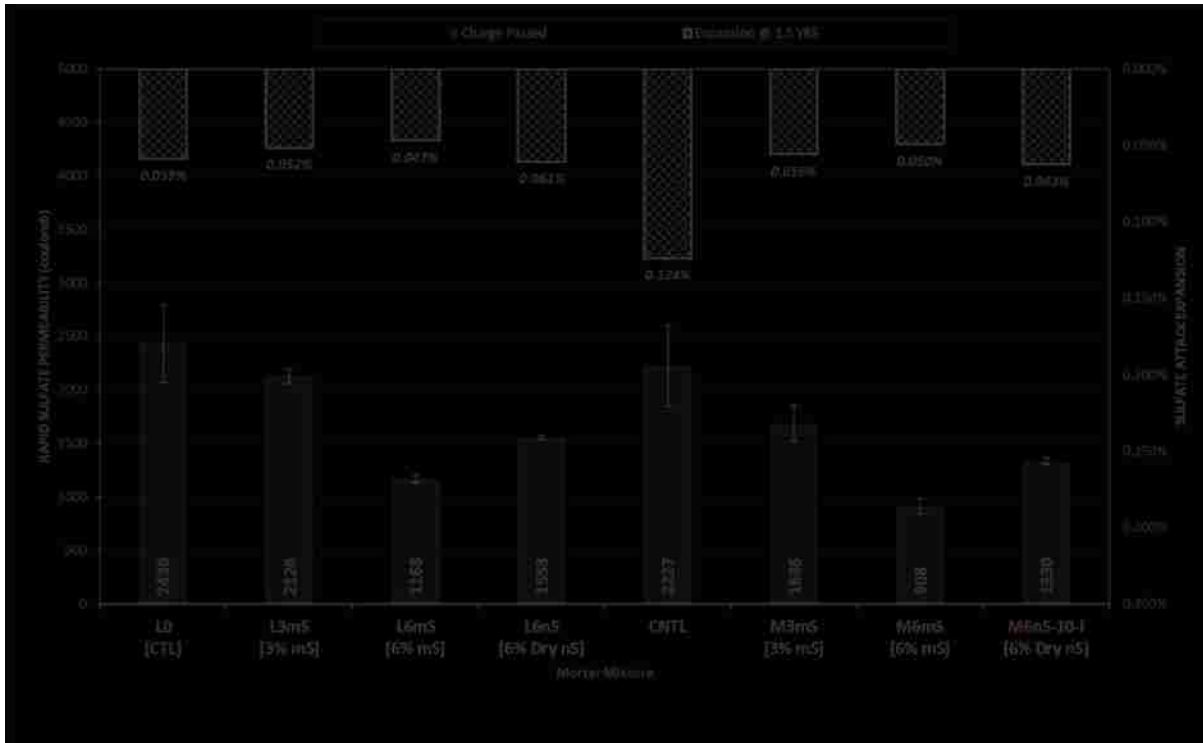


Figure 6-6: RSPT vs Expansion at 1.5 years of Sulfate Attack for Select Mortar Mixtures (error bars represent $\pm SD$)

The absorption results were not presenting the full story. The results of the RSPT test performed on the same selection of mortars are shown in **Figure 6-6**. This 6-hour test performed on 28 days cured mortars measures the penetration rate of sulfate ions which accounts for both the pore structure permeability and the free ion binding capacity. The coulomb charge measurement also accounts for all free ion movement through the mortar which could include the free hydroxide and calcium ions (Stanish et al. 1997). The mobility of these ions would reflect how effective the pozzolans were at reducing the Ca(OH)_2 available for reaction with the sulfate ions.

For cement L, the 6% nS mortar L6nS exhibited a higher penetrability compared to the 6% mS mortar L6mS which had the lowest coulomb readings. For cement M, the trend was the same. There is a significant decrease in the ion penetrability when the mS replacement is increased from 3% mS to 6% mS. The combination replacement mortars, although not tested, likely exhibit a similar coulomb

reading to the 3% mS mortars. The RSPT test correlates the relative sulfate expansion readings of the select mortars tested for RSPT to their sulfate attack expansion readings after 1.5 years as presented in the secondary axis of *Error! Reference source not found.* Although the nS mortars might be overall less porous according to the absorption test, they allow greater ion penetrability than the mS mortars. Greater ion mobility in the nS mortar mixtures indicates the nS was not as effective as a pozzolan compared to the mS. The higher diffusion rates of the nS mortars also results in a greater supply of sulfate ions deeper into the mortar to react with hydroxide and calcium ions and generate more expansive ettringite.

6.4.4 Mercury Intrusion Porosimetry (MIP)

The absorption test may indicate permeability in terms of the total permeable void volume but that is not always the case as quality durable concrete could have high porosity yet a low permeability. The pore size distribution, pore interconnectivity, and their tortuosity influence the permeability of the mortars and therefore their response to sulfate attack (Richardson 2002). A mortar may have a higher porosity as measured by absorption, but it may be composed of smaller less interconnected and impermeable voids or larger entrapped air voids that do not facilitate the generation of the expansive stresses that lead to volume instability and cracking from sulfate attack. Pores in the mortar are of different sizes and types and some contribute to permeability and some do not (Neville 1998). To better understand the nature of the silica contained mortars' pore size distribution, cement M mortars M0, M6mS, and M6nS were submitted for mercury intrusion porosimetry (MIP) testing to identify the effects of the mS and nS used in this study. Those results are presented in *Figure 6-7*.

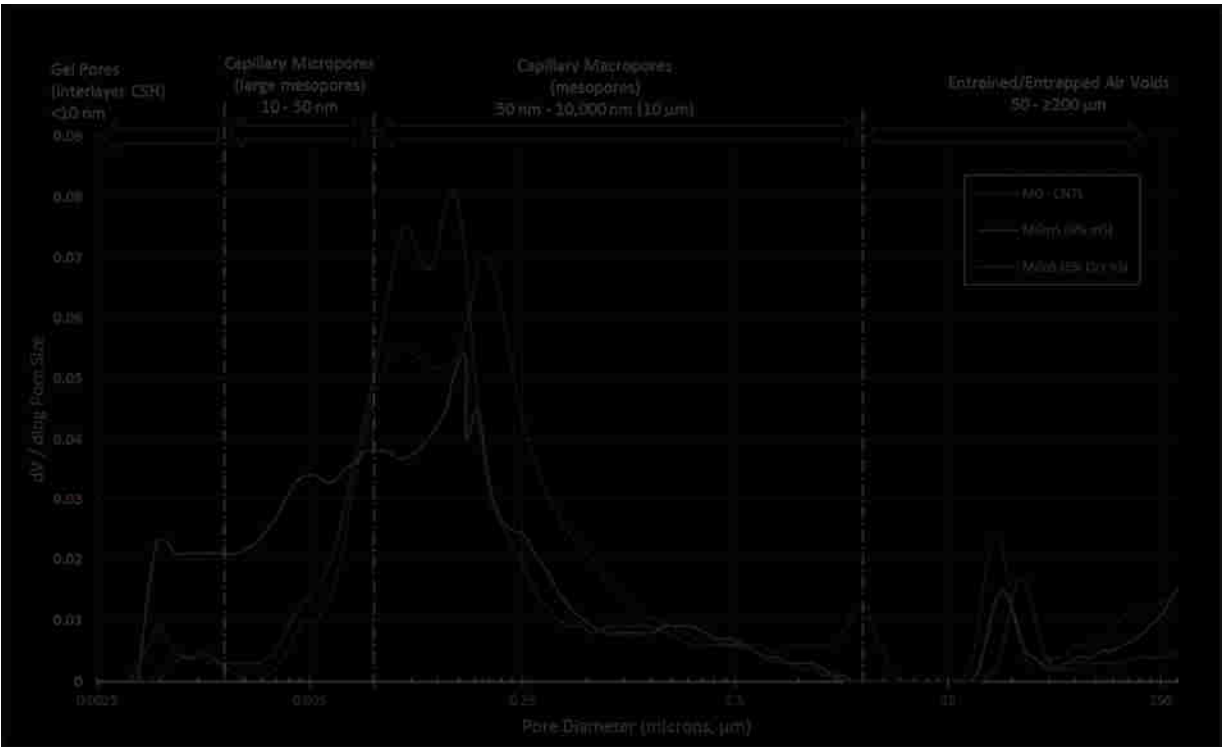


Figure 6-7: MIP Pore Size Distribution for Cement M Mortars

Pores in hydrated cement paste have been classified in several categories dependent on their size and influence on the hydrated cement properties. Gel pores are generally less than or equal to 10 nm and they are integral to the densely layered C-S-H phase; they are considered impermeable and do not contribute to transport processes. Pores ranging from 10 to 50 nm are considered capillary micropores and although tortuous, these can in small part contribute to permeability. The bulk of permeability and diffusivity occurs in the interconnected capillary macropores ranging from 50-10,000 nm (0.05 to 10 μm) (Tobón et al. 2015; Du et al. 2014b; Mindess et al. 2003). The most significant pore refinement is evident in the 6% mS contained mortar M6mS. There is a significant shift in its pore size distribution into the gel pore and micropore ranges. The average pore diameter for M6mS is 30.5 μm . The results also indicate that the 6% nS mortar had a higher volume of pores in the macropore range compared to M6mS and the control M0. This could be attributed to the

agglomeration of the dry nS powder during mixing. Agglomerated nS fails to serve as nucleation sites that can densify the cement paste and as other researchers have found may trap water during mixing that later becomes a porous weak zone (Li et al. 2004). There is evidence of this considering that even in agglomerated form, during mixing of M6nS, the demand for HRWRA quadrupled when compared to M6mS to achieve a similar workability and flow. A similar trend could be assumed for the combination mortar M3mS+3nS given that for M3mS, no HRWRA was required but 9 grams of HRWRA were necessary for the combination mixture. The total mercury intrusion volume measured for M0, M6mS, and M6nS was 0.082 cm³/g, 0.0808 cm³/g, and 0.0687 cm³/g, respectively. These intrusion volumes correlate with the trend observed with absorption. The mixture with nS might have the lowest total void volume, but most of it is concentrated in the capillary macropore range of pore sizes which negatively impacts the mortar's permeability.

6.4.5 Compressive Strength

Four cubes of the sulfate exposed and four cubes of the moisture room cured mixtures for each cement type were tested in compression at the 28 days, 12, 26, and 52 weeks (1 year). The results for the 26 and 52 week testing of cement L and cement M are presented in **Figure 6-8** and **Figure 6-9**, respectively. The strength ratio added as the secondary y-axis represents the compressive strength of the sulfate solution exposed samples over that of the cure room counterparts. When over the 1.0 line, it indicates that the average compressive strength of the sulfate exposed samples was higher than that of those tested from the curing room for that particular mortar mixture. Since almost all sulfate solution-to-moist room cured mortar strength ratios were greater than 1, except for L3mS at 52 weeks, there was no evidence of strength loss due to sulfate attack.

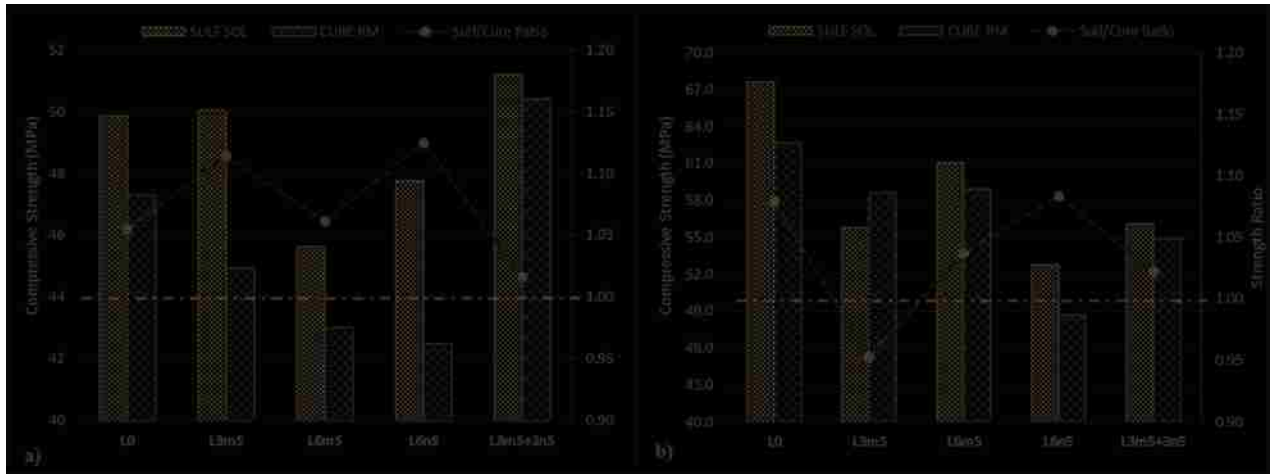


Figure 6-8: Cement L Mortar Cube Compressive Strengths at, a) 26 Weeks, b) 52 Weeks

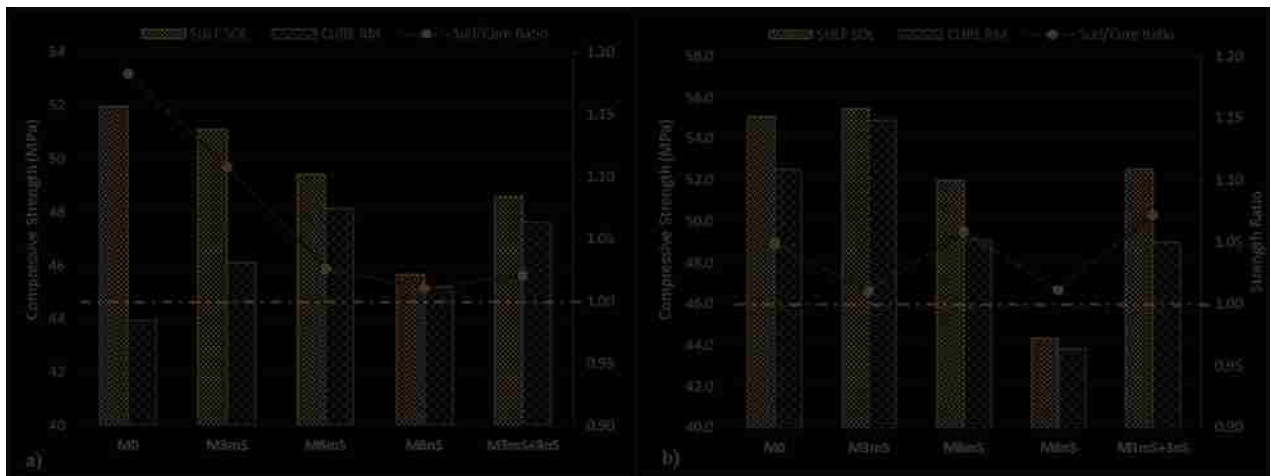


Figure 6-9: Cement M Mortar Cube Compressive Strengths at, a) 26 Weeks, b) 52 Weeks

Other researchers have reported an increase of strength due the filling and compaction effect of the sulfate attack related expansive compounds such as ettringite (Rundong et al. 2010). Upon a longer exposure to sulfate attack, when available pores are filled, the expansive compounds may begin developing micro-cracks that can reverse the trend between the sulfate and curing room samples.

In terms of comparing strength, the combination silica mixtures M3mS+3nS and L3mS+3nS outperformed the 6% nS mortars both at 26 and 52 weeks. The compression strengths of the 6% nS mortars for both cements are the lowest at 52 weeks indicating that the agglomerated nS weakened the cement paste matrix in comparison to the control and other silica replacement mixtures. The compressive strength measurements at 52 weeks for L3mS and L3mS+3nS were similar in nature and those of M3mS are higher than M3mS+3nS, indicating that the additional 3% nS for cement M had a negative effect. This further supports the hypothesis that in the combination mortar most of the beneficial effects due to the silica content stems from the 3% mS portion.

6.5 Conclusion

The objective of this study was to determine if combined nS and mS contained mortars would exhibit superior sulfate durability over comparable mortars mixtures featuring either only nS or mS cement replacement. The outcomes of this study were as follows:

1. M3mS performed almost as well as the combination mortar M3mS+3nS which suggests that most of the beneficial contribution to sulfate resistance in the combination mortar stems from the mS replacement when poorly dispersed dry nS is used. The positive contribution of the agglomerated nS replacement might only be that of reducing the overall availability of C₃A by reducing the cement content by another 3%.
2. With a sulfate resistant cement, increasing the mS dose resulted in diminishing returns as the smaller dose of 3% mS is almost as effective as doubling it. Similarly to the moderate C₃A cement, combining agglomerated dry nS with mS is not preferable to pure mS.
3. The results also indicated that the 6% nS mortar had a higher volume of pores in the macropore range of the pore size distribution that are conducive to permeability and diffusivity compared to M6mS and the control. It is believed this is attributed again to the agglomeration of the dry nS powder during mixing. The agglomerated nS failed to serve as

nucleation sites that could densify the cement paste and may have trapped mixing water within the agglomerates during hydration that later resulted in weak and permeable zones. This was supported by the RSPT testing and the observed high HRWRA demand of the agglomerated nS considering that the nS was not well dispersed and not exhibiting the desired high surface area.

4. The compressive testing results also indicated that, given the poor performance of the 6% nS replacement mortars, and the comparable performance between the 3% mS and combination mixtures after 1 year curing or sulfate exposure, most of the beneficial effects due to the silica content for the mS+nS mixtures is contributed by the mS when paired with agglomerated nS.

Considering the many forms and gradations of commercially available nano and micro-silica, the effect of nS+mS combination mixtures on resistance to sulfate attack warrants more research. Further testing of mortars with combined mS and nS cement replacement, where the nS is in a better dispersed form, such as a verifiable stabilized aqueous solution, is recommended. Nanosilica that better exhibits its high surface area and aggressive pozzolanic nature through its dispersed nanoscale particles, possibly will better pair with mS and more effectively resist sulfate attack than when either silica is applied individually.

7 INFLUENCE OF DISPERSION METHODS ON SULFATE RESISTANCE OF NANOSILICA CONTAINED MORTARS

7.1 Abstract

This study evaluates the influence of various dispersion methods on the sulfate attack resistance of nanosilica (nS) contained mortars. Multiple mechanical or ultrasonic dispersion methods, HRWRA dosing procedures, and both dry and aqueous solution forms of nS were used to prepare a series of mortars with 0%, 3%, and 6% replacement of Portland cement with nS. Mortars were subjected to 6 months of exposure in a 5% sodium sulfate solution. Expansion, compressive strength, water absorption, rapid sulfate ion permeability, and porosity were measured. Results indicate that, use of the aqueous form of nS results in a more sulfate resistant and impermeable mortar than all other tested methods of dry form nS. HRWRA dosage proved most effective when added directly to the mixer after all water, binders, and fine aggregate were combined. Excessive ultrasonic dispersion of dry nS in the mixing water may cause further agglomeration of the nS that proved deleterious to permeability and sulfate resistance. In terms of compressive strength, mortars with 3% nS content performed similarly to those with double the nS content. Increasing the nS content seemed to have the least influence on the compressive strength of the better dispersed aqueous nS mixtures.

7.2 Introduction

Concrete's broad application and dominance as the most ubiquitous construction material in part due to its inherent versatility, durability, and low cost, has made it a focus of innovative efforts (Kosmatka et al. 2002). These efforts include improving performance, durability, and reducing the associated high carbon cost of its production, estimated at 1.6 billion tons of CO₂/year. This represents 6% of the global man-made CO₂ production (Mann 2006). Concrete is a multi-phase composite material. Its performance is influenced by the molecular assemblages, chemical bonds,

and nano and microscale processes that occur both during hydration and under the ageing processes it is subjected to over its service life (Sanchez & Sobolev 2010). Nanotechnology developments have made significant impacts to multiple industries. Research into nano-engineered construction materials has garnered a lot of attention over the last 50 years since P. Feynman discussed the significance of manipulating matter at the nanoscale in his 1959 lecture "*There's Plenty of Room at the Bottom*" (Sanchez & Sobolev 2010; Sahin & Oltulu 2008). The surge of interest in nanomaterials and their potential applications in producing high performance, sustainable, and durable concrete has pushed nano-sized (<100 nm) SiO₂ in the limelight as a very promising mineral admixture. This attention is due to the material's fine particle size and aggressive pozzolanic nature. The high pozzolanic reactivity stems from its inherently high surface area that surpasses that of its predecessor microsilica (mS), also known as silica fume (Singh et al. 2013; Pengkun Hou et al. 2013). Nanosilica (nS) is commercially available in various nano-scale sizes dependent on the method of synthesis and may be offered in dry powder form or in a dispersant stabilized suspension (Campillo et al. 2004). Nanosilica has shown to improve segregation resistance of concrete or mortars in the fresh state, boost early strength, improve the packing density, refine the paste pore size distribution, reduce overall pore volume, densify the C-S-H paste and ITZ zone, and generates additional secondary C-S-H through its pozzolanic activity (Singh et al. 2013; Tobón et al. 2015). Nanosilica also pairs well with other mineral admixtures such as fly ash and slag. It helps accelerate hydration and early strength gain which are drawbacks of larger cement replacements with the aforementioned cementitious materials (Said et al. 2012; Peng-kun Hou et al. 2013; Kawashima et al. 2013).

Although the fresh rheological and hardened properties of cement pastes, mortars, and concrete with nS replacement have been studied over the recent years there is still limited literature on the sulfate durability effects of nS. Based on the densifying effect of the nanomaterial and its behavior as both a fine filler and a pozzolan, it has been observed that nS can improve durability (Tobón et al. 2015; Du

et al. 2014a). Nanosilica achieves this by both, making the cement paste and ITZ at the aggregate interface more impermeable to sulfates, and binding up the Ca(OH)_2 that is commonly first to be targeted for hydroxide (OH^-) and calcium (Ca^+) ions during sulfate attack for the formation of deleterious ettringite and gypsum. When nS comes in contact with water it forms $\text{H}_2\text{SiO}_4^{2-}$ which reacts with the calcium ions freed from Ca(OH)_2 to form secondary C-S-H (Singh et al. 2013). This pozzolanic effect albeit less aggressive, is similar with the application of silica fume.

Van der Waals and electrostatic forces strongly affect ultrafine particles in a solution such as nS, and cause them to agglomerate which reduces their free surface area (L Senff et al. 2010; Park et al. 2005). This recognized tendency of nS to agglomerate when in solution, that hinders its full potential as a nanomaterial, has motivated researchers to test a wide variety of mixing procedures and methods in their studies to improve the dispersion of nS in cementitious mixtures. Some of these studies are summarized in **Table 7-1**. These often include either mechanical or ultrasonic dispersion of the dry nS powder with the mixture water or the use of a dispersant stabilized aqueous solution. The aqueous solutions contain a certain percent of solid nS typically in the ranges of 20-50% and dispersants such as Na_2O , ammonia, or ethylene glycol (Campillo et al. 2004). Based on the weight of pure solid nS, the suspension solutions typically come at a higher cost than the dry nS powder, but are better at mitigating the tendency for the nS to agglomerate when introduced to the mixture water. Additionally there seems to be no general agreement on when the use of a superplasticizer (SP) or high-range water reducing admixture (HRWRA) in the mixing process is most effective at both dispersing the nS and achieving a good target workable flow of the mortar or concrete. In some studies, the admixture is introduced in the preliminary mechanical dispersion of the dry nS powder with water, sometimes in the mixer once all the binders and aggregates are combined, and sometimes it is split between the two.

Table 7-1: Literature Review of Different nS Forms and Methods of Dispersion or Mixing

Nanosilica (nS) Product	Method of Dispersion/Mixing	Superplasticizer/ Water Reducer	Reference
Dry Powder [15±5 nm]	Dispersant was dissolved in water and then the nano-particles were added and mechanically stirred at high speed for about 2 min. Then the other ingredients were added and stirred for another 1 min.	Sulfonated naphthalene formaldehyde condensate (UNF) added during mechanical mixing of nS	(Li et al. 2004)
Dry Powder [40 nm] 60 m ² /g	nano-SiO ₂ particles were stirred with the mixing water at high speed (120 rpm) for 1 min.	Polycarboxylate added in mixer	(Jo et al. 2007)
30% Aq. Dispersion [15 nm] (ammonia stabilized)	Colloidal silica directly added to the mixing water	Polycarboxylate added in mixer	(Dolado et al. 2007)
- Dry Powder 1 [20 nm] - Dry Powder 2 [5 nm] - 30% Ethylene Glycol Dispersion [20 nm] - 30% Aq. Sol. [30 nm] (0.15% Na ₂ O stab.) - 15% Aq. Sol. [15 nm] (ammonia stab.)	For colloidal silica, the suspension was directly added to the mixing water Dry nS was added to the cement and mechanically homogenized	No SP used	(Campillo et al. 2004)
30% Aq. Dispersion [5-15 nm] - 200 m ² /g	Cement , aggregates, and silica fume were dry mixed in a rotary mixer for 30 sec, then 80% of mixing water was added and mixed for 30 sec, then a ready-mixed liquid including super plasticizer and nano-SiO ₂ was added to the 20% remained water and then the liquid poured into the rotary mixer slowly. The concrete mixture was mixed wet for additional 1.5 min.	Polycarboxylate ether polymer or Sulfonated naphthalene formaldehyde SP mixed with 20% water and added to mixer	(Zaki & Khaled .s.Ragab 2009)
30% Aq. Dispersion [97-157 nm] - 51.4 m ² /g	Mortars prepared in accordance with ASTM C 305 The homogenization was done previously with the mixing water corrected for the amount of water incorporated by the suspension.	Polycarboxylate ether homogenized with the mixing water	(Tobón et al. 2010)
45% Aq. Dispersion [30 nm] (Na ₂ O stabilized)	ASTM C 305 mixing procedure followed	Not Discussed	(Mondal et al. 2010)
30% Aq. Dispersion [9 nm] - 300 m ² /g (Na ₂ O stabilized)	Not discussed	Polycarboxylate	(L Senff et al. 2010)
15% Aq. Dispersion [5 nm]	75% of mixing water added to concrete and mixed for 2.5 min, 25% mixing water which was premixed with the SP and the nS was added and mixed for 1.5 min	Polycarboxylate added to 1/4 of mixing water and nS and added to mixer	(Khanzadi et al. 2010)
50% Aq. Dispersion [50-60 nm] - 80 m ² /g	nS was mixed with SP and half of the mixing water. Then added with the coarse aggregate to mixer after sand, cement, half of the mixing water and half of the SP content were mixed in pan mixer for 1 minute.	Polycarboxylate ether added to mixer with 1/2 of mixing water	(Nili et al. 2010)

30% Aq. Dispersion [9 nm] - 300 m ² /g	Solid components dry mixed inside a plastic bag for 1 min, then poured into mixing water with SP, mechanical mixing for 3.5 min	Polycarboxylate added to water in mixer	(Luciano Senff et al. 2010)
15% Aq. Dispersion [5-50 nm] - 364 m ² /g	nS pre-mixed with demanded amount of water in a mixer with special blades for mixing liquids	Polycarboxylate added to small portion of mixing water in mixer	(Koohdaragh & Mohamadi 2011)
30% Aq. Dispersion [10 nm] - 345 m ² /g (Na ₂ O stabilized)	(1) Mechanical mixing for 2 min at 120 rpm, (2) hand mixing to break up clumped cement particles (1 min), and (3) mechanical mixing for other 2 min at 60 rpm.	Polyacrylic type superplasticizer added to mixer after nS and OPC was added to water	(Berra et al. 2012)
50% Aq. Dispersion [35 nm] - 80 m ² /g	Constituent materials mixed in a mechanical mixer according to ASTM C 192	Polycarboxylic acid added to the mixer in solution in the mixing water	(Said et al. 2012)
Dry Powder [3 nm] 710.4215 m ² /g (lab synthesized)	Cement, admixtures and nS blended and then water added	Not Discussed	(Choolaei et al. 2012)
- Dry Powder [12 nm] 200.1 m ² /g - Dry Powder [7 nm] 321.6 m ² /g	Mechanical mixing where nS added with cement and sand in mixer before adding water and SP or ultrasonic mixing of nS + water for 5 min	Polycarboxylate SP added to mixer 1 min after water	(Zhang et al. 2012)
30% Aq. Dispersion [10 nm] - 345 m ² /g (Na ₂ O stabilized)	nS was hand-stirred in the mixing water prior to adding the other materials	not used	(Peng-kun Hou et al. 2013)
- 30% Aq. Dispersion [10 nm] (Na ₂ O stabilized) - 30% Aq. Dispersion [20 nm] (Na ₂ O stabilized)	For nanoclays tested (30nm x 1.75µm) blended with household blender for 3 minutes For inert limestone powder (nanoCaCO ₃ : 15-40 nm) either sonicated 30 min at 15% wt. with water with 0.06% SP or blended for 3 minutes in household blender	Polycarboxylate SP added to nanoCaCO ₃ sonicated for 30 minutes	(Kawashima et al. 2013)
30% Aq. Dispersion [10 nm] (Na ₂ O stabilized)	Not discussed, nS in dispersed suspension		(Peng-kun Hou et al. 2013)
Aq. Dispersion [25 nm] - 109 m ² /g	Water, SP and nS were premixed for 1.5 min at 120 rpm. Fine aggregate, cement and SF (if used) were mixed first for 2 min at 60 rpm. The process was followed by addition of previously mixed water and SP.	Polycarboxylate SP blended with water and nS at 120 rpm for 1.5 min	(Zapata et al. 2013)
Dry Powder [13 nm] 200 m ² /g	nS was dissolved in 500 mL water with SP. Prior to ultra-sonication, the aq. sol. was hand-mixed for 1 min. The sonication period was 10 min at 400W. Aggregates and OPC were dry mixed for 1 min before adding the remaining mixing water. Finally, the nano-silica aqueous solution was added into the wet mixture. Additional SP was added into the concrete mixture to keep the consistency.	Surfactant (DARACEM 100 HRWRA Aqueous Solution of Na/K Naphthalene Sulfonates, Lignin and Hydrocarboxylic Acid Salts added during ultrasonication	(Du et al. 2014a)
40% Aq. Dispersion [98.65 nm] - 51.4 m ² /g (ammonia stabilized)	NS-particles suspension was pre-mixed with the mixing water.	Polycarboxylate SP homogenized with mixing water prior to use in mixer	(Tobón et al. 2015)

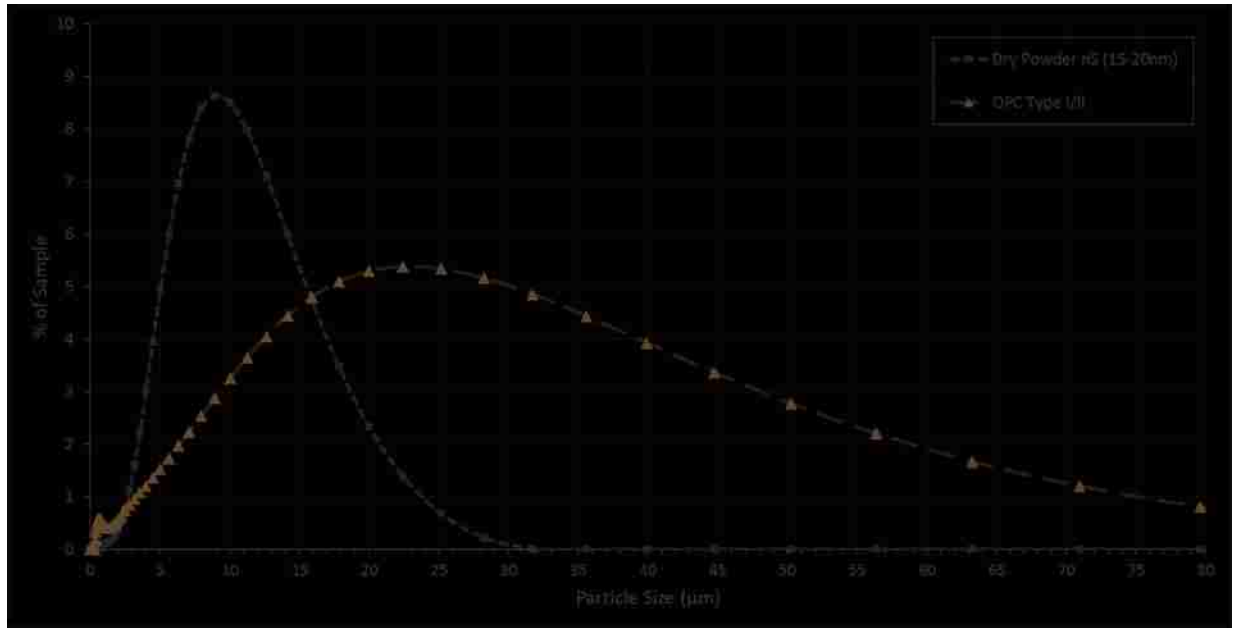


Figure 7-1: Laser Diffraction Particle Size Analysis of dry nS and OPC

Some agglomeration of the dry nS particles used in this study is anticipated and was directly observed and measured using laser diffraction particle analysis. Samples of the dry powder nS used in the study were tested along with samples of the OPC. Prior to measurement, the nS samples were ultrasonically mixed in water for 5 minutes. The results as presented in **Figure 7-1** indicated that the average particle size measured for nS was 7 to 10 µm which was multitudes larger than the manufacturer specified nS particle size of .015-0.020 µm. Even with ultrasonic dispersion, the dry nS particles introduced in a plain water suspension tend to agglomerate to a graded size of clusters significantly larger than the individual nS particles. Nevertheless the scope of the presented work is to investigate how different methods of dispersing the nanomaterial available in both dry and aqueous form, will impact the sulfate durability of the mortars. There are different levels of agglomeration directly influenced by the method of mixing and method of adding the dispersive HRWRA that, as widely explored in much of the referenced work in **Table 7-1**, have different effects on the performance of mortars. The focus of the work is to investigate this effect on the durability of mortars against sulfate

attack. It is was hypothesized that even in various degrees of agglomeration, nS could prove an effective pozzolanic admixture, but it is of particular interest to confirm a preferable form of nS and identify a recommended mixing procedure. This work serves to directly compare different dispersion methodologies and different HRWRA dosing procedures, and to investigate how they impact the sulfate durability, compressive strength, and permeability of mortars. Both mechanical dispersion and ultrasonic dispersion were compared against an equal nS dose by weight using an aqueous solution of nS.

7.3 Experimental Procedure

The studied mortars were subjected to a 26 week (6 month) full submersion exposure in a 5% sodium sulfate (Na_2SO_4) solution. The linear expansion of mortar bars, mortar cylinder compressive strength, water absorption, rapid sulfate ion penetration (RSPT), and mercury intrusion porosimetry (MIP) were measured.

7.3.1 Materials

An Ordinary Portland Cement (OPC) Type I/II was used with a moderate 7.2% C_3A content. The chemical and physical properties of the cement are presented in

Table 7-2. The dry nS used was supplied in porous white dry powder form with particle sizes ranging from 15-20 nm and a specific surface area of 640 m^2/g . The aqueous nS dispersion contained 25% by weight of 5-35 nm amorphous nS particles. Matching dry and aqueous form of nS were not commercially available but considerations were made to choose products with overlapping average particle size ranges. The chemical and physical properties of the nanosilica are also presented in

Table 7-2. A polycarboxylate based HRWRA was utilized for nS dispersion and achievement of the desired flow per ASTM C 109. The fine aggregate used for the mortars in this study was from a Nevada-based quarry and had an oven-dry specific gravity of 2.76, absorption of 0.81% and a

fineness modulus of 2.64. Its gradation was well inside the upper and lower limits of ASTM C 33. Mortar mixing water and water used for the preparation of the sodium sulfate solution was commercially available distilled water obtained from a single source.

Table 7-2: Chemical Composition and Physical Properties of Cement and nS

	OPC Type I/II Cement	Dry Powder nano-Silica (nS)	Aqueous Solution nano-Silica (AQnS)
<i>Chemical Composition</i>			
Silicon Dioxide (SiO ₂), %	21.1	99.5	99.9
Aluminum Oxide (Al ₂ O ₃), %	4	0.002	--
Ferric Oxide (Fe ₂ O ₃), %	2	0.001	--
Calcium Oxide (CaO), %	62.7	0.002	--
Magnesium Oxide (MgO), %	2.1	0.001	--
Sulfur Trioxide (SO ₃), %	2.8	--	--
Loss on Ignition, %	1.8	--	--
Insoluble Residue, %	0.71	--	--
Total Alkali (Na ₂ O + K ₂ O), %	0.59	--	--
Free Lime (CaO), %	0		
<i>Physical Properties</i>			
Time of Set Initial Vicat, min	145	--	--
Specific Surface Area, m ² /g	0.341 ^a	640 ^b	--
325 Mesh (45 μm), % passing	--		
Avg. Particle Size (APS), μm	20-30 ^c	0.015-0.020	0.005-0.035
<i>Per Bogue Calculation^d</i>			
Tricalcium Silicate (C ₃ S), %	57.0	--	--
Dicalcium Silicate (C ₂ S), %	17.5	--	--
Tricalcium Aluminate (C ₃ A), %	7.2	--	--
Tetracalcium Aluminoferrite (C ₄ AF), %	6.1	--	--
(C ₃ S) / (C ₂ S) Ratio	3.26	--	--

^aby Blaine air-permeability test

^bby BET Analysis

^cEstimated from MasterSizer Particle Distribution Analysis

7.3.2 Mixture Proportions

Table 7-3 presents the mixture proportions of the mortar series tested in this study. As can be seen besides the control mixture with 0% nS replacement, the study featured ten mortar mixtures prepared with mechanical blending of either 3% or 6% nS; four mortar mixtures prepared with ultrasonic blending of 3% or 6% nS replacement; and two mortars that contained either 3% or 6%

solid weight of the aqueous form nS. In a prior study (Ghafoori et al. 2016), the authors tested mechanically dispersed dry nS replacements from 1.5% to 6% in progressive 1.5% increments. The authors found that 3% and 6% nS are representable for identifying trends between lower and higher doses of nS. The water content of the aqueous solution was accounted for to maintain the desired water-to-binder (w/b) ratio. The (w/b) was 0.485 for all mixtures according to ASTM C 1012. The fine aggregate-to-binder ratio was 2.75-to-1 by mass as specified in ASTM C 109.

Table 7-3: Mortar Mixture Proportions

Sample Designation	nS Dispersing Method	HRWRA, mL		Binder, %			3-Day Compr. Strength,		
		Blender	Mixer	Cement	Dry nS	Aq. nS	Measured Flow, %*	MPa	psi
CTRL	n/a	--	5.0	100%	--	--	130%	31.2	4,527
M3nS-10-I	10 min. mechanical	--	10.0	97%	3.0%	--	101%	40.9	5,926
M3nS-10-II	10 min. mechanical	5.0	5.0	97%	3.0%	--	95%	48.6	7,051
M3nS-10-III	10 min. mechanical	10.0	--	97%	3.0%	--	85%	47.1	6,836
M3nS-10-IV	10 min. mechanical	10.0	5.0	97%	3.0%	--	106%	43.5	6,314
M3nS-20-I	20 min. mechanical	--	10.0	97%	3.0%	--	84%	47.8	6,930
M6nS-10-I	10 min. mechanical	--	20.0	94%	6.0%	--	98%	48.8	7,080
M6nS-10-II	10 min. mechanical	10.0	10.0	94%	6.0%	--	88%	49.4	7,158
M6nS-10-III	10 min. mechanical	20.0	--	94%	6.0%	--	75%	51.4	7,448
M6nS-10-IV	10 min. mechanical	20.0	5.0	94%	6.0%	--	103%	48.7	7,064
M6nS-20-I	20 min. mechanical	--	20.0	94.0%	6.0%	--	79%	50.0	7,251
U3nS-10	10 min. ultrasonic	--	10.0	97%	3.0%	--	109%	44.3	6,427
U3nS-20	20 min. ultrasonic	--	10.0	97%	3.0%	--	102%	46.4	6,737
U6nS-10	10 min. ultrasonic	--	20.0	94.0%	6.0%	--	90%	49.6	7,191
U6nS-20	20 min. ultrasonic	--	20.0	94%	6.0%	--	74%	47.9	6,951
AQ3nS	aqueous solution	--	13.0	97.0%	--	3.0%	80%	43.4	6,290
AQ6nS	aqueous solution	--	30.0	94%	--	6.0%	49%	44.6	6,473

*Flow measured according to ASTM C 1437 with flow table conforming to ASTM C 230

7.3.3 Mixing and Testing Program

Mortar mixtures were batched using an electrically driven epicyclic mechanical mixer following the mortar preparation procedure of ASTM C 305. Another point of interest to the researchers was the optimum time to add the HRWRA in the mixture procedure both to aid with the dispersion of the nS

when used in dry form and to effectively improve the fresh workability of the mortar after mixing. Therefore, the scope of the study included a comparison between four different methods of adding a preset dose of the HRWRA. The same dose of HRWRA was added in each dry nS mixture and based on the method that mortar was assigned as either Type I, II, III, or IV. For Type I mixtures, the full HRWRA dose was added in the mortar mixer after the fine aggregate was combined with the water and binders. For Type II, the dose was split evenly between both the blender and mixer. For Type III, the full dose was added in the blender with the mixing water and dry nS during the mechanical blending stage. For Type IV mixtures, similarly to Type III, the preset dose of HRWRA was added in the blender but supplemented by any additional HRWRA required during mixing of the mortar to achieve the ASTM C 109 recommended flow of $110\pm 5\%$. For the ultrasonic dispersion and aqueous solution nS mortars, the HRWRA was added to the mixer after all binders and fine aggregate were combined which aligned with the Type I method. When using dry nS, it was mechanically blended in a commercial blender or ultrasonically mixed through the indirect method in a glass beaker using a Branson 1200 ultrasonic cleaner for 10 or 20 minutes with the premeasured mixing water, prior to placing in the mortar mixer. For the aqueous nS, the solution was stirred in with the water directly in the mixer bowl prior to adding the cement and fine aggregate.

For each mixture, three mortar expansion bars were prepared per ASTM C 1012 for measuring expansion and nine, 2-in (500mm) \varnothing x 4-in (100mm), mortar cylinder specimens were prepared for compressive strength testing. Additionally six, 4-in (10 cm), diameter disks were cast for any supplemental testing.

All mortar sample molds were hand packed and compacted using an electromagnetic vibrating table. The sample molds for each mortar mixture were plastic wrapped and kept at room temperature 21 ± 3 °C (69.8 ± 5.4 °F) for 24 hours followed by 3 days of curing in a saturated lime solution to achieve the required minimum compressive strength of 20 ± 1.0 MPa (2900 ± 145 psi) per ASTM C 1012 prior to

sulfate exposure. After the 3-day lime solution cure, three mortar cylinders were tested for compressive strength to confirm the minimum. The mortar bars and three of the mortar cylinders were then transferred to the 5% sodium sulfate solution tank. The remaining 3 cylinders of each mortar were kept in the curing tank and tested in compression alongside the sulfate solution exposed samples after the 26 week (6 month) test period. An absorption test, based on ASTM C642, was conducted for all samples. A rapid sulfate penetration test (RSPT) as reported by Cement Concrete & Aggregates Australia (CCAA 2011) and mercury intrusion porosimetry (MIP) were also conducted for select mortar mixtures. The RSPT test is similar to ASTM C1202 for rapid chloride penetration test, but setup using 10% sodium sulfate across the 0.3N NaOH instead of 3% NaCl.

7.3.4 Sulfate Solution

The 5% Na₂SO₄ solution was prepared per ASTM C 1012. A solution to mortar volume ratio of 4 was maintained and the solution was kept in circulation using submersible pumps. To replenish the sulfate ion concentration of the solution, the pH was continuously maintained at 6.5±1 with a pH controller and peristaltic pump system that dosed 0.5N H₂SO₄ as needed during the 6 month fully submerged test (Mehta 1975).

7.4 Experimental Results and Discussion

Presented first is a direct comparison between the 3 main methods of dispersion before delving in a deeper discussion that concludes with a focused look at the mechanical method of dry nS dispersion. The effects of the different HRWRA dosing methods tested are discussed alongside the results of the mechanical blending method of nS dispersion.

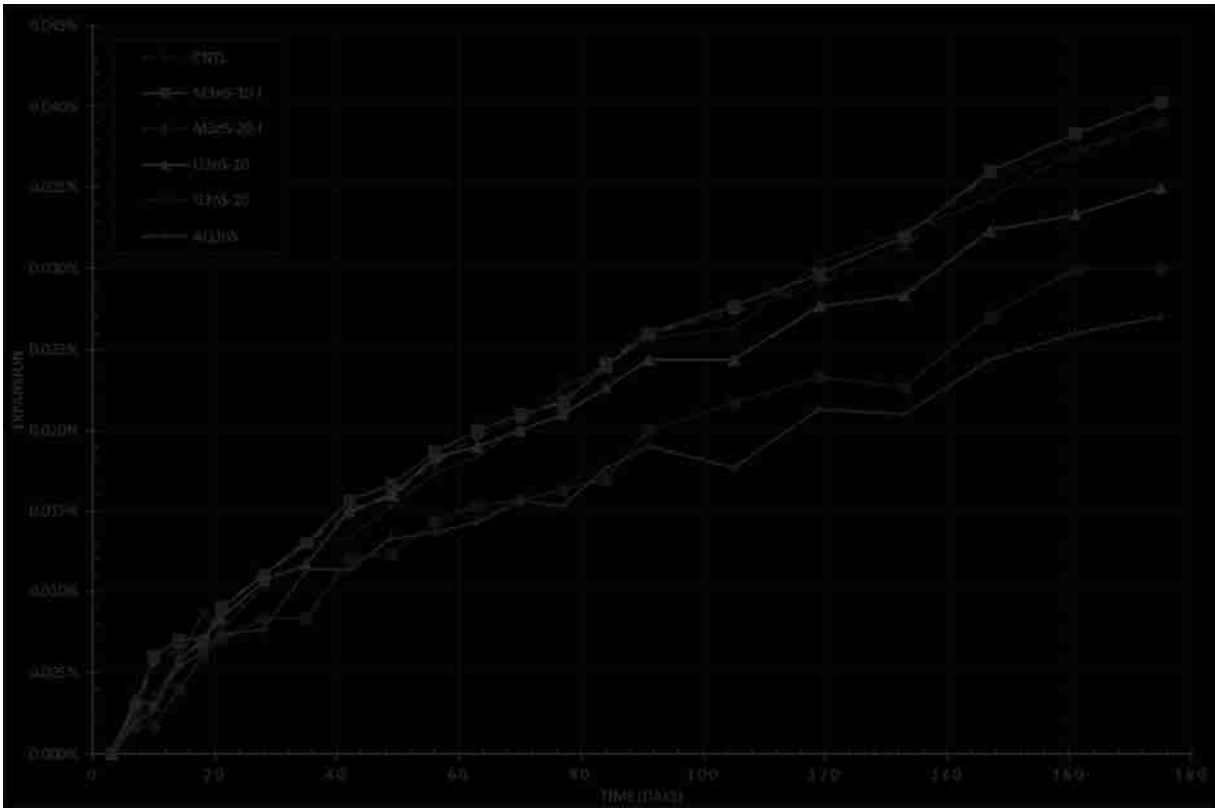


Figure 7-2: Expansion of the Mechanical Dispersion, Ultrasonic Dispersion, and Aqueous Solution 3% nS Mortars

7.4.1 Sulfate Expansion – Aqueous Solution VS Ultrasonic Dispersion VS Mechanical Dispersion

As evident in **Figure 7-2** and **Figure 7-3**, the aqueous solution mortars AQ3nS and AQ6nS exhibited the least expansion of all mechanical and ultrasonically dispersed nS mortars. On the other hand, the ultrasonic mortars U3nS-10 and U3nS-20 showed more expansion than M3nS-20-I, the mortar featuring 20 minute mechanical blending of 3% dry nS. Only M3nS-10-I and M3nS-20-I mortars are presented in **Figure 7-2** because they are the only directly comparable mechanically dispersed 3% nS series that had the HRWRA added in the mixer similarly to the ultrasonic and aqueous series. The rest of the M-series mortars will be further discussed later in the results. With the 6% nS mortars in **Figure 7-3**, the ultrasonic and mechanically blended nS mortars are not significantly distinguishable. These results indicate that at higher levels of nS replacement, there aren't any significant benefits of

ultrasonic over the mechanical method of dry nS dispersion. At lower levels of nS replacement, as shown with the 3% nS mortars in **Figure 7-2**, a longer period of mechanical blending results in less expansion than that measured for both 10 and 20 minute ultrasonically dispersed dry nS mixtures.

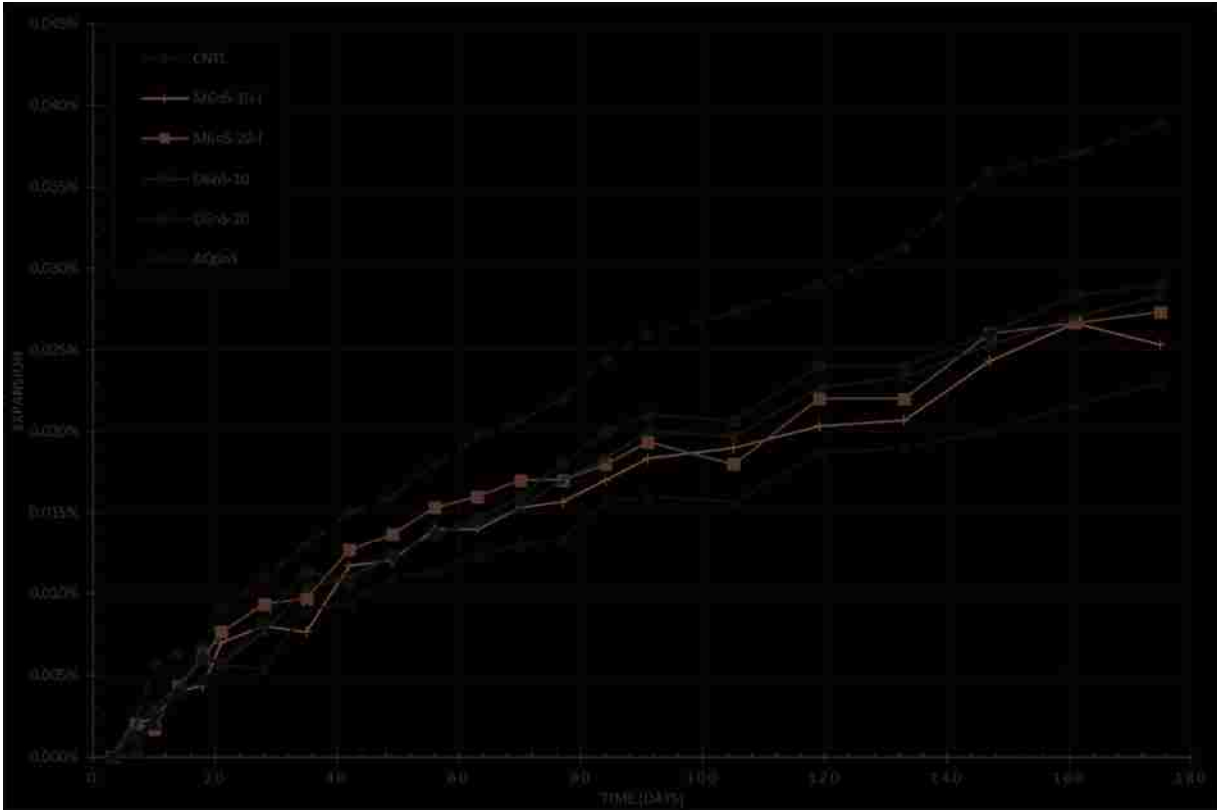


Figure 7-3: Expansion of the Mechanical Dispersion, Ultrasonic Dispersion, and Aqueous Solution 6% nS Mortars

7.4.2 Sulfate Expansion – Ultrasonic Dispersion and Aqueous Solution

All ultrasonically dispersed nS mortars are presented alongside their aqueous solution counterparts in **Figure 7-4**. The general trend observed was that the higher 6% nS replacement dose and aqueous solution form of nS produced the most sulfate durable mortar with the least expansion during the duration of the experiment. In terms of reducing sulfate expansion, the 3% nS mortar U3nS-10 showed some improvement over the control but the longer sonicated U3nS-20 surprisingly did not.

A longer period of dispersion using the ultrasonic method actually resulted in a negative effect on the mortar durability. Note that both U3nS-10 and U6nS-10 exhibited less expansion than their 20 minute sonication counterparts. This was against the original expectations that longer sonication would improve nS dispersion and therefore the paste density and impermeability.

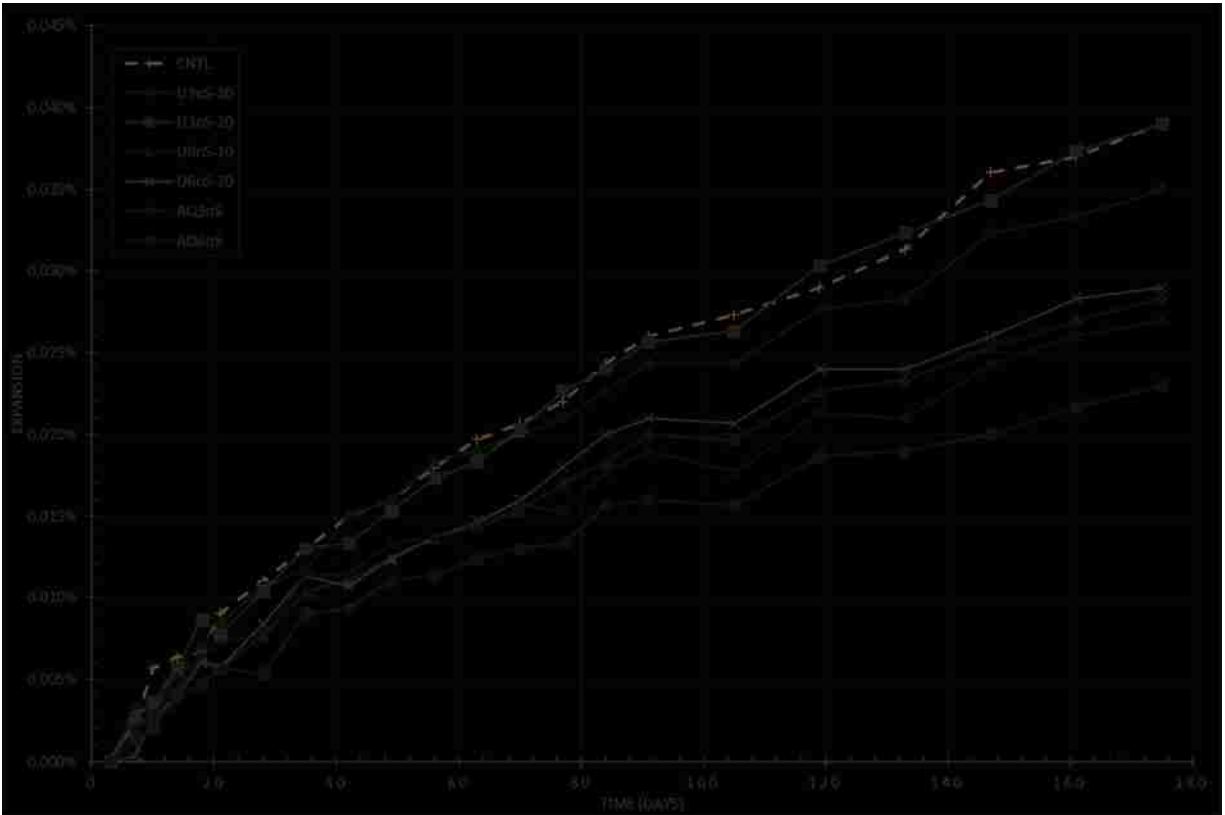


Figure 7-4: Expansion of the 3% and 6% nS Ultrasonic Dispersion VS Aqueous Solution Mortars

Both aqueous solution mortars AQ3nS and AQ6nS performed significantly better than the control mortar. AQ3nS and AQ6nS exhibited 36.4% and 51.6% less expansion than the CNTL mortar at 26 weeks. There was an observable challenge with workability for these two mixtures as can be seen in **Table 7-3**. The measured flow for the AQ3nS mortar was 80% and that required an additional 3 mL over the preset 10 mL of HRWRA used for all 3% nS mortars. The flow of AQ6nS was even less at 49% after the addition of 30 mL of HRWRA, 10 mL more than the preset 20 mL dose. These workability

challenges stem from the superior dispersion of the nS in the aqueous solution through which the nS better expressed its large surface area. The originally preset 20 mL dose of HRWRA based on 6% of dry nS was not nearly enough to get a workable mortar that could be tested for flow and adequately compacted into the molds. Nevertheless even under unfavorable workability, the aqueous solution mortars showed less expansion than all ultrasonic mixtures. Better performance of the aqueous solution mortars was hypothesized but not the difference in workability in comparison with the other forms of nS replacement.

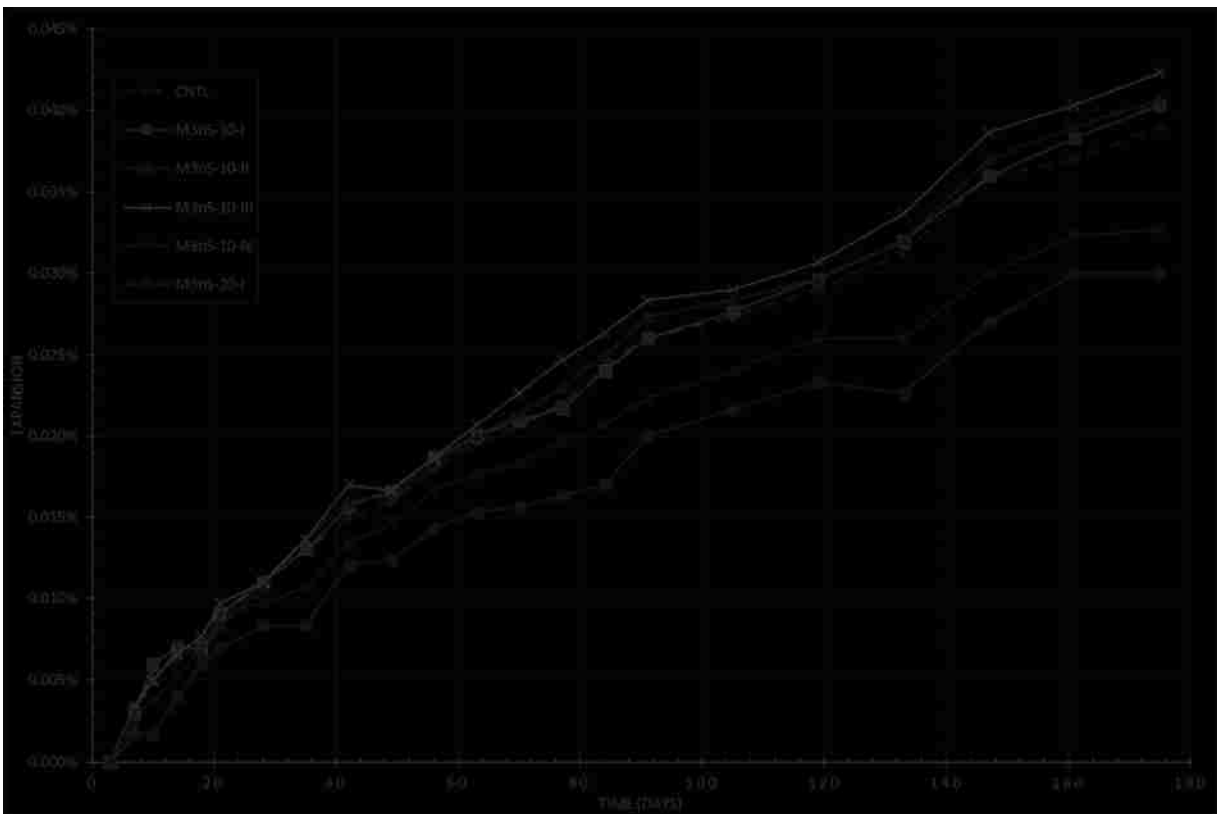


Figure 7-5: Expansion of the Mechanical Dispersion 3% nS Mortars

7.4.3 Sulfate Expansion – Mechanical Dispersion & HRWRA Dosing Method

The following results and discussion focus on the various forms of mechanical dispersion tested in this study. **Figure 7-5** presents the different expansion readings between mechanically blending the 3% dry nS with mixing water for 10 or 20 minutes and any observable trends between the different approaches for adding the HRWRA. Half of the 3% nS contained mortars generally showed higher levels of expansion in comparison to the CNTL (0% nS) mixture. The mortars that exhibited more expansion than the control at 26 weeks (175 days) were M3nS-10-I, M3nS-10-II, and M3nS-10-III. These were all the mortars where the same fixed dose of 10 mL HRWRA was used, and the nS and mixing water was blended for 10 minutes. The mortar with the consistently low levels of expansion during the 6 month exposure was M3nS-20-I. This mortar had the same 10 mL of HRWRA added in the mixer but the nS and mixing water were blended for 20 minutes instead of 10 minutes. At 12 weeks the expansion for M3nS-20-I was 0.016% which was 29.6% less than that of the control at 0.022%. At the 6 month mark, M3nS-20-I had 0.030%, which was 26.1% less than the control. Mortar M3nS-10-IV also performed better than the control. At 6 months, its expansion of 0.033% was 17.7% less than the control. M3nS-10-IV had all 10 mL of HRWRA added to the mixing water before it was blended with the nS for 10 min, and an additional 5 mL were added during mixing to achieve a flow within the target range. The intent of the Type IV mortar was to both optimize the effect of the HRWRA as a dispersant of the nS during mechanical blending, and also achieve an ideal workability for mixing and compacting by adding supplemental HRWRA above the preset dose. At the 3% nS level of replacement the results indicate that shorter periods of blending nS regardless of when the HRWRA was added will result in unfavorable dispersion of nS or mortar workability that will perform poorly against sodium sulfate. Based on these results, recommendations for mechanical dispersion of dry nS would primarily be blending the nS with the mixing water for a longer period of time; 20 minutes proved effective in this study. If the HRWRA is added during blending of nS with the mixing

water to aid dispersion, additional HRWRA should be added to the mixer to achieve desired workability.

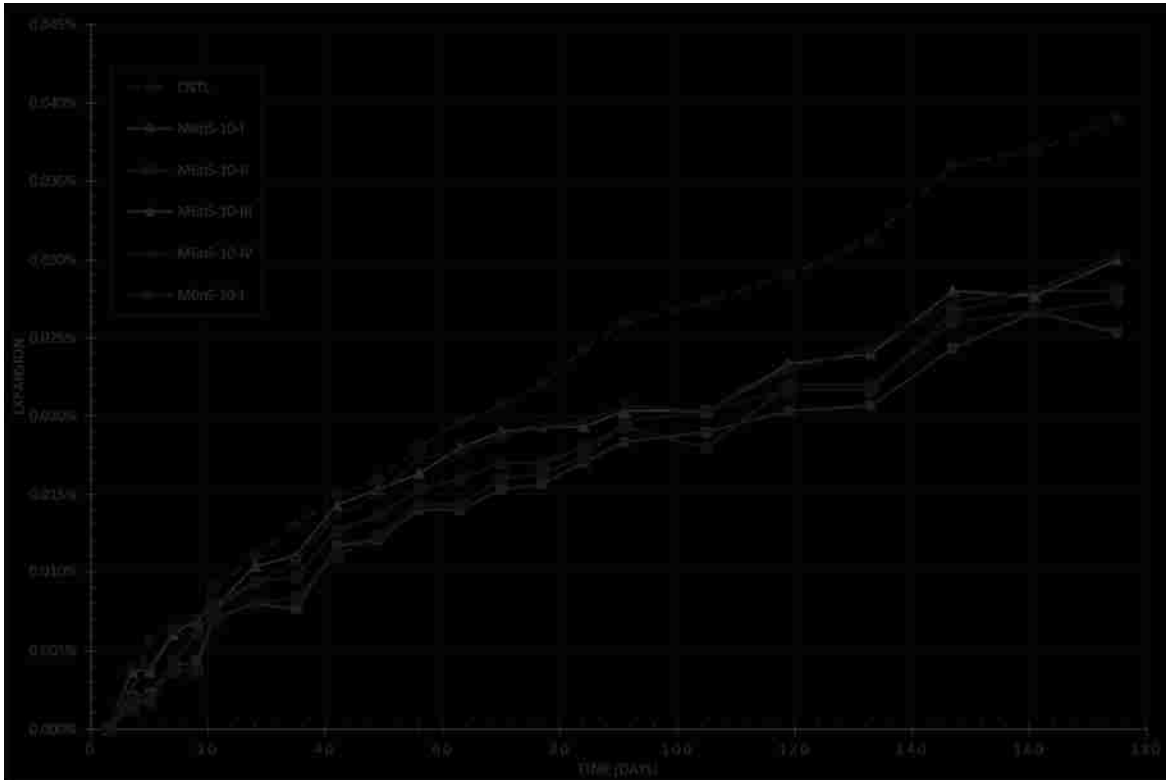


Figure 7-6: Expansion of the Mechanical Dispersion 6% nS Mortars

The mechanically blended dry nS mortars with a 6% level of cement replacement are presented in **Figure 7-6**. There are observable differences in expansion behavior of the mortars in this series compared to the 3% replacement. All 6% nS contained mortars exhibited less expansion than the 0% nS control. This indicates that a higher level of replacement is an effective approach to countering the negative effects of poorly dispersed nS. As evident in **Figure 7-6**, all five 6% nS mortars had a very similar level of expansion and M6nS-10-IV or M6nS-20-I did not show any less expansion than the rest. Actually the M6nS-10-I mortar seemed to consistently show the least expansion and these results suggest that adding the HRWRA in the actual mixer once all binders and aggregate are

together is a better approach than adding it all in the blender which similarly with the 3% nS mortars did not result in any improved durability due to a better dispersed nS. The authors suspect that the hydrophobic effect of the HRWRA polycarboxylate long chain molecules on the dry nS particles begins to wane under the prolonged period of blending with the water. Additionally, by the time the water, nS and HRWRA are added with the cement and fine aggregate, both the hydrophobic effect on nS is weakened and the remaining available HRWRA is not sufficient for de-flocculation of the cement particles. Insufficient HRWRA in the combined fresh mortar paste would limit the intermixing of the cement particles with the nS. This was suspected since the measured flow, as reported in **Table 7-3**, for the HRWRA added to the blender mortars was less than that of Type I and Type IV mortars. The Type I and IV mortars had sufficient HRWRA added to the mixer directly, the dose and quantity of all other mortar constituents being the same across all mixtures.

The 20 min mechanically blended dry nS mortar M6nS-20-I also performed well similarly to its 3% nS counterpart but not quantifiably better than the rest of the mortars. The higher volume of nS not only replaces more of the C₃A containing cement but also consumes more Ca(OH)₂ through the increased level of pozzolanic activity. That Ca(OH)₂ when consumed by the pozzolan for the generation of secondary C-S-H, will not be available for reaction with sulfate ions. The additional nS, even if in agglomerated form, acts as a filler that at those higher proportions reduces the permeability of the paste and slows the egress of sodium (Na⁺) and sulfate (SO₄²⁻) ions. Another reason why M6nS-20-I might not have performed better is that the workability of the mix at the end was not optimal at only 79%. There was a measurable warming of the mix water with dry nS after 20 minutes of blending that reduced the workability of the mortar in its fresh state. In a follow up continuous temperature monitoring test, the same volume of mixing water with either 3% or 6% nS replacement linearly increased in temperature from 24.8±0.1 °C to 46.7±0.1 °C after 20 minutes of blending, approximately at the rate of 1.0 °C/min. This warming could have adversely affected compaction and

therefore permeability. Although it also impacted the workability of M3nS-20-I (84% flow), the warmer mixing water did not seem to significantly affect its sulfate attack related expansion. Nevertheless the loss of workability for M6nS-20-I was sufficient to potentially prevent its ability to exhibit better resistance to sulfate attack than the other mortars in the 6% nS M-series. Dosage rate and duration of dispersion mixing should be considered to avoid unaccounted for increases in cementitious reactivity and reduced setting time.

7.4.4 Effects on Absorption, Sulfate Ion Permeability, and Porosimetry

Absorption of all mortars was performed to seek correlation between changes in the mortar permeable void volume due to the various forms of nS replacement and the sulfate expansion results. The results of the absorption testing are presented in **Figure 7-7**.

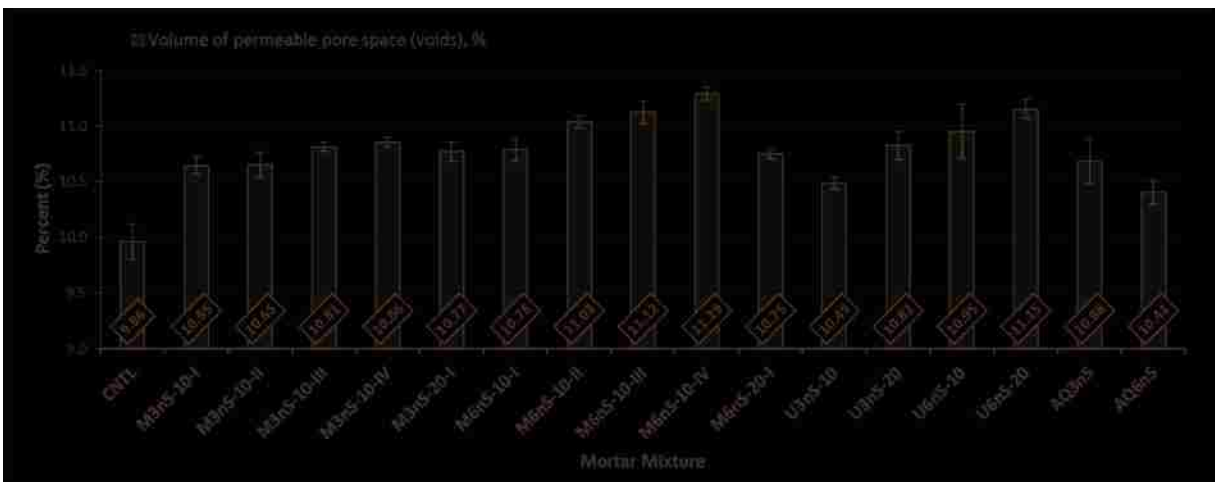


Figure 7-7: Water Absorption Results (error bars represent \pm SD)

The control mixture tested with the lowest overall permeable void volume of 9.96%. The lowest permeable pore volume of the silica contained mortars were for the U3nS-10 and AQ6nS mortars, 10.49% and 10.41% respectively. The AQ6nS mortar mixture that exhibited the best sulfate

durability in terms of least expansion in the 6 month test also exhibited the smallest percent permeable pore space of the silica replacement mortars. Nevertheless, the absorption of AQ6nS and the rest of the silica replacement mortars was higher than the control. Absorption alone could not explain the expansive behavior of the mortars under sulfate attack. The additional RSPT and MIP testing of select mortars that follow the absorption discussion provided further insight.

U3nS-10 exhibited low absorption, but its sulfate attack related expansion as reported earlier was not as impressive since it was surpassed by both 6% nS ultrasonic mixtures, AQ3nS and some of the mechanical dispersion mortars. It may be that U3nS-10 is physically more impermeable than the 6% mortars that surpassed it in terms of less expansion, but the smaller 3% nS dose meant more C₃A and free Ca(OH)₂ were available for ettringite and gypsum formation under sulfate attack. Note in **Figure 7-7** that the increased content of dry nS from 3% to 6% resulted in an overall increased permeable pore space between the ultrasonic method of dry nS dispersal. Not only did a higher nS content increase the pore volume measured but increasing the period of sonication from 10 minutes to 20 minutes also caused an increase in the pore volume. That correlates with the expansion results where both U3nS-10 and U6nS-10 exhibited less expansion than U3nS-20 and U6nS-20, respectively.

Based on sonication literature in other fields of research such as biology and toxicology (Taurozzi et al. 2011; Jiang et al. 2009), the authors suspect that certain sonication methods of nS for longer periods of time can foster further agglomeration. This is a phenomenon that has been observed with other nano-sized particles such as ZrO₂, where after a certain period of ultrasonic treatment the de-agglomeration effect can reverse and re-agglomeration of the particles can occur as shown in **Figure 7-8** (Vasylykiv & Sakka 2001).

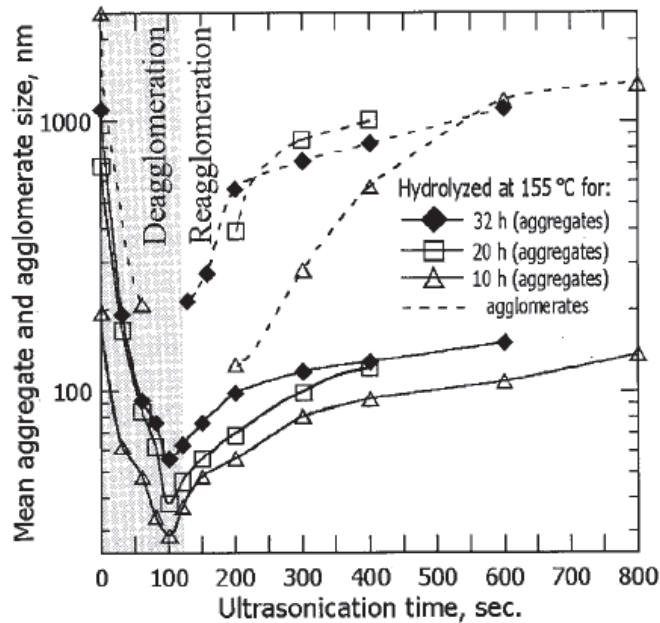


Figure 7-8: Example of Ultrasonically Induced Re-Agglomeration of ZrO_2 Particles due to Excessive Ultrasonic Treatment (Vasylykiv & Sakka 2001)

The effect of ultrasonic mixing on a liquid medium like water, is that as high frequency (20-40 kHz) waves propagate through the medium, they create alternating high and low pressure cycles that form microscopic vapor bubbles. Under the high pressure phase of each cycle these bubbles collapse in localized shockwaves that can generate extreme localized temperatures up to 10,000 K (9,727 °C), rapid temperature changes, significant pressure bursts, and 400 km/hr (364.5 ft/s) liquid jet streams. These ultrasonic cavitation effects are what break up agglomerates, but with excessive energy input, certain nano-materials can experience re-agglomeration, physiochemical alterations of the material, and even thermally induced inter-particle fusion (Taurozzi et al. 2011). These would all be undesirable effects on dry nS due to sonication and could explain the observed negative trend due to longer sonication times. Similarly to the mechanical form of mixing, temperature increases of the same volume of mixing water were also measured over a 20 minute period in a follow up test. Due to sonication, the water temperature increased $4 \pm 0.1^\circ\text{C}$ after 20 minutes indirect exposure to the ultrasonic bath. As reported in **Table 7-3**, this warming of the mixing water could be in part

responsible for the loss of workability which would pair with any directly negative effects from sonication. Warming of the mixing water, re-agglomeration, and any other adverse effects of sonication on dry nS in water, could all contribute to the negative impact longer sonication exposure had on the absorption and measured sulfate attack expansion. Save for the minor reduction between the 20 minute mechanical dispersion mortars M3nS-20-I and M6nS-20-I, the aqueous solution mortars AQ3nS and AQ6nS are the only other mortars where an increase of the nS content resulted in a tangible reduction in the permeable pore volume.

With the mechanically-dispersed nS mortars, it can be observed that the 20 minute blended mortars M3nS-20-I and M6nS-20-I had drops in the permeable void volume compared to the other types of dispersion. HRWRA was added to the water and dry nS during blending with an intent to improve dispersion of the nS and therefore reduce mortar permeability. As more of the HRWRA was moved to the blender for dispersion with the water and dry nS, the results indicate a trend of increasing void volume from Type I to Type IV mixing for both 3% and 6% nS contained mortars. Generally with mechanical blending of the dry nS powder, the smallest absorption readings measured were with the Type I mortars where all the HRWRA was added to the mixer. Here, the absorption results collaborate those of expansion. Possibly due to its limited period of effectiveness, by the time the HRWRA was introduced to the full mortar mixture, it could no longer improve workability and nS dispersion. This reduced effectiveness results in higher permeability and a reduction in the sulfate durability. It is of importance to also note that similarly to the ultrasonic mortars, the increased content of dry nS from 3% to 6% resulted in an overall increased permeable pore volume between the mechanical forms of nS dispersion.

The superior performance of the aqueous solution nS mortars was further verified after performing a six-hour accelerated rapid sulfate permeability test (RSPT) alongside the water absorption testing

of the 28 day cured samples. This test measures the penetration rate of sulfate ions which accounts for both the pore structure permeability and the sulfate ion binding capacity of the mortar. As **Figure 7-9** indicates, the AQ6nS mortar had less than half the coulomb charge passed than the mechanically blended M6nS-10-I. The RSPT test supports the low expansion measured for AQ6nS that is based both on a low permeability and a low penetration rate of sulfate ions. This is due to a refined pore structure, CSH densification, and stronger pozzolanic activity of aqueous solution nS. The RSPT results also indicate that the 6% dry nS mortar M6nS-10-I has a lower permeability than that of AQ3nS, which has half the nS content. Although the water absorption results indicate that the permeable void volume of AQ3nS is 1% less than M6nS-10-I, the expansion for AQ3nS at 26 weeks is 0.027%, and that of M6nS-10-I is 0.025%, which is a 6.4% difference. In terms of sulfate attack durability, a higher replacement of nS in dry form can result in a durable mortar considering that the dry nS replacement is performing at a level marginally better than what could be expected of half the replacement with aqueous form of nS.

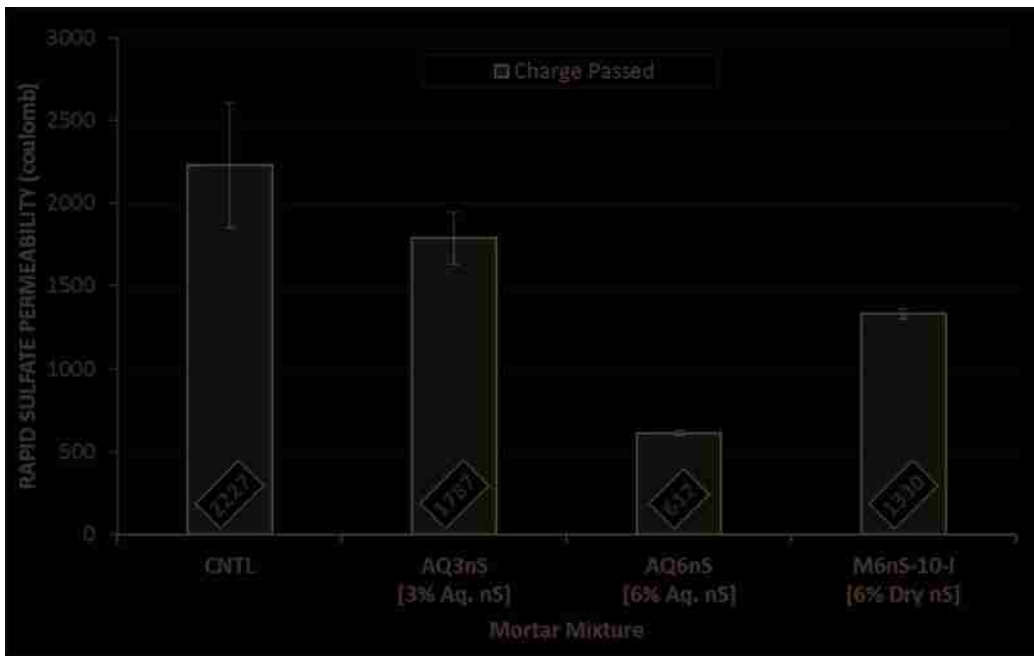


Figure 7-9: RSPT Test of Select nS Contained Mortars (error bars represent $\pm SD$)

Earlier it was pointed out that although all 6% dry or aqueous forms of nS contained mortars showed better resistance to sulfate attack in terms of less expansion than the control, the control mortar had the lowest permeable pore volume in the absorption testing. Permeable void volume does not always directly correlate with permeability since durable concrete could exhibit relatively high porosity yet a low permeability. The pore size distribution, pore interconnectivity, and their tortuosity influence the permeability of the mortars and therefore their response to sulfate attack (Richardson 2002). Therefore it is possible for a mortar like AQ6nS to exhibit higher porosity as indicated by absorption, but that void volume might be a function of finer, more tortuous and impermeable voids. That void volume could also be larger due to bigger entrapped air voids that do not facilitate the expansive causing stresses generated from the products of sulfate attack. Pores in concrete widely vary in size and certain ranges of them affect durability properties such as permeability and diffusivity. To understand the effects of dry and aqueous nS on the pore size distribution of the mortars tested against the control, the MIP test was performed on the CNTL, M6nS-10-I, and AQ6nS mortar. Those results are presented in **Figure 7-10**. As defined on the graph, based on their pore diameter and influence on the hydrated paste properties, pores are classified in several categories. Gel pores are generally less than or equal to 10 nm and they are integral to the densely layered C-S-H phase; they are considered impermeable and do not contribute to transport processes. Pores ranging from 10 to 50 nm are considered capillary micropores and although tortuous, these can in small part contribute to permeability. The bulk of permeability and diffusivity occurs in the interconnected capillary macropores ranging from 50-10,000 nm (0.05 to 10 μm) (Tobón et al. 2015; Mindess et al. 2003; Du et al. 2014b). There is stark difference in the capillary macropores for each of the three mortars tested. The CNTL and M6nS-10-I mortars exhibit similar peaks but those between 0.05 μm and 0.25 μm are more pronounced for the 6% dry nS mortar. There is evidence of some pore refinement in the macropore range after 0.1 μm for the 6% dry nS mortar which could explain its favorable

performance under sulfate attack but as the RSPT and expansion results show, that refinement is not as effective as the aqueous form of nS. There is a significant shift in the pore size distribution for the aqueous nS mortar AQ6nS. The two distinguishable peaks seen in the control and the 6% dry nS are not present. There is a significant increase in the gel pores and capillary micropores which indicates good C-S-H paste densification. For AQ6nS, although there is a peak around the 2.5 μm macropore size, overall, the total % pore volume in the capillary macropore range is significantly less than the rest (49.1%); those of the control and M6nS-10-I are 71.5% and 68.4%, respectively. AQ6nS has 31.4% of the total pore volume within the gel and capillary micropore range. The dry nS contained M6nS-10-I has 23.7%, and that of the CNTL is merely 13.2%. The RSPT and MIP results corroborate the sulfate attack expansion results for these three mortars. They help explain how both 6% nS contained mortars showed better sulfate attack resistance than the CNTL in terms of reduced expansion, even when the CNTL mortar had the lowest overall volume of permeable pore space from the absorption test.

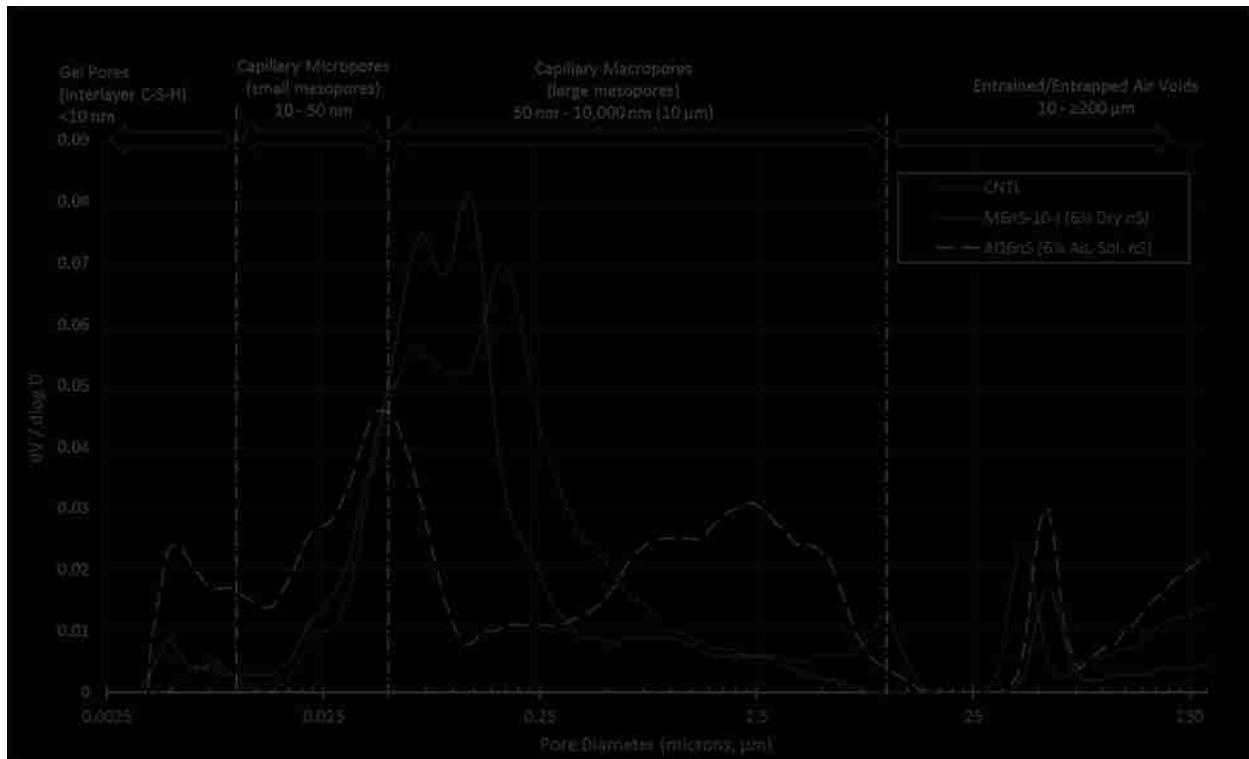


Figure 7-10: MIP Pore Size Distribution for CNTL, M6nS-10-I, and AQ6nS Mortars

7.4.5 Compressive Strength

The compressive strength of the samples was measured at 3 days of curing and at the 26 week mark where the sulfate solution exposed samples were tested against those kept in the cure tank. Each test is the average of three 2-in (500mm) \varnothing x 4-in (100mm) cylinders. Test results are summarized in **Figure 7-11**. A clear trend between the mixtures at 3 days is not evident. It can be observed that all nS contained mortars show significant early strength improvements over the control which correlates with existing research (Singh et al. 2013; Sanchez & Sobolev 2010; Kawashima et al. 2013; Pengkun Hou et al. 2013). It indicates that the pozzolanic activity of the nS has generated additional strength contributing C-S-H. Physically, the nS has served as a filler even in various degrees of agglomeration. Additionally as verified with the MIP test, different levels of paste densification have taken place to push all 3 day strengths for nS contained mortars at least 10 MPa above the control mixture.

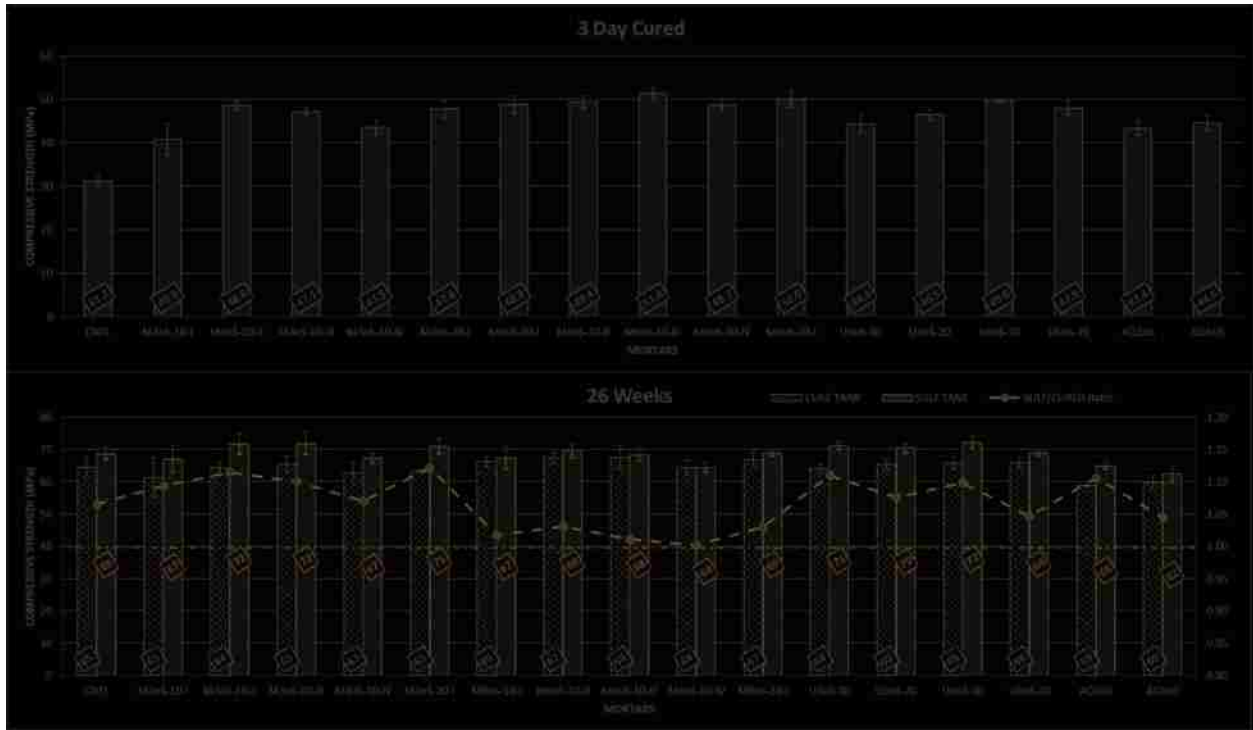


Figure 7-11: Compressive Strength of Mortars at 3 Days and 26 Weeks (error bars represent ±SD)

There do not appear to be significant improvements in compressive strength between 3% and 6% nS content. Between AQ3nS and AQ6nS there is a 2 MPa (2.9%) improvement. Between the U3nS-10 and U6nS-10 there is a 6MPa (11%) improvement and between U3nS-20 and U6nS-20 there is a 2 MPa (3.1%) improvement. Between the corresponding types of HRWRA dosing method, the compressive strength improvement from doubling the nS content between the mechanically blended series ranges between 1-8 MPa (5-18% difference). Irrespective of the form of nS used or method of dispersion, doubling the dose of nS has more of an impact on sulfate expansion and permeability than on compressive strength. At 26 weeks the difference between the 3% nS and 6% nS contained mortars is even smaller. With sonication, the improvement was only 2.4% between U3nS-10 and U6nS-10. For the aqueous solution mortars less of a difference still, only 1.5%. For the mechanically mixed dry nS mortars, the biggest improvement was between M3nS-10-I and M6nS-10-I at 7.6%; for

all others, there was a 2.5-5.5% improvement for doubling the nS content. Results indicate that with a better dispersed nS, the impact of increasing nS content on compressive strength is reduced.

What can be deduced from the 26 week compressive strength testing is that at the 6-month period of exposure to the 5% Na₂SO₄ solution, the mortars were generally still experiencing a strength improvement over their water-cured counterparts. **Figure 7-11** also includes a ratio of sulfate solution-to-water cured mortar strength ratio and for all mortars tested it is above 1. This development could be attributed to the generally observed trend for initial increases in strength due to the filling and compaction effect of the sulfate attack related expansive compound ettringite (Rundong et al. 2010). The effect is not permanent and given a longer period of continuous sulfate exposure, strength loss can develop.

Additionally, the lower water/binder ratio of 0.485 utilized in this study resulted in generally more impermeable mortars. In some of the studies listed in **Table 7-1** a higher water/binder ratio such as 0.50 or 0.55 was selected that increases the permeability of the samples and can accelerate sulfate attack deterioration. For the mortars in this work, the lower w/b ratio meant that the chemical sulfate attack could not successfully deteriorate the paste sufficiently enough to show any strength loss in the 6 months test period. The formation of gypsum is generally responsible for softening and strength loss and it should occur in conditions where the sodium sulfate solution pH is maintained below 8.0 (Mehta 1993; Mehta 1975). That was the case in this test with the automatic dosage of 0.5N H₂SO₄ and the pH controller that maintained a pH of 6.5±1. Nevertheless the 6-month period could have simply been too early to observe sulfate related strength loss with Na₂SO₄ attack. If the test were to be repeated with the more aggressive MgSO₄, the authors suspect that more decalcification of the Ca(OH)₂ and C-S-H phases would have occurred due to the participation of Mg ions and a more aggressive deterioration would have resulted with measurable strength loss.

7.5 Conclusions

The following are conclusions drawn from the presented comparison study between mortars prepared with different methodologies of mechanically dispersing dry nS versus mixtures containing ultrasonically dispersed and aqueous solution forms of nS.

1. Generally the higher 6% nS replacement and aqueous solution form of nS application produced the more sulfate resistant mortars. After 6 months of sulfate attack, the 6% aqueous nS contained mortar exhibited the least expansion (52% less than CNTL); a low permeable void volume as measured by absorption (10.41% permeable pore space volume); the lowest measurement of diffusivity from the RSPT test; and a high level of paste densification and pore size refinement as shown through MIP. Due to superior dispersion and a more fully expressed surface area, aqueous forms of nS require larger doses of HRWRA to achieve comparable workability to same dose replacements of dry nS replacement mortars.
2. Longer periods of dry nS sonication showed negative effects in terms of sulfate durability related to expansion and the measured absorption of the mortars. This effect seemed to be exasperated by doubling the nS content. While further research is needed, results indicated that longer periods of purely ultrasonic dispersion may result in more agglomeration of the nS particles. Authors recommend testing the addition of dispersants typically used in aqueous nS solutions to the nS water slurry during or after sonication, as well as other means of sonication to observe if improvements can be made.
3. With mechanical blending of dry nS, agglomerated nS will perform poorly against sulfate attack unless measures are taken to mechanically mix for a longer period of time or additional HRWRA is used to achieve optimal workability. The 3% nS M3nS-20-I (0.030% exp.) had 29.4% less expansion than M3nS-10-I (0.040% exp.) when blended for 20 versus 10 minutes. Adding the HRWRA in the mixer once all binders and aggregate are together is

the recommended approach to improve workability and durability over adding it in the nS blending phase.

4. A higher level of cement replacement with nS is an effective approach to countering the negative effects of poorly dispersed nS if used in dry form whether dispersed through mechanical blending or sonication with the mixing water.
5. Irrespective of the form of nS used or method of dispersion, doubling the dose of nS has more of an impact on durability in terms of expansion and permeability than on compressive strength.

8 INFLUENCE OF NANOSILICA ON PHYSICAL SULFATE ATTACK RESISTANCE OF MORTARS

(UPDATE ON ONGOING RESEARCH ACTIVITY ONLY)

8.1 Abstract

The objective of this study was to evaluate the effectiveness of colloidal nanosilica as a nanomaterial and pozzolanic admixture to prevent effects of physical sulfate attack on mortars. Physical sulfate attack is simulated via partial submersion in 10% sodium sulfate solution and either a constant or cyclic ambient condition. This work is still ongoing in order to collect results after more severe deterioration of the mortar samples is observed and quantified via mass loss and a visual rating system.

8.2 Update on Research Activities

A manuscript for this Phase III of the testing program has still not been prepared since the testing period was extended beyond the originally scheduled window of 3 to 6 months. Existing literature on physical sulfate attack of cementitious materials is in its infancy as most existing research done on salt weathering at this point is on various porous rock where deterioration seemed to manifest more rapidly than what has been observed in this study. That is likely due to weaker strength and a more porous void network of the rock materials tested such as limestone (Schiro et al. 2012). For details of the experimental set up for this phase of the testing program, please refer to Section 3.4.3. For background information on the physical form of sulfate attack, please refer to Section 1.3.

The first test mixtures were batched June of 2015. The original planned date of completion, where all mixtures were subjected to a minimum of 6 months of partial submersion in Na_2SO_4 solution in either exposure environment, was January 2016. At that time the samples were cleaned and inspected and it was observed that minimal evidence of salt weathering was present in any of the samples to

quantify mass loss or rate mixtures on a visual scale of deterioration. It was decided to extend the Phase III testing period beyond 6 months and continue to monitor the salt weathering effects over time in an effort to collect more useful data. The lack of measurable deterioration at that time was attributed to a few possible causes for each condition and some measures were taken, all of which is discussed next.

1. The constant low humidity (25-30% RH) and room temperature (23 ± 2 °C) condition was likely unable to force the evaporative front of the sulfate solution below the surface of the specimen so subflorescence of crystalline Thenardite could occur. Subflorescence of thenardite is a critical step towards forcing mirabilite precipitation from the supersaturation of the sulfate solution and result in damaging expansive stresses within the mortar pore structure (Haynes & Bassuoni 2011). A lot of surface formed thenardite was observed in the form of efflorescence but that is considered generally harmless. No tangible deterioration of the mortars was observed as well. A box fan was added after the 6 month condition assessment in an attempt to increase the evaporation rate above the rate of solution supply via capillary action by moving more air over the exposed surfaces of the samples, see **Figure 8-1**. This was done in an attempt to force the evaporative front below the surface of the mortars and hopefully observe an increase in physical sulfate attack. After almost another 6 months from that point, based on more severe weathering noted on samples in the cyclic exposure environment (see **Figure 8-2**) in comparison to those at the constant condition (see **Figure 8-3**), it is likely that the most mortars in the latter case will not exhibit significant salt weathering at the conclusion of the test. This being the case even with the attempted increase in the rate of surface evaporation.



Figure 8-1: Constant Low Humidity Exposure Setup for Physical Sulfate Attack



Figure 8-2: Specimens Exposed to Cyclic Exposure Conditions after 12 Months



Figure 8-3: Specimens Exposed to Constant Condition Exposure after 12 Months

2. The cyclic exposure of mortars to 24 hours of high humidity/lower temperature ($>85\% \text{ RH} / 24 \pm 2 \text{ }^\circ\text{C}$) followed by 24 hours of low humidity/higher temperature ($< 35\% \text{ RH} / 40 \pm 2 \text{ }^\circ\text{C}$) was started after the first 6 months of the testing period in the environmental chamber in an attempt to increase the aggressiveness of the exposure conditions. The original experimental set up in the environmental chamber attempted to control the hydrous to anhydrous sulfate phase changes only via a cyclic changes from high to low RH at a constant temperature of ($23 \pm 2 \text{ }^\circ\text{C}$). The former experimental set up only had a humidifier on a RH controller set up to run every other 12 hours to bring the RH above 80%. Then, an automated duct flap would open and a vent fan would come ON during the alternating 12 hours to rapidly bring the RH of the chamber down to ambient laboratory levels of 35% RH or less. The updated cyclic conditions have resulted in a more observable ration of physical sulfate attack.

3. The testing specimens prepared for this study were mortars instead of concrete, which do not feature coarse aggregate. It is shown that the addition of aggregate increases permeability and more so the larger the aggregate meaning that concrete would be more permeable than mortar, and mortar more permeable than neat cement paste (Mehta & Monteiro 2006). This increase in permeability has largely been attributed to micro-cracks at the interfacial-transition zone (ITZ) which would have a bigger presence with coarser aggregate (Mehta & Monteiro 2006). Mortars are preferable for chemical sulfate attack so a more rapid rate of reactions takes place, the size of the samples can be smaller, and the chemical characteristics of the binders can play a bigger role in the matrix. With physical attack, concrete might exhibit physical deterioration faster than mortar due to the increased permeability and presence of more microcracks that become weak spots that salt crystallization can exploit. For these reasons, concrete might be preferable over mortar for physical sulfate attack since salt weathering effects then are likely more pronounced and faster occurring. Most of the recent literature on physical sulfate attack is in fact performed on concrete (Suleiman 2014; Haynes & Bassuoni 2011; Liu et al. 2012).

In conclusion, Phase III of the testing program is ongoing and at this time results are deemed inconclusive beyond the observations discussed so far. Final results of this test, likely to come to completion after 2 years of total exposure or more, will be presented and published in a manuscript that is at this time beyond the scope of work presented in this thesis.

9 CONCLUSION AND RECOMMENDATIONS

9.1 Summary of Research Activities

During the first phase research, a side-by-side comparison study was carried out intended to identify the effects of nanosilica (nS) on chemical sulfate attack resistance of Portland cement (PC) mortars and its effectiveness in comparison to similar replacement levels of the more widely implemented microsilica (mS). Several mortar mixtures were prepared with a 4.1 and 7.2% tricalcium aluminate (C_3A) PC by progressive cement replacement with nS or mS. Cements of contrastingly different fineness and C_3A content were chosen to test in combination with nS. Several mortar mixtures of incrementally higher cement replacement with nS or mS were prepared with a 4.1 and 12.3% tricalcium aluminate (C_3A) PC of different fineness. Concurrently to testing of the aforementioned mixture designs, the effect of combined nS and mS on the sulfate resistance of moderate C_3A (7.2%) and a low C_3A (4.1%) PC mortars was evaluated against all cement control mortars and mixtures with equivalent contents of only one form of silica. Silica contained mortars had 6% cement replacement of either nS, mS, or 3% of each. The mortars tested were measured for expansion, compressive strength, and mass loss. Additional testing for absorption, rapid sulfate penetration, and mercury porosimetry of select mortar mixtures paired with laser diffraction particle analysis of the suspended silica particles supplemented the interpretation and explanation of the results. In the second phase of the study, the influence of various dispersion methods on the sulfate attack resistance of nanosilica (nS) contained mortars was evaluated. Multiple mechanical or ultrasonic dispersion methods, HRWRA dosing procedures, and both dry and aqueous solution forms of nS were used to prepare a series of mortars with 0%, 3%, and 6% replacement of Portland cement with nS. Mortars were subjected to 6 months of exposure in a 5% sodium sulfate solution. Expansion, compressive strength, water absorption, rapid sulfate ion permeability, and porosity were measured.

There is a third phase where physical sulfate attack is simulated via partial submersion in 10% sodium sulfate solution and either a constant or cyclic ambient condition. This work is still ongoing in order to collect results after more severe deterioration of the mortar samples is observed and quantified via mass loss and a visual rating system.

9.2 Summary of Conclusions

Work during the first phase of research indicated that nS replacement benefited the tested moderate 7.2% C₃A cement mortars. However, in the dry powder form and method of mixing used in this study, poor dispersion and agglomeration of the nS was suspected to hinder mortar permeability in comparison to mS and low C₃A cement mortars. The results indicated nS in its dry form was an inferior mineral admixture alternative to mS for chemical sulfate attack durability due to the inherent dispersion challenges of the significantly finer particles. Mortars with mS outperformed those with dry powder nS for all cements tested. Poor dispersion of the dry powder nanosilica used in this study is suspected to increase mortar permeability and hinder the reported filler, paste, and ITZ densification effects of nS. Mortars made with a lower Blaine and low C₃A cement paired with the agglomerated nanosilica exhibited more sulfate attack expansion in comparison to the control. Microsilica resulted in both pore and grain refinement of the mortar pastes. Increasing cement fineness proved beneficial in combination of either pozzolan regardless of the cement's C₃A content. Replacement with nS in aqueous dispersion, however, proved to be significantly more effective than equivalent replacement of dry powder nS and mS. The expansion measurements indicated that mS replacement mortars outperform both nS only, and nS+mS combination replacement mixtures. A negative effect of the dry nS powder replacement attributed to agglomeration of its fine sized silica particles during mixing negated the expected superior pozzolanic activity of the nanomaterial. The nS+mS combination mortar mixtures performed better than those with nS only but not better than the mS only mortars. Combining both silica types did not merge the strengths of both forms of

pozzolan admixtures as hypothesized. In light of the results, most of the beneficial contribution from the cement replacement with the combination mixtures could be attributed to the mS proportion given that the combination mixtures' expansion performance was comparable to that of the 3% mS only mortars. Results indicated that, use of the aqueous form of nS results in a more sulfate resistant and impermeable mortar than all other tested methods of dry form nS. HRWRA dosage proved most effective when added directly to the mixer after all water, binders, and fine aggregate were combined. Excessive ultrasonic dispersion of dry nS in the mixing water may cause further agglomeration of the nS that proved deleterious to permeability and sulfate resistance.

Currently, nS is a relatively expensive synthetically manufactured nanomaterial, and unlike mS, it is not a byproduct of another industrial process. Therefore, it would seem more economical to procure and properly mix a smaller quantity of well dispersed nS than use excessive cement replacement levels of agglomerated nS.

9.3 Future Research Needs

Based on the research work presented herein, nanosilica proved to be an effective mineral admixture for increasing the sulfate resistance of cementitious composites as long as it is in a well dispersed state. This nanomaterial can exhibit superior pozzolanic and paste densification effects in comparison to microsilica, but if poorly dispersed, it can compromise the permeability and be less effective than microsilica. Use of dry nanosilica powder proved challenging and it would be of value to explore dispersion methods of nanosilica in more detail. The author believes ultrasonic dispersion could be an effective method of dispersing dry nanosilica powder and a testing program that explores different means of applying ultrasonic treatment and stabilizing the nanoparticles in solution would be valuable to the concrete research community. This work only tested the application of sonication energy indirectly using an ultrasonic bath. There is ultrasonic equipment such as sonication probes

and horns that can apply sonication energy directly into the solution and might prove more effective at dispersion. Stabilizing the dispersion by increasing the zeta potential before or after sonication using electrostatic or steric stabilizing additives might prevent the re-agglomeration effect of nS under prolonged sonication exposure.

As mentioned upfront there are other forms of sulfate attack that were outside the scope of this study and would be worthwhile exploring. Testing programs that feature exposure of nS contained mixtures to other forms and combinations of sulfates or testing nanosilica contained mixtures in lower temperatures environments conducive to thaumasite formation would be insightful. The testing in all phases in this study used mortars; further testing using concrete samples with coarse aggregate could better highlight the effects of nS on the interfacial transition zone and that might influence the sulfate resistance of nS contained mixtures more or less significantly than what was observed in this study. Field tests of actual structures or larger specimens of nS contained mixture designs placed in natural high sulfate environments might cause unique effects otherwise elusive to laboratory conditions and would be of value as well.

APPENDIX A: CONVERSION FACTORS

$$1 \text{ mm} = 10^{-3} \text{ m} = 3.937 \times 10^{-2} \text{ inch}$$

$$1 \text{ }\mu\text{m} = 10^{-6} \text{ m} = 3.937 \times 10^{-5} \text{ inch}$$

$$1 \text{ nm} = 10^{-9} \text{ m} = 3.937 \times 10^{-8} \text{ inch}$$

$$1 \text{ kg} = 2.20 \text{ lbs}$$

$$^{\circ}\text{C} = (5/9)(^{\circ}\text{F} - 32)$$

$$^{\circ}\text{F} = (9/5)(^{\circ}\text{C}) + 32$$

$$1 \text{ MPa} = 145 \text{ psi} = 0.145 \text{ ksi}$$

$$1 \text{ kg/m}^2 = 1.684 \text{ lb/yd}^3 = 0.0624 \text{ lb/ft}^3$$

$$1 \text{ mL} = 10^{-3} \text{ L} = 3.38 \times 10^{-2} \text{ fl oz}$$

$$1 \text{ ppm} = 1 \text{ mg/L} = 0.0001\%$$

APPENDIX B: RELEVANT COMPOUND FORMULAS & CEMENT CHEMISTRY

Compound Name	Oxide Notation	Chemical Formula	Cement Chemistry Abbreviation
Tricalcium silicate (Alite)	$3\text{CaO} \cdot \text{SiO}_2$	Ca_3SiO_5	C_3S
Dicalcium silicate (Belite)	$2\text{CaO} \cdot \text{SiO}_2$	Ca_2SiO_4	C_2S
Tricalcium aluminate (Aluminate)	$3\text{CaO} \cdot \text{Al}_2\text{O}_3$	$\text{Ca}_3\text{Al}_2\text{O}_6$	C_3A
Tetracalcium aluminoferrite (Ferrite Phase)	$4\text{CaO} \cdot \text{Al}_2\text{O}_3 \cdot \text{Fe}_2\text{O}_3$	$\text{Ca}_2(\text{Al}_x\text{Fe}_{1-x})_2\text{O}_5$	C_4AF
Calcium hydroxide (portlandite)	$\text{CaO} \cdot \text{H}_2\text{O}$	$\text{Ca}(\text{OH})_2$	CH
Calcium silicate hydrate	$3\text{CaO} \cdot 2\text{SiO}_2 \cdot 8\text{H}_2\text{O}$ (common form) $x\text{CaO} \cdot \text{SiO}_2 \cdot y\text{H}_2\text{O}$	$\text{Ca}_3\text{Si}_2\text{O}_{15}$	C-S-H
Calcium sulfate dihydrate (Gypsum)	$\text{CaO} \cdot \text{SO}_3 \cdot 2\text{H}_2\text{O}$	$\text{CaSO}_4 \cdot 2\text{H}_2\text{O}$	$\text{C}\bar{\text{S}}\text{H}_2$
Hemihydrate	$\text{CaO} \cdot \text{SO}_3 \cdot 0.5\text{H}_2\text{O}$	$\text{CaSO}_4 \cdot 0.5\text{H}_2\text{O}$	$\text{C}\bar{\text{S}}\text{H}_{0.5}$
Anhydrite	$\text{CaO} \cdot \text{SO}_3$	CaSO_4	$\text{C}\bar{\text{S}}$
Tetracalcium aluminates hydrate	$4\text{CaO} \cdot \text{Al}_2\text{O}_3 \cdot 13\text{H}_2\text{O}$	$((\text{CaO})_4\text{Al}_2\text{O}_3 \cdot 13\text{H}_2\text{O})$	C_4AH_{13}
Calcium sulfoaluminate hydrate, AFm phase (monosulfate)	$3\text{CaO} \cdot \text{Al}_2\text{O}_3 \cdot \text{CaSO}_4 \cdot 12-18\text{H}_2\text{O}$	$\text{Ca}_4\text{Al}_2(\text{OH})_{12} \cdot \text{SO}_4 \cdot 6\text{H}_2\text{O}$	$\text{C}_4\text{A}\bar{\text{S}}\text{H}_{12-18}$
Calcium aluminate trisulfate, AFt phase (ettringite)	$3\text{CaO} \cdot \text{Al}_2\text{O}_3 \cdot 3\text{CaSO}_4 \cdot 32\text{H}_2\text{O}$	$\text{Ca}_6\text{Al}_2(\text{OH})_{12} \cdot (\text{SO}_4)_3 \cdot 26\text{H}_2\text{O}$	$\text{C}_6\text{A}\bar{\text{S}}_3\text{H}_{32}$
Calcium silicate sulfate carbonate hydrate, (Thaumasite)	$[\text{Ca}_3\text{Si}(\text{OH})_6 \cdot 12\text{H}_2\text{O}] \cdot (\text{SO}_4) \cdot (\text{CO}_3)$ <i>or</i> $3\text{CaO} \cdot \text{SiO}_2 \cdot \text{CO}_2 \cdot \text{SO}_3 \cdot 15\text{H}_2\text{O}$	$\text{Ca}_6(\text{Si}(\text{OH})_6)\text{CO}_3 \cdot \text{SO}_4 \cdot 12\text{H}_2\text{O}$ <i>or</i> $\text{Ca}_6(\text{Si}(\text{OH})_6)_2(\text{SO}_4)_2(\text{CO}_3)_2 \cdot 24\text{H}_2\text{O}$	$\text{C}_3\text{S}\bar{\text{C}}\bar{\text{S}}\text{H}_{15}$

Cement Chemistry Abbreviation	Oxide	Name
C	CaO , CO ₂ **	Calcium Oxide (free lime),
S	SiO ₂	Silica
A	Al ₂ O ₃	Alumina
F	Fe ₂ O ₃	Ferric Oxide
M	MgO	Magnesium Oxide
S̄	SO ₃	Sulfur Trioxide (Sulfite)
N	Na ₂ O	Sodium Oxide
K	K ₂ O	Potassium Oxide
C̄	CO ₂ , CO ₃ **	Carbon Dioxide , Carbon trioxide (carbonate)
H	H ₂ O , OH ⁻	Dihydrogen Monoxide (water) , Hydroxyl ion
**Note some abbreviations may be used for multiple oxides depending on the reaction compounds		

BIBLIOGRAPHY

- ACI Committee 201, 2008. *201.2R-08 Guide to Durable Concrete*, Farmington Hills, MI.
- ACI Committee 234, 2006. *234R-06 Guide for the Use of Silica Fume in Concrete*,
- ASTM International, 2004. *ASTM C 1012 Standard Test Method for Length Change of Hydraulic-Cement Mortars Exposed to a Sulfate Solution*, West Conshohocken, PA.
- ASTM International, 2002. *ASTM C 109/C 109M Standard Test Method for Compressive Strength of Hydraulic Cement Mortars*, West Conshohocken, PA. Available at: <http://scholar.google.com/scholar?hl=en&btnG=Search&q=intitle:Standard+Test+Method+for+Compressive+Strength+of+Hydraulic+Cement+Mortars#7>.
- ASTM International, 2001. *ASTM C 1437 Standard Test Method for Flow of Hydraulic Cement Mortar*, West Conshohocken, PA.
- ASTM International, 2003a. *ASTM C 230 Standard Specification for Flow Table for Use in Tests of Hydraulic Cement*, West Conshohocken, PA.
- ASTM International, 1999. *ASTM C 305 Standard Practice for Mechanical Mixing of Hydraulic Cement Pastes and Mortars of Plastic Consistency*, West Conshohocken, PA.
- ASTM International, 2003b. *ASTM C 33 Standard Specification for Concrete Aggregates*, West Conshohocken, PA.
- ASTM International, 1997. ASTM C 642 Standard Test Method for Density, Absorption, and Voids in Hardened Concrete. *Annual Book of ASTM Standards*, pp.1-3.
- ASTM-C150, 2007. Standard Specification for Portland Cement. *Annual Book of ASTM Standards*, pp.1-8.
- Atahan, H.N. & Dikme, D., 2011. Use of mineral admixtures for enhanced resistance against sulfate attack. *Construction and Building Materials*, 25(8), pp.3450-3457. Available at: <http://dx.doi.org/10.1016/j.conbuildmat.2011.03.036>.
- Bache, H.H., 1981. Densified Cement/Ultrafine- Particle-Based Materials. In *Second International*

Conference on Superplasticizers in Concrete. Ottawa, Ontario, Canada.

- Bassuoni, M.T. & Nehdi, M.L., 2009. Durability of self-consolidating concrete to sulfate attack under combined cyclic environments and flexural loading. *Cement and Concrete Research*, 39(3), pp.206–226. Available at: <http://dx.doi.org/10.1016/j.cemconres.2008.12.003>.
- Bentur, A. & Cohen, M.D., 1987. Effect of Condensed Silica Fume on the Microstructure of the Interfacial Zone in Portland Cement Mortars. *Journal of the American Ceramic Society*, 70(10), pp.738–743.
- Berra, M. et al., 2012. Effects of nanosilica addition on workability and compressive strength of Portland cement pastes. *Construction and Building Materials*, 35, pp.666–675. Available at: <http://linkinghub.elsevier.com/retrieve/pii/S0950061812003364>.
- Bibby Scientific, *Technical Note T11-001: pH of Distilled Water*, Available at: http://www.stuart-equipment.com/adminimages/t11_001_ph_of_distilled_water.pdf [Accessed April 7, 2016].
- Bihari, P. et al., 2008. Optimized dispersion of nanoparticles for biological in vitro and in vivo studies. *Particle and fibre toxicology*, 5, p.14.
- Binda, L. & Baronio, G., 1987. Mechanisms of Masonry Decay Due to Salt Crystallization. *Durability of Building Materials*, 4(3), pp.227–240.
- Bizi, M., 2012. Stability and flocculation of nanosilica by conventional polymer. *Natural Science*, 4(6), pp.372–385.
- Brown, P.W. & Taylor, H.F.W., 1999. The Role of Ettringite in External Sulfate Attack. In *Materials Science of Concrete: Sulfate Attack Mechanisms*. pp. 73–94.
- Campillo, I., Dolado, J.S. & Porro, A., 2004. High-Performance Nanostructured Materials for Construction. In W. Z. Peter J M Bartos, John J Hughes, Pavel Trtik, ed. *Nanotechnology in Construction*. The Royal Society of Chemistry, pp. 215–225.
- CCAA, 2011. *Technical Note: Sulfate-Resisting Concrete*, Australia.
- Choolaei, M. et al., 2012. The effect of nanosilica on the physical properties of oil well cement.

- Materials Science and Engineering: A*, 538, pp.288–294. Available at: <http://linkinghub.elsevier.com/retrieve/pii/S0921509312000810>.
- Cohen, M.D. & Bentur, A., 1988. Durability of Portland Cement-Silica Fume Pastes in Magnesium Sulfate and Sodium Sulfate Solutions. *ACI Materials Journal*, 85(3), pp.148–157.
- Collett, G. et al., 2004. The role of carbon dioxide in the formation of thaumasite. *Cement and Concrete Research*, 34, pp.1599–1612.
- Cook, R.A. & Hover, K.C., 1993. Mercury porosimetry of cement-based materials and associated correction factors. *Construction and Building Materials*, 7(4), pp.231–240.
- Cook, R.A. & Hover, K.C., 1999. Mercury porosimetry of hardened cement pastes. *Cement and Concrete Research*, 29(6), pp.933–943.
- Dolado, J.S. et al., 2007. Effect of Nanosilica Additions on Belite Cement Pastes Held in Sulfate Solutions. *Journal of the American Ceramic Society*, 0(0), p.070916231959005–??? Available at: <http://doi.wiley.com/10.1111/j.1551-2916.2007.02034.x>.
- Donaldson, S., Courtois, D. & Walker, M., 2012. *Drinking Water Quality in Nevada : Common Problems for the Well Owner*,
- Du, H., Du, S. & Liu, X., 2014a. Durability performances of concrete with nano-silica. *Construction and Building Materials*, 73, pp.705–712. Available at: <http://www.sciencedirect.com/science/article/pii/S0950061814011544>.
- Du, H., Du, S. & Liu, X., 2014b. Durability performances of concrete with nano-silica. *Construction and Building Materials*, 73, pp.705–712.
- Dyer, T., 2014. *Concrete Durability*, Boca Raton, FL: CRC Press.
- Ferraris, C., Stutzman, P. & Snyder, K., 2006. Sulfate resistance of concrete: a new approach. *PCA R&D Serial No. 2486*, (2486), p.78. Available at: <http://citeseerx.ist.psu.edu/viewdoc/download?doi=10.1.1.152.4715&rep=rep1&type=pdf>.
- Flatt, R.J., 2002. Salt damage in porous materials: how high supersaturations are generated. *Journal*

- of Crystal Growth*, 242(3–4), pp.435–454. Available at:
<http://www.sciencedirect.com/science/article/pii/S002202480201429X>.
- Ghafoori, N., Batilov, I.B. & Najimi, M., 2016. Sulfate Resistance of Nanosilica and Microsilica Contained Mortars. *ACI Materials Journal*, 113(4), pp.459–469.
- Haynes, H. & Bassuoni, M.T., 2011. Physical Salt Attack on Concrete. *Concrete International*, (November), pp.38–42.
- Haynes, H., O'Neill, R. & Mehta, K.P., 1996. Concrete Deterioation from Physical Attack by Salts. *Concrete International*, 18(January), pp.63–68.
- Henderson, C. of, 2015. *2015 Water Quality Report*,
- Hewlett, P.C. & Massazza, F., 2003. Lea's Chemistry of Cement and Concrete. *Lea's Chemistry of Cement and Concrete*, pp.471–635.
- Holland, T.C., 2005. Silica Fume User's Manual. *FHWA-IF-05-016*, p.194.
- Hou, P. et al., 2013. Effects of colloidal nanosilica on rheological and mechanical properties of fly ash-cement mortar. *Cement and Concrete Composites*, 35(1), pp.12–22. Available at:
<http://linkinghub.elsevier.com/retrieve/pii/S0958946512001916>.
- Hou, P. et al., 2013. Modification effects of colloidal nanoSiO₂ on cement hydration and its gel property. *Composites Part B: Engineering*, 45(1), pp.440–448. Available at:
<http://linkinghub.elsevier.com/retrieve/pii/S1359836812003952>.
- ICRI, 2006. Vision 2020 : A Vision for the Concrete Repair Protection and Strengthening Industry. In Chicago, IL: International Concrete Repair Institute, pp. 1–25. Available at:
https://www.icri.org/GENERAL/Vision2020-Version1.0_May2006.pdf.
- ISO 14887, 2000. ISO 14887 Sample Preparation—Dispersing Procedures for Powders in Liquids. *ISO*, 2000.
- Jiang, J., Oberdörster, G. & Biswas, P., 2009. Characterization of size, surface charge, and agglomeration state of nanoparticle dispersions for toxicological studies. *Journal of*

Nanoparticle Research, 11(1), pp.77–89.

Jo, B.-W. et al., 2007. Characteristics of cement mortar with nano-SiO₂ particles. *Construction and Building Materials*, 21(6), pp.1351–1355. Available at: <http://linkinghub.elsevier.com/retrieve/pii/S095006180600136X>.

Kawashima, S. et al., 2013. Modification of cement-based materials with nanoparticles. *Cement and Concrete Composites*, 36(1), pp.8–15. Available at: <http://dx.doi.org/10.1016/j.cemconcomp.2012.06.012>.

Kelham, S., 1996. The Effect of Cement Composition and Fineness on Expansion Associated with Delayed Ettringite Formation. , 9465(95).

Khanzadi, M. et al., 2010. Influence of nano-silica particles on mechanical properties and permeability of concrete. In *Second international conference on sustainable construction materials and technologies, Ancona, Italy, June*.

Khatri, R.P., Sirivivatnanon, V. & Yang, J.L., 1997. Role of permeability in sulphate attack. *Cement and Concrete Research*, 27(8), pp.1179–1189. Available at: <http://www.scopus.com/inward/record.url?eid=2-s2.0-0031213143&partnerID=40&md5=8a272529307f930dcd1d9d1890871032>.

Kong, D. et al., 2012. Influence of nano-silica agglomeration on microstructure and properties of the hardened cement-based materials. *Construction and Building Materials*, 37, pp.707–715. Available at: <http://dx.doi.org/10.1016/j.conbuildmat.2012.08.006>.

Kontoleonos, F. et al., 2012. Influence of Colloidal Nanosilica on Ultrafine Cement Hydration : Physicochemical and microstructural characterization. *Construction and Building Materials*, 35, pp.347–360. Available at: <http://dx.doi.org/10.1016/j.conbuildmat.2012.04.022>.

Koohdaragh, M. & Mohamadi, H.H., 2011. Comparison of mechanical of the concrete samples containing micro-silica and nano-silica. *Australian Journal of Basic and Applied Sciences*, 5(10), pp.560–563. Available at: <http://www.scopus.com/inward/record.url?eid=2-s2.0->

84864469371&partnerID=tZOtx3y1.

Kosmatka, S.H., Kerkhoff, B. & Panarese, W.C., 2002. *Design and Control of Concrete Mixtures* 14th ed., Skokie, Illinois: Portland Cement Association.

Kosmatka, S.H. & Wilson, M.L., 2016. *Design and Control of Concrete Mixtures* 16th Editi., Skokie, Illinois: Portland Cement Association.

Kurdowski, W. & Nocuń-Wczelik, W., 1983. The Tricalcium Silicate Hydration in the Presence of Active Silica. *Cement and Concrete Research*, 13(3), pp.341–348.

Li, H. et al., 2004. Microstructure of cement mortar with nano-particles. *Composites Part B: Engineering*, 35(2), pp.185–189.

Lin, K.L. et al., 2008. Effects of nano-SiO₂ and different ash particle sizes on sludge ash-cement mortar. *Journal of Environmental Management*, 88(4), pp.708–714.

Liu, Z. et al., 2012. “Salt Weathering” Distress on Concrete by Sulfates? *Advances in Crystallization Processes*, pp.431–464. Available at: http://cdn.intechopen.com/pdfs/36366/InTech-_salt_weathering_distress_on_concrete_by_sulfates_.pdf \n<http://www.intechopen.com/books/advances-in-crystallization-processes/salt-weathering-distress-on-concrete-by-sulfates> \n<http://cdn.intechopen.com/pdfs/363>.

Mann, 2006. *Report on Nanotechnology and Construction*, Available at: nanoforum.org.

Mather, B., 1967. *Field and Laboratory Studies of the Sulfate Resistance of Concrete*, Vicksburg, Mississippi.

McMillan, F.R. et al., 1949. Bulletin 30: Long-Time Study of Cement Performance in Concrete. In *Concrete Exposed to Sulfate Soils*. Chicago, IL: Research Laboratories of the Portland Cement Association.

Mehta, K.P., 1983. Mechanism of Sulfate Attack on Portland Cement Concrete - Another Look. *Cement and Concrete Research*, 13(3), pp.401–406.

Mehta, K.P., 1993. Sulfate Attack on Concrete - A Critical Review. *Materials Science of Concrete*, 3,

pp.105–130.

Mehta, P.K., 1973. Effect of Lime on Hydration of Pastes Containing Gypsum and Calcium Aluminates or Calcium Sulfoaluminate. *Journal of the American Ceramic Society*, 56(6), pp.315–319.

Mehta, P.K., 1975. Evaluation of Sulfate-Resisting Cements by a New Test Method. *ACI Journal Proceedings*, 72(10), pp.573–575.

Mehta, P.K. & Monteiro, P.J., 2006. *Concrete Microstructure, Properties, and Materials* 3rd ed., New York, NY: McGraw-Hill.

Mindess, S., Young, F.J. & Darwin, D., 2003. *Concrete* 2nd Editio., Upper Saddle River, NJ: Pearson Education, Inc.

Mondal, P. et al., 2010. Comparative Study of the Effects of Microsilica and Nanosilica in Concrete. *Transportation Research Record: Journal of the Transportation Research Board*, 2141(2141), pp.6–9. Available at: <http://trrjournalonline.trb.org/doi/10.3141/2141-02>.

Monteiro, P.J.M., Maso, J.C. & Ollivier, J.P., 1985. The aggregate-mortar interface. *Cement and Concrete Research*, 15(6), pp.953–958.

Nehdi, M.L., Suleiman, a. R. & Soliman, a. M., 2014. Investigation of concrete exposed to dual sulfate attack. *Cement and Concrete Research*, 64, pp.42–53. Available at: <http://linkinghub.elsevier.com/retrieve/pii/S0008884614001197>.

Neville, A.M., 1998. *Properties of Concrete* 4th ed., New York: John Wiley & Sons, Inc.

Nili, M., Ehsani, a & Shabani, K., 2010. Influence of Nano-SiO₂ and Microsilica on Concrete Performance. *Concrete*.

Odler, I., 1991. Expansive Reactions in Concrete. *Materials Science of Concrete*, 2, pp.221–247.

Odler, I. & Gasser, M., 1988. Mechanism of Sulfate Expansion in Hydrated Portland Cement. *Journal of the American Ceramic Society*, 71(11), pp.1015–1020.

Park, C.K., Noh, M.H. & Park, T.H., 2005. Rheological properties of cementitious materials containing mineral admixtures. *Cement and Concrete Research*, 35, pp.842–849.

- Poole, A.B. & Sims, I., 2016. *Concrete Petrography: A Handbook of Investigative Techniques* 2nd ed., Boca Raton, FL: CRC Press.
- Powers, T.C., 1958. Structure and Physical Properties of Hardened Portland Cement Paste. *Journal of the American Ceramic Society*, 41(1), pp.1–6.
- Quercia, G. & Brouwers, H.J.H., 2010. Application of nano-silica (nS) in concrete mixtures. *8th fib PhD Symposium in Kgs, Lyngby, Denmark*.
- Rahman, M.M. & Bassuoni, M.T., 2014. Thaumasite sulfate attack on concrete: Mechanisms, influential factors and mitigation. *Construction and Building Materials*, 73, pp.652–662. Available at: <http://dx.doi.org/10.1016/j.conbuildmat.2014.09.034>.
- Raupach, M., 2006. Concrete repair according to the new European Standard EN 1504. *Methods*, pp.9–18.
- Richardson, M.G., 2002. *Fundamentals of Durable Reinforced Concrete*, New York, NY: Spon Press.
- Rodriguez-Navarro, C. & Doehne, E., 1999. Salt weathering: influence of evaporation rate, supersaturation and crystallization pattern. *Earth Surface Processes and Landforms*, 24(3), pp.191–209. Available at: [http://doi.wiley.com/10.1002/\(SICI\)1096-9837\(199903\)24:3<191::AID-ESP942>3.0.CO;2-G](http://doi.wiley.com/10.1002/(SICI)1096-9837(199903)24:3<191::AID-ESP942>3.0.CO;2-G)
http://www.design.upenn.edu/files/4-Rodrig_NavarroDoehne_EarthSurfProcLandf_24_2009.pdf
[http://doi.wiley.com/10.1002/\(SICI\)1096-9837\(199903\)24:3<191::AID-ESP942>3.0.CO;](http://doi.wiley.com/10.1002/(SICI)1096-9837(199903)24:3<191::AID-ESP942>3.0.CO;)
- Rosetti, V.A., Chiochio, G. & Paolini, A.E., 1982. Expansive properties of the mixture C4A \bar{S} H12 - 2C \bar{S} I. An hypothesis on the expansion mechanism. *Cement and Concrete Research*, 12(5), pp.577–585.
- Rundong, G. et al., 2010. Deterioration Mechanisms of Sulfate Attack on Concrete under Alternate Action. *Journal of Wuhan University of Technology-Materials*, pp.355–359.
- Sahin, R. & Oltulu, M., 2008. New Materials for Concrete Technology: Nano Powders. In *33rd Conference on OUR WORLD IN CONCRETE & STRUCTURES*. Singapore: Singapore Concrete

Institute.

- Said, a. M. et al., 2012. Properties of concrete incorporating nano-silica. *Construction and Building Materials*, 36, pp.838–844.
- Sanchez, F. & Sobolev, K., 2010. Nanotechnology in concrete – A review. *Construction and Building Materials*, 24(11), pp.2060–2071. Available at: <http://linkinghub.elsevier.com/retrieve/pii/S0950061810001625>.
- Scherer, G.W., 2004. Stress from crystallization of salt. *Cement and Concrete Research*, 34(9), pp.1613–1624. Available at: <http://linkinghub.elsevier.com/retrieve/pii/S0008884604000122>.
- Schiro, M., Ruiz-Agudo, E. & Rodriguez-Navarro, C., 2012. Damage Mechanisms of Porous Materials due to In-Pore Salt Crystallization. *Physical Review Letters*, 109(26), p.265503. Available at: <http://link.aps.org/doi/10.1103/PhysRevLett.109.265503>.
- Senff, L. et al., 2010. Effect of nanosilica and microsilica on microstructure and hardened properties of cement pastes and mortars. *Advances in Applied Ceramics*, 109(2), pp.104–110.
- Senff, L. et al., 2009. Effect of nano-silica on rheology and fresh properties of cement pastes and mortars. *Construction and Building Materials*, 23(7), pp.2487–2491. Available at: <http://dx.doi.org/10.1016/j.conbuildmat.2009.02.005>.
- Senff, L. et al., 2009. Influence of added nanosilica and/or silica fume on fresh and hardened properties of mortars and cement pastes. *Advances in Applied Ceramics*, 108(7), pp.418–428. Available at: <http://www.maneyonline.com/doi/abs/10.1179/174367609X422108>.
- Senff, L. et al., 2010. Mortars with nano-SiO₂ and micro-SiO₂ investigated by experimental design. *Construction and Building Materials*, 24(8), pp.1432–1437. Available at: <http://linkinghub.elsevier.com/retrieve/pii/S0950061810000243>.
- Shanahan, N. & Zayed, A., 2007. Cement composition and sulfate attack Part I. *Cement and Concrete Research*, 37(4), pp.618–623.

- Shih, J.-Y., Chang, T.-P. & Hsiao, T.-C., 2006. Effect of nanosilica on characterization of Portland cement composite. *Materials Science and Engineering: A*, 424(1-2), pp.266-274.
- Siddique, R. & Khan, M.I., 2011. *Supplementary Cementing Materials*, Berlin: Springer-Verlag.
- Sieger, B.H. et al., 2004. Controlling Surface Composition and Zeta Potential of Chemical Vapor Synthesized Alumina-Silica Nanoparticles. *Chemical Vapor Deposition*, 10(2), pp.71-76.
- Singh, L.P. et al., 2013. Beneficial role of nanosilica in cement based materials – A review. *Construction and Building Materials*, 47, pp.1069-1077.
- Skalny, J., Marchand, J. & Odler, I., 2002. *Sulfate Attack On Concrete*, London and New York: Spon Press.
- Sobolev, K. & Gutiérrez, M.F., 2005. How nanotechnology can change the concrete world. *American Ceramic Society Bulletin*, 84(10), pp.14-18.
- Stanish, K.D., Hooton, R.D. & Thomas, M.D.A., 1997. *Testing the Chloride Penetration Resistance of Concrete : A Literature Review*, Toronto, Ontario, Canada.
- Suleiman, A.R., 2014. *Physical Sulphate Attack on Concrete*. University of Western Ontario. Available at: <http://ir.lib.uwo.ca/etd/2058/>.
- Taurozzi, J.S., Hackley, V. a & Wiesner, M.R., 2012. Preparation of Nanoparticle Dispersions from Powdered Material Using Ultrasonic Disruption Preparation of Nanoparticle Dispersions from Powdered Material Using Ultrasonic Disruption. *NIST Special Publication 1200-2*.
- Taurozzi, J.S., Hackley, V. a & Wiesner, M.R., 2011. Ultrasonic dispersion of nanoparticles for environmental, health and safety assessment--issues and recommendations. *Nanotoxicology*, 5(4), pp.711-29.
- Taylor, H.F.W., 1997. *Cement Chemistry* 2nd ed., London: Thomas Telford.
- Thomas, M. et al., 2008. Diagnosing delayed ettringite formation in concrete structures. *Cement and Concrete Research*, 38, pp.841-847.
- Tobón, J.I., Payá, J. & Restrepo, O.J., 2015. Study of durability of Portland cement mortars blended with silica nanoparticles. *Construction and Building Materials*, 80, pp.92-97.

- Tobón, J.I., Restrepo, O.J. & Payá, J., 2010. Comparative analysis of performance of portland cement blended with nanosilica and silica fume . *Análisis comparativo del desempeño del cemento portland adicionado con nanosílice y humo de sílice*, 77(163), pp.37–46. Available at: <http://www.scopus.com/inward/record.url?eid=2-s2.0-80051560900&partnerID=40&md5=7e4c37f7474a4ba7ae0804ffdf64788>.
- Tsui, N., Flatt, R.J. & Scherer, G.W., 2003. Crystallization damage by sodium sulfate. *Journal of Cultural Heritage*, 4, pp.109–115.
- Vasylykiv, O. & Sakka, Y., 2001. Synthesis and colloidal processing of zirconia nanopowder. *Journal of the American Ceramic Society*, 84(11), pp.2489–2494. Available at: <http://onlinelibrary.wiley.com/doi/10.1111/j.1151-2916.2001.tb01041.x/abstract>.
- Verbeck, G.J., 1967. *Field and Laboratory Studies of the Sulphate Resistance of Concrete*, Skokie, Illinois.
- Vočka, R. et al., 2000. Mercury intrusion porosimetry and hierarchical structure of cement pastes - theory and experiment. *Cement and Concrete Research*, 30(4), pp.521–527.
- Wee, T.H. et al., 2000. Sulfate resistance of concrete containing mineral admixtures. , 97(5), pp.536–549.
- Winter, N.B., 2012a. *Understanding Cement*, Rendlesham, Woodridge, UK: WHD Microanalysis Consultants Ltd.
- Winter, N.B., 2012b. *Understanding Cement*, Woodridge, UK: WHD Microanalysis Consultants Ltd.
- Zaki, S.I. & Khaled .s.Ragab, 2009. How Nanotechnology Can Change Concrete. *1st International Conference on Sustainable Built Environment Infrastructures in Developing Countries*, pp.407–414. Available at: <http://enset-oran.dz>.
- Zapata, L.E. et al., 2013. Rheological performance and compressive strength of superplasticized cementitious mixtures with micro/nano-SiO₂ additions. *Construction and Building Materials*, 41, pp.708–716. Available at: <http://dx.doi.org/10.1016/j.conbuildmat.2012.12.025>.
- Zhang, M.-H., Islam, J. & Peethamparan, S., 2012. Use of nano-silica to increase early strength and

reduce setting time of concretes with high volumes of slag. *Cement and Concrete Composites*,
34(5), pp.650–662. Available at:
<http://linkinghub.elsevier.com/retrieve/pii/S0958946512000327>.

CURRICULUM VITAE

Department of Civil and Environmental Engineering and Construction

Howard R. Hughes College of Engineering

The Graduate College

Iani B. Batilov

Address:

897 Prairie Grass Drive, Las Vegas, NV, 89123

Degrees:

Bachelor of Science in Civil and Environmental Engineering, 2012

University of Nevada, Las Vegas

Master of Science in Civil and Environmental Engineering, 2016

University of Nevada, Las Vegas

Special Honors:

Graduate College and Graduate and Professional Student Association (GPSA) 2015 Research Forum Honorable Mention for poster presentation of "Sulfate Resistance of Nano Silica and Micro Silica Contained Mortars"

Manuscript "Effect of Combined Nanosilica and Microsilica on Resistance to Sulfate Attack" recognized as Award Winning Paper at the Fourth International Sustainable Construction Materials & Technologies (SCMT4)

Tau Beta Pi, Nevada Beta Chapter, 2011

Publications:

Ghafoori, N., Batilov, I.B. & Najimi, M., 2016. "Sulfate Resistance of Nanosilica and Microsilica Contained Mortars," *ACI Materials Journal*, 113 (4), pp.459–469.

Ghafoori, N., Batilov, I.B. & Najimi, M., Sharbaf, M. 2016. "Effect of Combined Nanosilica and Microsilica on Resistance to Sulfate Attack" *Proceedings of the Fourth International Sustainable Construction Materials & Technologies (SCMT4)*, August 7-11, 2016, Las Vegas, NV, USA.

Thesis Title: Sulfate Resistance of Nanosilica Contained Portland Cement Mortars

Thesis Examination Committee:

Chairperson: Dr. Nader Ghafoori, Ph.D.

Committee Member: Dr. Samaan Ladkany, Ph.D.

Committee Member: Dr. Mohamed S. Kaseko, Ph.D.

Graduate College Faculty Representative: Dr. Mohamed Trabia, Ph.D.